A computational model of hepatic energy metabolism: Understanding the role of zonation in the development and treatment of non-alcoholic fatty liver disease (NAFLD).

William Ashworth

A thesis submitted for the degree of

Doctor of Philosophy

at

University College London

Declaration

I, William Ashworth, confirm that the work presented in this thesis is my own. Where information has been derived from other sources, I confirm that this has been indicated in the thesis.

Acknowledgements

I would like to express my sincere gratitude to Dr Nathan Davies and Prof. David Bogle for their guidance, supervision and motivation throughout my research. I would like to thank Dr Andreola, Dr Jones, Ms Habtesion, Dr De Chiara, Mr Apostolidis and the liver failure group for their invaluable help and advice with experiments. I am very grateful to the Engineering and Physical Sciences Research Council (ESPRC) and the Centre for Mathematics and Physics in the Life Science and Experimental Biology (CoMPLEX) at UCL for their financial support without which this work would not have been possible. Finally, I would like to thank my family and friends for their support over the last 4 years.

Abstract

Non-alcoholic fatty liver disease (NAFLD) is a highly prevalent condition associated with increased risk of liver failure, diabetes and numerous further conditions. In NAFLD, lipid build-up and the resulting damage occurs most severely in hepatocytes at the pericentral end of the capillaries (sinusoids) which supply the cells with blood [1-3]. Due to the complexity of studying individual regions of the sinusoids, the causes of this zone specificity and its implications on treatment have largely been ignored in previous research. In this study, a computational model of liver glucose and lipid metabolism was developed which includes zone-dependent enzyme expression. This model was then used to study the development of NAFLD across the sinusoid. By simulating insulin resistance and high intake diets leading to the development of steatosis in the model, we propose a novel mechanism leading to pericentral steatosis in NAFLD patients. Sensitivity analysis on the rate parameters in the model was then used to highlight key inter-individual variations in hepatic metabolism with the largest effect on steatosis development.

Secondly, the model, in combination with cell culture experiments, was used to assess potential drug targets for clearing steatosis across the sinusoid without disrupting other aspects of metabolism. Adverse effects were highlighted when targeting (stimulating or inhibiting through altering the rate constants) for most processes in the model, and these were largely validated in the hepatocyte-like cell culture line through the addition of small molecule inhibitors. However, inhibition of lipogenesis combined with stimulation of β-oxidation was predicted to clear steatosis, reduce hepatic FFA levels, reduce excess ETC flux and increase hepatic ATP concentrations across the sinusoid without causing adverse effects elsewhere in metabolism. Furthermore, in the cell culture model, inhibition of lipogenesis combined with stimulation of β-oxidation using acetyl-CoA carboxylase inhibitor TOFA, resulted in clearance of steatosis, improved cell viability, reduced oxidative stress and increased mitochondrial function.

Contents

Frequently Used Abbreviations

NAFLD – Non-alcoholic Fatty Liver Disease
NASH – Non-alcoholic Steatohepatitis
T2DM – Type 2 Diabetes Mellitus
IR – Insulin Resistance
FA – Fatty Acid
FFA – Free/Non-esterified Fatty Acid
HDL – High density lipoprotein
LDL – Low density lipoprotein
VLDL – Very Low Density Lipoprotein
ALF – Acute Liver Failure
AFLD – Alcoholic Fatty Liver Disease
SREBP-1c – Sterol-Regulatory Element Binding Protein 1c
ChREBP – Carbohydrate Responsive Element Binding Protein
ROS – Reactive Oxygen Species
ETC – Electron Transport Chain

CoA – Coenzyme A
DAG – Diacylglycerol/Diglyceride
G6P – Glucose-6-Phosphate
GADP – Glyceraldehyde-3-Phosphate
G3P – Glycerol-3-Phoshate
ATP – Adenosine Triphosphate
ADP – Adenosine Diphosphate
AMP – Adenosine Monophosphate
UTP – Uridine Triphosphate
UDP – Uridine Diphosphate
GTP – Guanosine Triphosphate
GDP – Guanosine Diphosphate
P_i – Inorganic Phosphate
NAD+/NADH – Nicotinamide Adenine Dinucleotide (oxidised/reduced)
FADH – Flavin Adenine Dinucleotide
FAS – Fatty Acid Synthase
ACC – Acetyl-CoA Carboxylase
FATP – Fatty Acid Transport Protein
GK – Glucose Kinase
G6Pase – Glucose-6-Phosphatase
PFK – Phosphofructokinase
FBPase – Fructose-Bisphosphatase
PK – Pyruvate kinase
PEPCK – Phosphoenolpyruvate Carboxykinase
GS – Glycogen Synthase
GP – Glycogen Phosphorylase
PDH – Pyruvate Dehydrogenase
NDK – Nucleoside Diphosphate Kinase
AK – Adenosine Kinase
CYP2E1 – Cytochrome P450 2E1
ALT – Alanine Aminotransferase
AST – Aspartate Aminotransferase

List of Figures

List of Tables

Aims of the Project

Non-alcoholic fatty liver disease (NAFLD), the build-up of fats in the liver in the absence of alcohol abuse, drug abuse and viral infection, is present in around one third of US and UK adults [1-5]. High liver fat increases the probability of developing liver failure, type 2 diabetes, kidney failure, liver cancer and cardiovascular problems [6-14]. Due to the high prevalence of the disease, it is expected to become the largest cause of liver transplant in the coming decades [8]. No approved drug for reducing steatosis in NAFLD is currently available and lifestyle change, which is known to be associated with low compliance rates, remains the only effective treatment. Therefore, study of both the development and treatment of NAFLD is urgently required, particularly in the early, reversible stages.

Hepatocytes *in vivo* are known to show vast heterogeneity in enzyme expression depending upon their position along the liver sinusoid. This heterogeneity in enzyme expression causes groups of hepatocytes to specialise in different functions. In adult NAFLD, patients tend to show higher lipid content in cells near the central vein (pericentral) [15-17]. Additionally, the resulting damage tends to occur more rapidly in these cells. However, due to the experimental difficulty in studying a large number of variables (such as concentrations, enzyme activities or conversion rates) in specific regions of the sinusoid, researchers instead tend to study homogenised tissue and only measure averaged changes in the liver as a whole. Therefore, the causes of this increased pericentral susceptibility to steatosis remain unclear. Additionally, the implications of hepatic heterogeneity are rarely considered when assessing potential drug targets. It is possible that a drug may have beneficial effects on one region of the sinusoid whilst causing damage in another.

The aim of this project was to study the implications of zonation in NAFLD development and treatment through a combination of computational modelling and cell culture experimentation. These simulations and experimental data will provide a basis for targeted and minimised future *in vivo* experimentation.

The first objective was to build a model capable of representing hepatic glucose and lipid metabolisms across the sinusoid (chapter 2). This model should include blood flow and variation in enzyme activity across the sinusoid based on experimental data in the literature. It should additionally provide realistic output data when simulating both metabolically normal and insulin resistant individuals, when compared with a range of experimental data.

The second objective was to simulate conditions leading to the development of NAFLD (chapter 3). This included simulating the effects of high fat intake, IR and other metabolic dysregulation in the model and comparing with the metabolic changes known to occur in NAFLD. After establishing a representation of NAFLD, the next goal was to assess the major differences between periportal and pericentral cells that cause higher susceptibility to steatosis in pericentral cells. In a computational model, the concentrations of a large number of molecules and the rates of processes can be studied in individual regions of the sinusoid under a range of conditions, which would not be feasible experimentally. The model predictions can then be used to motivate targeted experimental validation.

The third objective was to assess the effects of inter-individual heterogeneity in hepatic metabolism on susceptibility to steatosis and on the pattern of steatosis development (chapter 3). Around 25% of obese individuals fail to develop steatosis whilst 16% of lean individuals show excess liver fat [18]. Furthermore, whilst pericentral cells tend to show the highest lipid content, variation is seen in the predominant location of steatosis from pericentral to azonal or pan-sinusoidal [15-17]. Computational modelling allows each parameter to be modified individually, or several parameters to be modified as required, where experimentally, large scale studies would be required to correlate liver fat percentage or liver fat distribution with enzyme activities and confounding factors would have to be accounted for. Furthermore, use of a computational model allows detailed study of the mechanisms leading to change in liver fat percentage or distribution.

The fourth objective was to assess the impact of pharmacologically targeting various processes in the model to clear steatosis in NAFLD without further disrupting energy metabolism (chapter 4). Through

changes to the rate constants of particular processes, pharmacological inhibition or stimulation of key enzymes can be simulated. By performing this analysis in a computational model, the effects on a wide range of variables can be studied under a range of conditions. Additionally, the effects of targeting each process can be studied in each individual region of the sinusoid.

The final objective was to provide validation of key model predictions using an *in vitro* HepG2 cell culture model (chapter 5). Firstly, the impact of FFA treatment on the cells was studied to ensure they replicate the major metabolic changes occurring in hepatocytes in NAFLD *in vivo* and seen in model simulations. Once a cell culture model of the metabolic changes had been established, the next goal was to treat the cells with a range of small molecule inhibitors to mirror the pharmacological targeting simulated in the model and assess the effects on metabolism, comparing with the simulated data.

1 Chapter 1: Introduction

In this chapter, a review of the relevant literature is provided. Firstly, in section 1.1, the structure and physiology of the liver are reviewed. In section 1.2 the causes and consequences of zonation in liver function across the sinusoid are discussed with a focus on zonation in metabolism. In section 1.3 a review of liver disease and failure is presented focussing on NAFLD, NASH and related conditions. Finally, in section 1.4 a brief review of previously published computational models relevant to hepatic metabolism or zonation across the sinusoid is presented.

1.1 *The Liver*

1.1.1 Structure of the Liver

The liver is the largest internal organ in the body (1.44-1.66kg) [19] and is involved in a vast range of essential processes including glucose and lipid metabolism, drug and xenobiotic detoxification, plasma protein synthesis and bile production. Despite its regenerative capacity, disease of the liver is the fifth largest cause of death in the UK and the only major cause of death to be rising year on year [1]. The following sections will review the structure and function of the liver.

1.1.1.1 Blood Supply and Microstructure

On the micro scale, the liver is built from ~1-2mm long structural units called lobules. In cross-section, these consist of rows of liver cells extending outwards from a central vein to form a hexagonal shaped unit which tessellates with adjacent lobules (see figure 1.1) [20]. Blood is supplied to the liver through two vessels, the hepatic artery and the portal vein. The hepatic artery supplies oxygenated blood from the heart. The portal vein provides blood which has passed through the gastrointestinal tract, spleen and pancreas containing the nutrients and toxins absorbed from food. Upon entering the liver, the hepatic artery and portal vein divide into branches which pass between the corners of neighbouring lobules. These branches subdivide into capillaries known as sinusoids which extend into the lobule between each row of cells, supplying them with oxygenated blood from the hepatic artery and nutrient filled blood from the digestive system [21] (figure 1.2). After passing through the sinusoid,

blood exits the lobule through the central vein. The central veins from each of the lobules join to form the hepatic vein, through which blood leaves the liver. As well as the blood vessels, intrahepatic bile ducts pass between each lobule which join and provide bile to the digestive system.

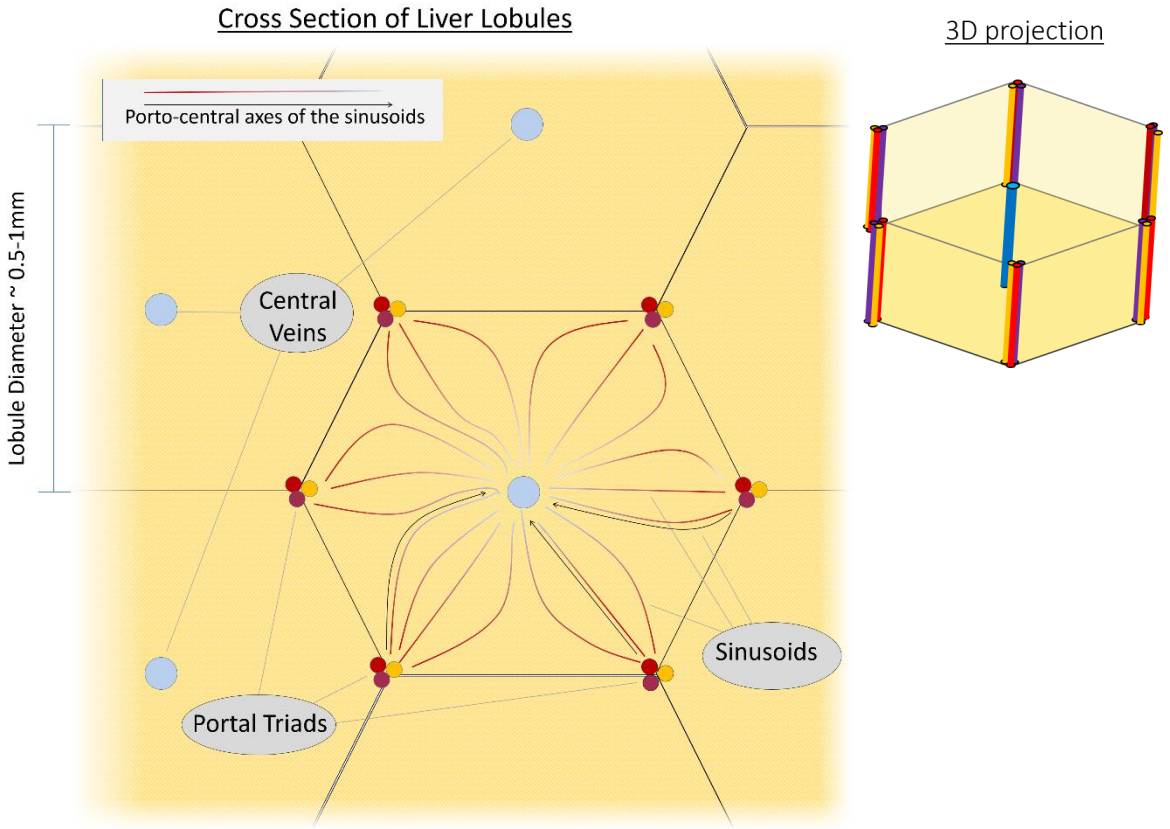

Figure 1.1: A cross sectional view of a hepatic lobule and its neighbouring lobules showing the portal triads, central veins and the sinusoids and a 3D projection of the lobule.

1.1.1.2 The Sinusoid – Cell types and zonation

Hepatocytes are the major cell types in the liver making up roughly 80% of its volume [20]. They are the worker cells of the liver, involved in the vast range of functions described in section 1.1.2. The other cells, referred to as non-parenchymal cells, make up roughly 40% of the total number of cells in the liver but only 6.5% of its volume [22]. These include sinusoidal endothelial cells, Kupffer cells (macrophages), hepatic stellate cells and liver associated natural killer cells. A fenestrated single cell wall composed largely of endothelial cells along with some Kupffer cells lines the sinusoid vessel [20]. The fenestrae are small enough to block platelets or cells from passing through, but allow plasma to enter the space between the wall and the hepatocytes known as the space of Disse [20]. The rare Pit

cells (the natural killer cells of the liver) also inhabit the sinusoid space, attached to the luminal surface [20]. Ito cells inhabit the space of Disse and are strongly bound to the endothelial cells. The liver also contains a residual stem cell population known as Oval cells that are thought to be involved in regeneration. Under normal conditions the liver contains relatively little connective tissue [23].

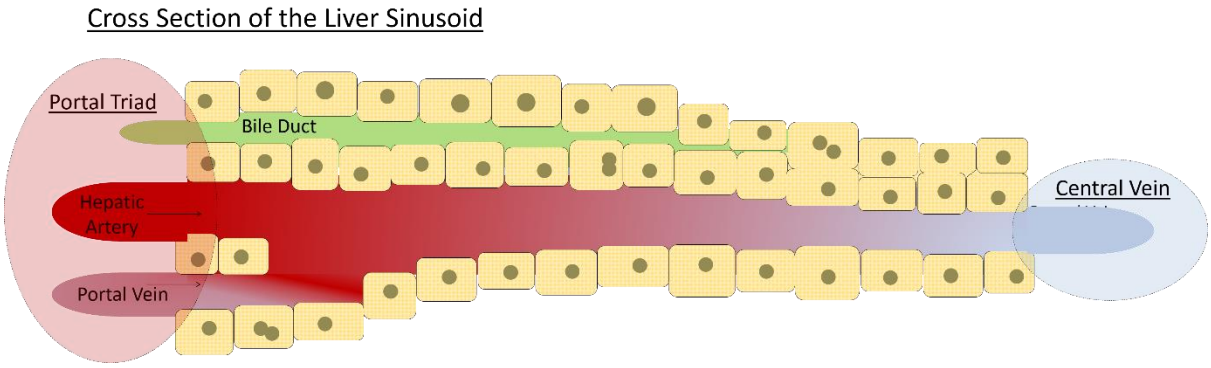

Figure 1.2: The liver sinusoid showing the portal triad (hepatic artery, portal vein, bile duct) and the central vein.

The focus of this study is on hepatocytes, the cells responsible for performing the major functions of the organ. Hepatocytes are large polarised cells, having distinct membranes on their basolateral and canalicular sides. The basolateral side faces the sinusoid and so is covered in microvilli to maximize the surface area presented to the blood. The canalicular surfaces of neighbouring groups of hepatocytes form bile canaliculi, the thin ducts which join to form the bile duct [20].

The relative contributions of each hepatocyte to different functions performed by the liver vary as a function of their position along the sinusoid. For example, in glucose metabolism, the cells in the region closest to the hepatic artery and portal vein, the periportal zone, tend to be more active in glucose production whilst cells in the region closest to the hepatic vein play a more prominent role in glucose uptake [24]. This heterogeneity, known as zonation, is seen in almost all functions of the liver [24]. The primary cause of zonation is the change in abundance of substances in the blood as it passes through the sinusoid. For example, the average blood oxygen concentration falls from 60-65mmHg in the periportal zone to 30-35 mmHg in the pericentral zone [24]. As well as changes in the enzymatic

content of hepatocytes across the sinusoid, there are also changes in the numbers and types of non-parenchymal cells. Zonation is reviewed in detail in section 1.2.

1.1.2 Liver Physiology

The liver performs a vast number of processes in the body such that, at rest, it produces 20% of the body's heat. These include roles in detoxification, synthesis and storage section.

Ammonia is the main toxic waste resulting from protein catabolism and its detoxification occurs mostly in hepatocytes [20]. It is generally converted to urea which is removed by the kidney, although specific subgroups of hepatocytes (pericentral) are able to convert ammonia to glutamine [25]. Bilirubin, a degradation product of haemoproteins, is conjugated with glucuronic acid to make it soluble. It is then removed in the bile. Bile acids are also produced in the liver using cholesterol as a substrate.

The liver is responsible for the breakdown of several hormones such as insulin and glucagon along with certain proteins [20]. It also removes most xenobiotics from the blood. Hydrophobic xenobiotics are solubilised so that they can be removed [20]. This is a two-stage process with different enzymes responsible for each process. The first step involves oxidation of the xenobiotic by attaching a polar group. In the second step, a second group of enzymes conjugate small hydrosoluble molecules (amino acids, glutathione, glucuronic acids etc.) to the protein [20]. It also has immunological roles containing many active cells which destroy pathogens in the portal vein [20].

The liver plays important roles in the synthesis of proteins, hormones (such as insulin-like growth factor-1) and amino acids [20]. The liver produces albumin, which makes up 50% of the protein content of blood, along with various coagulation factors and antithrombin [20].

The liver plays a vital role in carbohydrate metabolism, storing glucose and other sugars as glycogen (section 1.1.2.1). It also plays several roles in fatty acid (FA) metabolism (section 1.1.2.2). It is these roles in the metabolism of carbohydrate and fat which are studied in the subsequent chapters. As well

as glycogen, the liver stores a vast range of other substances including vitamins A, D, B and K, iron and copper [20].

1.1.2.1 Glucose and Carbohydrate Metabolism

Most carbohydrates and sugars are broken down to glucose in the digestive system before entering the blood stream in the intestine. Glucose is a simple monosaccharide that acts as the major source of energy for most cell types. After meals, glucose is absorbed into the blood stream whilst between meals, especially during exercise, sugars are utilised in organs and muscle for energy. Since these rates of input and consumption are not constant, excess glucose must be stored to stop the blood concentration rising above or falling below safe bounds. This storage occurs in liver and muscle cells where glucose molecules are attached to polysaccharide (glycogen) chains.

When blood glucose levels are high, the hormone insulin is released by the pancreas prompting the liver to remove glucose from the blood stream. Glucose molecules are converted to glucose-6-phosphate (G6P) by the enzyme glucokinase (GK) before the G6P is polymerised to glycogen by glycogen synthase (GS). Alternatively, G6P can also be converted to pyruvate through a process known as glycolysis (predominantly rate-limited by enzymes phosphofructokinase (PFK) and pyruvate kinase (PK)). Excess pyruvate is then converted to acetyl-CoA for use in oxidative ATP synthesis or lipid metabolism or released into the blood as lactate.

When blood glucose levels are low, the hormone glucagon is released triggering the breakdown of glycogen to glucose. Similarly, during exercise catecholamines such as epinephrine promote glucose release. This breakdown of glycogen to G6P is mediated by glycogen phosphorylase (GP). This G6P is converted to glucose by glucose-6-phosphatase (G6Pase) before being released into the blood. Additionally, under the influence of glucagon, the liver converts lactate, pyruvate and certain amino acids to G6P in a process known as gluconeogenesis (predominantly rate-limited by enzymes phosphoenolpyruvate kinase (PEPCK) and fructose-bisphosphatase (FBPase)).

GS and GP, along with the key enzymes in both glycolysis and gluconeogenesis, can exist in active and inactive states depending on their phosphorylation. When insulin, glucagon and other hormones bind to surface receptors on a cell, it triggers a series of downstream effects which alter the phosphorylation state of these enzymes. Through this feedback loop between the liver and pancreas, blood glucose levels are maintained in a safe range. Furthermore, transcription of glucose metabolism enzymes is increased or suppressed when exposed to long term increased insulin or glucagon concentrations [20]. Zonation in glucose metabolism is discussed in detail in section 1.2, whilst each of the individual processes and their representations in the model are discussed in chapter 2.

1.1.2.2 Fatty Acid Metabolism

Although adipose tissue is the major tissue responsible for mediating blood free fatty acid (FFA) and triglyceride concentrations, liver plays important role in synthesizing triglyceride (combining three FFAs with a glycerol molecule) and releasing them into the plasma, predominantly as very low density lipoproteins (VLDL). Although the majority of fats in liver arise from uptake of circulating FAs, some *de novo* lipogenesis also occurs in hepatocytes [26]. When studied in the livers of patients with NAFLD, around 26% of the FAs contained in hepatic triglycerides and VLDL were produced in liver [26].

FAs are taken up from the plasma by fatty acid transport proteins, FATP2 and FATP5 along with scavenger receptor CD36 and caveolins [27-33]. For *de novo* FA synthesis to occur, acetyl-CoA (and related malonyl-CoA) molecules, derived predominantly from sugars, proteins or previous FA oxidation, are combined into FA chains (under the influence of enzymes acetyl-CoA carboxylase (ACC) and fatty acid synthase (FAS)). This process is stimulated by insulin and inhibited by glucagon [34, 35]. However, *de novo* lipogenesis is counter-intuitively upregulated in insulin resistant livers [36-39]. Numerous FAs can be produced or absorbed from food with different chain lengths and with saturated and unsaturated tails. The most common of FA is palmitate in humans, plants animals and micro-organisms comprised of the equivalent of 8 acetyl-CoA molecules [40], whilst the most common FA in adipose tissue is oleic acid [41, 42].

Triglyceride synthesis (also promoted by insulin and glucagon) involves combining three FAs with a glycerol backbone for storage (rate-limited by enzyme glycerophosphate acyltransferase [43]). Post-prandially, when FFA and glucose concentrations are high, triglyceride synthesis removes the FFAs from the blood stream preventing damage. The liver also utilises FFAs as its primary source of energy through β-oxidation [44]. Here the FA chains are broken down to acetyl-CoA, which can in turn enter the citric acid cycle to produce cellular ATP [20]. The liver also plays a major role in the production of ketone bodies and in cholesterol synthesis. Zonation in lipid metabolism is reviewed in section 1.2, whilst each of the individual processes their representation in the model are discussed in chapter 2.

1.2 Zonation

Zonation is the variation of enzyme expression and liver function between hepatocytes across the sinusoid. Almost all functions performed by the liver show zonation. In some cases a very specific group of hepatocytes in a particular location perform a function, whilst in other cases a more gradient-like and variable distribution exists [45]. In section 1.2.1, the zonation of enzymes and functions involved in energy, glucose and lipid metabolism are reviewed. These follow the latter class of gradient-like changes in function across the sinusoid [45]. In section 1.2.2, possible mechanisms involved in the promotion of a zonated phenotype are discussed. Zone specific damage in liver disease is discussed in section 1.3.6.

1.2.1 Zonation of hepatic enzymes and function

1.2.1.1 ATP production through oxidative phosphorylation

Adenosine tri-phosphate (ATP) is produced from adenosine diphosphate (ADP) and inorganic phosphate (P_i) through the electron transport chain (ETC) in the mitochondrial membrane of cells. The ETC relies on nicotinamide adenine dinucleotide (NADH) or flavin adenine dinucleotide (FADH) as well as oxygen to occur. Since transporting cytoplasmic NADH into the mitochondria consumes energy, the majority of the NADH and FADH required are generated through the degradation of acetyl-CoA in the citric acid cycle inside the mitochondria. Periportal hepatocytes contain a greater volume of

mitochondria [46], a larger mitochondrial membrane area [46] and increased concentrations of key enzymes involved in both the citric acid cycle [47] and the ETC [48], demonstrating that they have a higher capacity for generating energy through this mechanism. This is consistent with the observation that pericentral cells inhabit a low oxygen environment. If the ETC is active in the absence of oxygen, it can lead to the production of toxic metabolites such as the superoxide anion radical, hydrogen peroxide or the hydroxyl radical [45, 49]. Therefore, these cells contain less of the machinery for oxidative energy production to avoid producing reactive intermediates in the absence of oxygen as an acceptor [45, 50].

Due to the reduced oxidative phosphorylation in pericentral hepatocytes, they tend to produce acetyl-CoA from glucose through glycolysis whilst periportal cells consume FAs through β-oxidation [45]. The breakdown of glucose to pyruvate through glycolysis produces a small amount of ATP without the requirement for oxygen. This pyruvate can then by converted to acetyl-CoA or released into the blood as lactate. Pericentral hepatocytes specialise in this process as an additional mechanism to produce ATP [45]. Generating acetyl-CoA from FAs meanwhile consumes a small amount of ATP. Periportal hepatocytes inhabit a higher oxygen environment and are able to generate sufficient acetyl-CoA from FA oxidation [45]. This is discussed in more detail in the following sections.

1.2.1.2 Carbohydrate metabolism

There is a bias for the glycogen stores in periportal hepatocytes to fill more quickly after feeding. However, glycogen is seen across the sinusoid, and the dominant section has been shown to vary from periportal to intermediate with feeding state [51].

The mechanism by which glycogen stores are filled varies across the sinusoid [45]. These differences are related to the heterogeneity in oxidative energy metabolism described in the previous section. Pericentral cells cannot produce sufficient ATP through the citric acid cycle alone and instead specialise in processes that produce additional ATP. Periportal cells meanwhile inhabit the high oxygen environment near the periportal artery and can specialise in the more ATP intensive processes.

In the context of glycogen storage, pericentral cells tend to fill their glycogen stores from glucose and release them as pyruvate and lactate. This is because the conversion of glucose or glycogen to pyruvate and lactate through glycolysis results in the production of ATP without the requirement of oxygen. Periportal cells show higher rates of gluconeogenesis and glycogen synthesis from lactate, which requires ATP to occur. Periportal glycogen stores are then released as glucose. The high oxygen environment allows periportal cells to produce sufficient ATP through oxidative phosphorylation to fuel gluconeogenesis. Evidence for this glucose-lactate cycling across the sinusoid (figure 1.3) firstly comes from studies looking at the relative concentrations and activities of enzymes involved in glycolysis and gluconeogenesis across the sinusoid ([52-73] see chapter 2: table 2.2). A number of studies have also shown higher gluconeogenesis in periportal cells than in pericentral cells [73-78] and higher glycolysis in pericentral cells [77, 79] either using metabolic flux analysis in perfused whole livers or using cultured primary periportal and pericentral hepatocytes.

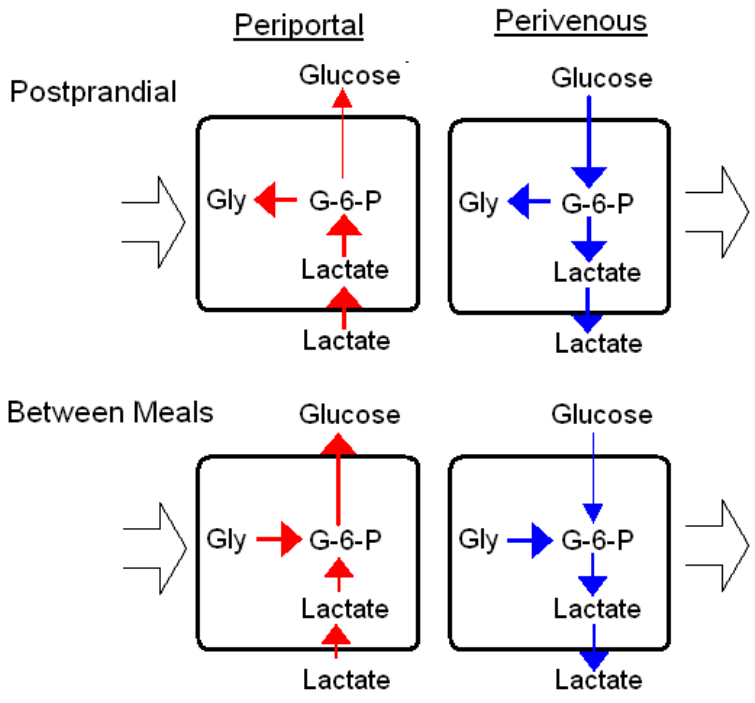

Figure 1.3: Glucose/lactate cycling in the liver.

Amino acids can also enter carbohydrate metabolism through conversion to intermediates in the citric acid cycle or to pyruvate or related molecules. Since periportal hepatocytes contain higher

concentrations of the components of both the citric acid cycle and gluconeogenesis, it is likely that these cells will specialise in both the catabolism of amino acids and the production of glucose from them (e.g. reviewed in [80]).

1.2.1.3 Lipid metabolism

The liver plays several roles the metabolism of lipids. FAs are broken down to form acetyl-CoA through β-oxidation. The majority of FFAs in the blood stream originate from dietary triglycerides or from adipose tissue [26]. However, the liver also synthesizes FAs from substrates such as glucose, lactate, amino acids and ethanol. Hepatocytes, along with adipose tissue, combine FAs and glycerol to form triglycerides and phospholipids. Hepatocytes also package triglycerides into VLDL and release them into the blood stream. The liver is the only organ responsible for the production of ketone bodies and the major organ responsible for cholesterol production [45].

Zonation in lipid metabolism is less clearly defined than in oxidative energy and glucose metabolisms and tends to vary with feeding state. However, as a general trend periportal cells are more involved in uptake and β-oxidation of FAs [81-87], whilst pericentral cells are more involved in *de novo* synthesis of FAs from acetyl-CoA [45, 81, 83, 86-89] (in turn produced from glucose through glycolysis) and the production and release of triglycerides [83, 86]. There is some evidence that ketogenesis is specialised to pericentral cells (e.g. increased β-hydroxybutyrate dehydrogenase expression in pericentral region [81, 90]), whilst cholesterol synthesis is restricted to a small number of cells surrounding the periportal artery [45, 91].

Guzman et al, used isotope labelling to show that that that β-oxidation of palmitate (the most common FA) occurred 1.2 and 1.5 times as quickly in isolated periportal hepatocytes from fed and starved animals respectively compared to the isolated pericentral hepatocytes [87]. However, when refeeding after starvation and in cold-exposed animals the pericentral section became more prominent in β-oxidation highlighting the flexibility in the zonation of lipid metabolism. Consistent with this, the rate of FA synthesis was higher in pericentral than periportal hepatocytes from fed and starved rats, whilst

the rate was higher in periportal hepatocytes in refed and cold-exposed animals [87]. Additionally Guzman and Castro showed that the rate of FA synthesis was 1.59 times higher in pericentral hepatocytes in the absence of hormones [83]. The rates of cellular and VLDL triglyceride, phospholipid and cholesterol production from FAs were all increased by 1.3-1.6 times in pericentral hepatocytes [83, 86]. Meanwhile, after liver perfusion with blood containing fluorescently labelled FAs, a higher signal was seen in periportal cells than in pericentral cells demonstrated increased uptake [92]. The triglyceride, phospholipid and cholesterol content of pericentral cells were slightly, but not statistically significantly, higher in this study. Zonation of key enzymes in lipid metabolism is discussed in chapter 2 and table 2.2.

1.2.1.4 Zonation in other liver functions

Zonation is seen in almost all liver functions including ammonia detoxification, protective metabolism, xenobiotic removal and bile formation. For a detailed review of zonation in liver function see [45].

1.2.2 Signals Promoting Zonation

The following section reviews the possible signals responsible for promoting a zonated phenotype *in vivo*. These include blood based metabolites along with nervous input.

1.2.2.1 Oxygen

The most important of signal promoting zonated enzyme expression is oxygen [50]. The average concentration of oxygen falls from 65mmHg to around 35mmHg between periportal and pericentral ends of the sinusoid [69]. Oxygen is required for ATP production via oxidative phosphorylation [50]. Studies have shown that the blood oxygen concentration at which cells begin to lose some of their ability to produce ATP is around 20-30mmHg [69]. One study calculates the half maximum oxygen uptake to be 14mmHg [93]. Although the average oxygen concentration remains above this across the sinusoid, there is a radial gradient in concentration from the centre of the sinusoid to the plasma membrane of cells. The actual oxygen concentration reaching the cells was on average was measured to be 25mmHg [94]. Therefore, as an approximation, we might expect the average concentration at

the cell surface to fall from 32.5mmHg at the periportal end to 17.5mmHg at the pericentral end across the sinusoid. It is, therefore, beneficial for hepatocytes near the hepatic artery to specialise in more ATP intensive processes, whilst pericentral cells should specialise in those the produce ATP without the requirement of oxygen.

In vitro experiments have demonstrated the importance of oxygen as a determinant of zonated enzyme expression. When cells are stored at higher oxygen concentration for 1-2 days in culture, it has been demonstrated that concentrations of PEPCK, an enzyme involved in gluconeogenesis, rise whilst concentrations of GK and PK, enzymes involved in glycolysis, fall [77]. It was also demonstrated that the rate of gluconeogenesis increases and the rate of glycolysis falls after pre-treatment increasing oxygen concentration (4->13% 02 in atmospheric gas) with the measurements being performed at equal oxygen concentrations. Furthermore, on a shorter time scale Nauck *et al.* showed that cells incubated in arterial oxygen concentrations show higher induction of PEPCK expression by glucagon than those incubated in venous oxygen concentrations [69]. It was also demonstrated that these increases results from increased synthesis rather than a change in the rate of degradation [45].

There is evidence to suggest that oxygen acts via reactive oxygen species (ROS), in particular hydrogen peroxide to provide a zonated phenotype [95]. Hydrogen peroxide is toxic substances created as a result of electron transfer in the oxidative phosphorylation chain. A smaller increase in expression of periportal enzyme PEPCK occurred as a result of increased oxygen concentrations when accompanied by an increase in catalase, the enzyme responsible for the conversion of the ROS hydrogen peroxide to water and oxygen [95]. Furthermore, it has been demonstrated that knocking out manganese superoxide dismutase, which catalyses the dismutation of superoxide to oxygen and hydrogen peroxide, leads to a loss of zonation [96].

1.2.2.2 Substrates and Products

There is evidence to suggest that zonated enzyme expression is linked with feeding state, most strongly in the enzymes mediating lipid metabolism (e.g. in lipogenesis [81, 88, 89] and β-oxidation

[81, 82]). Furthermore, it has been shown that in starvation, the prominent function of pericentral hepatocytes switches from glycolysis to gluconeogenesis [45, 97]. However, a full study of the effect of carbohydrates, lactate or fatty acids on enzyme expression has yet to be performed. Since oxygen and hormones are removed from the blood by hepatocytes across the sinusoid independent of feeding conditions, they are likely to provide stronger signal molecules for sustained zonation than metabolic substrates such as glucose which may be removed from or released into the blood by hepatocytes depending upon feeding conditions.

1.2.2.3 Hormones

The concentrations of insulin and glucagon are also thought to contribute to the development of zonation [45]. The rate at which insulin is removed across the sinusoid depends upon feeding state. Between meals the concentration falls by around 50% whilst postprandially only 15% of insulin is removed between periportal and pericentral sections [45]. The glucagon concentration meanwhile falls by around 50% independent of food intake [45]. As a result, a higher insulin to glucagon ratio is seen postprandially in pericentral than periportal cells consistent with their role in glucose uptake.

As discussed by Jungermann et al. [45], if enzyme synthesis was induced by absolute hormone concentration alone we would expect all enzymes to be upregulated in the periportal section due to the fall in concentration of both insulin and glucagon across the sinusoid. The induction of enzyme synthesis must instead either be dependent on the relative concentrations of hormones or dependent on a modulator formed as the blood passes through the sinusoid.

Some *in vitro* experiments suggest the former of these mechanisms. When hepatocytes are incubated with insulin alone, expression of GK increases [98]. However, when the cells are also incubated with glucagon, this induction is inhibited [98]. When hepatocytes are incubated with glucagon alone, expression of PEPCK is increased. In this case insulin and adenosine act as inhibitors [99-101]. It is therefore likely that the increasing insulin to glucagon ratio across the sinusoid is at least partially responsible for inducing the zonation enzyme expression. Furthermore, additional experiments have

looked at the overall gluconeogenic and glycolytic activity of cells incubated for 48 hours in varying quantities of either insulin or glucagon. In these experiments, incubation with insulin led to increased glycolysis whilst incubation with glucagon led to increased gluconeogenesis [77].

1.3 Liver Disease and Failure

In 2014, 11,597 people in the UK died of liver disease making it the fifth biggest cause of death and it is the only major cause of death to rise year by year [102]. Liver conditions can broadly be split into two categories, those which gradually increase in severity over time, known as chronic, and those in which severe symptoms suddenly arise, known as acute. A third category, where a sudden insult occurs in an individual with chronic liver disease is known as acute on chronic. This report focusses on NAFLD, a slowly developing chronic form of liver disease, and its interaction with IR.

1.3.1 Chronic Liver Disease

Chronic liver conditions occur when the liver experiences repeated damage over a long period of time. This repeated process of injury followed by regeneration leads to fibrosis, cirrhosis and problems stemming from the inflammatory response. There can be numerous causes of this such as alcohol and substance abuse, hepatitis B and C or NAFLD. If the condition persists until liver failure occurs, the only current proven treatment is transplant. Due to the limited availability of organ donors, the waiting list can be up to a year for low risk chronic patients (average 140-150 days [103, 104]). Between 1st April 2012 and 31st March 2013, only 52.7% of patients on the transplant list received transplants whilst 5.4% of patients the waiting list died [105]. The development of treatments to provide an alternative to transplant, and to prevent the progression from early to late stage liver disease is therefore crucial.

Numerous stages mark the progression of chronic liver disease. Steatosis, the build-up of excess fats occurs in the majority of liver diseases, including most notably NAFLD and excess alcohol consumption [106, 107]. Simple fatty liver alone is asymptomatic in the vast majority of patients but increases the probability of development of liver disease and cardiovascular disease [8, 106, 108].

Fibrosis is the development of excessive fibrous tissue (extracellular matrix proteins such as collagen), generally as a result of repeated damage and repair [109]. It is associated with a stiffening of the liver and can prevent blood flow to regions of the liver. Fibrosis is often accompanied by inflammation and liver cell ballooning, particularly in NAFLD and non-alcoholic steatohepatitis (NASH) [110].

Once sufficient fibrosis and cell death occurs such that the liver no longer functions properly, the condition is referred to as cirrhosis. The precise definition for the transition from fibrosis and cirrhosis is ill-defined. Liver failure causes fatigue, weakness, swelling in the lower legs, ascites (fluid build-up in the abdomen that often becomes infected), spider angiomas (spider-like blood vessels in the skin) and yellow skin due to defective bilirubin clearance [20]. Additionally, increased plasma concentrations of nitrogen and other molecules due to defective liver function cause damage and reduced function in the brain, known as hepatic encephalopathy [109]. This can results in confusion, coma and death [109].

1.3.2 Acute Liver Failure (ALF)

Acute liver failure (ALF) results from the rapid loss of a large number of liver cells (80-90% of total cell mass) and leads to the sudden onset of severe symptoms. The most common cause of ALF in developed countries is paracetamol poisoning whilst in the developing world it is hepatitis [111]. Other causes include a wide range of viral infections, extreme alcohol abuse, idiosyncratic reaction to medication and causes linked to pregnancy. If ALF occurs in a patient with a chronic liver condition that was previously stable, it is known as acute-on-chronic liver failure (ACLF) [112]. While a small number of patients (~20%) will recover from ALF spontaneously, this is not true of the majority, and the only effective existing treatment is transplant [113].

1.3.3 Diabetes, IR and the Metabolic Syndrome

1.3.3.1 Diabetes Mellitus

Diabetes mellitus is the name given to a group of conditions in which either disrupted insulin release or reduced insulin reception lead to hyperglycaemia. Since insulin promotes glucose uptake, problems

in its release or detection result in dangerously high blood glucose levels post-prandially. Additionally, the lack of glycogen storage can then result in hypoglycaemia and diabetic coma between meals. Standard tests for diagnosis of diabetes include a fasting blood glucose concentration of greater than 7mM or a concentration of greater than 11mM two hours after a 75g oral glucose tolerance test [114].

Diabetes mellitus can be split in to two categories; type 1 diabetes mellitus (or insulin-dependent diabetes mellitus) resulting from deficient insulin production by the pancreas and type 2 diabetes mellitus (T2DM or non-insulin-dependent diabetes mellitus) resulting from problems with insulin reception. Type 1 diabetes results from loss of pancreatic β-cells, often caused by infection in genetically susceptible individuals [115].

T2DM is largely associated with lifestyle factors such as obesity and lack of exercise as well as genetic susceptibility[116]. Sustained increased FFA, glucose and insulin concentrations cause damage to hepatic insulin reception leading to decreased glucose uptake. This triggers a feedback cycle in which increased plasma FFA and glucose concentrations cause to worsening insulin release causing further hyperglycaemia, hyperlipidaemia and hyperinsulinaemia.

As of 2014, 3.2 million people in the UK, 32 million people in Europe and 29.1 million people in the USA were estimated to suffer from T2DM. Additionally, the number of people showing signs of 'prediabetes' increased from 10% to 33% in the UK between 1996 and 2011, and from 79 million to 86 million in the USA between 2010 and 2012 [1-5].

1.3.3.2 Metabolic Syndrome

Metabolic syndrome is the name given to a broader range of conditions associated with dysfunction of energy, lipid and carbohydrate metabolism. It is associated with lifestyle as well as genetic factors and is strongly linked with the development of heart disease and T2DM. Criteria for diagnosing metabolic syndrome vary but generally patients are required to show three of the following 5 conditions with varying definitions of the severity required: obesity, diabetes or hyperglycaemia, hypertriglyceridaemia, reduced HDL-cholesterol and raised blood pressure [114, 117-120].

Prevalence of the metabolic syndrome is the U.S has been estimated to be as high as 34% [121]. If the disease is still in its early form, the major treatment is lifestyle change. Later interventions tend to focus on treatment of the individual conditions and some publications have questioned the usefulness of grouping the disorders under one name [122, 123].

1.3.4 NAFLD and NASH

NAFLD is the abnormal retention of lipids in liver in the absence of alcohol abuse, drug abuse or viral infection [8]. As of 2004, prevalence of NAFLD in the United States was around 34% [124-126]. Similarly as of 2014, 25-30% of the UK adult population were thought to suffer from the condition [6] (30-40% in men and 15-20% in women [8, 124]). These numbers continue to rise year on year, and there is considerable overlap with patients showing 'prediabetes', which increased from 10% to 33% between 1996 and 2011 in the UK [1-3]. It is also becoming the most common cause of liver disease amongst children [127].

As discussed below, NAFLD can progress to NASH which can result in fibrosis, cirrhosis and liver failure. It is estimated that 30-40% of NAFLD progresses to NASH [108], which is associated with development of fibrosis in 40-50% of patients [108], cirrhosis in 20% of patients and liver-related death in 12% [6, 7]. Even in the absence of cirrhosis, NASH is associated with hepatocellular carcinoma [8-11], cardiac diseases [12], chronic kidney disease [13] and a range of further conditions [8, 14]. A meta-analysis study has suggested that, depending on the severity of fibrosis, NASH increases the probability of liver related death 5-10 fold [12]. It has additionally been suggested that NASH may also be responsible for many cases in which cirrhosis occurs with unknown causes [128, 129]. In terms of population, it is thought that 2-5% of adults in the UK suffer from NASH [1, 12].

The risk of mortality to each individual suffering from NAFLD is comparatively low (one study suggested a 57% increase in mortality in NAFLD individuals relative to individuals without hepatic steatosis largely due to liver failure or cardiovascular disease [12]), and the majority of patients are asymptomatic. However, due the vast prevalence of the disease, it has been predicted that NAFLD will

become the major cause of liver transplant by 2030 [8]. Even as of 2009, NASH was the third biggest cause of liver transplant in the United States, accounting for 10% of total transplants [130].

1.3.4.1 Risk Factors

1.3.4.1.1 Insulin Resistance and T2DM

NAFLD is strongly linked with IR, the metabolic syndrome and T2DM [18, 131-134]. The presence of IR, the metabolic syndrome and T2DM all increase the risk of NAFLD [135-137], and the presence of NAFLD increases the risk of T2DM (section 1.3.4.2.2). Around 70% of T2DM sufferers show excess liver fat [8, 138].

IR leads to increased plasma FFA and triglyceride concentrations resulting in increased lipid uptake into hepatocytes [139, 140]. IR in liver and muscle cells causes deficient glycogen synthesis, increasing the glucose concentration as a substrate for lipogenesis [139, 141]. Even in insulin resistant patients, insulin stimulation of lipogenesis appears to remain intact, further increasing the production of fats from sugars (see chapter 3) [36-39]. Additionally, IR in adipose tissue prevents insulin stimulation of triglyceride synthesis and inhibition of lipolysis in these tissues. This results in fats stored in adipose tissue being broken down and released into the plasma FFAs, which can then enter liver cells [142, 143]. It has been shown that diabetic individuals are 3 times more likely to die of liver failure than non-diabetics [144], and it has been suggested this is predominantly due to the increase NAFLD prevalence [8]. It should be noted, however, that many individuals with NAFLD are neither diabetic nor obese, and understanding the condition across the range of patients is vital to developing effective therapies [145, 146].

1.3.4.1.2 Obesity and Exercise

Obesity is strongly linked with the development of NAFLD. Firstly, the amount of fat in the liver correlates with percentage fat mass and BMI [147-154]. In obese individuals, higher plasma FFA concentrations result in increased uptake of FFAs in liver and muscle [146, 155]. NAFLD is also linked with high calorie intake, particularly with a high fat content [6, 18, 133]. In addition to overall adipose

tissue mass, the type of adipose tissue in an individual affects their probability of developing NAFLD. Liver fat shows an even stronger correlation with visceral fat mass than overall adiposity [147-152]. Visceral adipose tissue is both more active and less insulin sensitive than subcutaneous adipose tissues and performs lipolysis and lipogenesis at faster rates [156-160]. This contributes to an increased plasma FFA concentration, redirecting fats to liver and muscle. Numerous studies have demonstrated that increased hepatic lipid supply arising from either dietary intake or adipose tissue contribute significantly to hepatic steatosis [155, 158, 161, 162].

Adipocytes in obese individuals additionally release inflammatory cytokines such as tumour necrosis factor alpha (TNFα) and interleukin-6 (IL-6) and show reduced adiponectin release [163-167]. Although the role of cytokines and hormones in NAFLD and NASH development is not yet fully understood, the suppression of adiponectin release in particular is thought to have an effect on liver and muscle fat, where TNFα and IL-6 have a largely paracrine effect (within the adipose tissue) [155, 161, 165].

Regular physical exercise shows a negative correlation with liver fat mass, although it is not known whether this results from reduced visceral adipose mass rather than a direct effect [153, 154, 168, 169]. However, it has been suggested that exercise may metabolise lipids in muscle cells and promote non-insulin dependent glucose uptake, reducing IR both in muscle and around the body independent of weight loss [155, 168-172]. Aerobic fitness and mitochondrial function have been shown to inversely correlate with liver fat percentage and prevalence of NAFLD [172-176].

1.3.4.1.3 Lipoatrophy:

Despite the strong link between visceral fat mass and hepatic steatosis, NAFLD has been shown to develop in a notable percentage of lean individuals [145]. In a study by Wong *et al*, fatty liver was shown to develop in 8% of the individuals whose BMI was below the overweight threshold (23kg/m) at both baseline and follow up [153]. Similarly, Xu *et al.* studied the incidence of NAFLD in non-obese Chinese individuals. At baseline, NAFLD was measured in 7.27% of 6905 individuals [177]. Of 5562 lean individuals who did not show signs of NAFLD at baseline, 8.8% had developed the condition after 5

years [177]. In the US, 11613 individuals who did not frequently consume alcohol were assessed for NAFLD and NASH. 431 of 4457 normal weight individuals were observed to suffer from NAFLD compared with 2061 of 7156 overweight or obese individuals [178].

NAFLD does show a strong correlation with obesity, but given that a sizeable number of lean individuals develop NAFLD whilst many obese individuals show healthy liver fat content, additional factors must be considered. It has been hypothesized that the underlying factor causing the development of NAFLD is the inability to store excess plasma lipids correctly within adipose tissue, rather than the presence of excess adiposity itself [146]. As discussed above, it is particularly increased mass of the less insulin sensitive visceral adipose tissue which correlates with NAFLD. Therefore, it may be an excess of this less insulin responsive adipose tissue that causes improper storage of plasma FFAs and a build-up of fats in other organs around the body such as liver and muscle. Consistent with this, lipoatrophic mice lacking adipose tissue develop hepatic steatosis and IR [179, 180]. Transplantation of white adipose tissue protects against these factors [180]. It has been shown that FATPs and CD36 (proteins involved in FA uptake) both show increased hepatic expression but reduced adipose expression in individuals with NAFLD, compared with individuals of the same weight group without fatty liver [146, 181, 182].

Reduced overall activity of proliferator-activated receptor gamma (PPARγ), a protein which promotes adipose FA uptake, leads to increased susceptibility to NAFLD [183] whilst liver specific knockout of the protein protects against excess liver fat [184, 185]. This is consistent with the idea that it is not just excess fat, but the incorrect storage of excess fat which cases NAFLD. It should be noted that lean NAFLD patients show higher mortality than obese NAFLD, and treatment options for resolving NAFLD across the range of patient weights must be developed [186].

1.3.4.1.4 Genetics

Genetic variability is involved in the progression of NAFLD in the susceptibility to the build-up of fats in liver, the development of fibrosis and the rate of progression to cirrhosis. A brief review of the role

of genetics in NAFLD susceptibility is provided here. For more information see recent reviews by Anstee *et al.* [187, 188] and Marzuillo et al. [189]. No single gene has been identified as mediating NAFLD risk alone, and instead inter-individual variability results from the combined effect of common polymorphisms identified by both genome-wide association studies (GWAS) and candidate gene studies [187, 188]. However, across a range of studies two genes have been repeatedly highlighted as strongly associated with NAFLD; patatin-like phospholipase domain-containing protein 3 (PNPLA3) and transmembrane 6 superfamily member 2 (TM6SF2) [187, 188].

The Met148Ile allele of (PNPLA3), which is prevalent in Hispanic populations [190], has been linked with the development of NAFLD and IR [187, 188, 191-193]. A second SNP in the same gene has also been implicated. The mechanism by which this polymorphism of PNPLA3 alters hepatic liver triglyceride levels is unknown and the gene is likely to have wide ranging functions [146, 155, 187, 188]. However, it is thought to play a role in fatty-acid selective hepatic triglyceride remodelling [194]. PNPLA3 SNPs are not only associated with altered liver triglyceride content but also severity of steatohepatitis and fibrosis.

A number of studies have shown an association between a TM6SF2 SNP and both hepatic triglyceride content and the development of fibrosis [187, 188]. As with PNPLA3, the role of TM6SF2 has yet to be fully elucidated. However, the current hypothesized role of TM6SF2 is in hepatic VLDL assembly, suggesting reduced removal of triglycerides from liver [189, 195].

In addition to these two genes, NAFLD is associated with a wide range of common polymorphisms with roles in insulin sensitivity, carbohydrate metabolism, lipid metabolism, alcohol metabolism, oxidative stress, inflammation and fibrosis amongst others [187, 188].

1.3.4.1.5 Hormones:

It has been suggested that imbalance of several hormones may play a role in the development of hepatic steatosis. Hyperinsulinaemia and IR are both involved in the development of fatty liver [196, 197]. Insulin largely stimulates lipogenesis in hepatocytes through the action of sterol-regulatory

element binding protein 1c (SREBP-1c), which mediates expression of numerous FA and triglyceride synthesis enzymes [155, 158, 198]. However, as discussed in chapter 3, a counterintuitive increase in SREBP-1c expression is seen in insulin resistant and steatotic livers suggesting that this pathway continues to contribute to *de novo* lipogenesis [36-39]. However, it has been shown that sustained supplementary provision of insulin in hyperinsulinaemic T2DM individuals lowers rather than raises liver fat content [199]. An additional protein to SREBP-1c in stimulating this lipogenesis is the carbohydrate response element-binding protein (ChREBP), which is activated by hyperglycaemia and has similar stimulatory effects to SREBP-1c. In mouse models of NAFLD, both SREBP-1c and ChREBP show increased activity [36-39, 200].

Plasma adiponectin concentration negatively correlates with liver fat and hepatic IR [152, 201-203] while polymorphisms in the adiponectin receptor gene have been linked to variation in both hepatic fat content and IR [30]. Despite being released by adipocytes, plasma adiponectin concentration negatively correlates with adipose tissue mass. Adiponectin promotes lipid oxidation in liver and skeletal muscle via AMP-activated protein kinase (AMPK), whilst decreasing the activity of ACC and FAS [167, 204-206]. This provides an additional link between hepatic fat content and obesity via plasma FFA concentrations [207]. The drug pioglitazone (a thiazolidinedione) has been shown to both increase circulating adiponectin and reduce hepatic fat content in NAFLD individuals, although this may have additional mechanisms of action beyond stimulating adiponectin release [208].

Leptin, also produced in fat tissue, may also play a role in reducing hepatic steatosis. Beyond its role in reducing appetite and food intake, the hormone is also thought to have direct effects on lipogenesis and lipid oxidation [155, 209]. However, the magnitude of these effects relative to those of other hormones such as insulin and adiponectin are currently not known.

1.3.4.2 Consequences of NAFLD

1.3.4.2.1 Progression to NASH, Fibrosis and Cirrhosis

Early stage NAFLD is generally diagnosed when the liver fat concentration is greater than 5% after alcohol abuse, drug abuse and viral infection have been rules out as causes, although a higher threshold of 5.6% has been suggested based on the 95th percentile [15, 210, 211]. Once steatohepatitis develops, the condition is referred to as NASH. NASH is diagnosed when the presence of inflammation and hepatocellular ballooning is detected in addition to steatosis [212]. Around 30-40% of NAFLD patients progress to NASH [108]. 40-50% of NASH patients develop fibrosis [108], 20% develop cirrhosis and liver-related death occurs in 12% [6, 7].

Since NAFLD and NASH are generally asymptomatic in their early stages, diagnosis of both conditions tends to be notably delayed relative to onset. In general, measurements of individual biochemical markers do not allow for an effective judgement of the severity of lipid build-up in an individual [213]. The most accurate method of assessing NAFLD/NASH severity is biopsy [213]. However, this is inherently invasive and is not recommended for asymptomatic, incidentally discovered NAFLD [213]. Instead liver fat content is often measured using non-invasive imaging techniques (e.g. [214-224]).

Hepatic steatosis may progress to inflammation and steatohepatitis through a number of mechanisms [155]. Increased oxidative stress is seen in humans with NASH [225], which has been suggested to stimulate an inflammatory responses and mitochondrial dysfunction [155, 165, 226]. It has been shown that increased lipid availability is associated with a reduction in insulin stimulated ATP synthesis in muscle in obese and non-obese individuals [227]. Similarly it has been shown that hepatic ATP synthesis is lower in T2DM individuals, who were also demonstrated to have high hepatic fat content, than controls [228]. It is therefore possible that the progression from NAFLD to NASH results from a combination of inflammatory responses, reduced mitochondrial function, mitochondrial stress and the build-up of ROS [229, 230].

Changes in the microflora of the gut may promote inflammation through an effect on liver macrophages, the Kupffer cells [155]. NAFLD patients are more likely than controls to show intestinal bacterial overgrowth [231, 232]. Gut bacterial overgrowth results in both ethanol and bacterial lipopolysaccharide production [233]. Both of these molecules stimulate the production of pro-inflammatory cytokine TNF-α in Kupffer cells [155, 234]. Furthermore, alterations to the microbiome of the gut have been shown to reduce liver inflammation [235-238].

1.3.4.2.2 IR and T2DM

As discussed, diabetic individuals are far more likely to suffer from NAFLD than metabolically normal individuals. Furthermore, it has been shown in a large number of studies that individuals with excess liver fat are more likely to develop hepatic IR, peripheral IR and T2DM [150, 214-224, 239-243]. A number of these studies have shown that increasing severity of pre-existing NAFLD increases this risk of T2DM development [8, 218, 221, 223, 224]. It has also been shown that risk of incident T2DM returns to baseline in individuals who had pre-existing fatty liver, but whose liver fat percentage returned to a healthy level over a 5 year trial [224]. Similarly, individuals whose liver fat percentage increased over the period showed an increased risk of incident T2DM development [224]. This demonstrates a clear benefit to NAFLD patients of reducing steatosis level. NASH patients are more likely to develop T2DM than NAFLD patients. In a study by Ekstedt *et al.*, over a 13.7-year period 71% of individuals who suffered from NASH at the start of the study went on to develop T2DM period compared with 46% of individuals who suffered from NAFLD (p=0.01) [108]. In this study, NAFLD and NASH score were assessed by biopsy rather than non-invasive imaging, allowing greater confidence in the measurements [108]. As well as hepatic IR, hepatic steatosis is also associated with whole-body IR independent of visceral fat mass [240, 244-246].

Although hepatic fat build-up, predominantly in the form of triglycerides, is associated with increased risk of T2DM and other conditions, triglycerides are generally considered to be a less potent form of fat in promoting progression to NASH and IR. Instead, the adverse effects are thought to arise due to

the FAs themselves (in particular palmitic acid) [247], ceramides [248] and diacylglycerides (DAGs) [8, 146]. It is thought that the protein kinase C (PKC) family of kinases enzymes play a key role in the development of IR as reviewed in Birkenfeld et al [146]. In particular, PKCε is highly expressed in liver. PKCε knockout mice are protected against IR when fed a high fat diet leading to steatosis [249]. There is some evidence to suggest that this may involve DAGs [8, 146]. In particular, DAGs in contact with the plasma membrane of hepatocytes, rather than in lipid droplets or endoplasmic reticulum [250]. DAGs are an intermediate in the sequential addition of three FAs to a glycerol backbone in triglyceride synthesis. In a liposyn (intravenous fat emulsion) plus heparin infusion rodent model, muscle IR developed and protein kinase C-θ (PKC θ) became active before any changes in triglyceride or ceramide concentration, but at roughly the same time as the DAG concentration increased [251]. Similar results are seen in liver, where hepatic IR develops after DAG concentrations begin to rise and is accompanied by activation of PKCε [252]. This was accompanied by reduced glycogen synthesis as a result of reduced activity of insulin receptor kinase. This hepatic IR was noted before the onset of IR elsewhere in peripheral tissues [252]. However, DAGs are not thought to be the solely responsible for the development of inflammation and IR, and a number of molecules both derived from FAs and the FAs themselves are likely to contribute [247, 248, 253-259].

The link between the development of hepatic IR in NAFLD and the subsequent development of peripheral IR has yet to be fully understood. However, numerous hepatokines may be involved including retinol binding factor protein 4, fetuin A, fibroblast growth factor 21 or markers of inflammation such as IL-6, TNFα or C-reactive protein [260].

1.3.4.2.3 NAFLD and Hepatocellular Carcinoma

Obesity and T2DM are strongly linked with the development of hepatocellular carcinoma [261]. Similarly, NASH, and possibly NAFLD, are linked to increased susceptibility to hepatocellular carcinoma [9-11, 262]. This may occur as a result of the inflammation and metabolic stress common to both NASH

and T2DM patients. Furthermore, changes in the microbiota have been suggested as playing a potential role (discussed in [8]).

1.3.4.2.4 NAFLD and Cardiovascular Disease

It have been demonstrated that individuals with excess liver fat, with or without diabetes, are at greater risk of cardiovascular disease after other CVD factors have been accounted for [263-274]. Consistent with this, a meta-analysis of several cross-sectional studies showed an increase in several markers of atherosclerosis in individuals of NAFLD independent of other CVD risk factors [275]. As reviewed in Byrne *et al.* ([8]-table 2) around 20 retrospective and prospective studies show an overall trend of increased CVD risk in individuals suffering from NAFLD and NASH. In particular, the studies in which NAFLD presence and severity were assessed by biopsy rather than non-invasive imaging demonstrate an increase in risk of mortality resulting from both CVD and liver failure (along with overall mortality) in individuals with NAFLD [108, 276-281]. The presence of fibrosis has been highlighted as a particular determinant of risk of mortality [8].

Non-obese non-diabetic and diabetic adults with NAFLD have been shown to suffer from a higher risk of disturbed myocardial energy metabolism, cardiac steatosis, myocardial IR and (in most but not all studies) left ventricular diastolic dysfunction [282-290] than adults without excess liver fat. Additionally recent studies have suggested an association exists between NAFLD and both cardiac arrhythmias [291-296] and aortic valve sclerosis [289, 297-299] independent of other known risk factors (reviewed in [8]).

The mechanism linking NAFLD and CVD has yet to be fully established. Although it has yet to be conclusively shown that NAFLD is causative in the development of CVD rather than simply a marker, based on the strength and consistency of the data it is generally considered that this is the case [8]. It has also yet to be demonstrated that reducing hepatic liver fat content results in a reduced risk of CVD in individuals with pre-existing NAFLD.

1.3.4.2.5 NAFLD and Chronic Kidney Disease

Excess liver fat is additionally associated with increased prevalence of chronic kidney disease (CKD) in both diabetic and non-diabetic individuals [13, 300-313]. Furthermore, increased severity of NAFLD is associated with increased severity of CKD [306-309]. As with CVD, a causative link between NAFLD and CKD has yet to be demonstrated, and it has not yet been investigated whether improvement in hepatic lipid levels results in an improvement in either incident CKD risk or severity of pre-existing CKD. As a result, further large-scale studies with long follow-up periods are required to investigate these links.

1.3.5 Current Treatment of NAFLD

Despite the vast prevalence of NAFLD and the large number of deaths and liver transplants associated with it, as of 2016, there is no approved drug for the treatment of NAFLD or NASH [314]. Historically, liver fat was considered to be benign and large scale population studies (reviewed above) were required to demonstrate that excess liver fat (both in diabetic and non-diabetic individuals) is associated with an increase in risk of both liver failure-related and overall mortality. As discussed by Ratziu *et al.* [314], NAFLD has also often been considered a complication of diabetes and therefore would be treated by anti-diabetic drugs. However, metformin, sulfamides and insulin are ineffective in treating NASH [314] and, although diabetes greatly increases the risk of NAFLD, many individuals with excess liver fat are not diabetic. At present the only effective methods of treating NAFLD are improvement in diet and increased exercise. However, obese patients requiring treatment for NAFLD and NASH often have a long history of failed attempts at changes in diet and exercise such that the resources and expertise required to ensure successful sustained weight loss and increased exercise are often not feasible [314-316]. Additionally, as discussed in section 1.3.4.1.3, a significant proportion of NAFLD sufferers are neither obese nor diabetic. As reviewed below (and in detail by Ratziu *et al.* [314]), some potential drug target pathways have shown the potential to reduce hepatic damage in mouse models of insulin resistant NAFLD. However, when tested in humans these have been ineffective. These include anti-TNFα, PDE4 inhibitors, selective caspase inhibitors, resveratrol and omega 3 FA preparations [304, 317-320].

1.3.5.1 Dietary and Lifestyle Change

1.3.5.1.1 Physical exercise

Exercise has been shown to reduce hepatic fat content even in the absence of overall weight loss [321], although the effects on fibrosis and cirrhosis in later stage NASH have yet to be fully explored. Exercise also has known effects on IR, T2DM and hypertension [322, 323]. People who regularly exercise are less likely to develop NASH and NASH-derived fibrosis [322, 324].

Type and duration of exercise are also important, with cardiovascular exercise more effective than walking [322, 324]. Particular benefits have also been noted for resistance training [325, 326] despite no overall change in weight and adipose distribution [326]. It is thought this may result from the removal of fats from muscle and liver, where they are known to promote IR. Finally, minimising sedentary time has been shown to improve insulin sensitivity [327, 328].

However, NAFLD is associated with fatigue such that compliance with increased exercise plans can be low [314]. Furthermore, many individuals are unable to put additional stress on their cardiorespiratory system [148, 314, 325].

1.3.5.1.2 Dietary changes and weight loss

Given that NAFLD is strongly linked with obesity, excess calorie intake and over/under consumption of specific foods, it is unsurprising that dietary change has been demonstrated to provide an improvement in severity of NASH. In a randomised control trial (RCT), intensive lifestyle intervention was shown to be a significantly more effective treatment for NASH patients than standard education on how to lead a healthy lifestyle (67% resolution vs 20%; p=0.02) [329]. Additionally, it was demonstrated that, in either group, a 7% loss of weight correlates with an improvement in physiological score. A second RCT, conducted in diabetic individuals, also showed improvements in hepatic fat content as measured by non-invasive imaging after dietary intervention and exercise [330]. Peterson *et al.* demonstrated that small amounts of weight loss are associated with an improvement in insulin sensitivity and reduction in liver fat [239]. Another study by Suzuki *et al.* showed that weight

loss is associated with a reduced plasma alanine aminotransferase (ALT) concentration, a marker of liver injury [154].

Substantial weight loss following bariatric surgery is associated with improvements in liver steatosis, fibrosis and even cirrhosis in morbidly obese individuals [165, 331-333]. Reductions in pro-inflammatory molecules released from adipose tissue have also been demonstrated on weight loss [165, 334].

Some data exists to suggest that the dietary composition, rather than solely caloric intake, is important in the development of NAFLD. Firstly, it is thought that a diet containing higher amounts of polyunsaturated and monounsaturated FAs can improve hepatic steatosis in the absence of weight loss [335]. A number of studies have suggested that increased fructose intake is linked with increased liver fat and hepatic *de novo* lipogenesis [336-339]. However, other studies have suggested that fructose is no more damaging than alternative sugars [340-343]. High intake of saturated fats, cholesterol and meat are common amongst NAFLD patients along with low intake of vitamins and omega-3 FAs [314, 344-347]. Some trials have investigated the impact of omega-3 FA supplements and of L-carnitine supplements on NAFLD with variable results in both cases (reviewed in Ratziu et al. [348]).

1.3.5.1.3 Problems with lifestyle change as a therapy

It is clear that both weight lost and increased exercise (even in the absence of weight loss) are beneficial both in preventing the development of NAFLD. However, the major problem with lifestyle change as a treatment is the known low-compliance of individuals, even when incentivised in clinical trials [314-316, 349]. Increasing this compliance rate would require considerable resources unfeasible for most hepatology centres [314, 316]. As a result, given the increasing prevalence of NAFLD and its cost to health services, alternative therapies must be considered.

1.3.5.2 Pharmacological Intervention

As discussed, no approved drug exists for NAFLD or NASH. When considering NAFLD, any pharmacological treatment should focus on removing the lipids from the liver. When considering NASH, it may also be desirable for a pharmacological intervention to have anti-fibrotic effects. However, sustained removal of excess fats from liver cells alone is likely to lead to an improvement of fibrosis. A drug focussed purely on reducing fibrosis without removing steatosis may lead to some short-term improvements in liver histology, but would not remove the fundamental cause of fibrogenesis.

The largest scale trial to be performed for a NAFLD/NASH drug so far tested the effects of pioglitazone and vitamin E over 96 weeks in 247 individuals without diabetes [350]. Pioglitazone (a thiazolidinedione) is an insulin sensitizers which act primarily on adipose tissue [351]. Thiazolidinediones promote expansion of insulin sensitive adipose mass which, despite causing weight gain, also directs fats away from tissues such as liver muscle and heart where they are known to cause most damage [351-354]. Thiazolidinediones also promote adiponectin release which stimulates β-oxidation in liver and muscle [206, 355]. Vitamin E, meanwhile, is an antioxidant, reducing the production of ROS during β-oxidation and preventing the resulting mitochondrial toxicity as well as blocking apoptotic pathways [356-358].

Pioglitazone treatment caused a higher rate of improvement of NASH (34% vs 19% resolution; p=0.04), reduced ALT and (aspartate aminotransferase) AST, improved lobular inflammation and steatosis, partially improved IR but failed to cause an improvement in fibrosis score compared to placebo [350]. As would be expected from the drug's action on adipocytes, weight gain was also seen with pioglitazone compared with placebo [350]. Similar results have been reported in two smaller trials [359-361].

Unfortunately however, side effects have been noted with pioglitazone use. Firstly, the increased adipose proliferation and weight gain is undesirable, particularly since this often remains after an

individual ceases to take the drug [314, 362]. Pioglitazone is not available in parts of Europe due to concerns that it may raise the risk of bladder cancer, although this was not seen in large scale studies [361, 363, 364]. An increase in the rate of bone fractures in the hands, feet and upper arms of women has been noted for the drug. An additional major concern of pioglitazone as a treatment is that the benefits of Pioglitazone use on steatohepatitis, insulin sensitivity (HOMA) and liver damage (ALT) do not remain after termination of the treatment [365].

Vitamin E also cause an increase in the rate of resolution of NASH (46% vs 19%), improvements in ALT and AST, improvements in lobular inflammation and hepatic steatosis relative to placebo but no significant improvement in fibrosis score. No significant difference in weight gain was seen between the placebo and vitamin E groups. Additionally, in a paediatric trial vitamin E caused an improvement in resolution of NASH compared with placebo (58% vs 28%) but did not improve steatosis, fibrosis, inflammation of ALT [362]. In this case vitamin E, therefore, reduced the hepatic damage caused by NAFLD but did not remove the underlying cause itself [362].

It should be noted that the positive findings in these two studies are countered by alternative studies demonstrating no benefit from vitamin E consumption [366]. It has therefore yet to be fully proven that vitamin E has a positive effect on NAFLD [348]. Furthermore, fairly severe negative side effects of vitamin E consumption have been suggested in the literature including increased overall risk of mortality [367], increased risk of stroke [368] and increased risk of prostate cancer in over 50 year olds [369]. There are also concerns that at high doses vitamin E may act as a pro-oxidant [370].

An additional insulin sensitizer tested for use in NAFLD/NASH treatment is metformin. Metformin is a biguanide used in the treatment of T2DM due to its action in suppressing hepatic gluconeogenesis [371]. However, it has been demonstrated to have little effect on hepatic steatosis and NASH [213] (for review see Ratziu *et al.* [348]). Similarly there is no data to suggest that statins, commonly prescribed to reduce low density lipoprotein (LDL)-cholesterol levels, are beneficial to NAFLD/NASH other than a possible slight reduction in steatosis [213, 348, 372].

Some data exists to suggest that bile acids, and particularly Ursodeoxycholic acid (UDCA) may be effective in treating NAFLD. However, in relatively small scale trials, treatment with UDCA has shown variable results [348]. UDCA, therefore, requires a large-scale, well designed RCT to assess its impact in NAFLD and NASH.

Obeticholic acid, a farnesoid X receptor agonists, has recently been tested in a clinical trial involving 283 NASH patients [373]. It was associated with improvement in histological features of NASH, but its long-term efficacy and safety as a treatment require further study [373]. Additionally, synthetic farnesoid X receptor agonists aiming to mimic the effects of bile acids are in development [213].

Pentoxifylline, a phosphodiesterase inhibitor, has been shown to have a beneficial effect on NASH in animal models [374]. Additionally, in a small RCT, pentoxifylline was demonstrated to improve histological features of NASH, steatosis and NAS score. [375]. However, a large-scale human trial is still lacking [348].

Recent review papers have addressed treatment currently in development for NAFLD [314, 376].

1.3.6 Zonated Damage in NAFLD

Numerous studies have reported that pericentral cells tend to be most susceptible to triglyceride build-up in both NAFLD and alcoholic fatty liver disease (AFLD) [15-17]. Additionally, the inflammation and fibrosis tend to be more severe towards the pericentral end of the sinusoid [15-17, 377-379].

Although pericentral centred steatosis is widely reported in NAFLD, the causes of the zonation in fat build-up are not fully understood, and this forms the focus of the simulations run in chapter 3. Since pericentral cells show higher rates of in insulin stimulated lipogenesis whilst periportal cells show higher rates of FFA uptake, periportal-centred steatosis might be expected in NAFLD given the context of insulin resistance and increased plasma FFA levels. However, it is thought that insulin may continue to stimulate lipogenesis through transcription factor SREBP-1c despite insulin resistance in the rest of metabolism (discussed in more detail in chapter 3) [36-39, 380, 381]. Alternatively, it has been

suggested pericentral cells may retain insulin sensitivity after periportal cells become IR [380]. However, a complete explanation of the heterogeneous development of steatosis across the sinusoid has yet to be presented in the literature.

After development of steatosis, numerous factors are thought to contribute to the pericentral-centred hepatic damage. Firstly, enhanced lipid peroxidation, a marker of oxidative stress, is seen in the pericentral compartment [225, 382]. Secondly disruptions to energy metabolism are more severe in pericentral cells [229, 230]. Finally, direct lipotoxicity resulting from the increased concentration of FFAs may contribute to the higher cellular damage in pericentral cells [8, 146, 247, 248].

1.4 Existing Mathematical Models of Liver Processes Including Zonation

Previous computational models of glucose homeostasis and liver energy metabolism have varied from those studying liver metabolism within the body as a whole to those focussed in detail on the regulation of specific enzymes depending upon the particular purpose of the study. For example, Kim *et al.* [383] and Xu *et al.* [384] developed whole body models to study the hormonal regulation of glucose homeostasis during exercise (Kim *et al.* [383]) and under varying feeding conditions (Xu *et al.* [384]), whilst Liu *et al.* [385] developed a model focussed in detail on the GLUT proteins responsible for glucose uptake and output. Additionally, representations of glucose regulation vary from black box models, for example with the purpose of calculating optimal insulin input for insulin responsive diabetic patients [386], to mechanistic models aiming to understand the metabolic changes occurring in disease in detail [387-392]. Of these mechanistic models, the vast majority of existing models of the liver are single hepatic compartment models, and zonation in the context of hepatic energy metabolism has yet to be addressed.

Numerous models of glucose regulation and other processes in liver have been presented since as early as 1965 [386]. As a result, the following review will focus on key recent mechanistic models. For a more detailed discussion of liver metabolism and diabetes modelling, see the reviews of Bogle *et al.*

and Balakrishnan *et al.* [386, 393] and for a detailed discussion of the application of systems biology techniques to NAFLD see the review of Fisher et al. [394].

Most recently, Somvanshi *et al.* published a detailed single compartment model of glucose, lipid and amino acid metabolism, including regulation at both a signalling and transcription level [387]. This model, which incorporated a number of previously published sub-models, was used to understand the effects of varying dietary compositions on metabolism. König *et al.* developed a detailed model of enzymatic conversions in glucose homeostasis including much of the allosteric regulation known to occur in glucose regulation [388]. This model (a set of ordinary differential equations with 49 localised metabolites and 36 reactions) included all of the enzymatic conversions involved in gluconeogenesis and glycolysis, with separate cytoplasmic and mitochondrial compartments within hepatocytes. Hetherington *et al.* developed a composite model of hormone signalling in glycogen storage, comprising of established and *ab initio* developed sub-models [389]. This was used to understand key features of insulin signalling including ultradian oscillations [389, 390]. Chalhoub *et al.* developed a single hepatic compartment model focussing on gluconeogenesis and lipid metabolism in the hepatocyte [391]. The model was adapted to give results corresponding to the liver in either *in vivo* or in an *ex vivo* perfusion system to allow comparison with different experimental data. It was then used to simulate concentrations of various molecules and fluxes of different reactions in response to changes in the composition of the perfusion medium. Calvetti *et al.* developed a sophisticated spatially distributed model of glucose regulation in liver [392]. This used a set of grid points to measure fluxes of various molecules. However, despite the inclusion of spatial distribution, this model did not include zonation in enzyme expression.

Whilst single compartment, homogenous hepatocyte models are useful for studying the function of liver as a whole, they do not allow simulation of changes within specific regions of the sinusoid, and exclude the implications of zonation in disease progression. Only a few models have included a representation of hepatic zonation in enzyme expression, and none of these have focused on liver

energy metabolism. Ohno *et al.* investigated heterogeneity in ammonia detoxification [395]. They set up a model in which substances enter the sinusoids from the periportal tract, pass through 8 compartments (hepatocytes) in series, before exiting the sinusoid in the central vein. The model was tested with homogenous enzyme expression in all compartments and with zonated expression of carbonyl phosphate synthase, glutamine synthase and ornithine aminotransferase to understand the roles of zonated enzyme expression. Anissimov *et al.* created a similar model with 8 compartments to study hepatic availability and clearance [396]. A model by Sheikh-Bahaei *et al.* also studied hepatic zonation xenobiotic toxicity focussing on the development of zonation in key enzymes, rather than the effects of this zonation on metabolite concentrations [397]. Pang et al. looked at the various different ways of modelling heterogeneity for studying pharmacokinetics, starting with a simple compartmental PBPK model, followed by a zonal model and moving on to more complex circulatory and fractal models [398]. The compartmental and zonal models were compared with clinical data for digoxin and estradiol 17β D-glucuronide ($E_2$17G). For digoxin, the zonal model provided little improvement over the compartmental model. However, for $E_2$17G results improved significantly if Sult1e1 was expressed heterogeneously, suggesting that zonation is a more important for some drugs than others.

Other than this, models have been developed including zonation of closely related non-liver metabolism. König *et al.* published a model of glucose metabolism in cancer cells including localized gradients in metabolites and oxygen and regional hypoxia across a tumour [399]. Although this is for metabolism in cancer cells rather than liver, many similarities are seen including increased glycolysis and reduced oxidative phosphorylation in the most hypoxic cells. Davidson *et al.* studied the development of zonation within a bioartificial device [400]. This study did not model the metabolism in cells but instead focused on optimisation of oxygen input, blood flow and the dimensions of the device to try set-up a liver-like gradient in oxygen expression across the cells to promote a zonated phenotype.

1.5 Conclusions of Chapter

From the review presented in this chapter, it is clear that an understanding of the role of zonation within NAFLD is both important and currently missing. A description of the metabolic changes across the sinusoid leading to steatosis and damage centred focussed on pericentral cells has yet to be presented in the literature. This is vital for understanding the progression of the disease. Furthermore, as discussed above, no pharmacological treatment for NAFLD has yet to be approved. One confounding factor is that studies investigating the effects of pharmacological treatments tend to study the changes in the liver as a whole by investigating changes within homogenised tissue, rather than within individual hepatocyte groups. If a treatment disrupts energy production in a subset of hepatocytes, this may not be seen in preliminary studies but could adversely affect patients over time.

The role of zonation in NAFLD has largely been neglected because studying the effects of disease in individual regions of the sinusoid experimentally is time consuming and costly, especially given the vast number of variables when considering metabolism. However, integrating existing knowledge about hepatocyte heterogeneity into a computational model of metabolism across the sinusoid and using this to simulate NAFLD development and treatment would allow rapid analysis of changes in metabolic fluxes and metabolite concentrations under these conditions. These model simulations would then allow for more targeted experimentation, focusing on key predictions. Despite modelling of glucose metabolism having been performed for 50 years, a suitable model representing zonation in glucose, lipid and ATP metabolisms across the sinusoid is not available in the literature.

It is these gaps in our understanding of NAFLD and in the tools required for studying zonation in NAFLD that this study aimed to address according to the aims listed at the start of the chapter.

2 Model Development

2.1 Introduction to Chapter

In this chapter, the development of a computational model of hepatic glucose and lipid metabolisms capable of representing zonation is discussed in detail. The equations representing each conversion are presented along with the experimental data used to determine the forms of the equations and to set parameter values. In supplementary material S1, comparison of model simulations with experimental data are provided under a range of conditions including simulations for metabolically normal and insulin resistant individuals. In chapter 3 additional validation of the model simulations focussed specifically on representing NAFLD is provided. Several sections of this chapter were published in the supplementary material of Ashworth *et al.* [401].

2.2 Model Building

2.2.1 Model Structure, Blood Flow

The first aim of this study was to build a computational model of glucose and lipid metabolisms capable of representing the zone-specific changes occurring under conditions of IR and NAFLD. In order to include zonation, a computational model of liver function must firstly be able to represent the changes in concentrations of metabolites and hormones occurring as blood passes through the sinusoid. Secondly, it must include the variation in enzyme expression between hepatocytes dependent upon their position along the sinusoid. Conventional two compartment (blood/hepatocyte) models, which treat the hepatocyte as the repeating unit of the liver, are unable to include these features. Instead, following the structure suggested by Ohno *et al.* in a model of hepatic xenobiotic metabolism, we treat the porto-central axis of the sinusoid as the repeating unit [395]. The blood and surrounding hepatocytes in the sinusoid are split into compartments according to their position along this axis (proximal periportal -> distal pericentral) (figure 2.1).

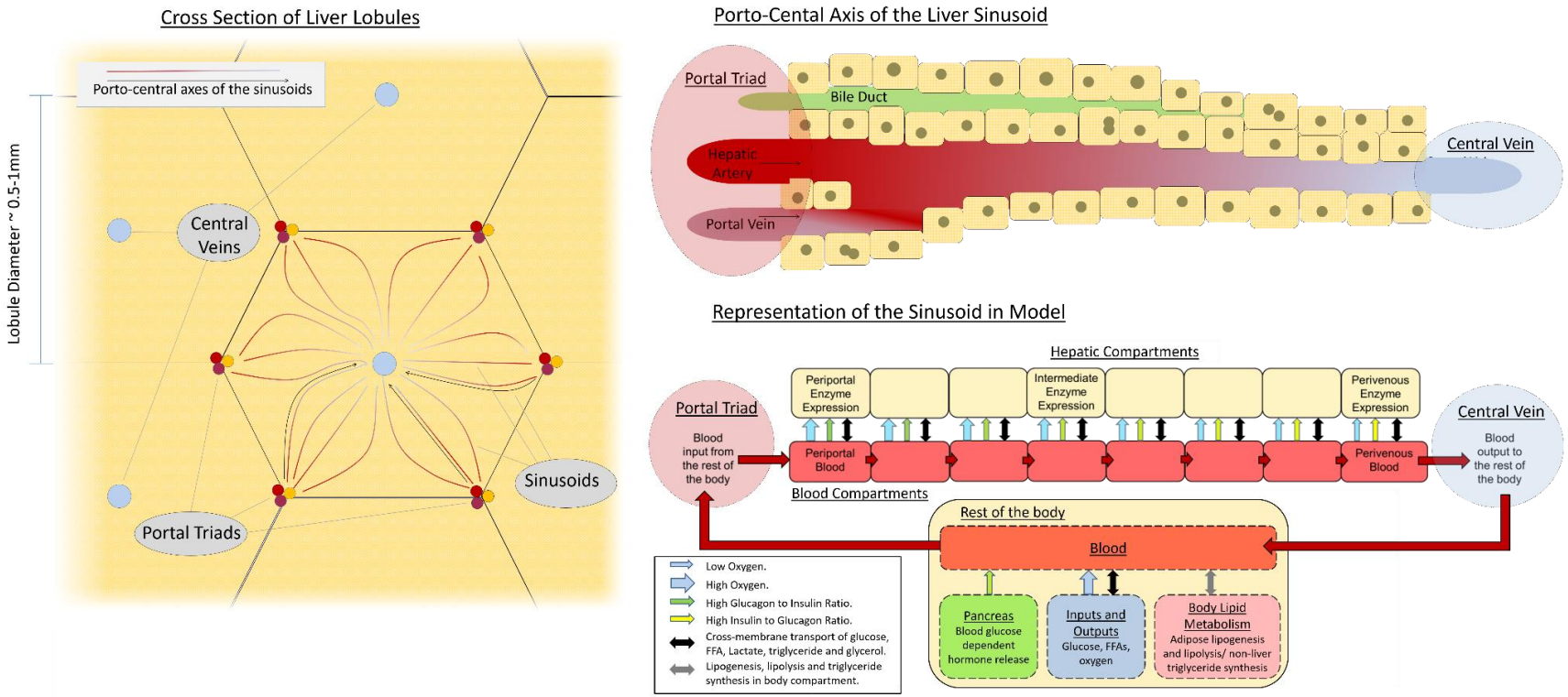

Figure 2.1 – The structure of the model. *The porto-central axis of the sinusoid is treated as the repeating unit of the liver. Cells and blood are compartmentalized into groups according to their position along the liver sinusoid. This allows the model to include changes in blood oxygenation, hormone concentrations and substrate and product concentrations across the sinusoid as well as differences in hepatic enzyme expression between compartments. Blood exits the sinusoid into a larger compartment representing the rest of the body. Blood in this compartment interacts with the pancreas, lungs and adipose tissue. Glucose and FFA inputs and consumption also occur in this compartment. Modified from diagrams in Ashworth et al. [402] and Ashworth et al. [401].*

Since blood is compartmentalized with average concentrations of variables in each compartment, rather than represented as a continuous change in plasma concentrations, a simplified representation of blood flow was used. In each time step, a proportion of the blood in each compartment moves to the subsequent compartment and is replaced by blood from the previous compartment. The plasma concentration of each metabolite or hormone (M) in each compartment changes according to the following equations.

$$\frac{dM_{i=1:n}}{dt} = bf * M_{i-1} - bf * M_i = bf * (M_{i-1} - M_i)$$

$$\frac{dM_0}{dt} = \frac{bf * (M_4 - M_0)}{s}$$

Rate of blood flow: $bf = 0.15 * n\ s^{-1}$ *-> (*$bf = 1.2s^{-1}$ *for the 8 compartments used in this report.)*

Rest of body to hepatic compartment ratio: $s = 5 * n$ *-> (*$s = 40$ *for the 8 compartments used in this report.)*

Compartments $i = 1 \rightarrow n$ correspond to the proximal periportal to distal pericentral sinusoidal compartments while compartment $i = 0$ is the body compartment. n is the number of hepatic compartments set to 8 for the simulations throughout this report (motivated below). The constant s is included since the body compartment is much larger than each liver compartment. The blood flow and relative size of the hepatic and body compartments were set such that blood takes around a minute to make a circuit of the body and so that the liver blood volume is equal to roughly 0.8L with a total blood volume of 5L [20, 403-405].

When building the model, simulations were run for both metabolically normal and insulin resistant individuals with varying compartment numbers to assess for an appropriate number to use. The number of compartments was increased from 3 (the minimum allowing separation of periportal, intermediate and pericentral zones) to well beyond the number after which no further qualitative changes in simulated data across the sinusoid (such as the appearance of missing maxima or minima) were seen when adding further compartments. Up to 48 were simulated, which is additionally several times larger than the actual number of hepatocytes per sinusoid (~10-13).

On the basis this preliminary data, 8 compartments were chosen for the simulations in this report since no under-sampling effects were noted when comparing with higher compartment numbers and because 8 compartments allows simple comparison with experimental studies which tend to split the sinusoid into 2-4 zones, up to a maximum of 8 (e.g. [406]). This is also consistent with previous computational models of zonation in liver [395, 396].

Blood flows from the periportal to the pericentral end of the sinusoid. After leaving the distal pericentral compartment, it enters a larger body compartment where it interacts with simple representations of the pancreas (hormone input), adipose tissue (FFA and triglyceride regulation) and with glucose and FFA inputs/outputs in the rest of the body (figure 2.1). The model simulates an individual at rest and does not include the blood flow, blood oxygenation and hormonal changes occurring during exercise.

Although this representation of the sinusoid allows inclusion of zonated enzyme expression, it remains a simplification. Several sinusoids extend between each portal triad and central vein following indirect paths through the cells, and the number of cells fed by each sinusoid will vary. Due to the hexagonal shape of the lobule, each sinusoid is likely to be supplying a larger number of cells nearer the portal triad than the central vein. Additionally, given that the oxygen concentration is the primary signal molecule promoting zonated expression [50], cells further from the capillary (but in the outer periportal region of the lobule) are likely to show more pericentral expression than those neighbouring the capillary. Therefore, there is scope for development of models to refine predictions in the future by representing distributed effects across 2D and 3D representations of the lobule.

2.2.2 Modelling and Parameterisation Strategy

2.2.2.1 Representation of Processes in the Model

Conversions are represented by Hill function dependences on the substrates and allosteric activators and inhibitors with a hormone dependent rate constant.

$$v = \frac{V_{max}[S]^{n_{Hill}}}{{K_M}^{n_{Hill}} + [S]^{n_{Hill}}}$$

Where K_M(mM) determines the substrate concentration at which enzymes are saturated, V_{max}(s^{-1}) is the maximum rate and n_{Hill} quantifies deviation from Michaelis-Menten behaviour. This form is based on Michaelis-Menten kinetics, a common method of representing enzymatic conversions. Michaelis-Menten kinetics are applicable to a reaction in which a substrate, S, reversibly binds to an enzyme, E, to form a complex, SE, before this complex then undergoes an irreversible reaction to form the product, P, as long as certain assumptions are met.

$$S + E \underset{\rightarrow k^+}{\overset{\leftarrow k^-}{}} SE \rightarrow^{k^{cat}} P + E$$

Defining $[x]$ as the concentration of x.

$$\frac{d[S]}{dt} = k^+[S][E] - k^-[SE]$$

$$\frac{d[SE]}{dt} = k^-[SE] - k^+[S][E] - k^{cat}[SE]$$

$$\frac{d[P]}{dt} = k^{cat}[SE]$$

One of the assumptions required for the derivation is that the substrate is in instantaneous chemical equilibrium with the substrate such that:

$$k^+[S][E] = k^-[SE]$$

The free enzyme concentration relative to the total enzyme concentration, $[E]_0$, can be calculated as:

$$[E] = [E]_0 - [SE]$$

Putting the previous three equations and rearranging gives:

$$v = \frac{d[P]}{dt} = k^{cat}[SE] = \frac{k^{cat}[E]_0[S]}{\frac{k^-}{k^+} + S}$$

$$v = \frac{V_{max}[S]}{K_M + [S]}$$

Where $V_{max} = k^{cat}[E]_0$ is the maximum rate of the process and K_M is the Michaelis-Menten constant which determines the saturation of the reaction with increasing substrate concentration. The

dependence of the reaction rate of the substrate concentration for an example reaction in which V_{max}=2s^{-1} and K_M=0.5mM is shown below.

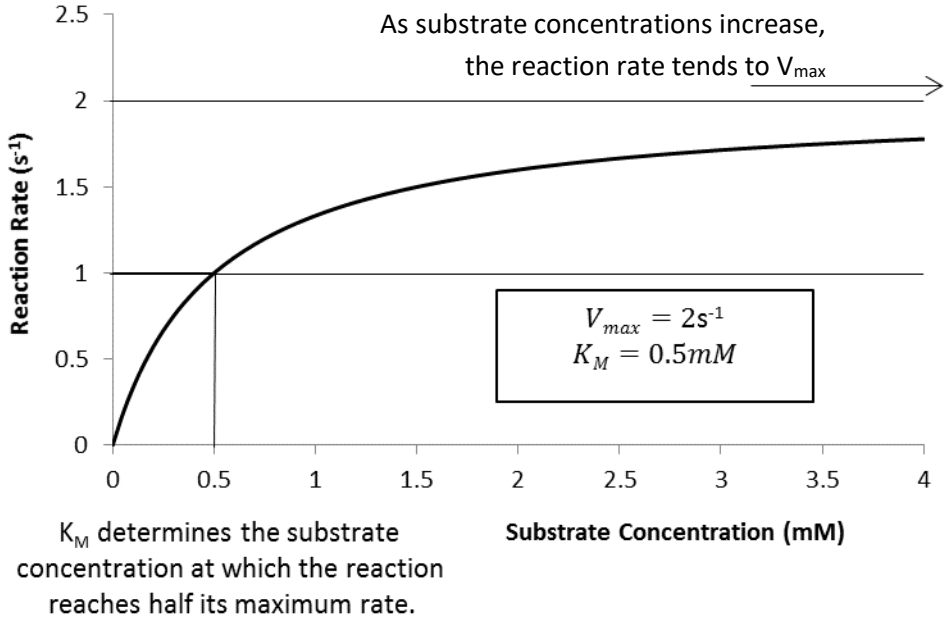

Hill coefficients, n_{Hill}, are used to represent conversions which deviate from the Michaelis-Menten assumptions. Higher Hill coefficients cause a more rapid increase towards the maximum reaction rate with increasing substrate concentration, but do not alter the maximum rate or the substrate concentration at which half maximum rate is reached. The change in the reaction rate vs substrate curve when n_{Hill}=2 compared with n_{Hill}=1 is shown.

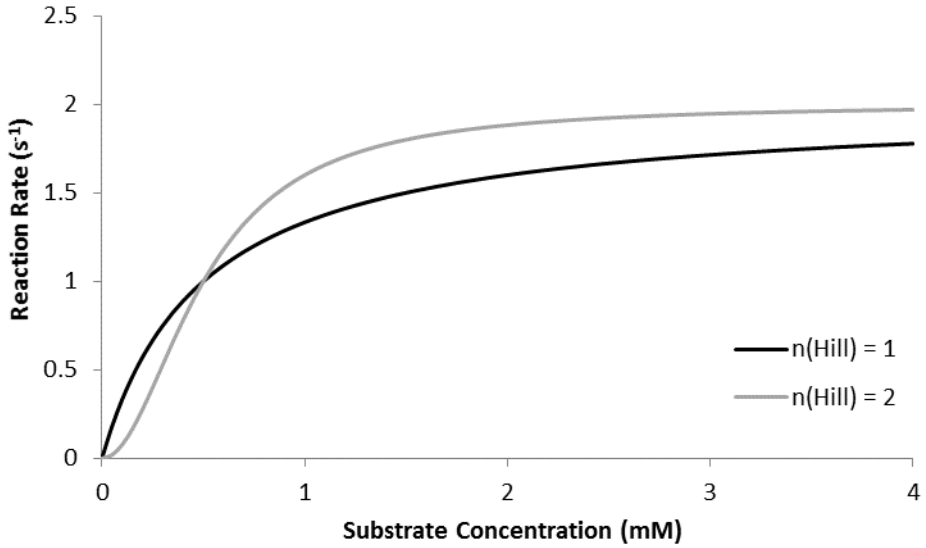

Many of the equations correspond to processes with a number of intermediate enzymes rather than a single enzyme. In these cases, Hill functions are still used to represent the substrate dependence of these processes, with K_M, and where applicable n_{Hill}, values based on the literature for the rate limiting enzyme in the process or estimated through fitting to experimental data.

Multiple substrates are represented in the model by multiplying the Hill function substrate dependences. E.g. for three substrate S1, S2 and S3.

$$v = \frac{V_{max}[S2]^{n_{S1}}}{{K_M^{S1}}^{n_{S1}} + [S1]^{n_{S1}}} * \frac{[S2]^{n_{S2}}}{{K_M^{S2}}^{n_{S2}} + [S2]^{n_{S2}}} * \frac{[S3]^{n_{S3}}}{{K_M^{S3}}^{n_{S3}} + [S2]^{n_{S3}}}$$

Allosteric inhibition and activation are represented using a similar dependence on the inhibiting or activating molecule with inhibition or activation constants taken from the literature. E.g. for an inhibitory molecule, i, with concentration $[i]$:

$$v = \frac{V_{max}[S]^{n_{Hill}}}{{K_M}^{n_{Hill}} + [S]^{n_{Hill}}}\left(1 - \propto_{inh} \frac{[i]^{n_{inh}}}{{K_i}^{n_{inh}} + [i]^{n_{inh}}}\right)$$

Where $\propto_{inh} \leq 1$ determines the maximum inhibition by i, ${K_i}^{n_{inh}}$ determines the concentration of i at which inhibition is at half maximum, and n_{inh} acts as the equivalent of the Hill coefficient.

In addition to the enzymatic conversions, the transport of molecules across the cell is represented in the model. A conversion factor $ctob = 4$ is used to account for the difference in sinusoidal plasma and sinusoid volume. For uni-directional active uptake, Hill functions are used, treating the plasma molecule as the substrate and the cytoplasmic molecule as the product. For bidirectional facilitated diffusion, a Hill-type equation dependent on the difference in concentration between the cytoplasm and plasma is used. It is assumed that molecules from both inside and outside the cell contribute to the saturation of the reaction (cross membrane transport protein is blocked by molecules moving both into and out of the cell) such that the reaction is represented by an equation of the form:

$$v_{plasma \rightarrow cyto} = \frac{V_{max}\left(\left[S_{plasma}\right] - \left[S_{cyto}\right]\right)}{K_M + \left[S_{plasma}\right] + \left[S_{cyto}\right]}$$

Although these are heuristic representations of cross-membrane transport based on the stated assumptions, previous experimental studies have used Hill-function equations with effective Michaelis-Menten constants to represent uptake [407-409], and these forms have been used in previous models of liver metabolism [388].

Hormonal regulation is represented in slightly different ways depending on how strongly and rapidly hormones are known to act on the process. In each case, hormonal regulation is based on the plasma concentration rather than modelling the receptors and downstream signalling in detail, as has been performed in previous models (e.g. [389]). The hormonal regulation of each process is discussed in the following sections.

2.2.2.2 Level of Detail

The model is limited to the major processes determining triglyceride levels, ATP concentrations and FA oxidation rates in liver, calculating the overall rates of these processes rather than for each intermediate enzyme. Furthermore, as discussed in section 2.2.4, only simple representations of essential processes occurring outside of liver are included, rather than including separate detailed adipose tissue and muscle compartments. A larger model may, for example, include cholesterol synthesis, include detailed adipose metabolism or individually simulate every enzyme mediating each process. Whilst these extra components would allow the model to simulate additional features of metabolism, for example regarding hepatic intermediate concentrations, it is not expected that they would alter the data presented in this report which were focussed towards a specific aim of understanding lipid build-up across the sinusoid. Conversely, given that each of the processes included in the model are fundamental to energy metabolism and regulation across the sinusoid, exclusion of any of the processes in the model would be expected to significantly alter the observations presented in this report. A major aspect of lipid metabolism which is relevant to current study of NAFLD but could not be studied within the model is the effect of changes in fatty acid compositions (chain length/saturation). In particular, the PNPLA3 gene, which is believed to play a role in determining the

fatty acid composition of triglycerides, is associated with changes in NAFLD and NASH susceptibility (see section 1.3.4.1.4). This is therefore a limitation of the model when considering interindividual variability. However insufficient data was available for the biochemical parameters of the enzymes interconverting between the different fatty acids and mediating oxidation and triglyceride synthesis from each individual fatty acid to include these in the model separately. Therefore, only overall changes in fatty acid concentration and triglyceride concentration can be studied using the model, and the heterogeneous effects of different fatty acid compositions are left to future work.

2.2.2.3 Parameterization

For each conversion, a search of the literature, along with online databases such as BRENDA [410], was first performed to establish allosteric and hormone dependences of the key enzymes mediating the process. The allosteric dependences of each process on other molecules in the model were included in the form of Hill functions with constants taken directly from the literature. The dependences on the various energy molecules in the model (ATP, GTP, UTP *etc.*) were also included as Hill functions with constants taken from the literature for each process. Where possible, the Hill function dependences on the various metabolic intermediates acting as substrates for each process were also taken directly from published experimental data. However, for some processes, e.g. glycolysis and gluconeogenesis, the rate limiting enzyme is not the first in the chain. As a result, in these cases, the substrate dependences were based on experimental data for metabolite concentrations and metabolic flux rates under varying conditions from a number of sources as described below and in supplementary material S1. For each process, the rate constant and constants mediating the insulin and glucagon dependences were also fitted to experimental data.

Since the exact rates at which glucose and lipids enter the bloodstream after feeding in experimental studies are unknown and would vary depending upon the size of the meal, the content of the meal and individual digestion rates, automated least-squares fitting parameters to any specific data set was not considered appropriate. Instead, the focus was placed on ensuring the simulated plasma and

hepatic concentrations both quantitatively remained within the experimentally measured ranges and matched qualitative features in the data such as periods of increase or decrease, and appropriately timed peaks and troughs when simulating a wide range of different feeding conditions and insulin sensitivities using a number of data sets. The fitting was performed by hand, first ensuring the model produced realistic hepatic and plasma concentrations and rates of oxidation when provided with constant inputs (comparing with concentration and rate ranges measured in the literature and with the simulations from an existing model of glycogen storage [389]), before extensively refining the parameter values by comparison with more complex data sets. Where possible, time-series measurements for variation in the concentrations of several molecules or rates of several processes before, during and after feeding were used, including data for both metabolically normal and insulin resistant patients. These comparisons of the model predictions with experimental data are provided in supplementary material S1. Due to inter-individual variability in metabolism, there is inevitably non-uniqueness in parameter values and the model can be considered to represent a single near-average individual. The sensitivity analysis performed in chapter 3 aims to understand the consequences of variability in these parameters.

To allow for the inclusion of zonated enzyme expression, the base values of the rate constant (which are zone-independent) were altered in each compartment according to whether the enzymes in each process are known to be upregulated or downregulated in that region of the sinusoid (figure 2.2). Since continuous changes in enzyme expression are seen for all of the processes included in the model, rather than the step-wise changes in, for example, cholesterol synthesis, the zonation of each process could be set based on the experimentally measured periportal to pericentral ratio of the rate limiting enzymes with a continuous change between compartments. The periportal to pericentral ratio used is stated for each process in table 2.2. The representation of zonation in the model along with the experimental data used to set the zonation in rate constants across the sinusoid is discussed in detail in section 2.2.6.

2.2.2.4 Simulations and Testing

Simulations were run using the XPPAUT ODE solver using a 4th order Runge-Kutta method. The model file was published in Ashworth *et al*. [401]. The concentrations of the various plasma and cytoplasmic molecules are calculated in μM (μmoles/L) except for the concentrations of hormones which are calculated in pM (pMoles/L). To allow easier comparison with experimental data, the hepatic concentration of triglycerides, roughly equal to the total lipid concentration, was converted to a percentage of total cell mass before being presented. Two assumptions were made for this calculation. Firstly, that in a cell containing no fat, the combined protein and cytoplasm concentration is 1000g/L. Secondly, that the protein and cytoplasm content of each cell remain constant independent of the lipid content, such that the cell volume (and total liver volume) expands as the lipid content increases, rather than the protein or cytoplasm content falling. In this case, the combined cytoplasm and triglyceride concentration becomes 1000g/v where v is the increased volume after including the lipid and the percentage lipid content is calculated as:

$$\frac{Triglyceride\ mass/volume}{Total\ mass/volume} = \frac{TG(g/v)}{TG(g/v) + Cyto(g/v) + Protein(g/v)}$$

$$= \frac{TG(g/v)}{TG(g/v) + 1000(g/v)}$$

An average molecular mass of 0.807 was used for triglyceride (equal to that of tripalmitin):

$$\frac{TG(g/v)}{TG(g/v) + Cyto(g/v) + Protein(g/v)} = \frac{(100\%) * 0.81 * TG(Mol/v)}{0.81 * TG(Mol/v) + 1000}$$

Due to the spatially discretised representation of blood flow and the discrete time steps used in simulations, several tests were performed to ensure the simulated data are stable and do not show numerical diffusion. Firstly, simulations were run with varying time steps and compartment numbers to assess stability in the model outputs. The time step was increased from 0.01 seconds to 1 second, and the simulated data were stable and consistent for time steps below 0.4 seconds. When running simulations for the data in the report, a time step of 0.05 seconds was used. Similarly, when the number of compartments was varied from 3 to 48, no numerical diffusion effects were seen for low

compartment numbers. For greater than 6 compartments, no qualitative changes in the simulated data for concentrations and rates across the sinusoid occurred due to under-sampling (such as the appearance of missing maxima or minima) for either metabolically normal or insulin resistant individuals. Finally, oxygen, insulin and glucagon are degraded at constant rates across the sinusoid in the model such that a theoretical concentration curve can be calculated and compared with the values produced by the model. In each case, when using 8 compartments and a time step of 0.05 seconds, the average difference between simulated and theoretical value was less than 0.1% of the average value.

2.2.3 Hepatic Metabolism

2.2.3.1 Summary

Figure 2.2 shows the variables and processes included in each hepatic compartment of the model. Each hepatic compartment interacts with a corresponding blood compartment as shown in figure 2.1. The model focusses on the storage of glucose as glycogen, the cycling between glucose and lactate, adenosine triphosphate (ATP) production, FFA synthesis and the storage of FFAs as triglycerides.

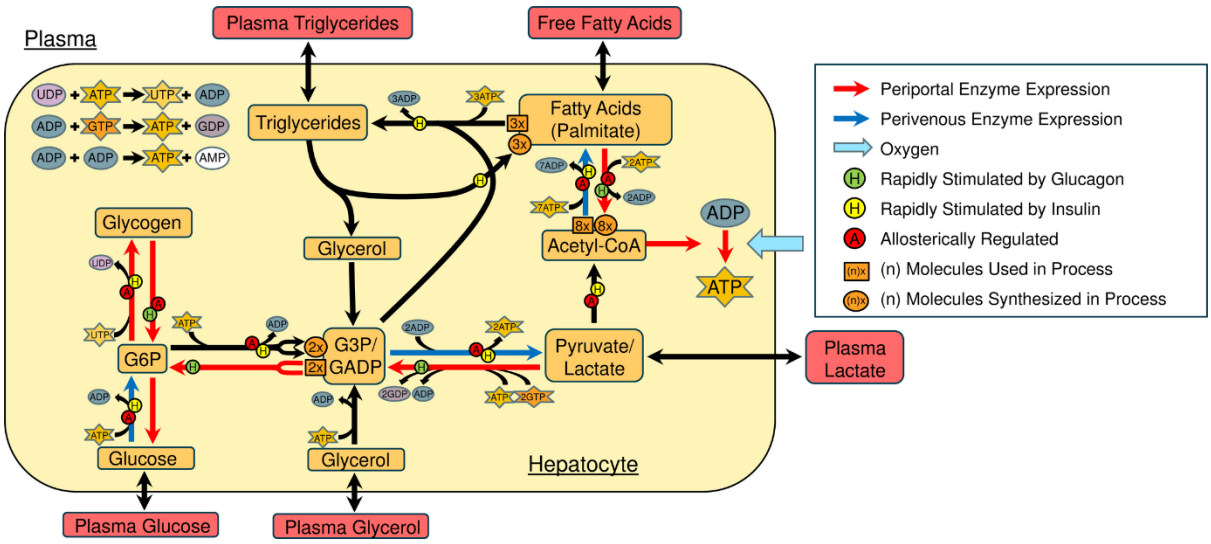

Figure 2.2 – Hepatic metabolism in the model. *The variables and conversions included in each hepatic compartment across the sinusoid (see figure 2.1). In addition to the hormonal regulation, almost all of the glucose and lipid metabolism conversions show some form of allosteric regulation. Lipolysis is also included but it occurs at very slow rate in hepatocytes. Diagram previously published in Ashworth et al. [401].*

2.2.3.1.1 Glucose Metabolism

The liver is the major organ responsible for the control of blood glucose concentrations. When blood glucose levels are high, glucose enters hepatocytes through the transmembrane carrier protein glucose transporter 2 (GLUT2) before being converted to glycogen via glucose-6-phosphate (G6P) under the influence of insulin (glycogenesis). When blood glucose levels are low, glucagon stimulates the release of glucose from glycogen stores (glycogenolysis). Insulin also stimulates the breakdown of glucose to two pyruvate molecules through glycolysis. This pyruvate can either be released into the blood as lactate or converted to acetyl-CoA for use in oxidative phosphorylation or in lipid metabolism. Glucagon, meanwhile, stimulates the reverse reaction converting pyruvate and lactate to glucose through gluconeogenesis. Glyceraldehyde-3-phosphate (GADP), an intermediate of glycolysis and gluconeogenesis, can be rapidly converted to glycerol-3-phosphate (G3P) which forms the glycerol backbone in triglyceride synthesis. Additionally, glycerol released in lipolysis is converted to G3P and GADP via the enzyme glycerol kinase. Most lipolysis occurs outside of the liver in adipose tissue. However, very little glycerol kinase activity is seen in adipose tissue and instead glycerol released in adipose tissue is recycled in the liver [411].

2.2.3.1.2 Lipid and Energy Metabolism

The liver plays an important role in lipid metabolism and there exists a strong link between lipid metabolism and liver disease. Hepatic steatosis is seen in a range of liver conditions most commonly linked with alcohol, viruses such as hepatitis c or metabolic dysregulation and is known to play a role in the development of IR.

Pyruvate is converted to acetyl-CoA by a complex of three enzymes known as the pyruvate dehydrogenase complex (PDC). These acetyl-CoA molecules can either enter the citrate cycle to provide fuel for oxidative phosphorylation of ADP to ATP or can be joined to form FA chains through *de novo* lipogenesis. Numerous FAs are produced *in vivo* with varying chain lengths. However, to reduce the computation required, the model assumes all FAs to be palmitate. Palmitate is the most

common FA in animals, plants and microorganisms and corresponds to a chain of 8 acetyl-CoA molecules (16 carbons). Both the production of acetyl-CoA and lipogenesis are stimulated by insulin whilst the breakdown of palmitate back to 8 acetyl-CoA molecules (β-oxidation) is stimulated by glucagon.

When blood glucose levels peak, it is beneficial to remove alternative cellular energy sources from the blood including FAs. Insulin stimulates the synthesis of triglycerides, in which three FAs are attached to a glycerol backbone for storage. While FFAs can be used as an energy source by the majority cells in the body, most cell types are unable to break down triglycerides. The liver has only a very small capacity to breakdown triglycerides through lipolysis [412]. Although the liver plays a role in lipid metabolism, adipose tissue is the primary regulator of blood lipid levels. As a result, it was also necessary to include a simple representation of adipose tissue in the model for it to produce valid blood FFA and triglyceride concentrations.

FFA uptake through the FATP proteins is included through two terms corresponding to passive concentration dependent uptake and the insulin dependent pumping of FFAs into the cytoplasm. Triglyceride release as VLDL is included along with a term representing triglyceride uptake from the blood.

2.2.3.1.3 Hepatic Rate Equations

A reduced description of the representation of metabolism in each hepatic compartment in the model is provided in tables 2.1 and 2.2 before a full description of each equation is provided in the following sections. Table 2.1 contains the differential equations for each hepatic variable in terms of the metabolic processes occurring. Table 2.2 defines the processes included in each hepatic compartment in the model and references the sections in which the full equations can be found.

Table 2.1 – The rate equations for the variables included in the hepatic compartments of the model.

Hepatic Variable	Rate Equations
Glucose	$\frac{dG_c}{dt} = -\mathbb{R}_{GK} + \mathbb{R}_{G6Pase} + \mathbb{R}_{Glut}$
G6P	$\frac{dG6P}{dt} = \mathbb{R}_{GK} - \mathbb{R}_{G6Pase} + \mathbb{R}_{GP} - \mathbb{R}_{GS} + \mathbb{R}_{FBP} - \mathbb{R}_{PFK}$
Glycogen	$\frac{dGly}{dt} = \mathbb{R}_{GS} - \mathbb{R}_{GP}$
G3P/GADP	$\frac{dG3P}{dt} = \mathbb{R}_{PEPCK} - 2\,\mathbb{R}_{FBP} + 2\,\mathbb{R}_{PFK} - \mathbb{R}_{PK} + \mathbb{R}_{GConv} - \mathbb{R}_{TSyn}$
Pyruvate/Lactate	$\frac{dLac_c}{dt} = \mathbb{R}_{Lact} - \mathbb{R}_{PEPCK} + \mathbb{R}_{PK} - \mathbb{R}_{PDH}$
Acetyl-CoA	$\frac{dACoA}{dt} = \mathbb{R}_{PDH} - 8\,\mathbb{R}_{Lgen} + 8\,\mathbb{R}_{\beta oxi} - \mathbb{R}_{ATPS}$
FFA (Palmitate)	$\frac{dFFA_c}{dt} = \mathbb{R}_{FFAt} + 3\,\mathbb{R}_{Lply} - 3\,\mathbb{R}_{TSyn} + \mathbb{R}_{Lgen} - \mathbb{R}_{\beta oxi}$
Triglycerides	$\frac{dTG_c}{dt} = \mathbb{R}_{TGt} + \mathbb{R}_{TSyn} - \mathbb{R}_{Lply}$
Glycerol	$\frac{dGly_c}{dt} = \mathbb{R}_{Glyt} - \mathbb{R}_{GConv} + \mathbb{R}_{Lply}$
ATP - Adenosine Triphosphate	$\frac{dATP}{dt} = 12\,\mathbb{R}_{ATPS} - \mathbb{R}_{AK} - 2\,\mathbb{R}_{PEPCK} - \mathbb{R}_{PFK} + 3.25\,\mathbb{R}_{PK} - \mathbb{R}_{GK} - \mathbb{R}_{NDKG} - \mathbb{R}_{NDKU} - \mathbb{R}_{ATPu} - 2\,\mathbb{R}_{\beta oxi} - 7\,\mathbb{R}_{Lgen} - \mathbb{R}_{GConv} + 2.5\,\mathbb{R}_{PDH} - 3\,\mathbb{R}_{TSyn}$
ADP - Adenosine Diphosphate	$\frac{dADP}{dt} = -12\,\mathbb{R}_{ATPS} + 2\,\mathbb{R}_{AK} + 2\,\mathbb{R}_{PEPCK} + \mathbb{R}_{PFK} - 3.25\,\mathbb{R}_{PK} + \mathbb{R}_{GK} + \mathbb{R}_{NDKG} + \mathbb{R}_{NDKU} + \mathbb{R}_{ATPu} + 7\,\mathbb{R}_{Lgen} + \mathbb{R}_{GConv} + \mathbb{R}_{\beta oxi} - 2.5\,\mathbb{R}_{PDH}$
AMP - Adenosine Monophosphate	$\frac{dAMP}{dt} = -\mathbb{R}_{AK} + \mathbb{R}_{\beta oxi} + 3\,\mathbb{R}_{TSyn}$
Pi - Inorganic Phosphate	$\frac{dPi}{dt} = -12\,\mathbb{R}_{ATPS} - \mathbb{R}_{GP} + \mathbb{R}_{G6Pase} + 2\,\mathbb{R}_{GS} - 2.25\,\mathbb{R}_{PK} + 2\,\mathbb{R}_{PEPCK} + \mathbb{R}_{FBP} - \mathbb{R}_{PReg} + \mathbb{R}_{ATPu} + 7\,\mathbb{R}_{Lgen} + \mathbb{R}_{\beta oxi} - 2.5\,\mathbb{R}_{PDH} + 7\,\mathbb{R}_{TSyn}$
UTP - Uridine Triphosphate	$\frac{dUTP}{dt} = \mathbb{R}_{NDKU} - \mathbb{R}_{GS}$
UDP - Uridine Diphosphate	$\frac{dUDP}{dt} = -\mathbb{R}_{NDKU} + \mathbb{R}_{GS}$
GTP - Guanosine Triphosphate	$\frac{dGTP}{dt} = \mathbb{R}_{NDKG} - \mathbb{R}_{PEPCK}$
GDP - Guanosine Diphosphate	$\frac{dGDP}{dt} = -\mathbb{R}_{NDKG} + \mathbb{R}_{PEPCK}$

The rates/processes ($\mathbb{R}$) are defined in table 2.2 and discussed in detail (along with the non-hepatic processes) in the following sections. References to the specific sections in which the full equation for each process can be found are also provided in table 2.2.

Table 2.2 – The processes included in each hepatic compartment in the model.

Process	**Conversion**
$\mathbb{R}_{Glut}$ – Glucose Uptake. *Section 2.2.3.2.1*	$G_B \underset{\longleftarrow}{\overrightarrow{\longleftrightarrow}} G_C$ (Blood Glucose $\underset{\longleftarrow}{\overrightarrow{\longleftrightarrow}}$ Cellular Glucose) Periportal to pericentral ratio in rate constant – 1:1
$\mathbb{R}_{GK}$ – GK. *Section 2.2.3.2.2*	$G_C + ATP \rightarrow G6P + ADP$ Periportal to pericentral ratio in rate constant - 1:2.5
$\mathbb{R}_{G6Pase}$ – G6Pase. *Section 2.2.3.2.3*	$G6P \rightarrow G_C + P_i$ Periportal to pericentral ratio in rate constant – 1.9:1
$\mathbb{R}_{GS}$ – Glycogen Synthesis. *Section 2.2.3.3.1*	$G6P + UTP \rightarrow Glycogen + UDP + 2\ P_i$ Periportal to pericentral ratio in rate constant – 3:1
$\mathbb{R}_{GP}$ – Glycogen Phosphorylation. *Section 2.2.3.3.2*	$Glycogen + P_i \rightarrow G6P$ Periportal to pericentral ratio in rate constant – 1:1
$\mathbb{R}_{PFK}$ – Glycolysis stage 1, primarily rate-limited by PDK. *Section 2.2.3.4.1*	$G6P + ATP \rightarrow 2\ GADP/G3P + ADP$ Periportal to pericentral ratio in rate constant – 1:1
$\mathbb{R}_{PK}$ – Glycolysis stage 2, primarily rate-limited by PK. *Section 2.2.3.4.2*	$\frac{GADP}{G3P} + 2ATP + P_i \rightarrow Pyr/Lac\ + 2ATP$ + additional indirect 1.25 ATP from NADH. Periportal to pericentral ratio in rate constant – 1:2.1
$\mathbb{R}_{PEPCK}$ – Gluconeogenesis stage 1, primarily rate-limited by PEPCK. *Section 2.2.3.4.3*	$Pyr/Lac + 2ATP + GTP \rightarrow GADP/G3P + 2ADP + GDP + 2\ P_i$ Periportal to pericentral ratio in rate constant – 2.4:1
$\mathbb{R}_{FBP}$ – Gluconeogenesis 2, primarily rate-limited by FBPase. *Section 2.2.3.4.4*	$2\ GADP/G3P \rightarrow G6P + P_i$ Periportal to pericentral ratio in rate constant – 1.75:1
$\mathbb{R}_{PDH}$ – Pyruvate oxidation mediated by PDH. *Section 2.2.3.5.1*	$Pyr/Lac \rightarrow ACoA$ + indirect 2.5 ATP from NADH Periportal to pericentral ratio in rate constant – 1:1
$\mathbb{R}_{\beta oxi}$ – β-Oxidation. *Section 2.2.3.5.2*	$FFA + 2\ ATP \rightarrow 8\ ACoA + ADP + AMP + 3\ P_i$ Periportal to pericentral ratio in rate constant – 1.6:1
$\mathbb{R}_{ATPS}$ - ATP Synthesis via the citrate cycle and electron transport chain. *Section 2.2.3.6.1*	$ACoA + 12ADP + 12\ P_i \rightarrow 12\ ATP$ Periportal to pericentral ratio in rate constant – 1.5:1
$\mathbb{R}_{NDKG}$/$\mathbb{R}_{NDKU}$ – NDKs. *Section 2.2.3.6.2*	(NDKG): $GDP + ATP \rightarrow GTP + ADP$ (NDKU): $UDP + ATP \rightarrow UTP + ADP$ Periportal to pericentral ratio in rate constant – 1:1
$\mathbb{R}_{AK}$ – AK. *Section 2.2.3.6.3*	$ATP + AMP \leftrightarrow 2\ ADP$ Periportal to pericentral ratio in rate constant – 1:1
$\mathbb{R}_{ATPu}$ – Cellular ATP consumption. $\mathbb{R}_{PReg}$ – P_i Regulation.	$ATP \rightarrow ADP + P_i$ $P_i \leftrightarrow -$

Section 2.2.3.6.4	Periportal to pericentral ratio in both rate constant – 1:1
$\mathbb{R}_{Lgen}$ – Lipogenesis. *Section 2.2.3.7*	$ACoA + 7\ ATP \rightarrow FFA + 7\ ADP + 7\ P_i$ Periportal to pericentral ratio in rate constant – 1:1.6
$\mathbb{R}_{TSyn}$ – Triglyceride Synthesis. *Section 2.2.3.8.1*	$3\ FFA + G3P/GADP + 3\ ATP \rightarrow\ TG + 3\ AMP + 7\ P_i$ Periportal to pericentral ratio in rate constant – 1:1
$\mathbb{R}_{Lply}$ – Lipolysis. *Section 2.2.3.8.2*	$TG \rightarrow Glyc + 3\ FFA$ Periportal to pericentral ratio in rate constant – 1:1
$\mathbb{R}_{GConv}$ - Glycerol Kinase. *Section 2.2.3.8.3*	$Glyc + ATP \rightarrow G3P/GADP + ADP$ Periportal to pericentral ratio in rate constant – 1:1
$\mathbb{R}_{Lact}$ – Lactate Output/Uptake. *Section 2.2.3.9.1*	$Lac_B \leftrightarrow Lac_C$ Periportal to pericentral ratio in rate constant – 1:1
$\mathbb{R}_{FFAt}$ – FFA Output/Uptake. *Section 2.2.3.9.2*	$FFA_B \underset{\longrightarrow}{\overset{\leftrightarrow}{}} FFA_C$ Periportal to pericentral ratio in rate constant – 1.5:1
$\mathbb{R}_{TGt}$ – Triglyceride Output/Uptake. *Section 2.2.3.9.3*	$TG_B \underset{\longleftarrow}{\overset{\leftrightarrow}{}} TG_C$ Periportal to pericentral ratio in rate constant – 1:1
$\mathbb{R}_{Glyt}$ – Glycerol Output/Uptake. *Section 2.2.3.9.4*	$Glyc_B \leftrightarrow Glyc_C$ Periportal to pericentral ratio in rate constant – 1:1
Hormone Reception	Periportal to pericentral ratio in insulin reception – 1:1.35 Periportal to pericentral ratio in glucagon reception – 1.35:1

Full equations along with the values of constants, the experimental data used as references and a detailed discussion are provided in the following sections, including the equations used to calculate the rates of processes occurring in the blood/body compartments in addition to the hepatic processes listed in the table.

2.2.3.2 Glucose Uptake and Output

2.2.3.2.1 Glucose uptake by GLUT2 – terms to represent pumping and passive diffusion

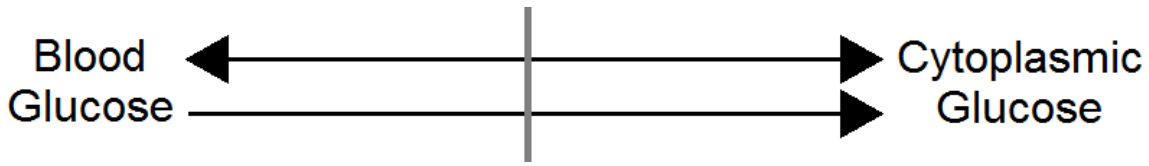

The major glucose transporter in the liver is GLUT2 [413]. Two terms represent pumping and diffusion of glucose into the cytoplasm. Uni- and bi- direction Michaelis-Menten equations are used to represent these terms respectively. GLUT2 has a higher K_M value than other common glucose transporters (GLUT1,3,4) allowing rapid uptake by hepatocytes when blood glucose levels rise for storage, where glucose uptake in other cells types would be determined by the energetic requirements of the cell.

$$\frac{v_{pump} * G_B}{\left(K_M^{pump} + G_B\right)} + \frac{v_{diff} * (G_B - G_C)}{\left(K_M^{diff} + G_B + G_C\right)}$$

$K_M^{pump} = 17mM$ *[407],* $K_M^{diff} = 17mM$ *[407].*

2.2.3.2.2 Glucokinase

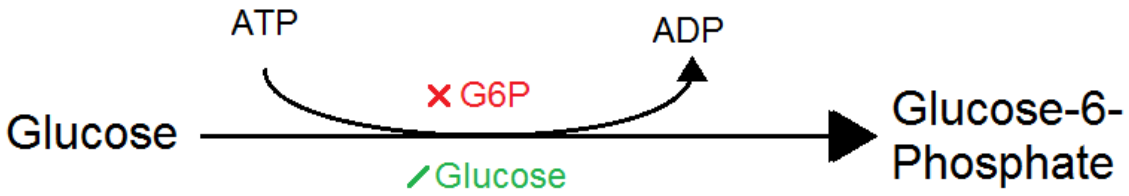

GK mediates the conversion of glucose to G6P taking a phosphate from ATP in the process. GK is allosterically dependent on the concentration of various molecules, either directly or indirectly via GK regulatory protein (GKRP). GKRP competitively binds to GK and moves the enzyme into the nucleus when glucose concentrations are low or when the concentrations of glycolysis intermediates such as F-6-P and F-1,6-P are high. G6P has a direct inhibitory effect. These dependences ensure increased uptake when glucose concentrations are high or when increased glycolysis is required to meet cellular energetic requirements. In the model, the effects glucose on GKRP (causing the release of GK) are included with constants taken from experimental data. Furthermore, the allosteric inhibition by G6P is included. F-6-P and F-1,6-P are not represented as independent variables in the model and their inhibitory effects (through GKRP) could not be included directly. However, conversion between G6P and F-6-P is rapid relative to the processes occurring in the model and so the two can be considered to be in constant equilibrium. In the model, a single G6P dependent inhibition term represents the allosteric inhibition of both G6P and F-6-P. The allosteric inhibition of F-1,6-P could not be included.

$$\frac{v_{gk} * {G_c}^{n_{free}}}{\left(K_M^{gkrp^{n_{free}}} + {G_c}^{n_{free}}\right)} * \frac{{G_c}^{n_g}}{\left(K_M^{G^{n_g}} + {G_c}^{n_g}\right)} * \frac{ATP}{(K_M^{ATP} + ATP)} * \left(1 - \frac{G6P^{n_{inh}}}{\left(K_i^{G6P^{n_{inh}}} + G6P^{n_{inh}}\right)}\right)$$

K_M^G *= 7.5mM [414, 415],* K_M^{gkrp} *= 15mM [414, 416].*

n_{free} *= 2 [414, 416],* n_g *= 1.4 [414, 416].*

K_i^{G6P} *= 240μM - [417, 418].*

K_M^{ATP} = 240μM – a fairly wide range of values measured in the literature (e.g. 140μM [419], 410μM [415]). The value chosen for model is roughly in the middle of these. However, since the values are much lower than the average ATP concentration under all but severe pathological conditions, small changes in the K_M value do not notably affect results.

n_{inh} = 4 – As discussed, the activity of GK is strongly inhibited both directly by G6P and indirectly by intermediates of glycolysis such as F6P [420]. F6P is not included in the model as an independent variable. However, conversion between F6P and G6P occurs rapidly relative to other processes included in the model. Therefore, the two can be expected to remain in constant equilibrium and a single allosteric dependence is included to represent both. A high n_{inh} of 4 is used to provide strong allosteric inhibition when G6P (/F6P) concentrations rise and a rapid reduction in inhibition when the concentration falls [389].

2.2.3.2.3 G6Pase

G6P is converted to glucose by the enzyme G6Pase releasing the phosphate. No strong allosteric or hormonal regulation has been demonstrated for this enzyme.

$$\frac{v_{G6Pase} * G6P}{K_M^{G6P} + G6P}$$

K_m^{G6P} = 2.41mM [421, 422]

2.2.3.3 Glycogen Synthesis and Breakdown

In order to control the rates of glycogenesis and glycogenolysis, insulin and glucagon bind to surface receptors causing a downstream cascade which determines the phosphorylation state, and hence activity, of glycogen synthase (GS) and glycogen phosphorylase (GP). In the model, a hormone dependent maximum activity is calculated for each enzyme before multiplying by Michaelis-Menten-type substrate dependences. The hormone signalling pathways have been modelled in detail in

previous two compartment models (for example Hetherington *et al.* [389]). However, in this study, since the focus is placed on understanding the effects of zonation rather than hormone signalling, hormone dependences of processes are calculated directly based on the blood hormone concentration in the region of the cells, rather than including a detailed representation of the downstream signalling.

2.2.3.3.1 Glycogen Synthase

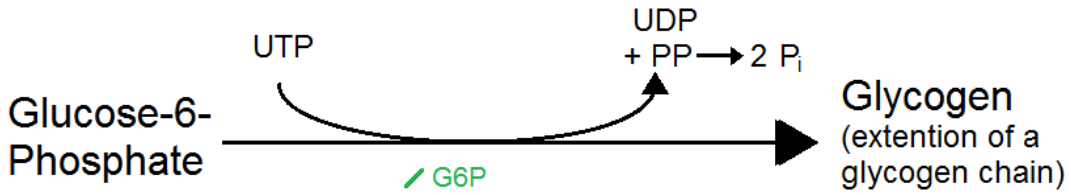

G6P is converted to glucose-1-phosphate (G1P) before binding with a uridine triphosphate (UTP) molecule to give UDP-glucose (and pyrophosphate (PP) which is rapidly broken down to give two phosphates (P_i)). GS, the rate limiting enzyme in glycogen synthesis, uses this UDP-glucose to extend a glycogen chain. As well as the hormonal regulation, GS is allosterically activated by an increased G6P concentration.

$$K_{syn}^{max} = \frac{(Ins + K_{IS})}{(Glgn + K_{LS})}$$

$$\frac{v_{syn} * K_{syn}^{max} * G6P^{n_{syn}}}{\left(G6P^{n_{syn}} + K_m^{G6P^{n_{syn}}}\right)} * \frac{UTP}{K_M^{UTP} + UTP}$$

K_m^{UTP} = 48μM [423, 424]

K_{IS} = 13.33pM, K_{LS} = 62.5pM, K_M^{G6P} = 50μM, n_{syn} = 4 set such that the simulated data match experimental data from [425-431] for plasma concentrations of key glucose metabolism molecules throughout a daily feeding cycle [425] (section S1.1.4), for hepatic glycogen and plasma concentrations after a mixed meal [428] (section S1.1.2), and for average glycogen and hepatic glucose metabolism intermediate concentrations [426, 427, 429, 430] (section S1.1.1) along with simulations from the model presented by Hetherington et al. [389, 390], which

contained a detailed representation of the pathways involved hormone reception and downstream regulation of GS and GP (see supplementary material S1 for comparison with experimental data). A low K_M value but high Hill coefficient (n_{syn}) was used for the G6P dependence. This rapidly reduces glycogen synthesis when G6P concentrations fall below their metabolically normal range due to the dependence on G6P both as a substrate (via G1P and UDP glucose) and as an allosteric activator (GS activity nearly doubles in the presence of high concentrations of G6P compared with no G6P [432]), whilst ensuring that the rate of synthesis is primarily determined by the effects of hormones under metabolically normal conditions. When G6P dependences that were less steep (lower n_{syn}) but reached saturation at higher G6P concentrations (higher K_M) were tested, glycogen stores failed to empty when simulating IR.

2.2.3.3.2 Glycogen Phosphorylase

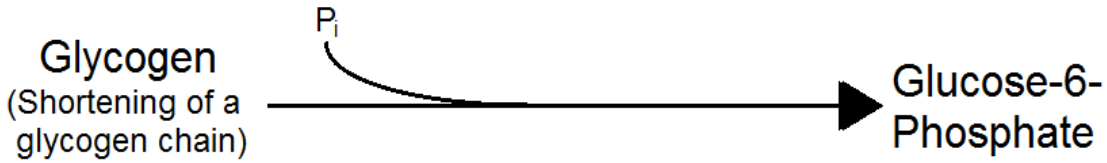

GP depolymerises glycogen adding a phosphate to give G1P. This G1P is then rapidly converted to G6P by phosphoglucomutase.

$$K_{phos}^{max} = \frac{(Glgn + k_{LP})}{(Ins + k_{IP})}$$

$$\frac{v_{brk} * K_{Phos}^{max} * Gly^{n_{brk}}}{\left(Gly^{n_{brk}} + K_m^{Gly^{n_{brk}}}\right)} * \frac{Phos}{K_M^{phos} + Phos}$$

K_M^{Gly} – 100mM (units of glucose), K_M^{phos} = 4000μM [433] – for the active form of GP

K_{IP} = 26.66pM, K_{LP} = 45pM, n_{brk} = 4 – set such that the model simulations match experimental data from [425-431] for plasma concentrations of key glucose metabolism molecules throughout a daily feeding cycle [425] (section S1.1.4), for hepatic glycogen and plasma concentrations after a mixed meal [428] (section S1.1.2), and for average glycogen and hepatic glucose metabolism intermediate concentrations [426, 427, 429, 430] (section S1.1.1)

along with the simulations of the model of hormone signalling and its effects on GS and GP presented by Hetherington et al. [389, 390].

2.2.3.4 Gluconeogenesis and Glycolysis

The rates of gluconeogenesis and glycolysis are strongly affected by the concentrations of insulin and glucagon (e.g. [431]). As with glycogenesis and glycogenolysis, when calculating the rates of the glycolytic and gluconeogenic processes a maximum enzyme activity is first calculated based on the blood hormone concentrations. This is then multiplied by Michaelis-Menten type substrate dependences.

2.2.3.4.1 Glycolysis 1: G6P to GADP

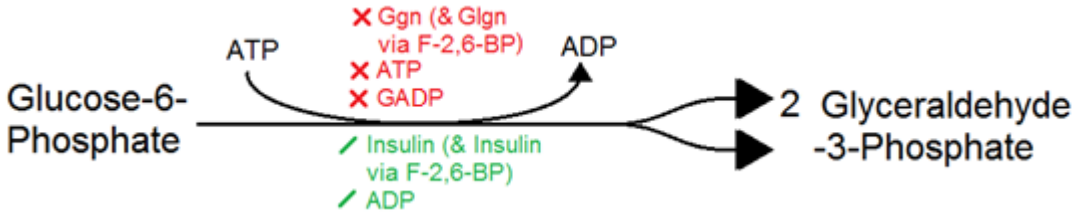

G6P is broken down to two GADP molecules via a sequence of enzymes. The rate limiting enzyme in this conversion is PFK (producing fructose-1,6-bisphosphate (F-1,6-BP)) which is highly allosterically regulated. It is also the only unidirectional enzyme in the chain, with the reverse conversion mediated by FBPase. PFK requires the removal of a phosphate molecule from ATP, releasing ADP. The enzyme is allosterically activated by ADP and inhibited by ATP such that the rate of glycolysis is increased or slowed depending on the energy (ATP) requirements of the cell. The effects of ATP and ADP are included with K_M, activation and inhibition constants taken from the literature. After the production of F-1,6-BP, the subsequent enzyme in the chain, fructose-bisphosphate aldolase, splits the F-1,6-BP into one GADP molecule and one dihydroxyacetone phosphate molecule, which is converted into a second GADP resulting in the production of two molecules from glycolysis for each glucose/G6P.

In addition, PFK is allosterically inhibited by GADP and phosphoenolpyruvate, products further down the glycolysis chain, as well as by intermediates of the citrate cycle, citrate and malate. As a result,

glycolysis is not only slowed when ATP levels are high but also when there is a surplus of substrate for the citrate cycle. Of these effectors, only GADP is included as an independent variable in the model and, therefore, the inhibition of the molecules further down cannot be directly included. Instead, the inhibition of GADP included in the model is assumed to represent the inhibition of all glycolytic intermediates. Finally, PFK is also allosterically activated by fructose-2,6-bisphosphate (F-2,6-BP). The concentration of F-2,6-BP is predominantly determined by the action of insulin and glucagon, such that the PFK activity increases when plasma glucose, and hence insulin, concentrations are raised. As a result, although F-2,6-BP is also not included in the model as an independent variable, this allosteric dependence is included in the fitted hormone dependences.

$$K_{PFK}^{max} = \frac{(Ins + K_{IPFK})}{(Glgn + K_{LPFK})}$$

$$\frac{v_{PFK} * K_{PFK}^{max} * G6P}{K_M^{G6P} + G6P} * \frac{ATP}{K_M^{ATP} + ATP} * \frac{ADP}{K_a^{ADP} + ADP}\left(1 - \beta_{ATP}\frac{ATP}{K_i^{ATP} + ATP}\right)\left(1 - \beta_{GAdP}\frac{GADP}{K_i^{GADP} + GADP}\right)$$

$K_{IPFK} = 2666.7pM$, $K_{LPFK} = 1250pM$ – *set so that the model simulations match the data in references [425-431, 434] for plasma concentrations of glucose and lactate throughout a daily feeding cycle [425] (section S1.1.4), after a glucose load [434] (section S1.2.2) and after a mixed meal [428] (section S1.1.2), for average hepatic glucose metabolism intermediate concentrations including glucose, G6P, pyruvate, lactate, G3P and GADP [426, 427, 429, 430] (section S1.1.1), and for the rates of glucose use in the various pathways after intake in the presence or absence of hormones [431] (section S1.1.3). Additionally set so that the model simulations match the data in references [141, 425, 435] for the FFA and triglyceride concentrations throughout a mixed meal [425] (section S1.1.4) and for average concentrations of FFAs and triglycerides in individuals of varying weight and with varying insulin sensitivities [141, 435] (section S1.2.1) due to the role of GADP/G3P in triglyceride synthesis.*

K_M^{G6P} = 5 µM – Since PFK doesn't act directly from G6P, a K_M value couldn't be taken from the literature. A very low value was used based on the observation that the rate of glycolysis does not increase when the glucose concentration is increased in insulin resistant patients [434]. This suggests that in metabolically normal individual's glycolysis increases due to the effects of insulin rather than increased substrate when plasma glucose concentrations are raised.

K_M^{ATP} = 42.5µM [436], β_{ATP} = 1, K_a^{ADP} = 83.6µM [436, 437], K_i^{ATP} = 2.1mM [436, 437], $\beta_{GADP} = 0.75$, K_i^{GADP} = 20.7 µM [438]

2.2.3.4.2 Glycolysis 2: GADP to Lactate/Pyruvate

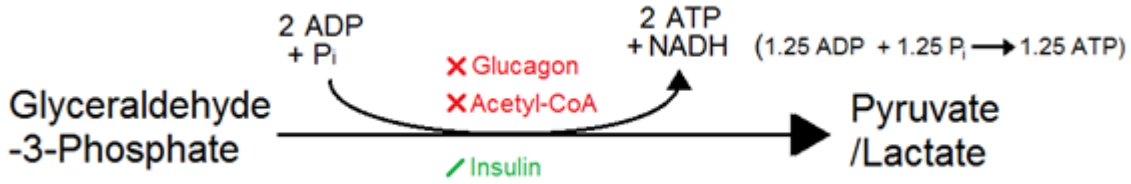

In the second half of glycolysis, each GADP molecule is converted to pyruvate (and lactate). Since conversion between pyruvate and lactate is reversible and relatively rapid, they are represented by a single variable in the model. Here we assume a constant pyruvate to lactate ratio. *In vivo*, the ratio is altered under conditions which effect the NAD:NADH ratio such as after heavy ethanol intake. Therefore, if in future work the model is used to study the metabolism of ethanol (or other drugs) across the sinusoid, modifications would be required to represent pyruvate and lactate as separate variables and to include NAD/NADH as separate variables rather than just through their effects on ATP concentrations.

The rate limiting enzyme in the conversion of GADP to pyruvate is PK. Both the phosphate contained in the GADP and an additional free inorganic phosphate are combined with ADP molecules to produce two ATP molecules in this part of glycolysis. One ATP molecule is released by phosphoglycerate kinase and the second by PK. Additionally an NAD+ molecules is converted to NADH. Note that because 2 GADP molecules are produced per glucose in the previous stage of glycolysis, when considering the

glycolysis of each glucose molecule, 4 ATP, 2 NADH and 2 pyruvate/lactate molecules are produced in this stage.

NADH can produce a theoretical maximum of 3 ATP when entering the ETC. However, a ratio of closer to 2.5 ATP per NADH is achieved for mitochondrial NADH. In the case of PK, the NADH is cytosolic and cannot cross the mitochondrial membrane. Instead a shuttle reactor of $NADH_{cyto} + NAD^{+}_{mito} \rightarrow NADH_{mito} + NAD^{+}_{cyto}$ occurs to transport NADH into the mitochondria which requires the consumption of 1 ATP molecule. Here a relatively low rate of 1.25 ATP per cytosolic NADH is assumed to account for these difficulties in transport and further inefficiency in the use of NADH. PK is allosterically inhibited by acetyl-CoA.

$$K_{PK}^{max} = \frac{(Ins + K_{IPK})}{(Glgn + K_{LPK})}$$

$$\frac{v_{PK} * K_{PK}^{max} * GADP}{K_m^{GADP} + GADP} * \frac{ADP}{K_M^{ADP} + ADP}\left(1 - \beta_{allos}\frac{aCoA}{K_i^{aCoA} + aCoA}\right)$$

$K_{IPK} = 1066.6pM$, $K_{LPK} = 500pM$, K_m^{GADP} *= 250μM – set so that the model simulations match the data in references [425-431, 434] for plasma concentrations of glucose and lactate throughout a daily feeding cycle [425] (section S1.1.4), after a glucose load [434] (section S1.2.2) and after a mixed meal [428] (section S1.1.2), for average hepatic glucose metabolism intermediate concentrations including glucose, G6P, pyruvate, lactate, G3P and GADP [426, 427, 429, 430] (section S1.1.1), and for the rates of glucose use in the various pathways after intake in the presence or absence of hormones [431] (section S1.1.3). Additionally set so that the model simulations match the data in references [141, 425, 435] for the FFA and triglyceride concentrations throughout a mixed meal [425] (section S1.1.4) and for average concentrations of FFAs and triglycerides in individuals of varying weight and with varying insulin sensitivities [141, 435] (section S1.2.1) due to the role of GADP/G3P in triglyceride synthesis.*

K_M^{ADP} *= 240μM [439],* K_i^{aCoA} *= 30μM [440],* β_{allos} *= 0.8 [440]*

2.2.3.4.3 Gluconeogenesis 1: Lactate/Pyruvate to GADP (Glyceroneogenesis)

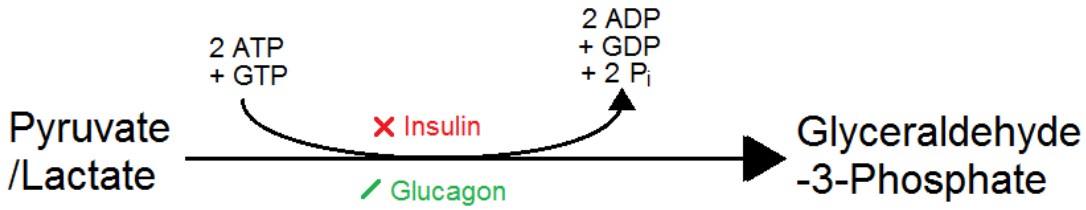

The conversion of pyruvate to GADP is highly energy intensive, requiring the removal of phosphates from 2 ATPs and a GTP. The rate limiting enzyme in this conversion is PEPCK which hydrolyses GTP to provide a phosphate, allowing the production of phosphoenolpyruvate. PEPCK is not known to be strongly allosterically regulated.

$$K_{PEPCK}^{max} = \frac{(Glgn + k_{LPEPCK})}{(Ins + k_{IPEPCK})}$$

$$\frac{v_{PEPCK} * K_{PEPCK}^{max} * Lac}{K_M^{Lac} + Lac} * \frac{ATP}{K_M^{ATP} + ATP} * \frac{GTP}{K_M^{GTP} + GTP}$$

$K_{IFBP} = 2266.6$, $K_{LFBP} = 1062.5$, K_M^{Lac} = 500mM – set so that the model simulations match the data in references [425-431, 434] for plasma concentrations of glucose and lactate throughout a daily feeding cycle [425] (section S1.1.4), after a glucose load [434] (section S1.2.2) and after a mixed meal [428] (section S1.1.2), for average hepatic glucose metabolism intermediate concentrations including glucose, G6P, pyruvate, lactate, G3P and GADP [426, 427, 429, 430] (section S1.1.1), and for the rates of glucose use in the various pathways after intake in the presence or absence of hormones [431] (section S1.1.3). Additionally set so that the model simulations match the data in references [141, 425, 435] for the FFA and triglyceride concentrations throughout a mixed meal [425] (section S1.1.4) and for average concentrations of FFAs and triglycerides in individuals of varying weight and with varying insulin sensitivities [141, 435] (section S1.2.1) due to the roles of GADP/G3P in triglyceride synthesis and pyruvate in lipogenesis.

K_M^{ATP} = 10 μM – set very low since, although ATP is required for the conversion of lactate to GADP, the ATP is required by enzymes which, under normal conditions, are not rate-limiting.

Using a low K_M value means that large drops in ATP concentration will inhibit the process but variation in the physiological range will not affect the rate.

K_M^{GTP} = 64μM - [441]

2.2.3.4.4 Gluconeogenesis 2: GADP to G6P

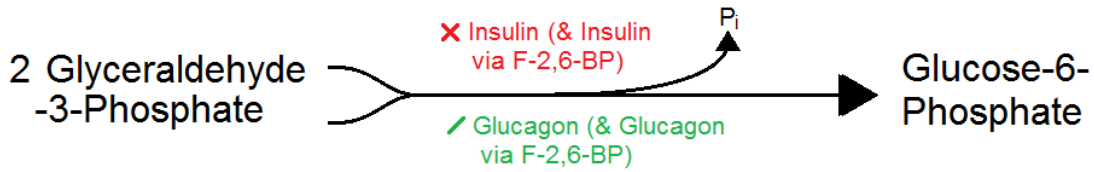

The rate limiting enzyme in the conversion of two GADP molecules to G6P is FBPase. FBPase is allosterically inhibited by F-2,6-BP. The F-2,6-BP concentration is primarily determined by the action of insulin and glucagon, such that hepatic glucose production is reduced when plasma glucose (and hence insulin) concentrations are high. Therefore, although F-2,6-BP is not included as an independent variable, its allosteric effects are included in the fitted hormone dependences.

$$K_{FBP}^{max} = \frac{(Glgn + k_{LFBP})}{(Ins + k_{IFBP})}$$

$$\frac{v_{FBP} * K_{FBP}^{max} * GADP}{K_m^{GADP} + GADP}$$

$K_{IFBP} = 2666.6$, $K_{LFBP} = 1250$, K_m^{GADP} = 250μM – *set so that the model simulations match the data in references [425-431, 434] for plasma concentrations of glucose and lactate throughout a daily feeding cycle [425] (section S1.1.4), after a glucose load [434] (section S1.2.2) and after a mixed meal [428] (section S1.1.2), for average hepatic glucose metabolism intermediate concentrations including glucose, G6P, pyruvate, lactate, G3P and GADP [426, 427, 429, 430] (section S1.1.1), and for the rates of glucose use in the various pathways after intake in the presence or absence of hormones [431] (section S1.1.3). Additionally set so that the model simulations match the data in references [141, 425, 435] for the FFA and triglyceride concentrations throughout a mixed meal [425] (section S1.1.4) and for average concentrations of FFAs and triglycerides in individuals of varying weight and with varying insulin sensitivities*

[141, 435] (section S1.2.1) due to the roles of GADP/G3P in triglyceride synthesis and pyruvate in lipogenesis.

2.2.3.5 Acetyl-CoA Production

2.2.3.5.1 Pyruvate Oxidation.

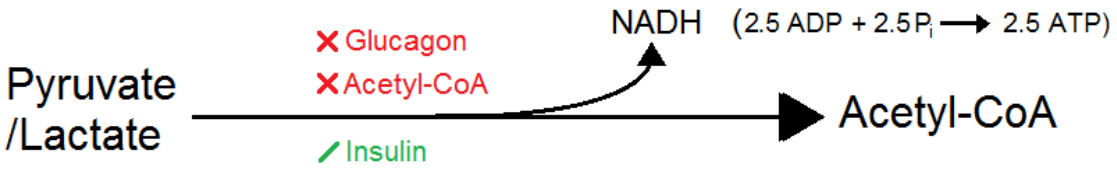

The conversion of pyruvate to acetyl-CoA is mediated by PDC. PDC is allosterically inhibited by acetyl-CoA to ensure that excessive acetyl-CoA does not enter the citrate cycle causing mitochondrial stress. PDC also converts a mitochondrial NAD+ to NADH allowing for the production of 2.5 ATP molecules through the ETC.

$$K_{PDH}^{max} = \left(1 + \frac{Ins}{Ins_{ref}^{asyn}} - \frac{Glcgn}{Glcgn_{ref}^{asyn}}\right)$$

$$\frac{v_{asyn} * K_{PDH}^{max} * Lac}{K_M^{Lac} + Lac}\left(1 - \frac{ACoA}{ACoA + k_i^{CoA-inhib}}\right)$$

$k_i^{CoA-inhib}$ = 35 μM [442]

K_M^{Lac} = 540, Ins_{ref}^{asyn} = 1.33nM, $Glcgn_{ref}^{asyn}$ = 375pM – *set so that the model simulations match the data in references [141, 425-431, 434, 435, 443, 444] for plasma concentrations of key glucose and lipid metabolism molecules throughout a daily feeding cycle [425] (section S1.1.4), after a glucose load [434] (section S1.2.2) and after a mixed meal [428] (section S1.1.2), for average hepatic glucose metabolism intermediate concentrations including acetyl-CoA, pyruvate, glucose, G6P, lactate, G3P and GADP [426, 427, 429, 430] (section S1.1.1), for average concentrations of FFAs and triglycerides in individuals of varying weight and with varying insulin sensitivities [141, 435] (section S1.2.1), and for the rates of glucose use in the various pathways after intake in the presence or absence of hormones [431, 443, 444] (section S1.1.3).*

2.2.3.5.2 Acetyl-CoA production from FAs (β-oxidation)

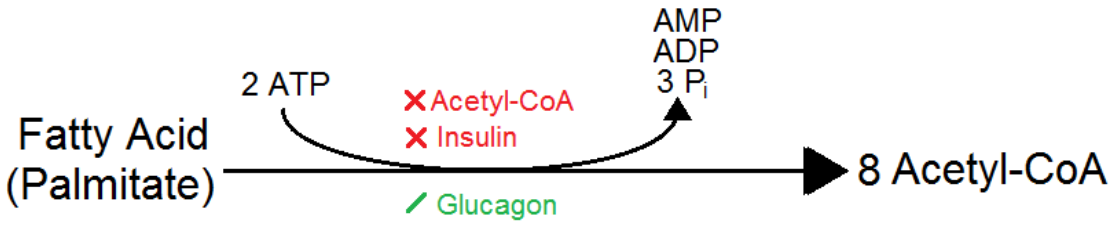

In β-oxidation, acetyl-CoA molecules are produced from the breakdown of FAs. *In vivo*, numerous FAs are found with varying chain lengths and with varying properties. As discussed, in the model all FAs are synthesized from 8 acetyl-CoA molecules corresponding to palmitate, the most common FA in animals. Initially the FA is combined with a CoA molecule requiring the conversion of an ATP to AMP. An additional ATP molecule is required to transport the resulting acyl-CoA into the mitochondria, where it is sequentially broken down. The transfer across the mitochondrial membrane, mediated by carnitine palmitoyltransferase 1 (CPT1), is considered to be rate-limiting in this process. β-oxidation is allosterically inhibited by its product acetyl-CoA to ensure a steady acetyl-CoA supply for the citrate cycle [445, 446].

$$K_{\beta oxi}^{max} = \left(1 - \frac{Ins}{Ins_{ref}^{\beta oxi}} + \frac{Glcgn}{Glcgn_{ref}^{\beta oxi}}\right)$$

$$\frac{v_{\beta oxi} * K_{\beta oxi}^{max} * FA}{K_M^{FA} + FA}\left(\frac{ATP}{(K_M^{ATP} + ATP)}\right)\left(1 - \beta_{inh}\frac{ACoA}{ACoA + k_i^{CoA-inhib}}\right)$$

K_M^{FA}=5 μM – it is difficult to define a single K_M value for all FAs. K_M values for palmitate and a few additional FAs are provided below for fatty acid synthetase, the enzyme responsible for the initial activation of the FFA with CoA, when measured in rats. All K_M values are in the range 1-10μM. 5-8.6μM Palmitate (16:0) [447]; 3.6-8.6μM Palmitate (16:0), 3-8.6μM Oleate (18:1), 6.5-10μM Arachidonate (20:4) [448]; 2.78μM Palmitate (16:0), 2.04μM Palmitoleate (16:1), 1.39 μM Oleate (18:1), 2.22μM Linoleate (18:2), 1.64μM Linolenate (18:3) [449].

K_M^{ATP} = 87μM [450]

$k_i^{CoA-inhib}$ = 47.8μM, [451] β_{inh} = 0.4 [451]

$Ins_{ref}^{\beta oxi}$ = 666.7pM, $Glcgn_{ref}^{\beta oxi}$ = 875pM - set so that the model simulations match the data in references [141, 425-431, 434, 435, 443, 444, 452, 453] for plasma concentrations of key glucose and lipid metabolism molecules throughout a daily feeding cycle [425] (section S1.1.4), after a glucose load [434] (section S1.2.2) and after a mixed meal [428] (section S1.1.2), for average hepatic glucose metabolism intermediate concentrations including acetyl-CoA, pyruvate, glucose, G6P, lactate, G3P and GADP [426, 427, 429, 430] (section S1.1.1), for average concentrations of FFAs and triglycerides in individuals varying weight and with varying insulin sensitivities [141, 435] (section S1.2.1), and for the rates of lipid and glucose use in the various pathways after intake in the presence or absence of hormones [431, 443, 444, 452, 453] (sections S1.1.3, S1.3).

2.2.3.6 Oxidative phosphorylation and the energy molecules

2.2.3.6.1 Oxidative phosphorylation/the citrate cycle

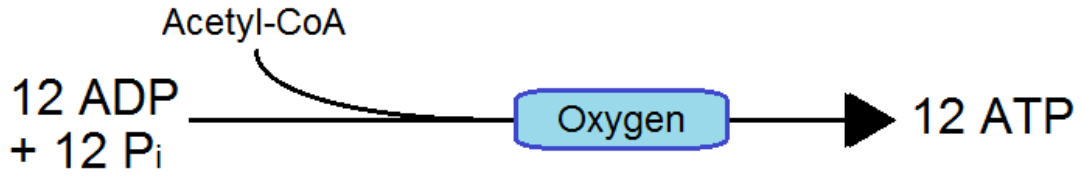

Rather than modelling the citrate cycle and ETC in detail, they are represented by a single equation. For each acetyl-CoA molecule that enters the citrate cycle, 12 ATP molecules are produced from ADP and P_i (based on the system working slightly below its maximum efficiency yield of 14 ATP per acetyl-CoA). An oxygen dependence is included based on the plasma oxygen concentration reaching the cells.

$$\frac{v_{ATPS} * ACoA}{K_M^{ACoA} + ACoA} * \frac{Oxy_B}{K_M^{Oxy_B} + Oxy_B} * \frac{Phos}{K_M^{Phos} + Phos} * \frac{ADP}{K_M^{ADP} + ADP}$$

K_M^{ACoA} = 0.4 μM – [454] (measured in heart)

$K_M^{Oxy_B}$ = *28mmHg for the oxygen concentration in the blood near the cell, based on the value of 14mmHg from Matsumura et al. [93] which was doubled since it is estimated the the blood concentration of oxygen reaching cells is half of the average concentration in the sinusoid [94].*

K_M^{Phos} = *3830mM based on the average phosphate concentration in the model – The constant hasn't been measured for humans in the literature and widely ranging values have been measured for other organisms (8.9mM [455], 0.55mM [456], ~10mM [457]). However, when simulating normal conditions, less than a 5% change in phosphate concentration is seen throughout the day, so ATP production is not strongly affected by phosphate concentration in the model.*

K_M^{ADP} = *410 µM – not measured in human or other mammals, based on data for thermophilic Bacillus PS3 [455].*

2.2.3.6.2 Nucleoside Diphosphate Kinases

Nucleoside diphosphate kinases (NDKs) mediate the exchange of phosphate groups between various nucleoside di- (and tri-) phosphates. K_M values were taken from the literature whilst the rate constants were fitted to average values for the 3 sets of di- and tri- phosphates included in the model.

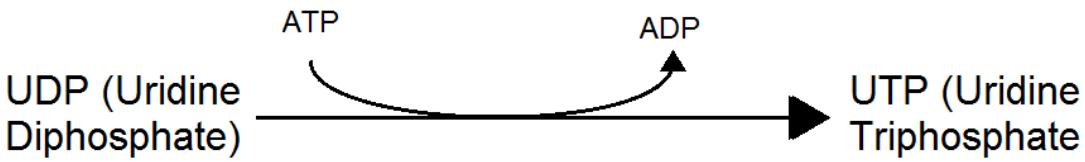

$$v_{NDKG}\left(\frac{ATP * GDP}{(K_M^{ATP} + ATP)(K_M^{GDP} + GDP)} - \frac{ADP * GTP}{(K_M^{ADP} + ADP)(K_M^{GTP} + GTP)}\right)$$

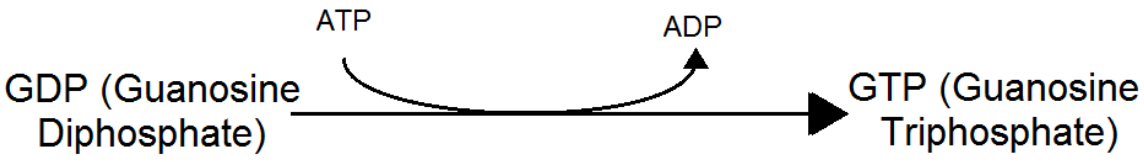

$$v_{NDKU}\left(\frac{ATP * UDP}{(K_M^{ATP} + ATP)(K_M^{UDP} + UDP)} - \frac{ADP * UTP}{(K_M^{ADP} + ADP)(K_M^{UTP} + UTP)}\right)$$

K_M^{ATP} = 290μM (200-380μM [458]), K_M^{GDP} = 33.5μM (31-36 [459]), K_M^{ADP} = 24μM [458], K_M^{GTP} = 120μM [458], K_M^{UDP} = 175μM (160-190 [459]), K_M^{UTP} = 21.5mM (16-27mM [460]).

2.2.3.6.3 Adenosine Kinase

Adenosine kinase (AK) mediates the bi-directional transfer of a phosphate from ATP to AMP, providing two ADP. K_M values were taken from the literature whilst the rate constant was fitted to experimental data for average hepatic ATP, AMP and ADP concentrations

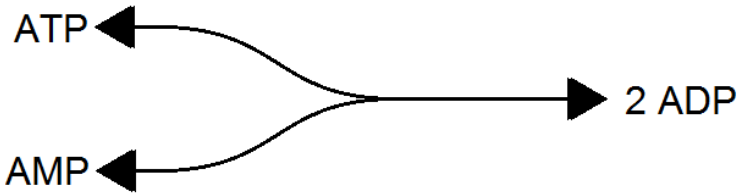

$$v_{AK}\left(\frac{ATP * AMP}{(K_M^{ATP} + ATP)(K_M^{AMP} + AMP)} - \frac{ADP^2}{\left(K_M^{ADP^2} + ADP^2\right)}\right)$$

K_M^{ATP} = 90μM [461], K_M^{AMP} = 80μM [461], K_M^{ADP} = 110μM [461].

2.2.3.6.4 Additional ATP Consumption

2.2.3.6.4.1 Cellular ATP usage term

ATP is consumed by hepatic processes other than the glucose and lipid metabolism represented in the model. A single Michaelis-Menten type equation was introduced to represent this consumption of ATP. The rates of ATP production and use were fitted so that the average ATP, ADP and P_i concentrations matched that measured in [429] (section S1.1.1). Additionally, Ainscow and Brand performed a study in which they determined the relative rates of various processes under conditions of rapid glycogen breakdown in cultured hepatocytes [444] (section S1.1.3). Under these conditions, 10% of G6P derived from glycogen breakdown entered glycolysis but was not released as lactate (46% overall entered glycolysis). Of this 10%, the vast majority would be expected to have entered the citrate cycle given that a very low rate of lipogenesis was measured. This allows an estimation of the

rate of use of glucose for ATP production. Finally, the simulated data were compared with experimental data published by Edgerton *et al.* for the rates of various metabolic processes in canine livers under varying insulin concentrations [443], and by Mandarino *et al.* for the rates of glucose disposal and glucose oxidation and β-oxidation in muscle cells experiencing different insulin concentrations [431] (section S1.1.3). While the liver derives a higher percentage of its energy from plasma FFAs than muscle, this gives an idea of the effects of hormonal stimulation.

$$\frac{v_{atpuse} * ATP}{(K_M^{ATP} + ATP)}$$

K_M^{ATP} = 2500 – roughly equal to the average ATP concentration in pericentral compartment.

2.2.3.6.4.2 Control of cellular phosphate levels

The rate of cytosolic phosphate production or usage in glucose metabolism is strongly dependent on the feeding state and, in initial simulations, the concentration varied massively over time. As a result, an additional heuristic term was added representing the control of the cytosolic phosphate concentration.

$$v_{con}(P_i - ref_{P_i})$$

v_{con} = 0.1, ref_{P_i} = 4.15mM fitted so that the average phosphate concentration matched that presented in Veech et al. [429] and didn't fluctuate significantly from this value under different feeding conditions (section S1.1.1).

2.2.3.7 Lipogenesis

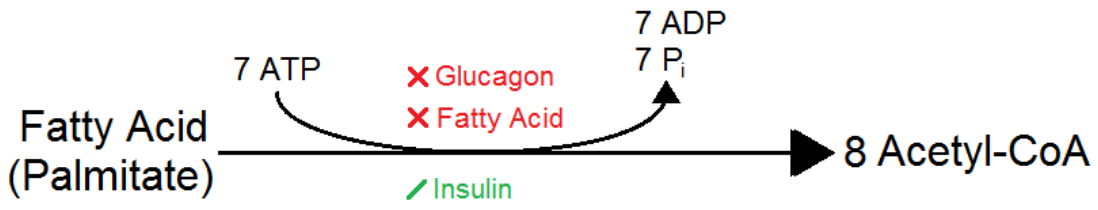

An acetyl-CoA molecule is converted to malonyl-CoA by ACC before combining with a second acetyl-CoA molecule under the influence of FAS. FAS then mediates the addition of subsequent malonyl-CoA molecules forming the FA chain. Of the two ACC isoforms, only ACC1 contributes to lipogenesis. The malonyl-CoA produced by mitochondrial ACC2 is physically separated from FAS under normal physiological conditions and, instead, is involved in the allosteric inhibition of β-oxidation [462]. In the model, all FAs are produced from 8 acetyl-CoA molecules corresponding to palmitate (16:0). Lipogenesis is allosterically inhibited by various FAs.

$$K_{lgen}^{max} = \left(1 + \frac{Ins}{Ins_{ref}^{lgen}} - \frac{Glcgn}{Glcgn_{ref}^{lgen}}\right)$$

$$\frac{v_{lgen} * K_{lgen}^{max} * ACoA}{K_M^{ACoA} + ACoA} * \frac{ATP}{K_M^{ATP} + ATP}\left(1 - \frac{FA}{FA + k_i^{FA-inhib}}\right)$$

K_M^{ACoA} = 58μM [463] for ACC. FAS also directly requires acetyl-CoA in the initial step of lipogenesis where an acetyl-CoA molecules is joined with a malonyl-CoA molecule before additional malonyl-CoA molecules are added to the FA chain. However, the K_M value for FAS is very low such that under normal physiological conditions further increase in acetyl-CoA will not increase the rate. Instead, FAS is rate limited by the malonyl-CoA produced by ACC [464, 465].

$K_m^{FA-inhib}$ = 300μM, Ins_{ref}^{lgen} = 8000pM, $Glcgn_{ref}^{lgen}$ = 875pM – set so that the model simulations match experiment data for plasma concentrations of key glucose and lipid metabolism molecules throughout a daily feeding cycle [139, 425] (sections S1.1.4, S1.2.1), after a glucose load [434] (section S1.2.2) and after a mixed meal [428] (section S1.1.2), for average hepatic glucose metabolism intermediate concentrations including acetyl-CoA, pyruvate, glucose, G6P, lactate, G3P and GADP [426, 427, 429, 430] (section S1.1.1), for average plasma concentrations of FFAs and triglycerides in individuals varying weight and with varying insulin sensitivities [141, 435, 466] (section S1.2.1), for the hepatic triglyceride concentration [211] (section S1.1.1), and for the effects of insulin and glucagon on the rate of lipogenesis and activity of ACC (in adipose tissue rather than liver) [467-469].

K_M^{ATP} = 120μM [463].

2.2.3.8 Triglyceride Synthesis and Breakdown

2.2.3.8.1 Triglyceride Synthesis

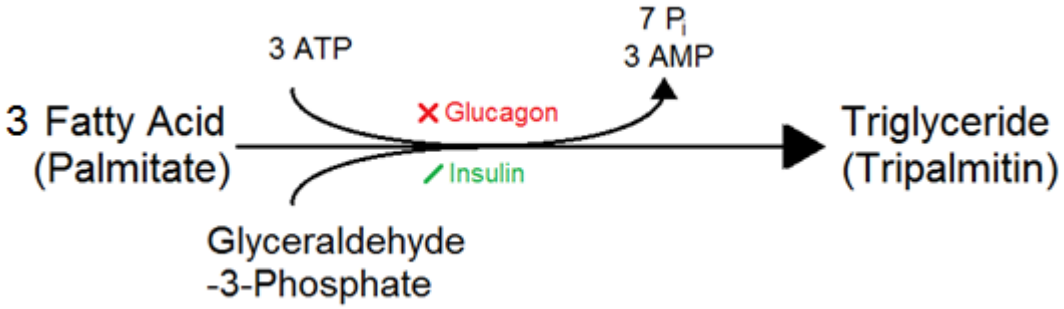

Each FFA must be joined with a coenzyme A (CoA) to form acyl-CoA before being used for triglyceride synthesis, requiring the conversion of 3 ATP molecules to AMP. An acyl-CoA is attached to a glycerol backbone derived from glycerol-3-phosphate (G3P) by G3P-acyltransferase forming a monoacylglycerol. Since conversion between G3P and GADP is rapid and reversible they are represented by a single combined variable in the model. Another two acyl-CoA molecules are sequentially added by acyltransferases forming DAGs followed by triglycerides. In the model these conversions are currently represented by one equation rather than as individual reactions. Triglyceride synthesis is promoted by insulin and inhibited by glucagon. Note that DAGs are also used to produce various phospholipids not currently included in the model.

$$K_{tsyn}^{max} = \left(1 + \frac{Ins}{Ins_{ref}^{tsyn}} - \frac{Glcgn}{Glcgn_{ref}^{tsyn}}\right)$$

$$\frac{v_{TGsyn} * K_{tsyn}^{max} * FA}{K_M^{FA} + FA} * \frac{GADP}{K_M^{GADP} + GADP}$$

K_M^{GADP} = 460μM [470].

$Glcgn_{ref}^{TGsyn}$ = 500pM, Ins_{ref}^{TGsyn} = 1.066nM – set so that the model simulations match experiment data for plasma concentrations of key glucose and lipid metabolism molecules throughout a daily feeding cycle [139, 425] (sections S1.1.4, S1.3.1), after a glucose load [434] (section S1.2.2) and after a mixed meal [428] (section S1.1.2), for average hepatic glucose

metabolism intermediate concentrations including acetyl-CoA, pyruvate, glucose, G6P, lactate, G3P and GADP [426, 427, 429, 430] (section S1.1.1), for average plasma concentrations of FFAs and triglycerides in individuals varying weight and with varying insulin sensitivities [141, 435, 466] (section S1.2.1), for the hepatic triglyceride concentration [211] (section S1.1.1), and for the effects of hormones on the rate of triglyceride synthesis and the activities of various triglyceride synthesis enzymes (in adipose tissue rather than liver) [467, 471].

K_M^{FA} = 645μM – as discussed for β-oxidation, it is not possible to measure a single K_M value for all FFAs in general. The value used is high relative to the low cellular FFA concentration such that the dependence of the rate on the concentration is almost linear. This ensures that triglyceride synthesis increases and falls when hepatic FFA concentrations fluctuate throughout the day.

2.2.3.8.2 Lipolysis

Each triglyceride is broken down to three FFAs and a glycerol molecule by a sequence of lipases (predominantly rate limited by the first enzyme in the chain, triacylglycerol lipase [472]. Hepatic lipolysis is stimulated by glucagon and suppressed by insulin.

$$K_{lply}^{max} = \left(1 - \frac{Ins}{Ins_{ref}^{lply}} + \frac{Glcgn}{Glcgn_{ref}^{lply}}\right)$$

$$\frac{v_{lply} * K_{lply}^{max} * TG}{K_M^{TG} + TG}$$

K_M^{TG} = 50.715mM – It is difficult to base a K_M value on experimentally measured values since numerous triglycerides exist and widely ranging K_M values are measured for both different triglycerides and in different studies of the same triglyceride (e.g. tripalmitin (three palmitic acids attached to a glycerol backbone) [473, 474]). A relatively high value was chosen relative to the average hepatic concentrations such that increases in hepatic triglyceride levels cause

increased lipolysis. However, since the rate of lipolysis is very slow in hepatocytes, hepatic lipolysis is not a major determinant of the hepatic or plasma triglyceride concentrations and has very little effect on the rest of hepatic metabolism. When triglyceride breakdown is required this predominantly occurs in adipose tissue.

Ins_{ref}^{lply} *= 1.067nM,* $Glcgn_{ref}^{lply}$ *= 625pM – set so that the model simulations match experiment data for plasma concentrations of key glucose and lipid metabolism molecules throughout a daily feeding cycle [139, 425] (sections S1.1.4, S1.2.1), after a glucose load [434] (section S1.2.2) and after a mixed meal [428] (section S1.1.2), for average plasma concentrations of FFAs and triglycerides in individuals varying weight and with varying insulin sensitivities [141, 435, 466] (section S1.2.1), for the hepatic triglyceride concentration [211] (section S1.1.1), and for the effects of hormonal regulation on triglyceride synthesis [467] (section S1.1.1 – discussed but not presented).*

2.2.3.8.3 Conversion of glycerol of G3P/GADP

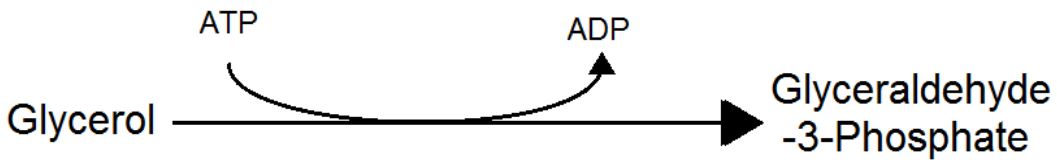

Glycerol is converted G3P by glycerol kinase requiring the conversion of ATP to ADP. G3P is then rapidly and reversible converted to GADP.

$$\frac{v_{gconv} * Glycerol}{K_M^{Glycerol} + Glycerol} * \frac{ATP}{K_M^{ATP} + ATP}$$

K_M^{Gly} *= 41µM – 36-46µM measured in rat [475]*

K_M^{ATP} *= 15µM – no data for human, ranging from 6µM to 3mM for different bacteria (BRENDA enzyme database). Changes in the glycerol concentration are very small compared to the glucose, lactate and lipid concentrations so changes in the parameters defining this term do not have a large effect on the system as a whole.*

2.2.3.9 Membrane Transport

2.2.3.9.1 Lactate

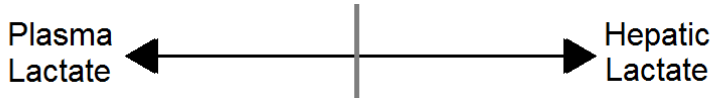

Lactate uptake/output is represented through a diffusion term dependent on the relative blood and cytoplasmic lactate concentrations.

$$\frac{v_{lact} * (Lac_B - Lac_C)}{(K_M^{Lac} + Lac_B + Lac_C)}$$

K_M^{Lac} = 1.2mM – Roughly equal to the average lactate concentration. K_M^{Lac} and v_{lact} were set so that the model simulations match the experimental data for plasma concentrations of glucose and lactate throughout a daily feeding cycle [425] (section S1.1.4), after a glucose load [434] (section S1.2.2) and after a mixed meal [428] (section S1.1.2), for average hepatic glucose metabolism intermediate concentrations including glucose, G6P, pyruvate, lactate, G3P and GADP [426, 427, 429, 430] (section S1.1.1), and for the rates of glucose use in the various pathways after intake in the presence or absence of hormones [431] (section S1.1.3).

2.2.3.9.2 Free Fatty Acids

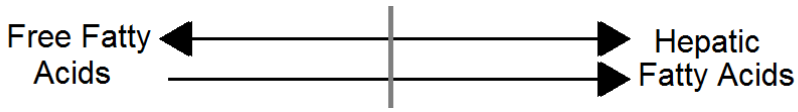

FFA uptake is complex and not fully understood [29]. It is known FA transport proteins FATP2 and FATP5 play an important role since uptake is reduced in mice lacking either protein [27-29]. Additionally, overexpression of scavenger receptor CD36 (known to occur in NAFLD) promotes increased uptake [30-32]. Knockout of liver-type FA binding protein also reduces FFA uptake [33]. Passive, unfacilitated diffusion also contributes to hepatic uptake although this process is relatively slow [476, 477]. Once FFAs enter the liver they are rapidly bound to a CoA molecule to form acyl-CoA preventing efflux. Cellular FFAs are rapidly utilized in β-oxidation or attached to a glycerol backbone to form di- and triglycerides. As a result, the hepatic concentration is low (<50μM).

Insulin causes increased FFA uptake by stimulating FATPs [478-480]. In the model, FFA uptake is represented by two terms. Firstly, an insulin-dependent, unidirectional uptake term corresponding to the active scavenging by transport proteins. Secondly a non-hormone dependent, bidirectional term accounting for both unfacilitated diffusion and bidirectional facilitated diffusion. Given that the cellular concentration is very small compared to the plasma concentration, these both act strongly as uptake terms, even when simulating IR.

$$\frac{v_{active} * FFA_B}{\left(K_M^{active} + FFA_B\right)}\left(1 + \frac{Ins}{Ins_{ref}^{active}}\right) + \frac{v_{diff} * (FFA_B - FFA_C)}{\left(K_M^{diff} + FFA_B + FFA_C\right)}$$

K_M^{active} = 2μM, K_M^{diff} = 200μM, Ins_{ref}^{active} = 21.333pM – set so that the model simulations match experiment data for plasma concentrations of key glucose and lipid metabolism molecules throughout a daily feeding cycle [139, 425] (sections S1.1.4, S1.2.1), after a glucose load [434] (section S1.2.2) and after a mixed meal [428] (section S1.1.2), for average hepatic glucose metabolism intermediate concentrations including acetyl-CoA, pyruvate, glucose, G6P, lactate, G3P and GADP [426, 427, 429, 430] (section S1.1.1), for average plasma concentrations of FFAs and triglycerides in individuals varying weight and with varying insulin sensitivities [141, 435, 466] (section S1.2.1), for the rates of lipid and glucose use in the various pathways after intake in the presence or absence of hormones [443] [431, 444, 452, 453] (sections S1.1.3, S1.3), for the hepatic triglyceride concentration [211] (section S1.1.1), and for the effects of hormones on the rate of lipogenesis and release, and the activities of various lipogenic enzymes (in adipose tissue rather than liver) [467, 471].

2.2.3.9.3 Triglycerides

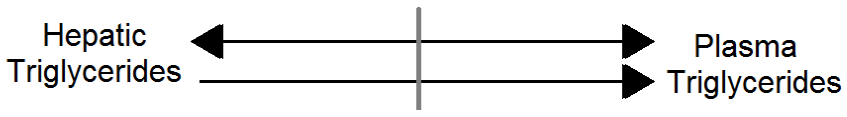

Two terms represent movement of triglycerides between the cytoplasm and the blood stream. The first term represents the production and release of VLDL. Liver is the major organ responsible for packaging triglycerides into VLDL such that this is the major cause of triglyceride output from the cell

[481]. It should be noted that, in the model, once triglycerides are in the blood, free triglycerides along with triglycerides contained in lipoproteins are represented by a single variable. The second term represents very slow uptake of triglycerides from transporter molecules in the plasma and the slow output in forms other than VLDL. It has been shown in numerous species that hepatocytes are able to uptake triglycerides from plasma lipoproteins, although the proteins involved in the transport have yet to be fully characterised [482-484]. Therefore, a simple bidirectional Hill function with K_M value based on the average plasma and hepatic triglyceride concentration was used. Since the hepatic triglyceride concentration is much higher than the plasma concentration (healthy livers store up to 5% fat), a conversion constant TG_{ref} was included to ensure this bi-directions transfer term did not result in constant output.

$$-\frac{v_{VLDL} * TG_C}{(K_M^{VLDL} + TG_C)} + \frac{v_{diff} * \left(TG_B - \frac{TG_C}{TG_{ref}}\right)}{\left(K_M^{diffi} + TG_B + \frac{TG_C}{TG_{ref}}\right)}$$

K_M^{VLDL} = 33.81mM, K_M^{diffi} = 1mM, TG_{ref}=33.81 – Roughly equal to experimental data for average plasma [141, 435, 466] (section S1.2.1), and hepatic TG concentrations [211] (section S1.1.1). Due to the slow rate of lipogenesis, short-term variations in the hepatic concentration have little effect on the rest of metabolism.

2.2.3.9.4 Glycerol

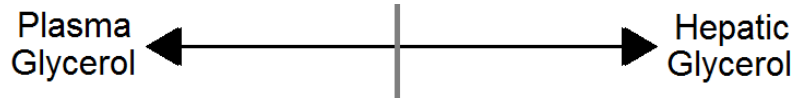

Glycerol released primarily by WAT during lipolysis is cleared from the blood by hepatocytes. Uptake is represented by a simple diffusion term.

$$\frac{v_{Glyct} * (Glyc_B - Glyc_C)}{\left(K_M^{Glyc} + Glyc_B + Glyc_C\right)}$$

K_M^{Glyc} = 270μM (250-402μM measured in rat [475]) – In simulations, glycerol kinase is rate-limiting in glycerol clearance rather than uptake such that moderate changes in K_M^{Glyc} do not have a large effect on the overall rate of uptake.

2.2.4 Adipose Tissue, Muscle and Dietary Inputs and Outputs

In addition to the liver, organs including the intestine, adipose tissue and muscle play important roles in FFA and glucose metabolism and consumption required for the model to produce realistic data. Given that the focus of this report is on hepatic metabolism rather than the gut or adipose tissue, rather than treating these organs as separate compartments containing complex sets of pathways, a minimal representation of these lipid metabolism processes was included which produces plasma lipid levels consistent with those measured experimentally in metabolically normal and insulin resistant individuals, but does not include the changes occurring in the concentrations of metabolites within the adipose tissue.

Lipids enter the body compartment of the model as FFAs. A single equation then calculates the synthesis of triglycerides in the gut (and other organs in the body excluding liver). Two equations represent adipose lipogenesis and adipose lipolysis. A final equation represents insulin dependent FFA uptake by muscle and other body cells. Since a separate adipose tissue compartment was not included in the model, adipose lipid storage could not be included. Instead, the adipose and muscle equations act directly on the blood concentrations of glucose, FFAs and triglycerides. The constants in these equations were fitted by eye so that the FFA and triglyceride concentrations matched those measured throughout the day for healthy patients by Daly *et al.* [425] (section S1.1.4), so that the average FFA and triglyceride concentrations matched those measured for diabetic and non-diabetic patients by Sindelka *et al.* [141] and Berndt *et al.* [435] (section S1.2.1) and so that the contribution of *de novo lipogenesis* to hepatic and plasma triglyceride content matched that presented by Donnelly *et al.* [26].

2.2.4.1 Adipose and Gut Equations

2.2.4.1.1 *De novo* synthesis

De novo FA synthesis is represented by a single equation in which 4 glucose molecules, and hence 8 acetyl-CoA molecules, are converted to a FFA.

$$\frac{v_{dnWAT} * G_B}{K_M^{G_B} + G_B}\left(1 + \frac{Ins}{Ins_{ref}^{dnWAT}} - \frac{Glcgn}{Glcgn_{ref}^{dnWAT}}\right)$$

$K_M^{G_B}$= 4.5mM, Ins_{ref}^{dnWAT}=1.87nM, $Glcgn_{ref}^{dnWAT}$=250pM

2.2.4.1.2 Triglyceride Synthesis and Lipolysis

When representing gut triglyceride synthesis and adipose lipolysis, time constants needed to be added to slow the effect of hormones. This is to compensate for the fact that adipose triglyceride storage was not included in the model. In initial model building, the rates of triglyceride synthesis and lipolysis were set to depend only on the current plasma insulin and glucagon concentrations (as with the rest of the equations in the model). However, this led to the rapid breakdown of triglycerides and a large spike in FFA concentration as soon as glucose concentrations dropped between meals. Instead, *in vivo*, the FFA concentration increases more steadily over time between meals, and FFAs continue to be released until the next meal (or lipid stores begin to empty). The difference between the simulated and experimental data is likely to be accounted for by the release of stored adipose triglycerides, not accounted for in the model. After the addition of time constants to account for this, the simulated FFA concentration was consistent with the values measured by Daly *et al.* [425], Sindelka *et al.* [141] and Berndt *et al.* [435] without the need to include adipose lipid storage.

2.2.4.1.2.1 Triglyceride Synthesis

Three FFAs attached to a G3P backbone corresponding to half of a blood glucose molecule to form a triglyceride.

$If\left(\frac{Glcgn}{Glcgn_{ref}^{trisyn}} - v_G\right) > 0$; then: $\frac{dv_G}{dt} = \frac{\left(\frac{Glcgn}{Glcgn_{ref}^{trisyn}} - v_G\right)}{\tau_G{}^{up}}$; else: $\frac{dv_G}{dt} = \frac{\left(\frac{Glcgn}{Glcgn_{ref}^{trisyn}} - v_G\right)}{\tau_G{}^{down}}$

$If\left(\frac{Ins}{Ins_{ref}^{trisyn}} - v_I\right) > 0$; then: $\frac{dv_I}{dt} = \frac{\left(\frac{Ins}{Ins_{ref}^{trisyn}} - v_I\right)}{\tau_I{}^{up}}$; else: $\frac{dv_I}{dt} = \frac{\left(\frac{Ins}{Ins_{ref}^{trisyn}} - v_I\right)}{\tau_I{}^{down}}$

$$v_{trisynH} = v_{trisyn} * (1 + v_I - v_G)$$

$$\frac{v_{trisynH} * G_B}{K_M^{G_B} + G_B} \frac{FFA}{K_M^{FFA} + FFA}$$

$K_M^{G_B}$=10mM, K_M^{FFA}=645mM, Ins_{ref}^{trisyn}=800pM, $Glcgn_{ref}^{trisyn}$=37.5pM

$\tau_I{}^{up}$ =1000s^{-1}, $\tau_I{}^{down}$ =15000s^{-1}, $\tau_G{}^{up}$=10000s^{-1}, $\tau_G{}^{down}$=700s^{-1}

2.2.4.1.2.2 Lipolysis

A triglyceride is removed from the blood and broken down into three FFAs and a glycerol.

$If\left(\frac{Glcgn}{Glcgn_{ref}^{lipoly}} - v_G\right) > 0$; then: $\frac{dv_G}{dt} = \frac{\left(\frac{Glcgn}{Glcgn_{ref}^{lipoly}} - v_G\right)}{\tau_G{}^{up}}$; else: $\frac{dv_G}{dt} = \frac{\left(\frac{Glcgn}{Glcgn_{ref}^{lipoly}} - v_G\right)}{\tau_G{}^{down}}$

$If\left(\frac{Ins}{Ins_{ref}^{lipoly}} - v_I\right) > 0$; then: $\frac{dv_I}{dt} = \frac{\left(\frac{Ins}{Ins_{ref}^{lipoly}} - v_I\right)}{\tau_I{}^{up}}$; else: $\frac{dv_I}{dt} = \frac{\left(\frac{Ins}{Ins_{ref}^{lipoly}} - v_I\right)}{\tau_I{}^{down}}$

$$v_{lipolyH} = v_{lipolysis} * (1 - v_I + v_G)$$

$$\frac{v_{lipolyH} * TG_B}{K_M^{TG_B} + TG_B}$$

$K_M^{TG_B}$= 2mM, $Ins_{ref}^{lipolysis}$= 800pM, $Glcgn_{ref}^{lipolysis}$=37.5pM

$\tau_I{}^{up}$=1000s^{-1}, $\tau_I{}^{down}$=15000s^{-1}, $\tau_G{}^{up}$=10000s^{-1}, $\tau_G{}^{down}$=700s^{-1}

2.2.4.2 Input

Carbohydrates are broken down to sugars before entering the blood stream. Dietary lipids are broken down to FFAs before being absorbed by the enterocytes of the intestinal wall. Short to medium chain

FFAs can enter directly into the portal vein. Longer chain FFAs are converted back into triglycerides and released into the bloodstream as chylomicrons via the lymph system, although some long chain FFAs have been shown to enter directly to the portal vein [485]. In the model, all dietary carbohydrates enter the bloodstream as glucose, whilst lipids enter the blood as FFAs. A triglyceride synthesis term represents both the reforming of triglycerides in the gut, and triglyceride synthesis around the body.

Glucose and FFA inputs of any form can be inputted to the model. Throughout this report, spiked glucose and FFA inputs with a period of 4 hours were used to approximate a daily feeding cycle excluding sleep.

$v_{input} * \sin^6\left(\frac{pi}{2(hours)}\right)$ -> Spiked inputs with 4-hour period

The additional changes to hormone release and energy metabolism occurring during sleep or prolonged starvation in addition to exercise were considered beyond the scope of the model at present. When simulating a moderate diet, the inputs were based on the average meal values in Daly *et al.* [425]. In this study, the three meals provided to subjects each day (breakfast, lunch and dinner) contained an average of 78.1g of carbohydrate and 22.2g of fat. In terms of the energy provided from these two sources this was a ratio of 1.648 to 1. When running the simulations, the size of the glucose and FFA inputs were set to match these values. Each intake cycle was set to provide 86.74mmoles of glucose per litre of blood into the body compartment. Presuming a blood volume of 5L, this corresponds to 78.1g. Since FFAs have a range of molar masses, the FFA input to the model in moles could not be calculated from the grams of fat per meal. Instead the relative contribution of glucose and FFAs to energy were used. In the model, each glucose molecules that undergoes glycolysis followed by oxidation provides a net total of 34 ATP. Each palmitate molecules that is oxidised provides a net of 114 ATP. Therefore, to attain the ratio of 1.648:1 provided in the study, the FFA input was set to provide 15.75mmoles of fat per litre of blood per intake cycle to the body compartment. Using the molar mass of palmitate and assuming 5L of total blood this would correspond to 20.2g of

fat. The outputted data are compared with experimental data when simulating this diet in section S1.1.4.

$v_{input}(Glucose)$=19.275μM/s - (78.1g/cycle assuming 5L of blood in the body compartment)

$v_{input}(FFA)$ =3.5μM/s - (20.2g/cycle assuming 5L of blood in the body compartment and the molecular mass of palmitate).

2.2.4.3 Consumption Terms (Muscle and Body cells)

In the model glucose is consumed by cells (outside the liver) according to a simple Hill function with a low K_M constant such that, under normal conditions, glucose is absorbed at a relatively constant rate by muscle and other body cells. In reality, other organs show hormone dependent uptake. However, the focus of this study is on liver which is the major determinant of plasma glucose concentration, hormone dependences of glucose uptake by other tissues around the body were not included.

$$\frac{v_{Gbuse} * G_B}{K_M^{G_B} + G_B}$$

$K_M^{G_B}$=1mM, v_{G_Buse} = 4.93μM/s

The rate of FFA consumption elsewhere in the body was represented by a similar term with the inclusion of an insulin dependence.

$$\frac{v_{FFAuptake} * FFA}{K_M^{FFA} + FFA}\left(\frac{(Ins + k_{Iup})}{(Glgn + k_{Lup})}\right)$$

K_M^{FFA} = 100 μM, k_{Iup} = 250pM, k_{Lup} = 125pM, $v_{FFAuptake}$ = 0.982μM/s

2.2.5 Oxygen and Hormone Inputs and Consumption

2.2.5.1 Hormone release by the pancreas

The representation of pancreatic hormone release developed by Hetherington *et al.* was used to calculate the rate of release of glucagon and insulin into the blood [389]. In this, insulin is only released when the blood glucose is above a threshold. Above this threshold, insulin is released according to a

Hill function acting on the logarithm of the glucose concentration relative to a reference concentration. Similarly, glucagon is only released when the blood glucose concentration is below the threshold. In this case, glucagon is released according to a Hill function acting on the inverse logarithm of the blood glucose concentration.

$$if\ G_B < G_{ref},\ Glucagon\ release = \frac{1}{\tau_{glgn}} \frac{\ln \frac{G_{ref}}{G_B}^{n_{glgn}}}{\left(K_m^{glgn\,n_{glgn}} + \ln \frac{G_{ref}}{G_B}^{n_{glgn}} \right)}$$

$$if\ G_B > G_{ref},\ insulin\ release = \frac{1}{\tau_{ins}} \frac{\ln \frac{G_{ref}}{G_B}^{n_{ins}}}{\left(K_m^{ins\,n_{ins}} + \ln \frac{G_{ref}}{G_B}^{n_{ins}} \right)}$$

Constants as in [389].

2.2.5.2 Hormone degradation across the sinusoid

In the model the hormones are degraded at a constant rate (per unit of hormone) as blood passes through the sinusoid. Experimentally, the concentration of glucagon has been measured to fall by around 50% between the blood entering the sinusoid and the blood exiting it [45]. To match this, the rate of degradation of glucagon was set to 0.03858 per unit of glucagon per second. *In vivo*, the insulin concentration falls by 50% across the sinusoid between meals but by only 15% post-prandially [45]. Since insulin is only released in the model when blood glucose levels are high, only the post-prandial rate of degradation was included and a rate of 0.01389 per unit of insulin per second was used. Therefore, an increase in the insulin to glucagon ratio is seen as blood passes through the sinusoid.

2.2.5.3 Oxygen input and degradation

A constant oxygen input was added to the body compartment along with a constant rate of consumption across the sinusoid. A constant rate of input of 1.35mmHg s^{-1} is provided to the body blood compartment and a constant output of 0.03525s^{-1} per unit of oxygen in each compartment of blood occurs across sinusoid. These were set such that the oxygen concentration falls from 65mmHg in the blood entering the proximal periportal compartment to 35mmHg in the blood leaving the distal

pericentral compartment [50]. Since no changes in oxygen input or blood flow were simulated in this study, the oxygen concentrations across the sinusoid remained fixed at the experimentally measured gradient for a healthy liver. However, the inclusion of a dynamic oxygen calculation may allow the model to be used to study changes in oxygen supply and blood flow in developing liver disease in the future. The rate of oxidative phosphorylation is oxygen dependent in the model, with a K_M value based on the measurements by Matsumura *et al.* [93].

2.2.6 Rate Constants and Zonation

Each equation in the model consists of a rate constant multiplied by a set of substrate, hormone and allosteric dependences. The rate constant for each process has a base-value (v_b) which is then modified in each compartment according to the zonation of the process. The base-values for each process were set by comparing the simulated plasma and average sinusoidal concentration of the various molecules in the model with experimental data from several sources (table 2.3). As discussed in the section 2.2.2.3, the exact rates at which glucose and lipids enter the bloodstream after feeding in experimental studies is unknown. As a result, rather than least-squares fitting the rate constants to any specific data, they were set such that, for a range of data sets, the simulated plasma and hepatic concentrations both quantitatively remained within the experimentally measured ranges and matched qualitative features in the data such as periods of increase or decrease, and appropriately timed peaks and troughs.

To allow for the inclusion of zonated enzyme expression, these base values of the rate constants were next altered in each compartment according to whether the enzymes in each process are known to be up-regulated or down-regulated in that region of the sinusoid.

Zonation is known to be primarily regulated by the blood oxygen concentration [50]. As a result, in the model the blood oxygen concentration is used to assign each compartment a value, z, dictating how periportal-like or pericentral-like the enzyme expression in that compartment is. The following function was used to define z.

$$If\ Oxy > 46.5mmHg\ then\ (\mathrm{z} = \tanh\left(\frac{(Oxy - 46.5)}{12}\right)\ else\ (z = 2 * \tanh\left(\frac{(oxy - 46.5)}{24}\right)$$

This function is plotted in figure 2.3 and was based on the data in Nauck *et al.* [69] and Wolfle and Jungermann [77] in which the concentrations of key periportal and pericentral enzymes were measured at a range of physiological oxygen concentration. A value of roughly z=1 is given at periportal oxygen concentrations (65-75mmHG) and a value of roughly z=-1 is given at pericentral oxygen concentrations (30-35mmHg). These were used as reference points for setting periportal-type and pericentral-type expression.

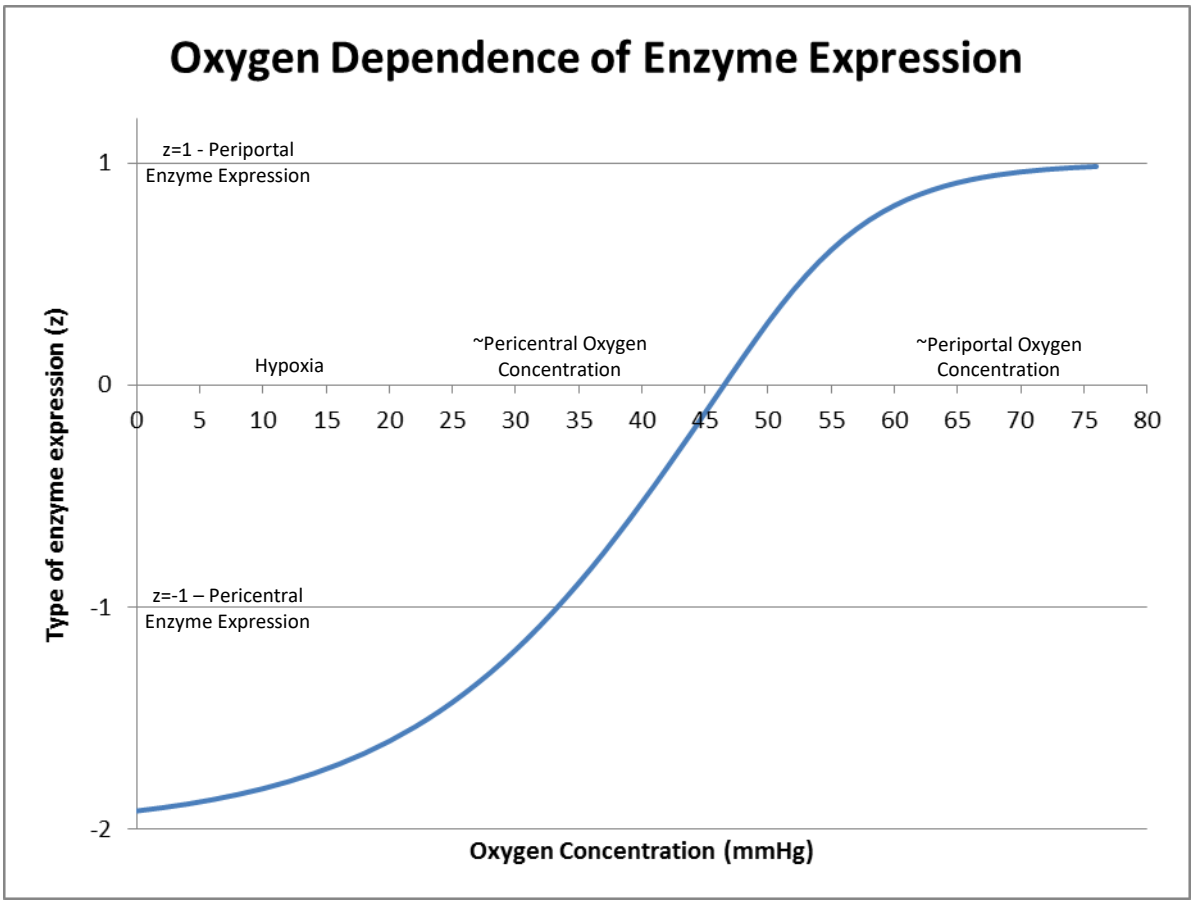

Figure 2.3: The dependence of enzyme expression type (pericentral -> periportal) on oxygen concentration in the model.

As shown in the experimental studies [69, 77], further induction of periportal-type enzymes does not occur at oxygen concentrations above that seen by periportal cells. However, in hypoxic conditions, additional induction of pericentral-type enzymes and suppression of periportal-type enzymes does occur.

Since continuous changes in enzyme expression are seen for all of the processes included in the model, rather than the step-wise changes in, for example, cholesterol synthesis, the zonation of each process could be set based on the experimentally measured periportal to pericentral ratio of the rate limiting enzymes with a continuous change between compartments. For a process where the base-value of the rate constant is v_b and the experimentally measured ratio of periportal expression to pericentral expression is k_{pp}:1, the altered rate constant in compartment x, (vx) is calculated by:

$$v_x = (1 + z_x * k_n)v_b$$

Where:

$$k_n = 1 - \frac{2 * k_{pp}}{|k_{pp}| + 1}$$

This equation gives the experimentally measured periportal: pericentral ratio between compartments with z=1 and z=-1 whilst leaving the average rate constant across the sinusoid unchanged at physiological oxygen concentrations. Table 2.4 shows the experimentally measured periportal to pericentral ratio in activity for the enzymes mediating each process along with the constant k_n used in the model.

Table 2.3: The baseline rate constants used in the model and the experimental data used for fitting.

Rate Constant	Base Value in Model, v_b	Data used for rate constant fitting (See supplementary material S1 for comparisons with experimental data)
Glucose Uptake	$v_{pump} = 118$ μM s^{-1}, $v_{diff}^{glu} = 224$ μM s^{-1},	[425-431, 443, 444, 466] – Concentrations of various glucose metabolism molecules in blood and in liver under a range of conditions:[425] – time series data for plasma concentrations throughout a daily meal cycle (section S1.1.4). [428] – time series data for glucose and glycogen concentrations after a single meal (section S1.1.2). [426, 427, 429, 430] – hepatic concentrations of several energy metabolism intermediates (section S1.1.1). [431, 443, 444] – the relative rates at which lipids and glucose are oxidised and the relative rates of glucose release, glycolysis, lactate release and acetyl-CoA synthesis under conditions of glycogenolysis (section S1.3). Further comparison with the postprandial rates of glucose and FA oxidation is presented in [452, 453] in section S1.3.
GK	v_{gk} = 112 s^{-1}	
G6Pase	v_{G6Pase} = 370 μM s^{-1}	
GS	v_{syn} = 55 μM s^{-1}	
GP	v_{brk}=5 μM s^{-1}	
Glycolysis 1 (PFK)	v_{PFK} = 160 μM s^{-1}	
Glycolysis 2 (PK)	v_{PK} = 87 μM s^{-1}	
Gluconeogenesis 1 (PEPCK)	v_{PEPCK}= 35 μM s^{-1}	
Gluconeogenesis 2 (FBPase)	v_{FBP}=68 μM s^{-1}	
Pyruvate Oxidation (PDC)	v_{asyn}= 15 μM s^{-1}	– set using [426, 427, 429] as a reference for the average cytosolic acetyl-CoA concentration, along with [425-431, 434, 443] for the glucose and lactate concentrations under different conditions, [141, 425, 435] for the FFA and triglyceride concentrations under different conditions and [431, 443, 444, 452, 453] for the relative rates of glucose and FA oxidation (sections S1.1-S1.3).
B-oxidation	$v_{\beta oxi}$= 3.3 μM s^{-1}	

ATP Production through the citrate cycle	v_{ATPS}=520 µM s^{-1}	– set such that the concentrations of the mono- di- and tri- phosphate molecules matched the following average values/ranges: P_i – 3.81 (3.55-4.07)mM [429]; ATP – 2.78 (2.71-2.85)mM [429]; ADP – .885 (.794-.976)mM [486]; AMP – .237 (.200-.272)mM [429]; UTP – .285 (.255-.315)mM [486]; UDP – .108 (.096-.120)mM [486]; GTP – .277 (.266-.288)mM [486]; GDP – .098 (.091-.105)mM [486] Rates of ATP production and consumption were estimated based on the data in [431, 443, 444] (section S1.1.3).
Nucleoside Diphosphate kinases	v_{NDKG}=3000 µM s^{-1} v_{NDKU}=30 µM s^{-1}	
Adenosine Kinase	v_{AK}= 100 µM s^{-1}	
ATP consumption	v_{atpuse} = 173 µM s^{-1}	
Lipogenesis	v_{lgen} = 5.5 µM s^{-1}	Overall lipogenesis (hepatic +WAT) was set such that the plasma concentrations and total lipogenesis rates matched to the data in [139, 425, 428, 466, 467] (see section S1). [426, 427, 429, 430] used as references for hepatic concentrations (section S1.1.1). [26] provides data for the relative contribution of liver to overall lipid metabolism (section 3.3.2.1).
Triglyceride Synthesis	v_{TGsyn}= 10 µM s^{-1}	Set such that the plasma triglyceride and FFA concentrations and overall (hepatic + WAT + gut *etc.*) triglyceride production and degradation matched data in [141, 425, 428, 431, 435, 443, 466, 467, 471] as closely as possible. However, since adipose triglyceride storage is not included in the model, larger variation occurs in the simulated plasma triglyceride concentration throughout each intake/output cycle than is seen *in vivo.* Given that short term variations in plasma triglyceride
Lipolysis	v_{lply}= 0.085 µM s^{-1}	
FFA Uptake	v_{active}^{FFA}=0.08µM s^{-1} v_{diff}^{FFA}= 1.2µM s^{-1}	

Triglyceride Uptake/Output	v_{VLDL}= 0.3μM s^{-1} v_{diff}^{TG}= 0.4μM s^{-1}	concentration have little effect on hepatic metabolism due to the slow rate of triglyceride uptake and lipolysis, emphasis was placed on ensuring the FFA concentration matched the experimentally measured at each time point, whilst only the time-averaged plasma triglyceride value matched the experimental data. The contribution of liver to triglyceride synthesis was based on the data in [26] (section S1.3.3). The hepatic triglyceride concentration was set to match the data in reference [487] (section S1.1.1).
Adipose Lipid Metabolism	v_{dnWAT}= .22μM s^{-1}	
	v_{trisyn}= 8.5μM s^{-1}	
	$v_{lipolysis}$= 2μM s^{-1}	
Glycerol Kinase	v_{gconv}= 5 μM s^{-1}	The average blood glycerol concentration was matched to the data in [425] (section S1.1.4).
Lactate Uptake	v_{lact}= 200 μM s^{-1}	Changes in lactate concentration are largely determined by the effects of hormonal and allosteric regulation on glycolysis. [425-430, 466] were used as reference values blood/hepatic concentrations of lactate and glycolysis intermediates.
Glycerol Uptake	v_{Glyct}= 100μM s^{-1}	Membrane transport is not considered rate limiting in the use of glycerol by hepatocytes. However, the plasma concentration was matched to the experimental data measured by Daly *et al.* [425] (section S1.1.4).

Table 2.4: The zonation of key enzymes in the model.

Process	PP:PC (model)	Zonation of key enzymes (experimental)	References	Zonation Constant (k_n) k_n=0 – no zonation 0<k_n<1 – periportal -1<k_n<0 – pericentral
Glucose Uptake (Glucose -> G6P)	1:2.5	Glucokinase (GK) 1 : 1.5-3.5	[52-61]	-0.429
Glucose Output (G6P -> Glucose)	1.9:1	Glucose-6-Phosphatase (G6Pase) 2.3-1.5 : 1	[54, 62-64]	0.31
Glycogenesis (G6P-> Glycogen)	3:1	Glycogen Synthase (GS) Periportal – no quantitative data found	[66]	0.5
Glycogenolysis (Glycogen -> G6P)	1:1	Conflicting data in literature – perhaps dependent on feeding conditions.	[65, 66]	0 (no zonation)
Glycolysis 1 (Glucose –> GADP)	1:1	6-Phosphofructo-kinase$_L$ (PFK$_L$) 1 : 1-1.3**	[488]** reported as statistically insignificant difference between sections	0 (no zonation)
Glycolysis 2 (GADP –> Pyruvate/Lactate)	1:2.1	Pyruvate Kinase$_L$ (PK$_L$) 1 : 1.66-2.5	Cited in [45] [67]	-0.355
Gluconeogenesis 2 (GADP -> Glucose)	1.75:1	Fructose-bisphosphatase (FBPase) 1.5-2:1	[52, 53, 68]	0.273
Gluconeogenesis 1 (Pyruvate/Lactate –> GADP)	2.4:1	Phosphoenolpyruvate carboxykinase (PEPCK) 1.9-2.9 : 1	Cited in [45] [61, 66, 69-72]	0.412
		Pyruvate Carboxylase 1.72:1	[73]	
Pyruvate Oxidation	1:1	Pyruvate dehydrogenase complex (PDC)	[73]	0 (no zonation)

		1 : 1.69 (insignificant due to large variability, especially in the pericentral compartment)		
Oxidative phosphorylation and the citrate cycle	1.5:1	Cristae volume:2.38:1	[46]	0.2
		Cristae Area: 2.05:1	[46]	
		Succinate Dehydrogenase:1.9:1 Malate Dehydrogenase 1.7:1	[47]	
		Cytochrome c oxidase >1:1	[48]	
Lipogenesis	1:1.6	Acetyl-CoA Carboxylase Fed : 1 : 1.58 (f), 1 : 1.64 (m). Starved: 1 : 1.13 (f), 1 : 1.32 (m). Refed: 1 : 1.61 (f), 1 : 1.60 (m).	[81]	−0.23
		Fatty Acid Synthase Fed 1 : 1.91 (f), 1 : 1.04* (m). Starved: 1 : 1.26* (f), 1 : 1.27* (m). Refed: 1 : 2.39 (f)1 : 1.34 (m).	[88]	
		ATP-dependent dependent citrate lyase Fed: 1 : 2.4 (f), 1 : 1.82 (m). Starved: 1 : 1.47 (f), 1 : 1.64 (m). Refed: 1 : 2.5 (f), 1 : 2.78 (m).	[89]	
		G6P dehydrogenase, 6-phosphogluconate dehydrogenase, Malic enzyme, Isocitrate dehydrogenase, Alcohol dehydrogenase, As a general trend 1 : >1 (pericentral)	For review see [45]	
β-oxidation	1.6:1	β-Hydroxybutyryl-CoA hydrogenase Fed: 1.52 : 1 (f), 1.59 : 1 (m) Starved: 1.58 : 1 (f), 1.80 : 1 (m)	[81, 82]	0.23

		Carnitine palmitoyltransferase-1 1.26 : 1 (in the absence of hormones)	[83]	
		Liver fatty acid binding protein (L-FABP) 1.6 : 1	[84, 85, 489]	
Triglyceride Synthesis	1:1	No data demonstrating zonation in triglyceride synthesis enzymes found		0 (no zonation)
Triglyceride Breakdown	1:1	No data demonstrating zonation in lipolysis enzymes found		0 (no zonation)
Insulin Reception	1:1.35	Insulin Receptor proteins Roughly 1:2 estimated from *in vitro* for physiological glucose concentrations. P.C. distribution demonstrated *in vivo*.	[490]	-0.15
Glucagon Reception	1.35:1	Glucagon Receptor Proteins 1-3.5:1 (for mRNA)	[491]	0.15
FFA membrane transport uptake	1.5:1	L-FABP expression - ~1.5-1.6:1	[84, 85, 489]	0.2

3 Understanding zonated steatosis and damage in NAFLD.

3.1 Introduction to Chapter

In this chapter, the model is used to simulate conditions of high fat intake and IR leading to the development of steatosis across the sinusoid. The major objectives addressed in this chapter were, firstly, to assess the contributions of high intake, IR and additional metabolic dysregulation to NAFLD. Secondly to identify the major differences between periportal and pericentral cells accounting for higher susceptibility to steatosis in pericentral cells. Finally, to identify key metabolic variations accounting for inter-individual differences in susceptibility to steatosis and inter-individual differences in NAFLD development in the model. The graphs in this chapter along with several sections of text were published in Ashworth *et al.* [401].

In adult sufferers of NAFLD, steatosis is often most severe in pericentral cells [15-17]. When assessed by Chalasani *et al.*, 38% of subjects showed steatosis predominantly in pericentral cells, 62% showed azonal or pan-sinusoid steatosis and less than 1% showed steatosis restricted to periportal cells [15]. Additionally, inflammation and fibrosis tend to be more severe towards the pericentral end of the sinusoid [15-17, 377]. When considering the effects of IR, this pattern of lipid build-up could be considered counter intuitive. Pericentral cells specialise in lipogenesis, whilst periportal cells show increased expression of FA uptake proteins. Given the context of reduced insulin stimulation but raised plasma lipid levels and increased hepatic FFA uptake, it would be expected that periportal cells to show the most severe steatosis [380, 492].

A potential solution to this apparent paradox suggested in the literature is that IR could be restricted to glucose metabolism, with insulin signalling remaining intact in lipid metabolism [380, 381]. Consistent with this, increased rates of lipogenesis and triglyceride synthesis are seen in insulin resistant NAFLD patients. Additionally, the expression of the lipid metabolism regulatory protein SREBP-1c, which is stimulated by insulin under metabolically normal conditions, is increased in insulin

resistant NAFLD livers [36-39]. Furthermore, increased expression of ChREBP, an additional transcription factor whose expression is primarily regulated by the presence of sugars, is seen in NAFLD as a result of hyperglycaemia [493, 494]. However, whilst hepatic lipogenesis is increased in NAFLD, it is known that the majority of the lipids in the livers of NAFLD patients arise from uptake, such that an explanation of pericentral-centred steatosis should not be based primarily on increased hepatic lipid production [26, 492, 495, 496]. Additionally, separate pathways for insulin reception required for a duel resistance/sensitivity effect have not been identified, and it is known that the two insulin receptors (IRS-1 and IRS-2) both act on glucose and lipid metabolisms [497-500]. The link between IR and the susceptibility of pericentral cells to steatosis, therefore, remains unexplained.

Fully characterising the development and consequences of metabolic diseases such as NAFLD in cells across the sinusoid experimentally would be a challenging task due to the small size of the sinusoid and the large number of potential variables. As a result, it is pertinent to study the system using a computational model such as the one presented here in order to make predictions and minimise the future experimentation required.

In section 3.3.1 we first assess whether the model can reproduce the changes to hepatic lipid levels, glucose storage and energy metabolism seen in steatotic livers *in vivo* when simulating IR. This provides validation of the model simulations when considering NAFLD, in addition to the comparison with experimental data presented in supplementary material S1 for metabolically normal and insulin resistant individuals. Additionally, the contributions of increased SREBP-1c expression and increased dietary intake to the changes in metabolism occurring in NAFLD were assessed. Ensuring that the model simulations under conditions of high caloric intake and IR are consistent with *in vivo* findings also provides the basis for the simulations run in chapter 4, in which the model is used to study the effects of inhibiting or stimulating various hepatic pathways as potential treatments for NAFLD.

Having validated that the model outputs are consistent with *in vivo* observations for NAFLD, in section 3.3.2 the model is used to investigate the key differences between cells at the periportal and

pericentral ends of the sinusoid that cause pericentral cells to be more susceptible to steatosis. Using the computational model, detailed predictions of the changes in the conversion rates and metabolite concentrations in specific regions of the sinusoid can be made under different feeding conditions for the healthy and disease states.

Finally, inter-individual variation is seen both in susceptibility to steatosis and in the pattern of steatotic build-up. Around 25% of obese individuals fail to develop steatosis whilst 16% of lean individuals show excess liver fat [18], and variation is seen in the predominant location of steatosis from pericentral to azonal or pan-sinusoidal [15-17]. In section 3.3.3, the model is used to identify variations in hepatic metabolism likely to account for these differences. Focussing on hepatic processes, sensitivity analysis was performed on the rate and zonation constants in the model to identify those with the largest effects on hepatic triglyceride and FFA levels.

3.2 Inputs and Model Set up

3.2.1 Inputs

Through this section, the 4-hour spiked input cycle discussed in section 2.2.4.2 was used to represent intake roughly equivalent to a daily feeding cycle excluding sleep. This provides both periods of post-prandial glycogen and triglyceride synthesis and periods of their breakdown to glucose and FFAs between meals. When using this input cycle, simulations were run until equilibrium was reached between subsequent cycles. The average concentrations and rates over each 4-hour cycle are then presented. When simulating a moderate diet the carbohydrate and lipid inputs over each cycle were set to match the average input per meal in a study performed by Daly *et al.* as discussed in section 2.2.4.2. [425].

Because a separate adipose compartment was not included, adipose lipid storage and adipocyte proliferation could not be included in the model. As a result, the short and medium term effects of high fat diets on plasma FFA and triglyceride concentrations are exaggerated because the fats are not

removed from circulation. To compensate, inputs representing high fat and very high fat diets were set by matching the resulting outputted plasma FFA and triglyceride concentrations to those seen in overweight and obese individuals, rather than matching the increase in dietary intake. A 12.5% increase in FFA input, used to represent high fat intake, results in simulated plasma triglyceride and glucose concentrations close to the average of those measured in overweight individuals by Sindelka *et al.* ($25kg.m^{-2}<BMI<30kg.m^{-2}$) [141]. A 25% increase was used to represent very high fat intake, which gives changes in triglyceride and FFA concentration towards the high end of the values measured in obese individuals ($BMI>30kg.m^{-2}$), consistent with a severe increase in dietary fat content [141, 435]. High and very high carbohydrate intake diets were simulated using equivalent percentage increases in glucose input.

3.2.2 Insulin Resistance and SREBP-1c

IR was simulated by multiplying the detected insulin concentration by an IR constant with a value of less than one ($K_{IR} < 1$) such that cells effectively experience an insulin concentration lower than the real concentration. Throughout this thesis, severe IR corresponds to a value of $K_{IR} = 0.015$ and developing IR to $K_{IR} = 0.05$. On a moderate diet, developing IR leads to hyperinsulinaemia but only a rise of 1.25mM in average glucose concentration as raised insulin levels compensate for decrease sensitivity. Severe IR, meanwhile, causes postprandial hyperglycaemia consistent with the development of T2DM.

As discussed, the pro-lipogenic regulatory protein SREBP-1c has been highlighted as playing a potential role in the development of NAFLD [36-39]. In metabolically normal individuals, SREBP-1c is stimulated by insulin and, therefore, a fall in expression would be expected insulin resistant NAFLD patients [155, 158, 198, 501]. However, an increase is seen in insulin resistant NAFLD patients [36-39]. To account for the counter-intuitive increase seen experimentally, simulations were run for an insulin resistant individual with continuous stimulation (corresponding to a high 1nM insulin concentration) of lipogenesis and triglyceride synthesis.

3.3 Results

3.3.1 Representing NAFLD in the Model

In the following section, IR with and without increased SREBP-1c expression and varying dietary intake are simulated to assess to what extent these account for the experimentally observed changes in lipid levels, glucose regulation, ATP levels and metabolic rates in NAFLD [18, 36, 37, 131-133].

3.3.1.1 Insulin Resistance and SREBP-1c

Figure 3.1 summarises the simulated effects of IR with and without increased SREBP-1c expression on bulk hepatic metabolism (figure 3.1a), on zonation in metabolism (figure 3.1b) and on key plasma concentrations (figure 3.1c). Figures 3.2 and 3.3 show the simulated effects of IR with and without increased SREBP-1c expression on concentrations of hepatic metabolites (figure 3.2) and rates of key hepatic processes (figure 3.3) across the sinusoid.

The majority of key metabolic changes known to occur in steatotic livers are seen when simulating the direct effects of IR alone (without increased SREBP-1c expression). Firstly, pericentral-centred steatosis occurs when simulating system-wide IR (figure 3.2a). For a severely insulin resistant individual on a moderate diet, the simulated average hepatic lipid content was more than doubled from 2.3% of total cell mass to 5.5%. The increase in concentration was largest in pericentral cells where the lipid content rose from 2.7% to 7.4%, consistent with the development of pericentral-centred steatosis. A 5% (50mg/g wet weight) liver triglyceride concentration is generally used as the criterion for diagnosing early-stage NAFLD [15].

Both experimentally and in the model simulations, insulin resistant livers are unable to store sufficient glycogen (figure 3.2d), leading to post-prandial hyperglycaemia (figure 3.1c). Consistent with experimental observations [502], pericentral cells show a more severe loss in their ability to store and release glucose throughout the meal cycle than periportal cells (Δ(compartment 1)=27.4mM vs Δ(compartment 8)=5.5mM (in units of glucose) (figure 3.2f)).

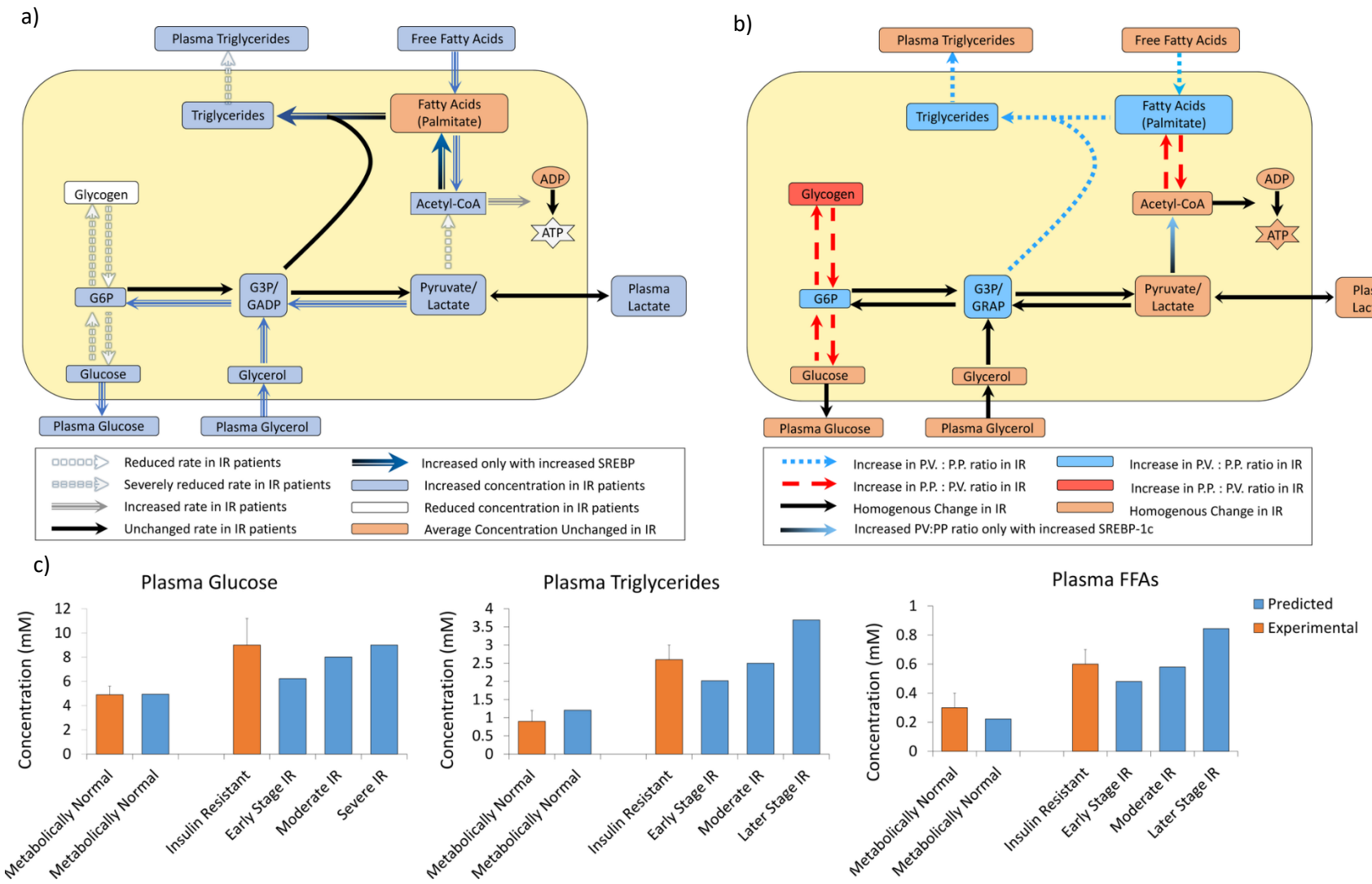

Figure 3.1 – The simulated effects of IR on metabolism. *(a) The effects of simulating IR on total hepatic metabolism (averaged across the sinusoid). (b) The heterogeneity in the effects of simulating IR across the sinusoid. (c) The effects of simulating increasing severities of IR on plasma triglyceride, glucose and FFA concentrations compared with experimental data from Sindelka et al [141] and Burnt et al. [435].*

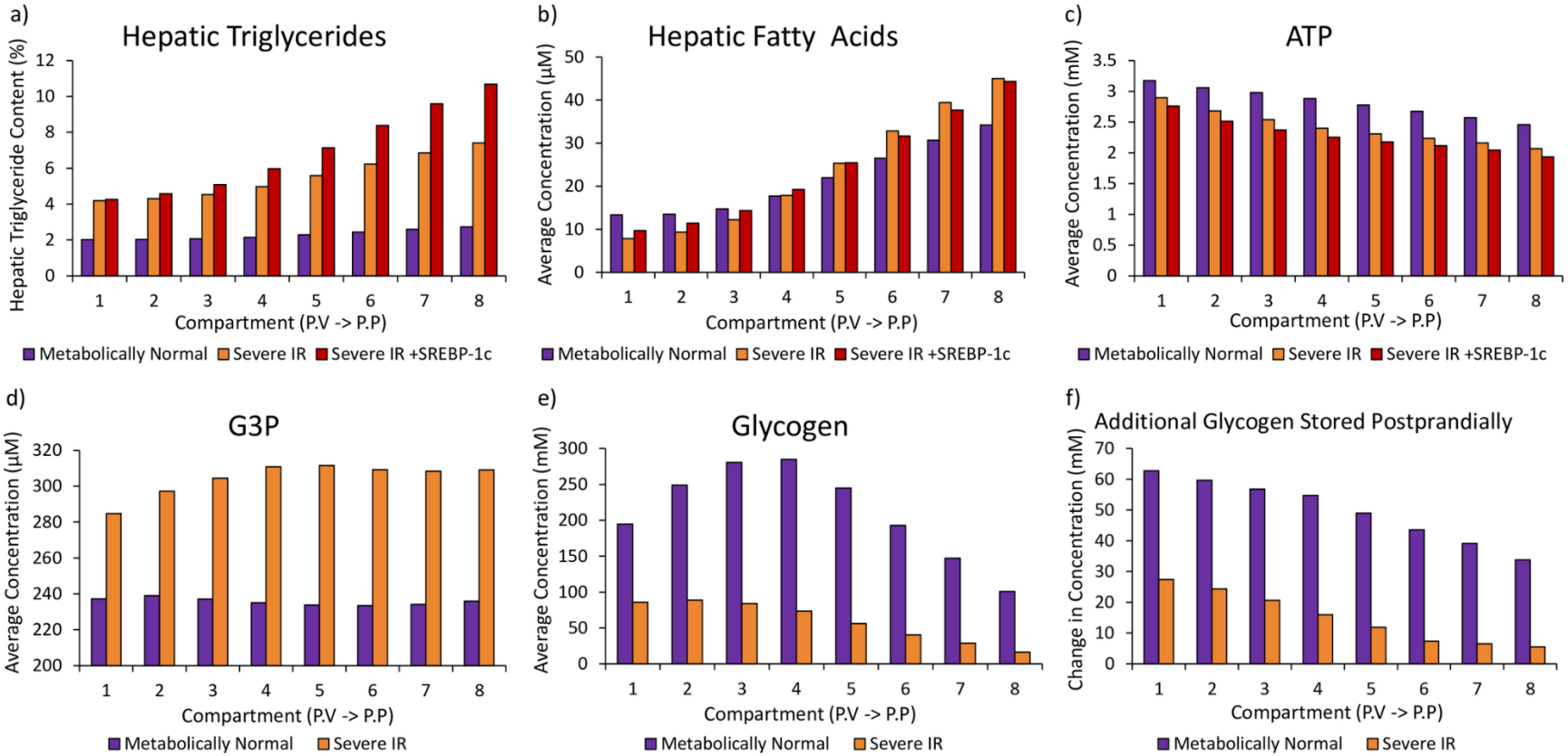

Figure 3.2 – Metabolite concentrations when simulating NAFLD. *(a) The average triglyceride (b) FFA, (c) ATP, (d) glycerol-3-phosphate and (e) glycogen concentration and (f) the difference between postprandial peak and pre-prandial trough glycogen concentrations in the different regions of the sinusoid when simulating (purple) a metabolically normal individual, (orange) the effects of IR alone and (red) IR with increase SREBP-1c expression using a moderate intake diet.*

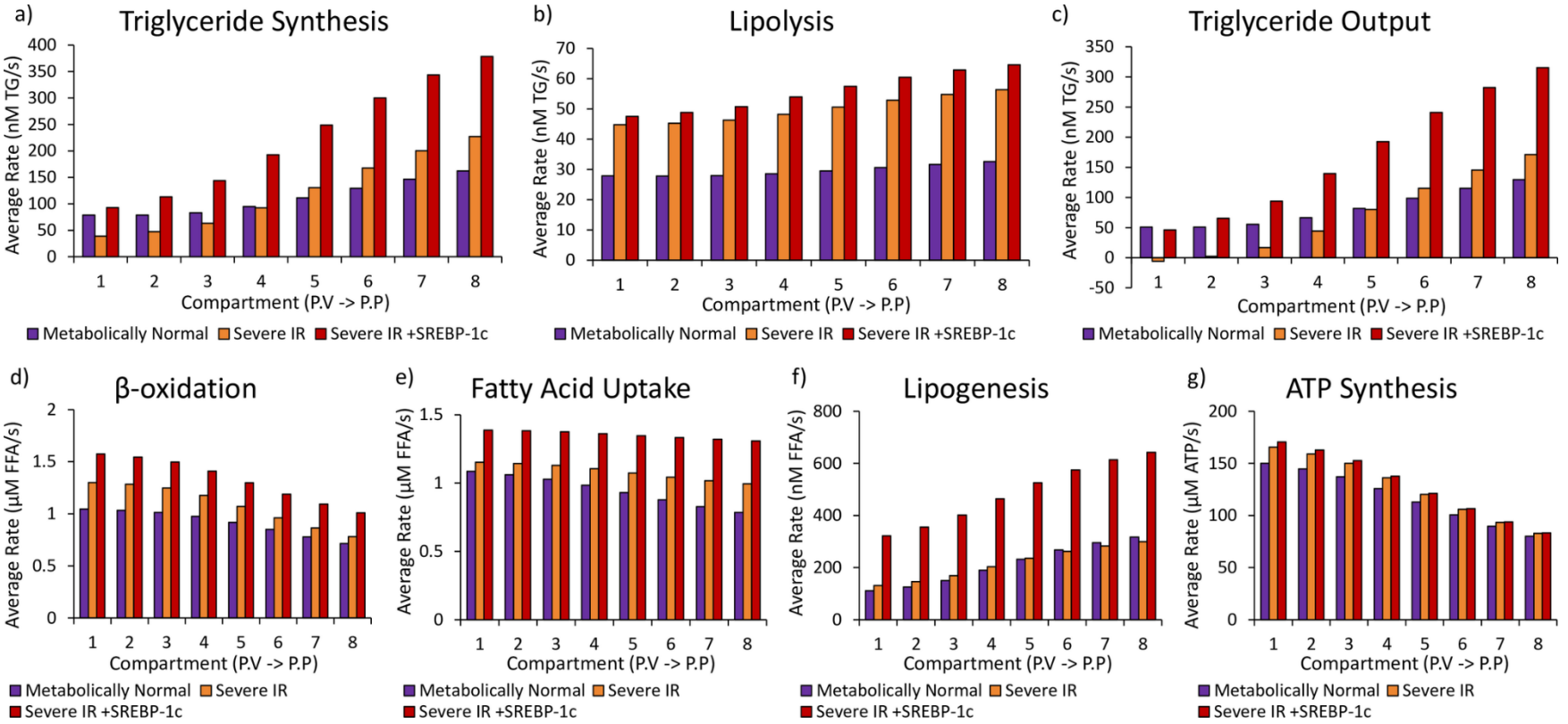

Figure 3.3 – Metabolic rates when simulating NAFLD. *The average rates of (a) triglyceride synthesis, (b) lipolysis, (c) triglyceride release as VLDL, (d) β-oxidation (e) FFA uptake, (f) lipogenesis and (g) ATP synthesis from acetyl-CoA in the different regions of the sinusoid when simulating (purple) a metabolically normal individual, (orange) the effects of IR alone and (red) IR with increase SREBP-1c expression using a moderate intake diet.*

However, in order for the model to fully recreate the metabolic changes seen *in vivo*, raised SREBP-1c expression must additionally be simulated. In particular, when simulating the direct effects of IR alone, the outputted data differ from *in vivo* findings for NAFLD in the lipogenesis rates. *In vivo,* although the majority of hepatic lipids in NAFLD are known to originate from uptake, increases have also been measured in the rates of *de novo* lipogenesis and triglyceride synthesis [26, 37, 503, 504]. When simulating IR in the model, the average rates of these processes were roughly unchanged (figures 3.3a, 5f) and hepatic steatosis arose as a result of increased lipid uptake alone (figures 3.3c, 3.3e). However, when additionally simulating increased SREBP-1c expression, the rates of lipogenesis and triglyceride synthesis increased to 2.31 and 2.05 times the metabolically normal rate respectively (figures 3.3a, 3.3f), consistent with *in vivo* NAFLD [26, 37, 503, 504]. Increased SREBP-1c expression led to more severe pericentral-centred steatosis, with the simulated compartment 8 (most pericentral) lipid content higher than 10% of total cell mass even, for the moderate intake cycle used (figure 3.3a).

When measured experimentally, hepatic glucose oxidation is markedly reduced in NAFLD, with almost all energy produced through β-oxidation [44, 227, 228, 505-508]. When simulating IR with increased SREBP-1c expression in the model, a 45% increase in β-oxidation (figure 3.3d) and a 13% reduction in glucose oxidation via glycolysis occurred, consistent with the experimental observations [44, 227, 228, 505-509] (figure 3.3d).

Despite the increase in FA oxidation, reduced ATP concentrations have been measured experimentally in NAFLD livers [44, 227, 228, 506, 510-513]. Also, increased mitochondrial ROS production has been measured, suggesting overactive but dysfunctional ATP synthesis pathways [501, 512, 514-516]. These findings are likely to be, at least partially, due to a reduction in activity in ETC proteins (reviewed in [501]). When simulating IR with increased SREBP-1c expression in the model, a 19.5% fall in ATP concentration (figure 3.2b) occurred despite a 9.3% increase in the rate of oxidation of acetyl-CoA in the citrate cycle (figure 3.3g). This occurred even though the model does not include the reduction in ETC protein activity, and results from increased ATP consumption in lipogenesis, triglyceride synthesis

and β-oxidation combined with reduced ATP production from glycolysis. As NAFLD develops *in vivo*, additional drops in ATP concentration would be seen due to reduced ETC protein activity [44, 227, 228, 505, 506].

Therefore, whilst pericentral-centred steatosis, reduced glycogenesis and key alterations to energy metabolism seen in NAFLD patients occur in the model when simulating IR alone, increased SREBP-1c expression is additionally required to fully replicate the metabolic changes occurring in NAFLD. In the following sections, both the effects of IR alone and IR combined with increased SREBP-1c expression are simulated.

3.3.1.2 Dietary intake and the development of steatosis

Figure 3.4 shows the simulated effects of high fat intake and very high fat intake diets on hepatic triglyceride, FFA and ATP concentrations. When simulating insulin sensitive individuals, high intake and very high intake of fats caused relatively moderate increases in the average hepatic triglyceride content from 2.3% on a moderate diet to 3.6% and 7.2% respectively (figure 3.4a). Therefore, hepatic lipid content is only higher than the 5% criteria at which early-stage NAFLD is diagnosed when simulating obese individuals with severe plasma hyperlipidaemia in the absence of IR. Hepatic FFA concentrations were increased from 21.5μM on a moderate diet to 28.6μM and 38.0μM when simulating high and very high fat diets respectively (figure 3.4e). A 5% reduction in ATP concentration occurred when simulating a very high fat diet due to increased allosteric inhibition of glucose oxidation (figure 3.4f). When high and very high carbohydrate diets were simulated, smaller increases in the simulated hepatic triglyceride content occurred than for increased lipid intake. Even for very high carbohydrate intake, the hepatic triglyceride concentration remained less than 5% (figure 3.4a).

When combined with IR, high dietary intake caused far more severe steatosis in the model. In the case of severe IR (K_{IR}=0.015) (figure 3.4b-d), the average concentration increased from 5.5% when simulating a moderate intake diet to 10.0% and 27.0% when simulating high carbohydrate and high fat intake diets respectively (figure 3.4c). Severe IR combined with increased SREBP-1c expression

caused even more extreme increases in hepatic triglyceride concentrations due to additional hepatic lipogenesis (figure 3.4d).

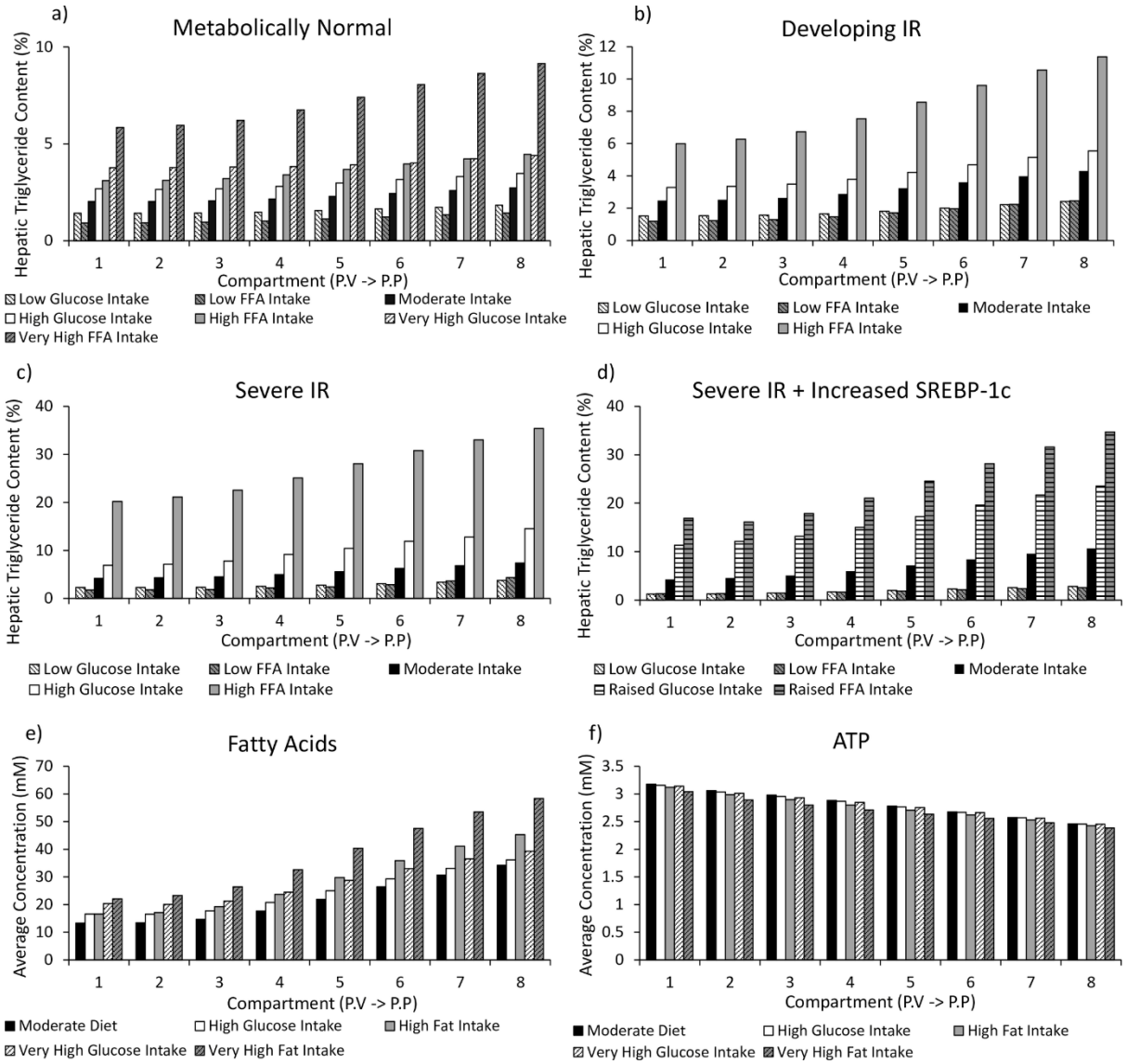

Figure 3.4 – The simulated effects of varying dietary intake in the model. *(a-d) The average hepatic lipid content across the sinusoid when simulating varying glucose and FFA intake diets in individuals with (a) metabolically normal insulin sensitivity (100%, K_{IR}=1), (b) developing IR (5%, K_{IR}=0.05), (c) severe IR (1.5%, K_{IR}=0.015) and (d) severe IR in combination with increased SREBP-1c expression. (e-f) The effects of high fat and carbohydrate (glucose) intake on (e) ATP concentrations and (f) FFA concentrations across the sinusoid when simulating a metabolically normal, insulin sensitive individual. High and low intakes correspond to a sustained 12.5% difference in intake relative to the moderate intake det. Very high and raised intakes correspond to 25% and 5% increases respectively. The average concentrations over a 4 hours intake/output cycle are depicted.*

In reality, adipose uptake of plasma lipids and increased adipocyte proliferation are likely to prevent such rapid rises in hepatic steatosis concentrations. However, these severely raised values are

consistent with the dangerous effects of high fat intake on metabolism in untreated insulin resistant individuals.

3.3.2 The causes of pericentral centred steatosis in insulin resistant NAFLD individuals.

In the following sections, the metabolic changes occurring across the sinusoid when simulating NAFLD resulting from IR and increased SREBP-1c expression are analysed in order to identify the key differences between periportal and pericentral cells accounting for pericentral-centred steatosis.

3.3.2.1 Triglyceride Synthesis, Output and Lipolysis

The processes directly determining the triglyceride concentration are triglyceride synthesis (figure 3.3a), lipolysis (figure 3.3b) and the net rate of triglyceride output (figure 3.3c) (release as VLDL minus the slow uptake from plasma). Lipolysis only occurs at a very slow rate in liver (88) and, although an increase in rate occurred when simulating IR, the process is not a major determinant of the hepatic triglyceride concentration. Triglyceride output and uptake, meanwhile, depend only on the plasma and hepatic triglyceride concentrations in the model, and cannot account for the variation in steatosis across the sinusoid. Instead, the zonal differences arise in the rate of synthesis.

Even when simulating metabolically normal individuals, the rate of triglyceride production was higher in the pericentral half of the sinusoid than in periportal cells. The simulated periportal to pericentral triglyceride synthesis ratio (pp:pc) was 1:1.64 (figure 3.3a), consistent with the ratio of 1:1.58±0.34 seen experimentally (89). When simulating metabolically normal individuals, this arises as a result of the upregulated lipogenic pathways in pericentral cells and upregulated β-oxidation in periportal cells. When simulating NAFLD (IR with increased SREBP-1c expression), the gradient in the rate of triglyceride synthesis across the sinusoid became steeper (pp:pc = 1:2.34), leading to greater steatosis in pericentral cells.

The enzymes mediating triglyceride synthesis are homogenously expressed across the sinusoid in the model. The large heterogeneity in rate across the sinusoid when simulating NAFLD instead results

from differences in the concentrations of the two substrates of triglyceride synthesis: glycerol-3-phosphate (G3P) and FFAs.

3.3.2.2 FFA concentration: Lipogenesis, Uptake and Oxidation

When simulating metabolically normal individuals, the FFA concentration was higher in the pericentral compartments (pp:pc=1:1.91) (figure 3.2c), which is intuitive given that pericentral cells specialise in lipogenesis whilst periportal cells predominantly utilise fats in β-oxidation (90). When simulating NAFLD, this gradient in FFA concentration becomes more pronounced (pp:pc=1:2.54). The processes directly determining the hepatic FFA concentration in the model are *de novo* lipogenesis (figure 3.3f), uptake and release (figure 3.3e), and β-oxidation (figure 3.3d) along with triglyceride synthesis (figure 3.3a) and lipolysis (figure 3.3b).

The majority of additional lipids in NAFLD arose from uptake in the simulations (ΔRate = 404nM FFA/s; figure 3.3e), although *de novo* lipogenesis also increased as a result of SREBP-1c expression (ΔRate =276nM FFA/s; figure 3.3f). The largest increase in uptake occurred in pericentral cells where it increased by 471nM FFA/s compared with 337nM FFA/s in periportal cells. FA uptake proteins have higher expression in periportal cells and even when simulating IR, the total rate of uptake was still larger in periportal than pericentral cells. However, under conditions of IR, where passive uptake dominates rather than insulin-stimulated scavenging, the simulated gradient in the rate of FFA uptake across the sinusoid was less steep. The increase in *de novo* lipogenesis was also larger in pericentral cells, where it increased by 311nM FFA/s compared with 242nM FFA/s in periportal (figure 3.3f). This is as a direct result of the pericentral zonation of lipogenesis enzymes.

The rate of β-oxidation is increased by 411nM FFA/s when simulating NAFLD providing a compensatory mechanism by which some of the extra fats are removed (figure 3.3d). In the model this occurred due to increased substrate and reduced insulin inhibition, although *in vivo* it is thought that additional signalling pathways may further increase β-oxidation (reviewed in (13)). The increase was largest in oxygen rich periportal cells (ΔRate =490nM FFA/s) where greater quantities of acetyl-

CoA are required for the citrate cycle compared with pericentral cells (ΔRate = 332nM FFA/s) (figure 3.3g). Since the largest increase in uptake occurred in pericentral cells whilst the largest increase in lipid oxidation occurred in periportal cells, FFA availability for triglyceride synthesis increased in pericentral cells.

3.3.2.3 G3P Concentration: Glycogen Storage and Carbohydrate Metabolic Intermediates

G3P, which is closely related to glyceraldehyde-3-phosphate (GADP), an intermediate of glycolysis, forms the carbon backbone in triglyceride synthesis. The G3P concentration was raised across the sinusoid when simulating insulin resistant individuals, and this increase was larger in the pericentral half of the sinusoid (75μM) than in the proximal periportal cells (48μM) (figure 3.2e). Increased SREBP-1c expression affects triglyceride concentrations through changes in lipogenesis and triglyceride synthesis, and has little effect on the G3P concentration.

The increase in G3P concentration when simulating IR individuals occurred because hepatocytes, particularly towards the pericentral end of the sinusoid, are unable to properly clear glucose intermediates. When simulating IR, glycogen concentrations were severely reduced across the sinusoid (figure 3.2d). However, as discussed above, pericentral cells showed a more severe reduction in glucose storage than periportal cells when simulating IR (Additional glucose stored postprandially: Δ(compartment 1)=27.4mM, Δ(compartment 8)=5.5mM) (figure 3.2f).

In addition, pericentral cells consume less glucose in oxidative metabolism than periportal cells due to their low oxygen environment (8.1μM acetyl-CoA/s vs 13.0μM/s when simulating NAFLD; figure 3.3g). These effects caused a build-up of carbohydrate metabolism intermediates, including G3P, particularly in pericentral cells.

This increase in G3P concentration, which remains lower than the K_M value for the glycerol backbone binding to glycerophosphate acyltransferase (460μM), means that FFAs are more rapidly converted to triglycerides, causing steatosis [470].

3.3.3 The effects of metabolic variation between individuals on steatosis development in NAFLD.

The results in the previous section investigated the development of NAFLD when running simulations with a single set of parameters. However, in reality, patients will show inter-individual variability in the activity of metabolic processes. In the following sections, the effects of this inter-individual variation in the activity of hepatic processes in the model on susceptibility to steatosis and on its pattern of development are assessed using two methods. Firstly, 15 example 'patients' were simulated with rate and zonation constants randomly generated from within a specified range of the standard values (section 3.3.3). These patients were simulated with both normal insulin sensitivity on a moderate intake diet and with developing IR on a high fat intake diet. Correlations were performed between each of the varied constants and the resulting triglyceride concentrations across the sinusoid. Secondly, sensitivity analysis was performed on both the rate and zonation constants to assess the impact of varying each constant in isolation on triglyceride concentrations across the sinusoid (section 3.4.3).

3.3.3.1 Simulating Individual Patients

To assess the impact of inter-individual variability across a wide range of processes, 15 patients with rate constants and zonation constants for a number of key processes randomly generated within bounded ranges were simulated. Metabolic variations in numerous tissues around the body are likely to affect hepatic steatosis via plasma lipid concentrations. However, because the model presented here is primarily of liver metabolism, we focus specifically on variations in the expression and activities of enzymes mediating hepatic energy metabolism. The constants which were altered include those for glycolysis (glucose->G6P, G6P->GADP and GADP->pyruvate), gluconeogenesis, pyruvate oxidation, lipogenesis, β-oxidation, oxidative phosphorylation and triglyceride synthesis.

The rate constants determine the overall maximum activity of the enzymes mediating each process. These were generated randomly using the Microsoft Excel RandBetween() function from within a 10%

range of the standard value (table 3.1). This function generates numbers within a range with equal weighting across the range of possible values. The zonation constants were selected using the same function from a range of ±0.2 of the standard value (table3.2). A zonation constant of 1 corresponds to completely periportal expression, a zonation constant of 0 corresponds to heterogeneous expression and a zonation constant of -1 corresponds to completely pericentral expression (see section 2.4.6). The altered parameter values for the 15 patients are shown in tables 3.1 and 3.2. For parameters not listed in the table, the standard values listed in chapter 2 were used. These ranges of parameter variability lie well within the inter-individual variability seen in the data used to set the parameters (tables 2.1 and 2.2).

3.3.3.1.1 Simulating Inter-Individual Variability

Figure 3.5 shows the hepatic lipid content, hepatic FFA concentration, hepatic ATP concentration, the plasma glucose concentration and the plasma lactate concentration when simulating the 15 example patients. The simulated data are shown for both normal insulin sensitivity with moderate lipid intake and developing insulin resistant with high fat intake.

In all cases, the average simulated concentrations across the patients are well within one standard deviation from the simulated values when using the standard parameter values, although a higher average hepatic lipid content was seen for the 15 simulated patients compared with the content when using standard parameter values (figure 3.5 a,b). In all cases, the simulated concentrations for the 15 example patients remain within the ranges measured experimentally.

Very little variation is seen between the patients for simulated plasma glucose (figure 3.5e) and hepatic ATP (figure 3.5d) concentrations, consistent with the strong allosteric and hormonal regulation in both glucose storage and ATP synthesis. A wider variation in plasma glucose concentration would have occurred if the rate constants for glycogen synthesis and glycogen phosphorylation were additionally altered between the patients.

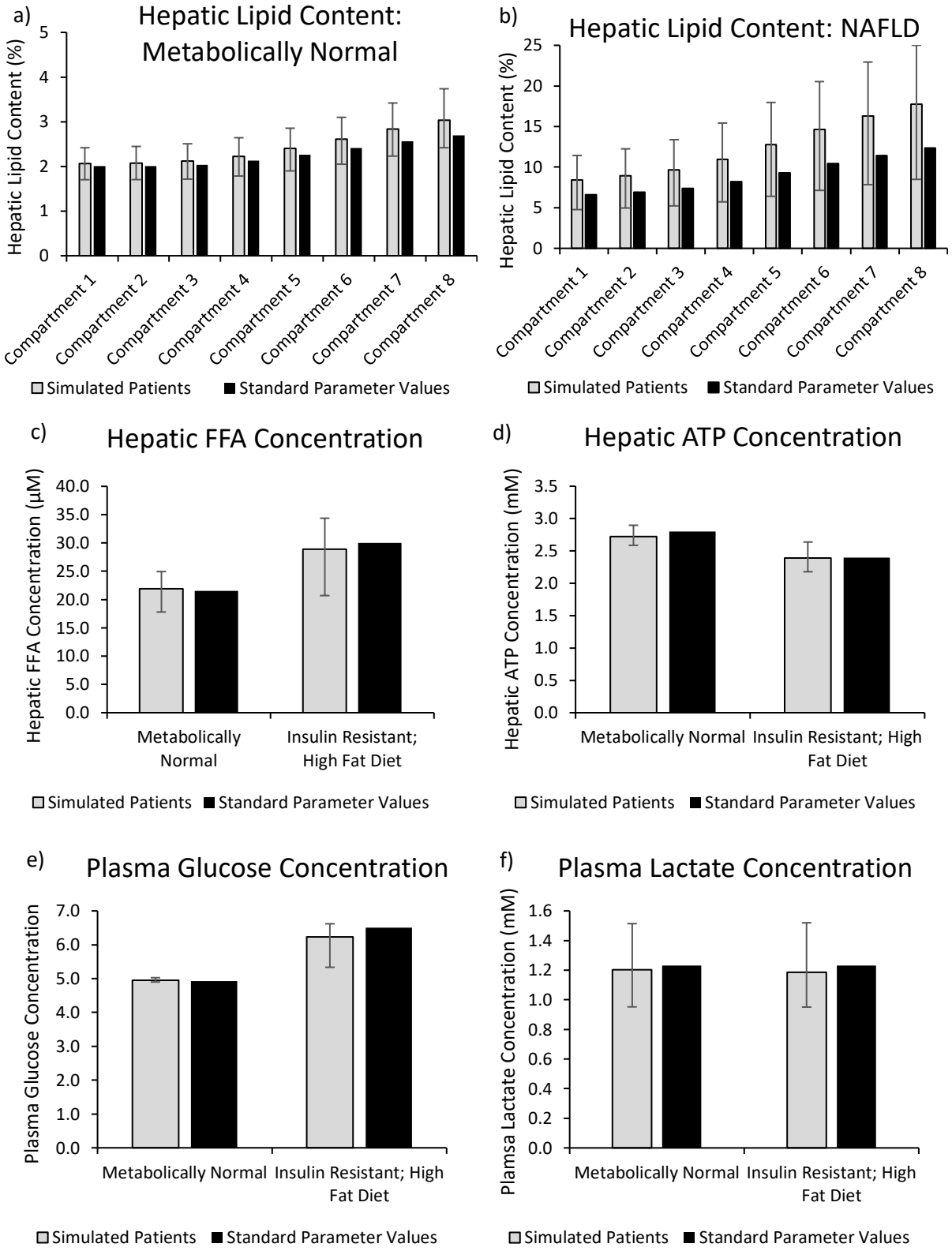

Figure 3.5: Plasma and hepatic concentrations when simulating randomly generated patients. *The simulated (a,b) hepatic lipid content, (c) hepatic FFA concentration, (d) hepatic ATP concentration, (e) plasma glucose concentration and (f) plasma lactate concentration when simulating the 15 sample patients compared with standard parameter values. The error bars show the 84.1th and 15.9th percentiles corresponding to the standard deviation in a central distribution.*

Table 3.1: The rate constants for the 15 simulated patients.

Rate Constants	**Simulated 'Patients'**														
	1	**2**	**3**	**4**	**5**	**6**	**7**	**8**	**9**	**10**	**11**	**12**	**13**	**14**	**15**
GK	122.03	133.11	144.7	143.97	136.71	140.24	125.63	141.73	134.42	144.54	139.65	120.51	141.78	124.44	129.07
G6Pase	400.87	370.26	379.47	370.43	361.99	350.18	387.13	360.86	353.5	372.49	352.46	384.54	342.74	404.15	374.47
Glycolysis 1: G6P->GADP	167.05	159.44	164.41	159.98	158.76	149.22	146.18	149.16	146.02	167.31	164.3	169.71	159.35	150.36	144.72
Glycolysis 2: GADP->Pyr/Lac	90.49	84.29	84.57	84.02	80.35	84.56	79.74	86.11	87.52	89.45	87.52	93.29	78.99	86.35	80.66
Gluconeogenesis 1: Pyr/Lac->GADP	36.46	31.56	37.26	32.38	37.53	33.04	31.67	34.71	37.61	33.45	32.34	33.32	36	34.28	35.81
Gluconeogenesis 2: GADP->G6P	74.78	74.75	69.6	61.71	61.24	70.52	73.24	71.71	72.97	67.87	68.42	66.38	72.54	65.83	68.48
Pyruvate Oxidation	12.86	14.9	13.73	15.02	14.96	13.93	15.28	12.69	13.47	15.33	13.88	13.96	15.32	15.32	12.83
Oxidative Phosphorylation	499.74	482.91	540.51	519.06	473.52	540.98	500.08	559.93	567.6	561.47	518.4	496.69	529.61	489	472.15
Lipogenesis	3.71	3.85	4.37	4.33	3.95	3.76	4.26	4.36	4.24	4.04	4.19	4.09	3.73	4.08	4.03
Beta Oxidation	3.29	3.54	3.27	3.09	3.51	3.05	3.31	3.55	3.41	3.55	3.53	3.07	3.57	3.21	3.47
Triglyceride Synthesis	8.23	8.57	9.79	9.03	8.15	8.15	9.16	8.88	9.18	9.79	9.02	8.26	9.62	8.41	8.38

Table 3.2: The zonation constants for the 15 simulated patients

Zonation Constants	**Simulated 'Patients'**														
	1	**2**	**3**	**4**	**5**	**6**	**7**	**8**	**9**	**10**	**11**	**12**	**13**	**14**	**15**
G6Pase	0.32	0.36	0.3	0.42	0.28	0.47	0.31	0.36	0.28	0.51	0.17	0.26	0.34	0.15	0.26
GK	-0.457	-0.309	-0.481	-0.502	-0.345	-0.331	-0.427	-0.401	-0.49	-0.278	-0.35	-0.44	-0.444	-0.422	-0.596
Glycolysis: GADP->Pyr/Lac	-0.473	-0.513	-0.538	-0.167	-0.381	-0.278	-0.35	-0.204	-0.552	-0.459	-0.175	-0.222	-0.214	-0.428	-0.175
Gluconeogenesis 1: Pyr/Lac->GADP	0.359	0.32	0.276	0.231	0.444	0.315	0.417	0.308	0.345	0.313	0.49	0.44	0.566	0.512	0.369
Gluconeogenesis 2: GADP->G6P	0.294	0.284	0.215	0.399	0.203	0.327	0.28	0.203	0.254	0.214	0.439	0.198	0.351	0.22	0.37
Pyruvate Oxidation	-0.14	0.07	-0.02	0.01	0	0.05	0	-0.02	0.18	0.02	-0.19	0.07	0.04	-0.01	0.15
Oxidative Phosphorylation	0.26	0.07	0.17	0.39	0.26	0.06	0.23	0.28	0.15	0.33	0.37	0.23	0.16	0.26	0.38
Lipogenesis	-0.16	-0.1	-0.41	-0.19	-0.42	-0.12	-0.13	-0.04	-0.23	-0.28	-0.09	-0.34	-0.37	-0.33	-0.36
Beta Oxidation	0.06	0.43	0.24	0.25	0.16	0.23	0.34	0.37	0.09	0.26	0.31	0.22	0.22	0.37	0.39
Triglyceride Synthesis	0.16	0.06	-0.11	-0.16	-0.11	-0.19	-0.14	-0.11	-0.09	-0.1	0.2	-0.13	-0.11	0.2	-0.05

Larger differences occurred in the simulated hepatic lipid content (figures 3.5a,b), hepatic FFA concentration (figure 3.5c) and plasma lactate concentration (figure 3.5f) between patients. When simulating metabolically normal individuals, the standard deviation in the hepatic lipid content is 19.5% of the average value. When simulating NAFLD this increased to 47.1%. Therefore, inter-individual variability in hepatic metabolism is predicted to have a marked effect on severity of steatosis once IR develops.

Little change in the simulated lactate concentration occurred between metabolically normal and NAFLD patients. However, a standard deviation of 29-30% of the average values was seen when simulating under the two sets of conditions, suggesting inter-individual variability predominantly determined the concentration in the two groups. The simulated patients with high lactate concentrations when simulating metabolically normal patients also showed a high concentration when simulating NAFLD (Pearson's coefficient=0.97).

3.3.3.1.2 Correlations between parameter values and key hepatic and plasma concentrations

Tables 3.3 and 3.4 show the Pearson's product-moment correlation coefficients between each varied parameter with the hepatic triglyceride concentration, with the zonation in hepatic triglyceride content (pericentral to periportal ratio) and with key plasma concentrations when simulating the patients with developing IR and high fat intake in the 15 patients. This is a measure of the linear dependence between two variables with 0 corresponding to independence and +1 and -1 corresponding to total positive and negative correlations respectively. Table 3.3 shows the correlations for the rate constants whilst table 3.4 shows the correlations for the zonation constants. The correlations are presented when simulating IR and high fat intake.

Only the rate constants for oxidative phosphorylation and for the second half of glycolysis, converting GADP to G6P, showed statistically significant (negative) correlations with hepatic triglyceride content. The rate constant for oxidative phosphorylation determines the rate of production of ATP from acetyl-CoA, and it is intuitive that a high rate constant would reduce the hepatic lipid content by promoting

increased FA oxidation. It also showed a statistically significant negative correlation with the plasma triglyceride and FFA concentrations. A relatively high, but non-significant, correlation was also seen between the rate constant for β-oxidation and the hepatic lipid content, consistent with the importance of the rate of oxidation of fats through these two pathways in determining susceptibility to steatosis. The zonation constants for both oxidative phosphorylation and β-oxidation also showed statistically significant correlations with the pericentral to periportal triglyceride ratio. Therefore, variability in the zonation of the enzymes mediating that oxidation of FAs via acetyl-CoA is predicted to at least partially account for the variability in steatosis location seen *in vivo*.

The rate constant for the second part of gluconeogenesis (GADP to G6P) showed statistically significant negative correlations with plasma triglyceride and FFA concentrations as well as the hepatic lipid content. Upregulation of this process not only reduces *de novo* lipogenesis from glucose, but also reduces G3P production for use in triglyceride synthesis. Furthermore, it reduces the allosteric inhibition of β-oxidation as a result of reduced acetyl-CoA synthesis from glucose. Finally, increased gluconeogenesis increases the rate of ATP consumption in the cell, increasing the required oxidation of acetyl-CoA to replenish ATP. The first three of these causes would be expected to be accompanied by an opposite correlation between glycolysis and triglyceride content. However, given the low correlation coefficients between the two glycolysis rate constants and hepatic triglyceride content, the increased ATP consumption in gluconeogenesis is likely to have been the major cause of the correlation between gluconeogenesis and hepatic lipid content. A relatively high, but non-significant, correlation was also seen between the hepatic lipid content and the first half of gluconeogenesis.

Table 3.3: The Pearson's product-moment correlation coefficients between several rate constants and key hepatic and plasma variables.

Rate Constants	Hepatic Triglyceride	PC:PP TG ratio	Plasma TG	Plasma FFA	Plasma Glucose	Plasma Lactate
GK	-0.35	0.00	-0.37	-0.32	-0.19	-0.30
G6Pase	0.41	0.18	0.42	0.43	-0.09	0.25
Glycolysis 1: G6P->GADP	0.25	0.22	0.23	0.32	**-0.59 ***	**0.60 ***
Glycolysis 1: GADP->Pyr	0.07	-0.13	0.08	0.14	-0.47	**0.56 ***
Gluconeogenesis 1: Pyr->GADP	-0.49	-0.51	-0.47	-0.54	**0.57 ***	-0.51
Gluconeogenesis 2: GADP->G6P	**-0.59 ***	-0.25	**-0.59 ***	**-0.60 ***	0.47	-0.35
Pyruvate Oxidation	0.31	0.16	0.31	0.38	-0.42	-0.01
Oxidative Phosphorylation	**-0.70 ***	**-0.52 ***	**-0.69 ***	**-0.64 ***	-0.10	-0.36
Lipogenesis	0.09	0.11	0.09	0.11	-0.34	0.07
Beta Oxidation	-0.35	0.30	-0.38	-0.38	0.32	-0.30
Triglyceride Synthesis	-0.40	-0.04	-0.41	-0.34	-0.19	-0.31

*The correlations when simulating high fat intake and developing IR using parameter values corresponding to 15 randomly generated patients shown in tables 3.1 and 3.2. * - statistical significance of correlation <0.05*

.

Table 3.4: The Pearson's product-moment correlation coefficients between several zonation constants and key hepatic and plasma variables.

Zonation Constants	Hepatic Triglyceride	PC:PP TG ratio	Plasma TG	Plasma FFA	Plasma Glucose	Plasma Lactate
GK	-0.25	-0.15	-0.25	-0.22	-0.06	-0.21
G6Pase	-0.10	0.12	-0.13	-0.01	-0.34	0.10
Glycolysis: GADP->Pyr	0.32	0.32	0.32	0.28	-0.16	0.36
Gluconeogenesis 1: Pyr->GADP	0.03	0.02	0.03	0.04	0.10	0.04
Gluconeogenesis 2: GADP->G6P	0.22	0.38	0.20	0.17	-0.03	0.18
Pyruvate Oxidation	-0.08	-0.34	-0.05	-0.14	0.29	-0.31
Oxidative Phosphorylation	0.43	**0.57 ***	0.42	0.41	-0.24	0.36
Lipogenesis	-0.10	0.13	-0.10	-0.08	-0.08	0.13
Beta Oxidation	0.32	**0.64 ***	0.31	0.31	-0.14	0.13
Triglyceride Synthesis	0.19	0.37	0.18	0.21	-0.05	0.28

*The correlations when simulating high fat intake and developing IR using parameter values corresponding to 15 randomly generated patients shown in tables 3.1 and 3.2. * - statistical significance of correlation <0.05.*

3.3.3.2 Sensitivity Analysis on Key Variables

As a second method of assessing key inter-individual variations in metabolism that account for differences in susceptibility to steatosis, sensitivity analysis was performed on the rate constants and zonation in the model. This involved altering each constant in turn and assessing the impact on metabolism. In addition to the processes varied in the previous section, the rate constants for glycogenesis, glycogenolysis, FA cross-membrane transport, triglyceride cross-membrane transport and active triglyceride release as VLDL were also included in the sensitivity analysis.

3.3.3.2.1 Key determinants of total hepatic triglyceride level

Each rate constant was increased or reduced by 10% when simulating an otherwise metabolically normal individual. Variations of this size are large enough to have a notable effect on hepatic and plasma concentrations and allow us to identify the relative importance of processes, but remain in a range which would realistically be expected between individuals under non-pathological conditions. The model was provided with constant glucose and FFA inputs such that, when using the unaltered parameter values, the plasma glucose, triglyceride and FFA concentrations remained at 5.03mM, 1.05mM, and 432µM respectively. Simulations were run for 36 hours from these initial values after changing each rate constant.

Hepatic and plasma triglyceride concentrations were most sensitive to the rate constants for β-oxidation and for ATP synthesis through the citrate cycle (table 3.5), particularly when these processes were inhibited. Reducing the rate constants for β-oxidation and ATP synthesis caused increases in the simulated hepatic triglyceride concentration of 2.78mM and 1.82mM over the 36 hours respectively. Increasing the rate constants, meanwhile, caused reductions of 0.81mM and 1.27mM respectively. These large changes suggest that metabolic variations affecting the rate of oxidation of fats are likely to be a major determinant of inter-individual susceptibility to the development of steatosis. Consistent with this, the hepatic triglyceride concentrations were also sensitive to changes in the rate constants mediating glycolysis, gluconeogenesis and pyruvate oxidation. All these processes alter the production

Table 3.5: Sensitivity analysis for the rate constants.

Process	Change in Cellular FFA (µM)		Change in Cellular Triglyceride (µM)		Change in Plasma FFA (µM)		Change in Plasma Triglyceride (µM)	
	Increased v_b (+10%)	Reduced v_b (-10%)	Increased v_b (+10%)	Reduced v_b (-10%)	Increased v_b (+10%)	Reduced v_b (+10%)	Increased v_b (-10%)	Reduced v_b (+10%)
β-oxidation	-2.7	5.4	-808.2	2782.5	-15.1	32.2	-36.6	125.7
Oxidative Phosphorylation	-1.9	2.1	-1271.9	1818.1	-12.2	13	-57.0	82.7
Glycolysis 1: (G6P to G3P) mediated by PFK	-0.6	0.6	562.6	-587.6	7.2	-7.7	17.9	-19.1
Gluconeogenesis 2 (G3P to G6P) mediated by FBP	0.0	-0.2	-517.1	599.3	-7.4	8.4	-18.5	21.1
Glycolysis 2: (G3P to Pyr) mediated by PK	2.3	-2.4	572.0	-588.9	12.0	-12.2	26.5	-27.2
Gluconeogenesis 2 (Pyr to G3P) mediated by PEPCK	-1.5	1.8	-464.9	550.4	-8.7	10.4	-21.0	24.8
Pyruvate Oxidation	1.6	-1.6	526.4	-549.9	9.4	-9.7	23.2	-24.3
VLDL Synthesis and Release	0.3	-0.3	-362.9	373.6	7.0	-7.0	23.0	-23.4
Triglyceride Synthesis	-1.5	1.8	237.5	-255.9	1.0	-1	4.5	-4.6
FFA Uptake	3.1	-3.0	260.7	-143.0	-28.5	36.4	-53.9	64.2
Lipogenesis	0.5	-0.5	183.0	-183.4	3.1	-3.2	7.8	-9.0
Glucokinase	1.6	-1.3	-90.4	262.8	79	-68.2	-56	65.9
Triglyceride Cross-Membrane Transport	-0.1	0.1	102.5	-114.8	-1.9	2.2	-6.4	7.2
G6Pase	-0.7	1.0	100.6	-45.5	-35	43.0	30	-31.2
Lipolysis	0.3	-0.4	-69.0	70.3	-0.5	0.4	-1.7	1.7
Glycogen Synthase	0.4	-0.4	-39.4	62.8	13	-14.0	-11	13.0
Glucose Uptake	0.5	-0.4	-24.4	63.8	21	-22.7	-15.5	19.8
Glycogen Phosphorylase	-0.2	0.2	16.2	-10.1	-5.6	5.9	4.4	-4.4

The effect of varying the baseline rate constants, v_b, for the various hepatic metabolism processes included in the model on cellular and plasma FFA and triglyceride concentrations.

Table 3.6: Sensitivity analysis for the zonation constants.

Enzyme Altered	**Periportal : Pericentral Triglyceride Ratio**		**Difference in the change in triglyceride concentration between pericentral and periportal cells.**
	Unchanged Metabolism: 1.80:1		
	20% More Periportal (Δk_n =+ 0.2)	**20% More Pericentral (Δk_n = - 0.2)**	$\frac{(\Delta TG_{pv} - \Delta TG_{pp})}{TG_{av}}$ $(\Delta\ from\ \Delta k_n = -0.2\ to\ \Delta k_n = +0.2)$
FA Uptake	1.27:1	2.62:1	0.91
Triglyceride Release as VLDL	2.22:1	1.47:1	-0.43
Oxidative Phosphorylation	2.09:1	1.53:1	-0.31
Pyruvate Oxidation	1.64:1	1.98:1	0.22
β-oxidation	2.01:1	1.64:1	`-0.22
Glycolysis 1 (G6P-> GADP)	1.73:1	1.86:1	0.08
Lipogenesis	1.75:1	1.85:1	0.08
Gluconeogenesis (GADP -> G6P)	1.88:1	1.74:1	-0.07
Gluconeogenesis 1 (Pyr -> GADP)	1.80:1	1.80:1	0.06
Glycolysis 2 (GADP -> Pyr)	1.79:1	1.80:1	-0.06
Triglyceride Synthesis	1.75:1	1.85:1	0.05
Triglyceride Uptake	1.75:1	1.89:1	0.04
Glucokinase	1.80:1	1.80:1	0.02
G6Pase	1.81:1	1.80:1	-0.00
Lipolysis	1.82:1	1.79:1	-0.00

The effect of altering the zonation constants k_n of lipid metabolism processes on steatosis location (compartment1: compartment 8 triglyceride ratio) when simulating for IR patients on a moderate diet.

of acetyl-CoA from glucose, and hence, the allosteric inhibition of β-oxidation. A 10% variation in the any of the five rate constants mediating these processes caused a 0.45-0.6mM variation in simulated hepatic triglyceride content after 36 hours (table 3.5).

In addition to the oxidation of FAs, hepatic triglyceride levels also showed moderate sensitivity to the rate constant for triglyceride release as VLDL. A 10% variation in rate constant caused a 0.36-0.37mM change in simulated hepatic triglyceride levels after 36 hours (table 3.5).

Hepatic lipid concentrations showed only a relatively weak sensitivity to changes in the rate constant for lipogenesis. Although *de novo* lipogenesis contributes less to hepatic lipid levels than FFA uptake,

its contribution is not insignificant and changes in the rate of lipogenesis would be expected to have a larger impact. However, lipogenesis is strongly allosterically regulated by the concentration of its product and alterations in maximum enzyme activity (rate constant) are partially compensated by changes in allosteric inhibition. Similarly, the rate constant for triglyceride synthesis only had a moderate effect on hepatic and plasma lipid levels. Due to the low concentration of cellular FFAs, the rate of triglyceride synthesis is predominantly determined by the availability of FFAs, rather than the enzyme activity.

Finally, hepatic triglyceride levels also showed a comparatively weak sensitivity to variations in the rate constant for FFA uptake. However, changes in FFA uptake did have a larger effect on plasma lipid levels.

3.3.3.2.2 Key determinants of sinusoidal steatosis location

10% variations in the rate constants of the processes in the model had little effect on the predominant location of steatosis across the sinusoid. Instead, to determine the hepatic metabolic variations most likely to account for differences in the location of steatosis, sensitivity analysis was performed on the zonation constants in the model (table 3.6). These constants determine the difference between periportal and pericentral activity of enzymes mediating each process. Positive values correspond to periportal zonation whilst negative values correspond to pericentral zonation. The constants were increased or reduced by 0.2 corresponding to a 20% increase in periportal and 20% reduction in pericentral cells or *vice versa*, which is well within the range of variation expected non-pathologically (chapter 2 – table 2.2). The effects of these increases and reductions on the pericentral to periportal triglyceride ratio are presented when simulating a severely insulin resistant individual (K_{IR}=0.015) with increased SREBP-1c expression on a moderate intake diet.

While total hepatic triglyceride levels were most sensitive to changes in the rate of lipid oxidation, the location of steatosis is most strongly sensitive to changes in the zonation constants mediating FFA uptake and triglyceride output (table 3.6). Variations in the zonation constant of FFA uptake had the

largest effect, causing the periportal and pericentral triglyceride concentrations to change from 1:1.80 to 1:1.27 when increased (20% more periportal expression) and 1:2.62 when reduced (20% more pericentral expression). Increasing the zonation constant for triglyceride release as VLDL caused more strongly pericentral steatosis with a ratio of 1:2.22, whilst reducing the constant gave a ratio of 1:1.47. This suggests that the inter-individual variation in the location of steatosis seen *in vivo* is likely to be at least partially accounted for by differences in the zonation of lipid uptake and output proteins.

The zonation constants for oxidative phosphorylation of acetyl-CoA, β-oxidation and pyruvate oxidation also had a notable effect on the location of steatosis (table 3.6). Alterations to the zonation constant for oxidative phosphorylation and β-oxidation directly affect the rate at which fats are oxidised and removed from the cells in each region of the sinusoid. Similarly, alterations to the zonation constant for acetyl-CoA synthesis from pyruvate alter the relative amount of acetyl-CoA produced from glucose in each region and, as a result, the allosteric inhibition of β-oxidation.

Consistent with the results when altering the rate constants, variations in the zonation constants for *de novo* lipogenesis and triglyceride synthesis have little effect on steatosis location in the model. This is despite the continuous stimulation of lipogenesis and triglyceride synthesis through increased SREBP-1c expression. Therefore, non-pathological inter-individual variations in the expression of lipogenesis enzymes are not predicted to account for differences in either susceptibility to steatosis or the distribution of fats across the sinusoid seen *in vivo*.

3.4 Discussion

3.4.1 Insulin resistance and increased SREBP-1c expression

Firstly, additional validation of the model was provided in this chapter, focussing on its representation of NAFLD under conditions of IR and high fat intake. It was demonstrating that, when the known disruptions to metabolism are simulated (IR, increased SREBP-1c expression and high intake), pericentral-centred steatosis occurs and the model replicates the major changes in hepatic

metabolism known to occur *in vivo*. The model allows simulation of the changes in the rates of a wide range of metabolic processes and concentrations of intermediates in specific regions of the sinusoid under different feeding conditions and disease states, which would not be feasible experimentally. Furthermore, having established the ability of the model to provide realistic data for NAFLD, it can be used to make predictions of the effects of different treatments (see chapter 4).

When simulating increased lipid intake in a metabolically normal, insulin sensitive individual, the hepatic triglyceride content was raised but this increase was fairly moderate. Unless a very high fat diet (resulting in plasma lipid concentrations at the high end of those seen in obese individuals) was simulated, the hepatic lipid concentration remained lower than the 5% cut off at which NAFLD is diagnosed. Similarly, high glucose intake primarily caused increased glycogenesis rather than steatosis in insulin sensitive individuals. For more serious steatosis to develop in the model, IR was required. Early stage steatosis arose even when simulating a healthy (moderate intake) diet in an insulin resistant individual. Severe build-up of lipids in the liver occurred when high lipid intake, or to a lesser extent high glucose intake, was simulated in addition to IR. Across the range of insulin sensitivities, low FFA or glucose intake returned simulated plasma triglyceride levels to a healthy range.

Therefore, loss of insulin sensitivity in addition to excessive calorie intake is predicted to be required for more than early stage steatosis to arise. Given that fats in liver are known to cause both hepatic and peripheral desensitivity to insulin, sustained excessive calorie intake will strongly increase the chance of developing hepatic steatosis over time. However, these predictions highlight the effectiveness of a low-fat diet as a treatment for NAFLD, even in insulin resistant patients.

In addition to the direct effects of IR, increased expression of SREBP-1c was required for the model to fully reproduce the metabolic changes seen in the early stages of NAFLD *in vivo*. In particular, increased SREBP-1c expression was required to replicate the increases in lipogenic rates seen *in vivo*. Additionally, both IR and increase SREBP-1c expression contributed to mitochondrial dysfunction, increased β-oxidation and reduced ATP levels in the simulations, consistent with *in vivo* observation.

SREBP-1c is a transcription factor which upregulates lipogenesis and triglyceride synthesis. Under normal conditions, its expression is stimulated by insulin. However, increased expression has been shown to occur in insulin resistant NAFLD patients. It is thought that insulin retains the ability to directly stimulate SREBP-1c expression despite the loss of insulin sensitivity [501, 517]. Alternatively, it is possible that SREBP-1c is stimulated by hyperglycaemia or by the fats themselves [501, 517], similar to the effects of ChREBP [493]. These results highlight the importance of the resulting increase in lipogenesis and triglyceride synthesis in the pathology of the disease. However, the presence of steatosis was seen when simulating the direct effects of IR alone.

3.4.2 Pericentral-centred steatosis in insulin resistant livers results from increases in FFA and G3P concentrations in pericentral cells

In addition to ensuring the model provided a valid representation of NAFLD, a major aim was to understand the metabolic changes leading to the development of steatosis in NAFLD, with a particular focus on understanding the increased susceptibility of pericentral cells to lipid build-up and the resulting damage. Changes in the rate of triglyceride synthesis, rather than output or lipolysis, accounted for the pericentral zonation in steatosis in simulations. A reduction in net triglyceride output also contributed to overall increased triglyceride levels but did not show zone specific differences. The enzymes involved in triglyceride synthesis are not zonated. The pericentral increase in triglyceride synthesis instead arose due to increases in the concentrations of G3P and FFAs.

Defective postprandial glycogen storage occurred when simulating IR and caused a build-up of glucose metabolism intermediates including G3P in hepatocytes. Pericentral cells show lower glycogen synthase activity than periportal cells [45]. When simulating insulin sensitive individuals, this was compensated by increased insulin receptor [490] and reduced glucagon receptor expression [491] in pericentral cells. However, when simulating IR, the zonation in hormone receptors no longer affects glycogen synthesis, and glycogen depletion is most severe in pericentral cells. Additionally, pericentral

cells have fewer mitochondria and downregulated oxidative phosphorylation due to their low oxygen environment [45]. As a result, pericentral cells cannot rapidly metabolise glucose intermediates.

Since glucose oxidation is suppressed in insulin resistant NAFLD patients and β-oxidation is upregulated, the periportal zonation of oxidative phosphorylation enzymes, along with those mediating β-oxidation, had an even larger effect on the simulated rate of oxidation of hepatic FFAs. Excess FFAs were metabolised more rapidly in periportal cells than pericentral.

Increased availability of hepatic FFAs arose from both uptake and *de novo* lipogenesis. The enzymes involved in glycolysis and lipogenesis show pericentral zonation and the increase in *de novo* lipogenesis was largest in pericentral cells. The enzymes mediating FFA uptake, meanwhile, show periportal zonation. When simulating metabolically normal individuals, FFA uptake is dominated by insulin stimulated scavenging leading to strongly periportal uptake. However, when simulating insulin resistant individuals, FFA uptake occurs due to the high plasma FFA concentration rather than insulin stimulation, and passive uptake dominates. Under these conditions, the periportal zonation of FA uptake proteins had a smaller effect on the rate of uptake. Therefore, although total uptake was still higher in periportal cells, a larger increase in rate occurred in pericentral cells.

Together these data suggest that the major differences between pericentral cells and periportal cells accounting for increased pericentral susceptibility to steatosis are lower expression of oxidative phosphorylation enzymes, β-oxidation enzymes and glycogen synthase along with higher expression of lipogenic enzymes in pericentral cells. These differences across the sinusoid account for a larger increase in FFA and G3P concentrations in pericentral cells in NAFLD and, therefore, result in higher triglyceride synthesis in these cells. Future experimental validation of these simulated data could be performed through the addition of radiolabelled substrates to measure the rates of conversion within individual regions of the sinusoid. As discussed supplementary material 1 (section S1.1.5), data of this form has previously been published for metabolically normal individuals, and the model outputs are consistent with experimental data in this case. Similar studies comparing metabolically normal and

NAFLD patients are required. Alternatively, experimental studies destroying specific regions of the sinusoids and measuring the remaining activity for various processes could also be used to provide additional insight [518].

3.4.3 Inter-individual variation in fatty acid oxidation rates most strongly affect susceptibility to steatosis.

Two methods were used to determine the processes most likely to account for variation in the development of steatosis seen between individuals *in vivo*. By varying rate and zonation constants for key processes, a set of simulated patients were created and used to investigate the correlations between expression of the enzymes mediating each process and lipid content across the sinusoid. Sensitivity analysis on the rate and zonation constants for each process was then used to assess the effects of alterations in the rates of key processes individually on steatosis development across the sinusoid.

Both sets of data suggest that any inter-individual variations in the rate of metabolism of hepatic fats will have a large effect on susceptibility to NAFLD development. In the sensitivity analysis, variations in the rate constants for β-oxidation and acetyl-CoA use in the citrate cycle had notably larger effects on hepatic lipid levels than equivalent variations in the rate constants of other processes. Furthermore, total hepatic lipid levels showed the next highest sensitivity to the rate constants for glucose uptake, glycolysis and acetyl-CoA synthesis from pyruvate, all of which play a role in the allosteric inhibition of β-oxidation by acetyl-CoA. When simulating the randomly generated sample patients, a strong negative correlation was also seen between oxidative phosphorylation and hepatic lipid content. Therefore, in both data sets, susceptibility to steatosis is predicted to be most strongly determined by the rate at which hepatocytes can metabolise fats.

As validation of this prediction, there is considerable evidence to suggest mitochondrial function, aerobic capacity and capacity for β-oxidation inversely correlate with liver fat percentage and prevalence of NAFLD [155, 172-176, 519-522]. Furthermore, consistent with the high sensitivity of fat

storage to oxidation rates, global knockout of ACC2 (resulting in reduced allosteric inhibition of β-oxidation) has been shown to reduce T2DM risk, obesity and adipose fat storage [523-525]. Liver specific knockout of ACC1 and ACC2 has been shown to reduce hepatic steatosis, although this resulted from both reduced lipogenesis and increased β-oxidation [526]. However, additional more directed studies are required to determine whether higher β-oxidation and oxidative phosphorylation capacities protect against hepatic steatosis independent of confounding factors such as exercise or caloric intake.

Whilst the predominant location of steatosis showed some dependence to the zonation of enzymes mediating oxidative phosphorylation and β-oxidation, it was far more sensitive to changes in the zonation constants for FA uptake and triglyceride release as VLDL. Therefore, inter-individual variation in the distribution of steatosis is predicted to be accounted for by differences in the zonation of proteins mediating lipid uptake and triglyceride release. At present, little experimental data exists to validate this prediction due to the difficulty involved in measuring the distributed activities of large numbers of enzymes. However, the model simulations allow for targeted potential future experiments. The activities of the proteins mediating lipid uptake and triglyceride release could be measured in each region of the sinusoid, before comparing this data with distribution of steatosis across a range of samples.

3.5 Conclusions of Chapter

Due to the large heterogeneity in metabolism across the sinusoid, a clear description of the metabolic changes occurring in each zone is required to fully understand NAFLD development and to optimise potential pharmacological interventions. In this chapter, the computational model of sinusoidal metabolism presented in chapter 2 was used to simulate the development of NAFLD, focussing on the metabolic changes in individual zones. Consistent with experimental observation, both IR and increased SREBP-1c expression were required for the model to fully replicate the metabolic changes seen in NAFLD *in vivo*.

Simulations were run to identify the key differences between periportal and pericentral cells which account for higher pericentral susceptibility to steatosis. The majority of additional FFAs in NAFLD arise from FA uptake rather than *de novo* lipogenesis both in the simulated data and experimentally [26, 492, 495, 496]. Although FA uptake enzymes show periportal zonation, the switch from predominantly insulin stimulated FA scavenging to passive diffusion reduced the effect of this heterogeneity on the rate of uptake across the sinusoid in the model simulations. Instead, the model simulations highlight the periportal zonation of oxidative phosphorylation and β-oxidation enzymes, along with the pericentral expression of lipogenesis enzymes as the key differences leading to a raised FFA concentration in pericentral cells when simulating insulin resistant NAFLD patients. Additionally, reduced insulin stimulation of glycogenesis caused the build-up of glucose intermediates, including G3P across the sinusoid. A more severe increase in pericentral and intermediate cells occurred due to the periportal zonation of glycogen synthase and of oxidative phosphorylation.

Two methods of analysis were performed investigating the effects of changes in the rate and zonation constants to determine likely inter-individual differences in enzyme activities accounting for variation in susceptibility to NAFLD and steatosis distribution seen *in vivo*. Hepatic triglyceride levels were most sensitive to inter-individual variations in the rate of FFA oxidation, either through differences in the overall rate of oxidation of acetyl-CoA or differences in the relative contribution of FFAs and glucose to oxidation. The predominant location of steatosis across the sinusoid meanwhile was most sensitive to changes in the zonation of proteins mediating FFA uptake or VLDL synthesis and release.

4 Analysis of potential drug targets for reducing steatosis in NAFLD

4.1 Introduction to Chapter

In this chapter, inhibition or stimulation of various pathways as potential pharmacological targets for treating NAFLD are simulated. As of 2016, there is no approved drug for NAFLD or NASH [314], and to prevent the large number of deaths resulting from excess liver fat and the development of NASH, it is essential to identify drug targets which clear excess liver fat. However, due to the fundamental importance of lipid metabolism pathways in various essential cellular processes, the impact of any intervention on metabolism as a whole must also be assessed. Additionally, the heterogeneity in enzyme expression and function in hepatocytes across the sinusoid means that any medication must reduce steatosis without causing adverse effects in all regions [50]. As discussed in the previous chapters, when assessed in NAFLD patients *in vivo*, pericentral hepatocytes are known to show higher susceptibility to developing steatosis and the resulting damage than periportal cells, although pan-sinusoidal and azonal steatosis patterns are also regularly seen [15-17, 377]. Experimentally studying the effects of targeting specific enzymes or hepatic processes on metabolism across the sinusoid would be time consuming, animal intensive and expensive due to the small size of the sinusoid and the large number of potential variables.

In this chapter, by simulating inhibition and stimulation of various potential targets, we aim to find targets which reduce steatosis across the sinusoid without adversely affecting ATP production or causing changes likely to lead to oxidative stress such as excess FFA hepatic concentrations when simulating different stages of fatty liver arising from both excess fat intake alone and from IR and metabolic dysregulation in addition to raised intake. Here we focus on targets for removing the excess lipids from hepatocytes and thereby removing the underlying cause of IR, fibrosis and cirrhosis development. To treat effectively, it is likely that medication reducing existing inflammation in the cells would also be required [314]. In the chapter 5, key findings are tested in a hepatocyte-like cell culture model.

4.1.1 Inputs, insulin resistance and representing NAFLD development

Throughout the simulations run in this chapter, the model was provided with spiked inputs at 4 hour intervals as a crude approximation to the intake of meals throughout the day (excluding sleep) as discussed in section 2.2.4.2. When simulating a moderate intake diet, the peak rates of glucose and FA intake were set so that each meal on average contained 78.1g of carbohydrate (glucose) and 22.2g of fat based on the meals provided to patients in a study by Daly *et al.* [425].

The effects of potential treatments were simulated for three stages of NAFLD development, from an early stage entirely caused by increased fat intake, to a later stage predominantly caused by IR and metabolic dysregulation. These stages were based on the simulations in the previous chapter, where it was shown that very high fat intake is required for hepatic steatosis to develop in insulin sensitive individuals but, as IR develops, lower intake was required for excess fats to build up in the liver. Early- to late stage refers to the extent of metabolic dysregulation, and therefore the loss of immediate reversibility of the condition, rather than a progressive increase in the liver fat content between the stages. As discussed in the previous chapter, since the model does not contain adipocyte proliferation or swelling, excess dietary lipids remain in the plasma rather than being stored in adipocytes and changes in input have a larger effect on metabolism. As a result, smaller increases in lipid intake (based on matching the plasma lipid concentrations to values measured experimentally (section 4.2.1)) were used in simulations. The parameter changes (corresponding to fat intake, IR and SREBP-1c expression) used to represent these changes are presented in table 4.1 and the resulting changes to metabolism are discussed in section 4.2.1.

In addition, the effects of targeting each pathway were simulated in metabolically normal individuals on a sustained low fat intake diet to identify possible dangers if medications are taken by those with reduced plasma FFA concentrations. For example, an individual may continue to take the medication after adopting a healthier diet and lifestyle. Finally, the effects of inter-individual variation in hepatic metabolism on key predictions are assessed in section 4.2.3. The effects of each intervention were

simulated until equilibrium was reached between successive input cycles. Once equilibrium was established, the average values over each 4 hour input cycle are presented.

Table 4.1: The parameter value changes used to simulate the various NAFLD stages.

NAFLD Stage	FFA Input v_{input}^{FFA}	Insulin Resistance k_{IR}	SREBP-1c: Lipogenesis v_{lipog}	SREBP-1c: Triglyceride synthesis k_{TGsyn}
Moderate Intake, Metabolically Normal	1	1	1	1
Early Stage: Very High FFA Intake, Metabolically Normal	1.25	1	1	1
Mid-Stage: Developing IR, High FFA Intake;	1.125	0.05	1	1
Later Stage: Severe IR, Raised FFA Intake	1.05	0.025	2.25 (1nM Insulin)	2 (1nM Insulin)
Low Fat Diet, Metabolically Normal	0.875	1	1	1

Values are presented relative to moderate intake in a metabolically normal individual.

4.1.2 Inhibitions simulated

Each process in the model is represented by a rate constant multiplied by a zonation constant and a series of substrate, hormonal and allosteric dependences (chapter 2). By simulating changes in these rate constants, which determine the maximum activity of the enzymes, we can assess the impact of stimulating or inhibiting key enzymes, not only on lipid concentrations but on metabolism as a whole across the sinusoid.

Only potential drug targets which reduce the hepatic lipid content by removing lipids from the system, rather than redirecting them into the blood, are considered in this report. When interventions such as stimulation of triglyceride release as VLDL or blocking FA uptake from plasma were simulated, rapid increases in plasma triglyceride and FFA concentration occurred. These are likely to cause damage as a result of lipid build-up in other tissues. Given that fats in liver in particular are known to cause both organ specific and peripheral IR, this may still be beneficial to an individual. However, NAFLD patients are known to often have increased visceral adipose mass which is less responsive to insulin and less effective at clearing plasma lipids [8, 155, 527, 528]. As a result, rather than being stored in adipose tissue, these additional excess fats are likely to build-up in other tissues where they are known to

cause harm such as the heart, muscle and pancreas, as has been demonstrated when blocking FA uptake *in vivo* [529]. Therefore, the focus was instead on hepatic targets which removed fat from the system, rather than redirect them elsewhere. This includes the conversion of glucose to G6P, the conversion of G6P to GADP, the conversion of GADP to pyruvate, pyruvate oxidation, lipogenesis, β-oxidation and triglyceride synthesis. These interventions are shown in figure 4.1.

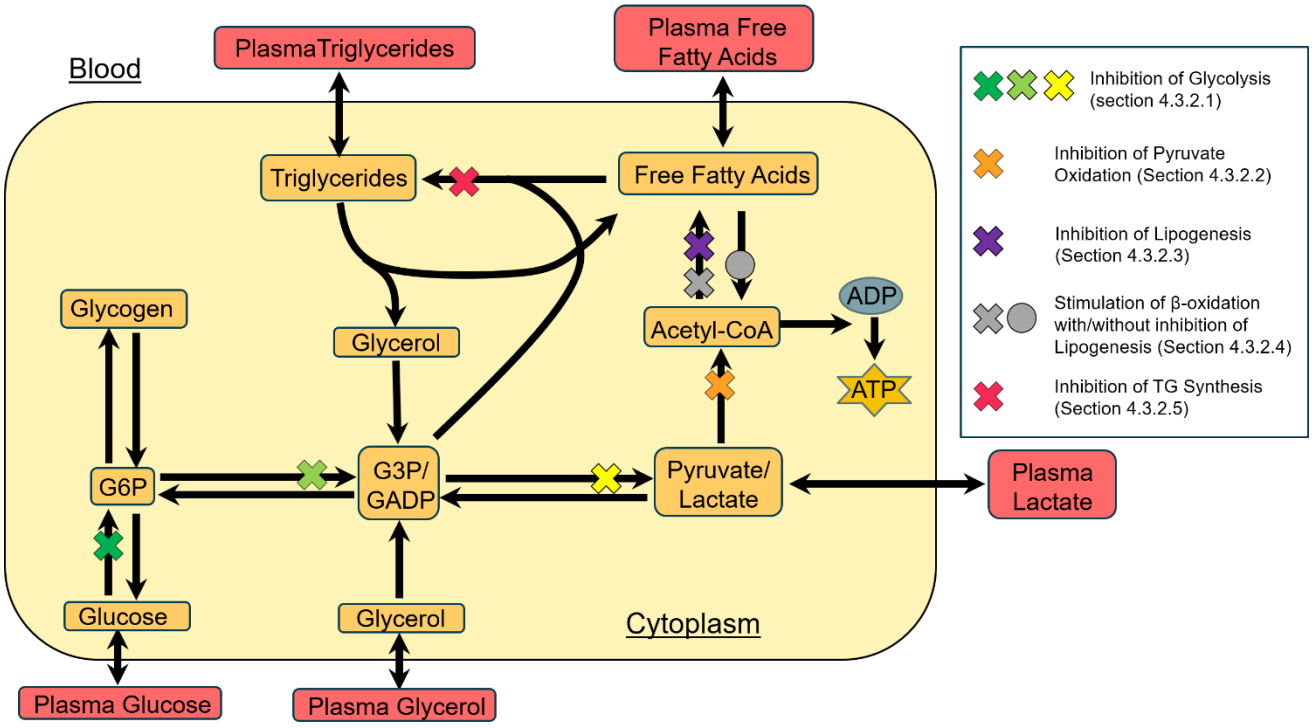

Figure 4.1: The processes investigated as potential targets for intervention in NAFLD.

Inhibiting the production of pyruvate through glycolysis provides a potential method of reducing the available substrate for *de novo* lipogenesis and forcing the cells to oxidise FAs rather than glucose. In the model, glycolysis is represented by the initial conversion of glucose to G6P, followed by the conversion of G6P to two GADP molecules (closely related to G3P) and the conversion of GADP to pyruvate. In preliminary simulations, a range of reductions of the three rate constants, corresponding to the degree of inhibition of the process, were assessed. Since notable disturbances to ATP synthesis were seen for high degrees of inhibition, for the data presented in this report the rate constants were reduced by $^{1}/_{3}$ to provide a balance between reducing *de novo* lipogenesis and promoting β-oxidation whilst allowing some glycolysis and glucose oxidation to occur for ATP synthesis when required.

Inhibition of pyruvate oxidation, mediated by the pyruvate dehydrogenase complex, allows a reduction in the production of acetyl-CoA from glucose without blocking glucose-lactate cycling. In initial simulations, a range of degrees of inhibition of the process were simulated. The data from these tests also showed that a balance was required between maximising the reduction in steatosis and minimising the disruption to energy metabolism. For the data in this report, the rate constant was halved to allow continued production of acetyl-CoA from glucose for use in oxidative phosphorylation when required.

Another potential method to reduce hepatic lipid concentration is to directly target the synthesis and elongation of FAs from acetyl-CoA, primarily mediated by ACC and FAS. Total inhibition of lipogenesis was simulated (reducing the rate constant to zero), since no notable adverse effects in energy metabolism were noted when the process was inhibited in preliminary simulations.

An alternative approach to clearing steatosis is to stimulate the oxidation of FAs. In initial simulations, various degrees of stimulation of β-oxidation were simulated. When simulating the data in this report, the rate was doubled to balance the reduction in lipid content resulting from high stimulation with potential disruptions to energy metabolism based on the preliminary simulations.

Finally, rather than attempting to reduce the hepatic FFA concentration, steatosis may be reduced by directly inhibiting the synthesis of triglycerides, preventing lipid storage. Since triglyceride synthesis does not directly affect either oxidative or non-oxidative ATP synthesis, complete inhibition of the process was simulated.

4.1.3 Criteria for judging effectiveness of a treatment

The following criteria were used to determine the effectiveness of a potential target. A process must firstly reduce hepatic triglyceride concentrations (roughly equal to the total lipid content) to a healthy level (below the 5% criteria used to define NAFLD). Lipids must be cleared in all regions of the sinusoid. As discussed above, potential targets which reduce the hepatic triglyceride concentration by forcing

lipids into the blood stream are not considered in this report since they would be associated with the build-up of fats in other tissues around the body.

Secondly, FFAs, along with closely related molecules including ceramides and DAGs, are known to be particularly potent in promoting mitochondrial stress and IR [8, 146, 247, 248, 253-259]. Although the mechanisms by which hepatic FFAs cause hepatic damage are not included in the model, potential drug targets which case reduction of the hepatic FFA concentration specifically, in addition to total lipid content, are likely to be associated with an improvement in liver injury.

Any pharmacological intervention must not further reduce ATP concentrations to avoid loss of function resulting from defective energy metabolism. Furthermore, to avoid mitochondrial stress and ROS production from the ETC, the treatment must not cause excess flux through the ETC. The combination of excess ETC flux and dysfunctional ETC enzymes seen in NAFLD is known to result in superoxide radical anion and hydrogen peroxide (ROS) production which should be resolved by a potential treatment [229, 230, 501, 512, 514-516]. The ETC flux and ATP concentration were assessed in each region of the sinusoid for all three stages of NAFLD and for individuals on a low fat diet, to ensure the intervention does not disrupt metabolism in the model.

Finally, any intervention should not cause excessively raised plasma glucose, lactate, FFA and triglyceride concentrations. In particular, glycogen synthesis should not be blocked. Although glycogen synthesis is defective in insulin resistant individuals, an improvement in hepatic steatosis would be expected to be associated with an improvement in insulin sensitivity *in vivo* (section 1.3.4.2.2).

4.2 Results

4.2.1 Simulated Stages of NAFLD Development

As discussed in chapters 3, when simulating an insulin sensitive, metabolically normal individual on a moderate diet, the average hepatic lipid content was 2.3% (figure 4.2c, table 4.2). This towards the low end of values measured in the US general population by Szczepaniak *et al.* [211], consistent with

a healthy individual on a healthy diet. The simulated concentration increased from 2.0% to 2.7% between periportal and pericentral ends of the sinusoid (figure 4.2c) similar to the increase measured by Guzman *et al. in vivo* [86]. The hepatic and plasma concentrations of various molecules when simulating the three stages of NAFLD, along with metabolically normal individuals on moderate and low fat diets are shown in table 4.2.

To represent steatosis arising from very high fat intake alone (early-stage), the rate of lipid intake was increased so that the simulated plasma FFA and triglyceride concentrations matched the highest values measured in obese individuals by Sindelka *et al.* [141] (FFA: 0.9mM, TG: 4.1mM, table 4.2). This is equal to the very high fat intake diet (27.75g/meal) simulated in chapter 3. When simulating these conditions, the average hepatic triglyceride content more than tripled to 7.2%, with a gradient in concentration from 5.8% to 9.0% across the sinusoid (figure 4.2c).

To represent a mid-stage in NAFLD development, developing IR (5% detection) was simulated in individuals with a sustained high fat intake diet (24.6g/meal). At this stage the system begins to become hyperglycaemic with an average plasma glucose concentration of 6.5mM, but hyperinsulinaemia compensates for the most severe effects of IR. The average hepatic triglyceride content was 9.1% with the largest rise in pericentral cells (12.3%) (figure 4.2c). The simulated plasma triglyceride (6.0mM) and FFA (1.1mM) concentrations were severely raised (table 4.2).

Finally, to represent a later stage, severe IR (2.5% detection) was simulated in individuals with a raised lipid intake diet (23.2g/meal). Additionally, as discussed in chapter 3, when studied *in vivo*, NAFLD patients show a counter intuitive increase in SREBP-1c expression, a protein which stimulates lipogenesis and triglyceride synthesis [36-39]. In chapter 3, it was shown that this increase in SREBP-1c expression must be simulated in addition to IR to fully replicate the metabolic changes seen in NAFLD patients *in vivo*. Therefore, to represent later-stage NAFLD, the effects of increased SREBP-1c expression were included through continuous stimulation of hepatic lipogenesis and triglyceride synthesis (equivalent to 1nM). When simulating these conditions, hyperglycaemia occurred post-

prandially, with a peak concentration of 12.7mM as insulin could no longer stimulate the storage of glucose as glycogen (table 4.2). The average hepatic triglyceride content was 8.9% (figure 4.2c). Due to the up-regulation of lipogenesis, which occurs primarily in pericentral cells, an increased periportal-pericentral gradient in triglyceride concentration was seen relative to the other stages of steatosis development (PP->PC: 6.0%->12.7%). Severe increases occurred in the simulated plasma triglyceride and FFA concentrations (table 4.2).

In addition to the total lipid content, the hepatic FFA concentrations were increased when simulating all three stages of NAFLD (figure 4.2b). The average concentration was markedly increased when simulating the early stage of NAFLD to 39.0μM from 21.5μM when simulating a metabolically normal individual on a moderate intake diet. When simulating the mid- and later disease stages, lower FFA inputs were used resulting in less severely raised FFA concentrations (mid stage 30.0μM, later stage 26.2μM).

The ATP concentration was progressively reduced when simulating early to later stages of NAFLD, as is seen *in vivo* [44, 227, 228, 505, 506] (figure 4.2a). For the later stage of NAFLD, the simulated average concentration fell by 18% to 2.3mM compared with 2.8mM in a metabolically normal individual. A switch to deriving ATP almost exclusively from FA oxidation reduced the additional ATP synthesized in glycolysis. Secondly increased SREBP-1c expression caused increased ATP consumption in lipogenesis [44, 227, 228, 505-509]. The decrease in ATP concentration was particularly severe in hypoxic pericentral cells which rely heavily on non-oxidative metabolism. In these cells, the simulated concentration fell from 2.5mM to 1.9mM in later-stage NAFLD. *In vivo*, in the later stages of NASH, further reductions in ATP concentration occur due to a loss of function in the oxidative phosphorylation enzymes [501].

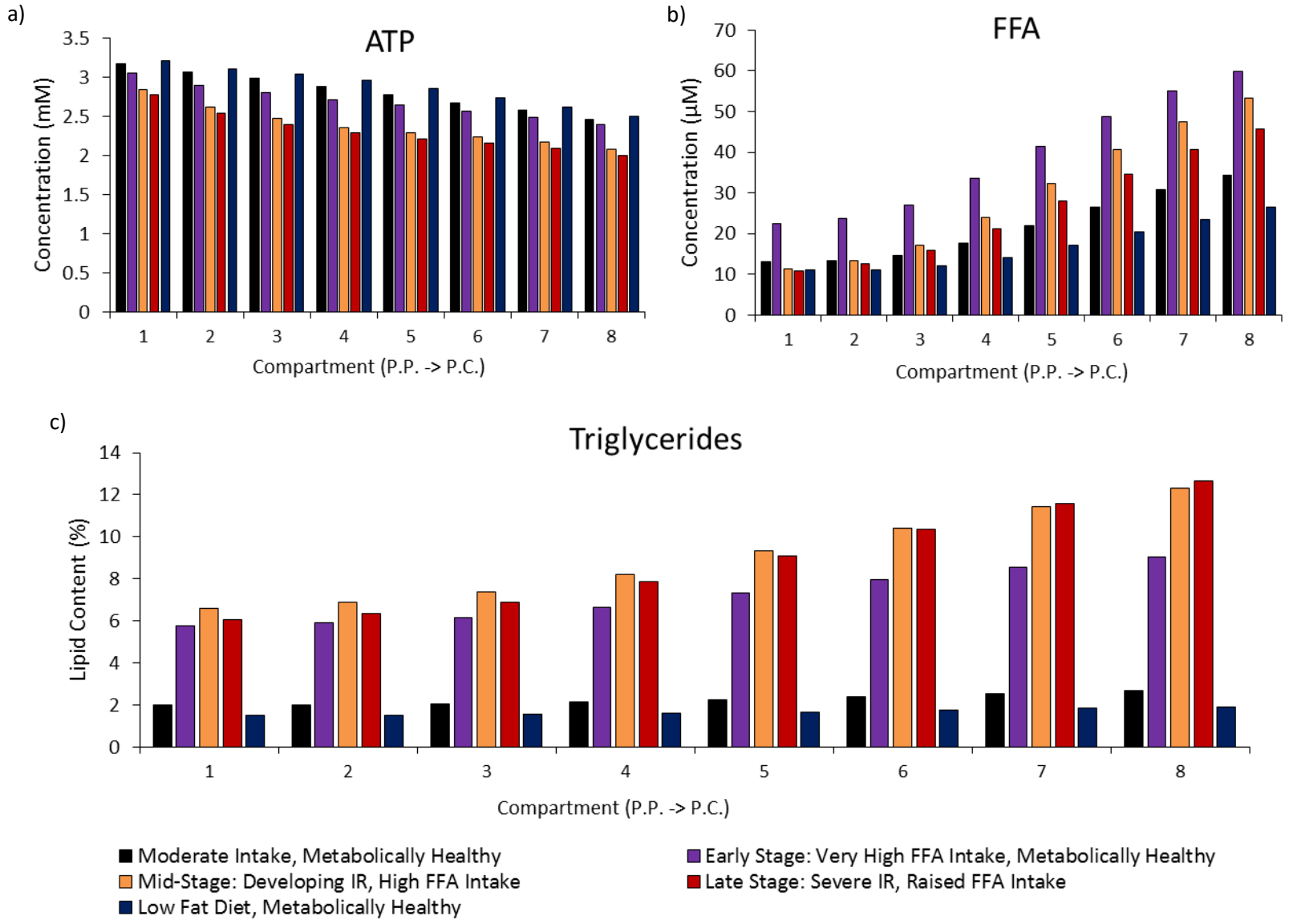

Figure 4.2: Simulated stages of NAFLD development. *The (a) the hepatic lipid content, (b) the hepatic FFA concentration and (c) the hepatic ATP concentration across the sinusoid when simulating the early, mid and later stages of NAFLD development. The average concentration is depicted when simulating a 4-hour intake/output cycle of the form discussed in the model building section.*

Table 4.2: The concentrations of key hepatic and plasma molecules when simulating different stages of NAFLD development.

	Average Hepatic FFA Concentration	Average Hepatic ATP Concentration	Average Plasma Triglyceride Concentration	Average Plasma FFA Concentration	Average Plasma Glucose Concentration	Average Plasma Lactate Concentration	Average Hepatic Triglyceride Content	Average Ox-Phos Rate (% of MN rate)
Moderate Intake, Metabolically Normal	21.5 µM	2.8 mM	1.2 mM	0.2 mM	5.0 mM	1.2 mM	2.3%	118 µM ATP/s
Early Stage: Very High FFA Intake, Metabolically Normal	39.0 µM	2.7 mM	4.1 mM	0.9 mM	5.0 mM	1.2 mM	7.2%	122 µM ATP/s
Mid-Stage: Developing IR, High FFA Intake;	30.0 µM	2.4 mM	6.0 mM	1.1 mM	6.5 mM	1.2 mM	9.1%	127 µM ATP/s
Later Stage: Severe IR, Raised FFA Intake	26.2 µM	2.3 mM	5.4 mM	3.9 mM	6.7 mM	1.4 mM	8.9%	128 µM ATP/s
Low Fat Diet, Metabolically Normal	17.0 µM	2.9 mM	0.9 mM	0.15 mM	5.0 mM	1.3 mM	1.7%	115 µM ATP/s

The hepatic triglyceride, FFA and ATP concentrations, hepatic rate of oxidative phosphorylation and plasma triglyceride, FFA, glucose and lactate concentrations when simulating the early to later NAFLD stages and a metabolically normal individual on a moderate and a low-fat intake diet.

Despite this drop in ATP concentration, the rate of ATP production through the citrate cycle was increased when simulating the mid- and later- stages of NAFLD by 8.4% and 9.2% respectively (table 4.2). Mitochondrial stress and ROS production occur in NAFLD *in vivo*, and this excess ETC flux, in addition to reduced mitochondrial function, is likely to contribute [501, 512, 514-516]. Excess ETC flux results in production of the superoxide anion radical, particularly when the ETC enzymes are not fully functional, which can in turn be converted to hydrogen peroxide. These disruptions to energy metabolism have been suggested as possible mechanisms for the progression of NAFLD to NASH [229, 230].

4.2.2 Targeting hepatic processes in the model

4.2.2.1 Glycolysis

Partial inhibition of the conversion of glucose to G6P prevented the uptake of glucose for storage or glycolysis, resulting in increased glucose and insulin concentrations when simulating all stages of NAFLD (table 4.3). For later stage NAFLD, the post-prandial peak plasma glucose concentration rose to 15.4mM, well above the acceptable range. Furthermore, the raised plasma glucose and insulin concentrations resulted in continuous lipogenesis in adipose tissue, in turn causing the hepatic lipid content to increase through uptake of excess plasma FFAs (figure 4.3a,b; table 4.3). Therefore, rather than improving steatosis, the treatment caused an increase in hepatic triglyceride concentration (later stage: 8.9%->12.5% when partially inhibited; figure 4.3a). In a NAFLD patient *in vivo*, a larger percentage of these excess lipids are likely to be stored in adipose tissue rather than released into the plasma. However, the simulated data show that partial inhibition of GK increases plasma glucose levels even in insulin sensitive individuals.

Targeting either of the two processes further along the glycolysis caused disruptions to pericentral energy metabolism when simulating all stages of NAFLD (figure 4.3c, table 4.3). This effect was small for the early stage of NAFLD (when either process was inhibited the ATP concentration fell to 2.6mM compared with 2.7mM when uninhibited). However, for the later stage of NAFLD, the pericentral ATP

Table 4.3: The effect of targeting the various hepatic processes on key hepatic and plasma molecules.

	Average Hepatic FFA Concentration	Average Hepatic ATP Concentration	Average Plasma Triglyceride Concentration	Average Plasma FFA Concentration	Average Plasma Glucose Concentration	Average Plasma Lactate Concentration	Average Hepatic Triglyceride Content	Average Ox-Phos Rate (% of MN rate)
Early Stage NAFLD/IR Development: Very high fat diet in insulin sensitive individuals								
Standard Parameter Values (Untreated)	39.0 µM	2.7 mM	4.1 mM	0.9 mM	5.0 mM	1.2 mM	7.2%	122 µM ATP/s
Partial Inhibition of Glucokinase	45.7 µM	2.8 mM	6.8 mM	1.0 mM	5.2 mM	1.3 mM	12.1%	119 µM ATP/s
Partial Inhibition of G6P->GADP	41.9 µM	2.6 mM	3.0 mM	0.5 mM	5.0 mM	0.7 mM	5.1%	120 µM ATP/s
Partial Inhibition of GADP->Pyr	26.3 µM	2.6 mM	2.9 mM	0.5 mM	5.0 mM	0.6 mM	5.1%	122 µM ATP/s
Partial Inhibition of Pyruvate Oxidation	25.0 µM	2.7 mM	2.4 mM	0.4 mM	5.0 mM	3.2 mM	4.1%	121 µM ATP/s
Inhibited Lipogenesis	29.6 µM	2.9 mM	2.9 mM	0.5 mM	5.0 mM	0.9 mM	5.1%	117 µM ATP/s
Stimulated β-oxidation	17.3 µM	2.5 mM	2.0 mM	0.3 mM	5.0 mM	1.3 mM	3.4%	125 µM ATP/s
Stimulation of β-oxidation with inhibition of DNL	14.3 µM	2.8 mM	1.8 mM	0.3 mM	5.0 mM	0.9 mM	2.9%	118 µM ATP/s
Inhibition of Triglyceride Synthesis	230.4 µM	2.7mM	2.3mM	0.4mM	5.0mM	1.1mM	2.5%	121 µM(ATP)/s
Mid-Stage NAFLD/IR Development: High fat diet in individuals developing insulin resistance								
Standard Parameter Values (Untreated)	30.0 µM	2.4 mM	6.0 mM	1.1 mM	6.5 mM	1.2 mM	9.1%	127 µM(ATP)/s
Partial Inhibition of Glucokinase	35.1 µM	2.5 mM	8.5 mM	1.6 mM	6.6 mM	1.1 mM	12.5%	126 µM(ATP)/s
Partial Inhibition of G6P->GADP	31.6 µM	2.4 mM	4.5 mM	0.7 mM	6.7 mM	0.7 mM	6.3%	125.7 µM(ATP)/s
Partial Inhibition of GADP->Pyr	19.2 µM	2.3 mM	4.3 mM	0.7 mM	6.7 mM	0.6 mM	6.2%	127 µM(ATP)/s

Partial Inhibition of Pyruvate Oxidation	15.8 µM	2.4 mM	3.1 mM	0.5 mM	6.6 mM	3.3 mM	4.0%	126 µM(ATP)/s
Inhibited Lipogenesis	20.8 µM	2.6 mM	4.0 mM	0.6 mM	6.8 mM	0.9 mM	5.6%	123 µM(ATP)/s
Stimulated β-oxidation	10.8 µM	2.2 mM	2.6 mM	0.4 mM	6.7mM	1.2 mM	3.6%	128 µM(ATP)/s
Stimulation of β-oxidation with inhibition of DNL	7.9 µM	2.5 mM	2.4 mM	0.4 mM	6.9 mM	0.8 mM	3.2%	123 µM(ATP)/s
Inhibition of Triglyceride Synthesis	122µM	2.4 mM	3.1 mM	0.6mM	6.7 mM	1.1 mM	3.2%	127 µM(ATP)/s
Later Stage NAFLD/IR Development: Severe insulin resistance + Increased SREBP-1c expression								
Standard Parameter Values (Untreated)	26.2 µM	2.3 mM	5.4 mM	3.9 mM	6.7 mM	1.4 mM	8.9%	128 µM(ATP)/s
Partial Inhibition of Glucokinase	25.6 µM	2.3 mM	7.4 mM	6.5 mM	9.6 mM	1.3 mM	12.5%	128 µM(ATP)/s
Partial Inhibition of G6P->GADP	25.8 µM	2.2 mM	5.9 mM	3.3 mM	7.3 mM	0.9 mM	9.3%	129 µM(ATP)/s
Partial Inhibition of GADP->Pyr	15.8 µM	2.1 mM	5.8 mM	3.4 mM	7.3 mM	0.7 mM	9.4%	130 µM(ATP)/s
Partial Inhibition of Pyruvate Oxidation	14.7 µM	2.2 mM	4.4 mM	0.6 mM	8.1 mM	6.0 mM	6.1%	128 µM(ATP)/s
Inhibited Lipogenesis	12.3 µM	2.6 mM	5.1 mM	0.6 mM	8.5 mM	1.0 mM	7.0%	123 µM(ATP)/s
Stimulated β-oxidation	8.9 µM	1.9 mM	3.5 mM	0.5 mM	8.2 mM	1.5 mM	4.8%	131 µM(ATP)/s
Stimulation of β-oxidation and inhibition of DNL	5.8 µM	2.5 mM	3.0 mM	0.4 mM	8.8 mM	0.9 mM	3.8%	124 µM(ATP)/s
Inhibition of Triglyceride Synthesis	135.1 µM	2.2 mM	3.9 mM	0.6 mM	8.3 mM	1.3mM	3.9%	130 µM(ATP)/s
Low fat diet in metabolically normal individuals								
Standard Parameter Values (Untreated)	17.0 µM	2.9 mM	0.9 mM	0.15 mM	5.0 mM	1.3 mM	1.7%	115 µM(ATP)/s

Partial Inhibition of Glucokinase	23.2 µM	3.0 mM	1.0 mM	0.2 mM	5.2 mM	1.3 mM	2.2%	113 µM(ATP)/s
Partial Inhibition of G6P->GADP	18.3 µM	2.9 mM	0.8 mM	0.1 mM	4.9 mM	0.7 mM	1.4%	112 µM(ATP)/s
Partial Inhibition of GADP->Pyr	12.5 µM	2.8 mM	0.8 mM	0.1 mM	4.9 mM	0.6 mM	1.4%	114 µM(ATP)/s
Partial Inhibition of Pyruvate Oxidation	12.1 µM	2.8mM ** notably reduced in periportal cells	0.7 mM	0.13 mM	5.0 mM	4.5 mM	1.4%	113 µM(ATP)/s
Inhibited Lipogenesis	12.3-13.6 µM	3.0 mM	0.8mM	0.13 mM	5.0 mM	1.0 mM	1.4%	110 µM(ATP)/s
Stimulated β-oxidation	8.9 µM	2.8 mM	0.7 mM	0.12 mM	5.0 mM	1.3 mM	1.3%	117 µM(ATP)/s
Stimulation of β-oxidation and inhibition of DNL	7.0 µM	3.0 mM	0.7 mM	0.11 mM	5.0 mM	0.9 mM	1.1%	111 µM(ATP)/s
Inhibition of Triglyceride Synthesis	89.3 µM	2.9mM	0.7 mM	0.13 mM	5.0mM	1.2mM	1.0%	114 µM(ATP)/s
Reference Values: Metabolically normal individuals on moderate diet								
Standard Parameter Values	21.5 µM	2.8 mM	1.2 mM	0.2 mM	5.0 mM	1.3 mM	2.4%	118 µM(ATP)/s

The effect of targeting the various hepatic processes on hepatic triglyceride, FFA and ATP concentrations, the hepatic rate of oxidative phosphorylation, and plasma triglyceride, FFA, glucose and lactate concentrations. The interventions simulated in each case are described in section 4.1.2.

Partial Inhibition of Glycolysis (3 stages)

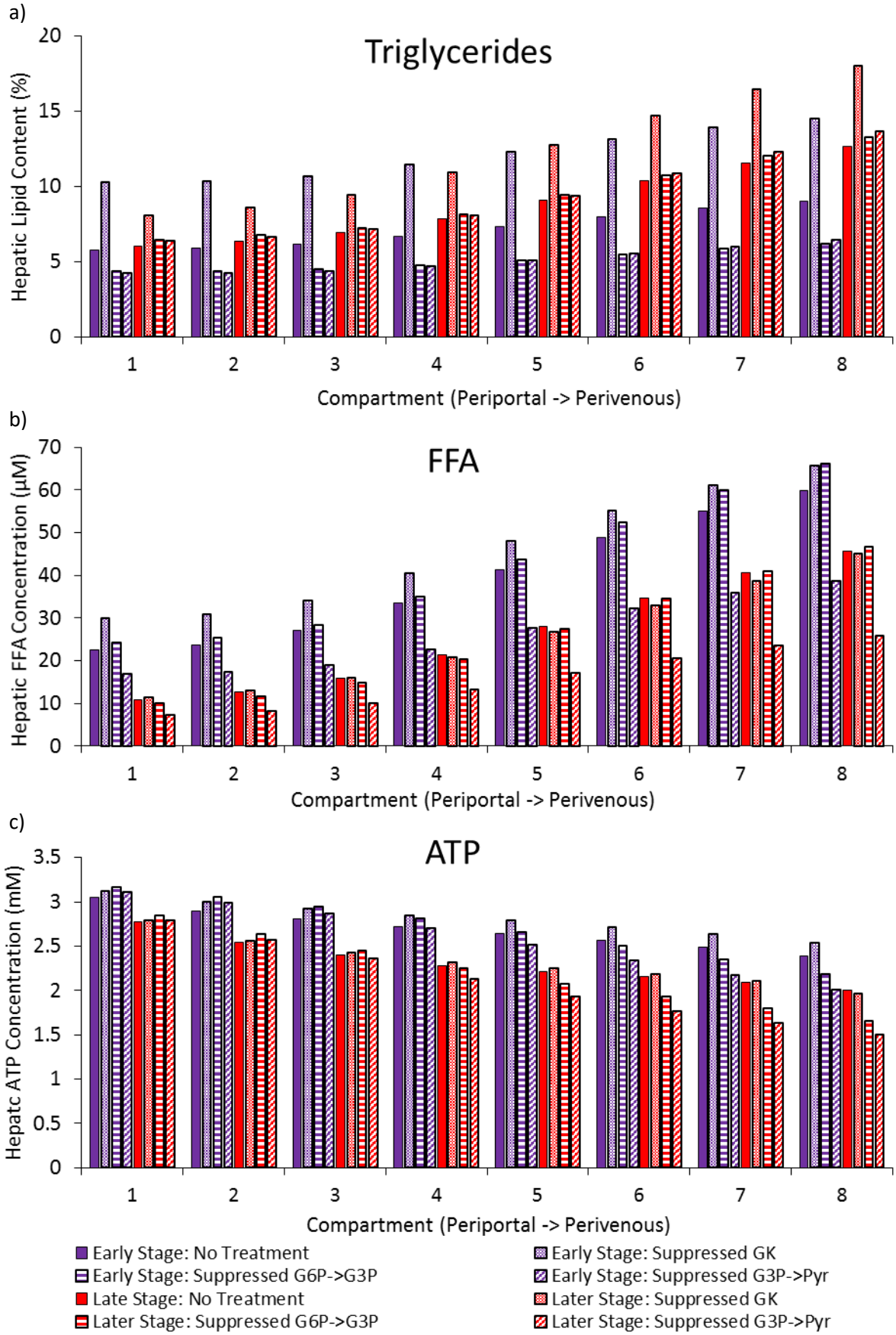

Figure 4.3: Simulating inhibition of glycolysis. *The simulated effects of reducing the rate constant for glycolysis by one third on (a) hepatic lipid content, (b) hepatic FFA concentration and (c) hepatic ATP concentrations when simulating the range of NAFLD stages.*

concentration fell to 1.7mM when simulating partial inhibition of the conversion of G6P to GADP and to 1.5mM for partial inhibition of the conversion of GADP to pyruvate glycolysis. These reductions in pericentral ATP concentration, compared with 2.5mM when simulating a metabolically normal individual, occurred because pericentral cells, which inhabit a hypoxic environment, rely on glycolysis to produce additional ATP. Furthermore, although the hepatic triglyceride concentration decreased slightly when simulating partial inhibition of these two glycolysis processes in early stage, insulin sensitive NAFLD (7.2% -> 5.1% when either process was inhibited; figure 4.3a), no notable change in triglyceride content occurred in any region of the sinusoid for the mid- and later NAFLD stages (figure 4.3a; table 4.3). A decrease in hepatic FFA concentration was seen when targeting the conversion of GADP to pyruvate (later stage 25.6-39.0μM -> 15.8-26.3μM), but not when inhibiting the conversion of G6P to GADP.

Due to the changes in ATP concentration and ineffective clearance of steatosis, none of the processes along the glycolysis chain are predicted to be suitable as a target for reducing steatosis.

4.2.2.2 Pyruvate Oxidation

Halving the rate constant of pyruvate oxidation reduced the hepatic lipid content to less than 5% when simulating the early and mid-stages of NAFLD development. However, when simulating the later stage, the average hepatic lipid content was only reduced to 6.1% and remained notably raised in pericentral cells. (4.8->8.2% from periportal to pericentral ends of the sinusoid) (figure 4.4a). Hepatic FFA concentrations were reduced for all three NAFLD stages (26.2-39.0μM -> 14.7-25.0μM when inhibited; figure 4.4b). Plasma FFA and triglyceride concentrations were additionally markedly reduced, particularly when simulating the early and mid-stages of NAFLD development (table 4.3).

However, some adverse metabolic changes were predicted when simulating the partial inhibition of pyruvate oxidation. Plasma lactate concentrations increased, particularly when simulating the later stage of the disease where the average concentration rose to greater than 6mM (figure 4.4c and table

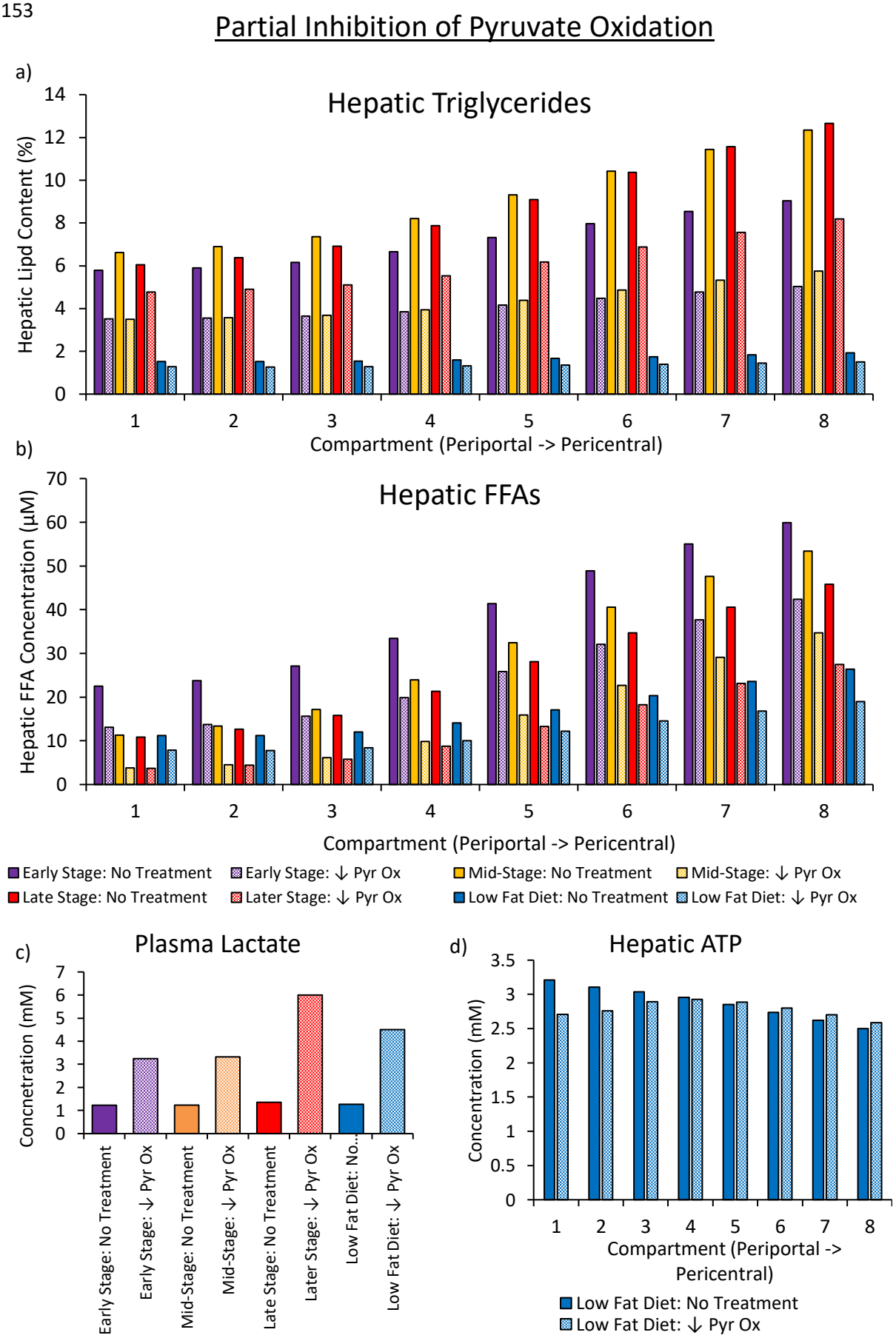

Figure 4.4: Simulating inhibition of pyruvate oxidation. *The simulated effects of reducing the rate constant for pyruvate oxidation by a half on (a) hepatic lipid content, (b) hepatic FFA concentration and (c) plasma lactate concentration when simulated the NAFLD stages and (d) the hepatic ATP concentration when simulating a low-fat diet.*

4.3). Lactic acidosis is diagnosed when plasma concentrations exceed 5mM [530]. Additionally, inhibiting pyruvate oxidation caused more severe post-prandial hyperglycaemia. When simulating the later stage of NAFLD development, the post-prandial peak in glucose concentration increased from an already hyperglycaemic value of 12.7mM to 14.9mM, well outside of a healthy range. Furthermore, when simulating a low-fat intake diet, ATP concentrations fell in periportal cells (compartment 1: 3.2mM -> 2.7mM when inhibited; figure 4.4d), even though only partial inhibition of pyruvate oxidation was simulated. In this oxygen rich part of the sinusoid, the cells do not supplement their ATP production through glucose-lactate cycling. With a normal or raised plasma FFA concentration, periportal cells are able to compensate for reduced glucose oxidation by increasing β-oxidation. However, when simulating conditions in which plasma FFAs were no longer available, insufficient acetyl-CoA was available for the citrate cycle.

4.2.2.3 Lipogenesis

When simulating the inhibition of lipogenesis, ATP concentrations were partially restored (later stage: 2.3mM->2.6mM) (figure 4.5c) and the excess ETC flux was reduced when simulating all three stages of NAFLD (table 4.3). However, only a small improvement in simulated hepatic lipid content occurred. The lipid content remained above the 5% criteria at which NAFLD is diagnosed for all stages of NAFLD (early stage: 7.6%->5.1%, mid stage: 8.7%->5.6%, later stage: 9.6%->7.0%) (figure 4.5a). FFAs were readily available from uptake to compensate for reduced hepatic synthesis and inhibition of lipogenesis caused an increase in G3P concentration, allowing more rapid triglyceride synthesis.

Despite not effectively clearing triglycerides, a decrease in hepatic FFA concentration occurred in all three stages of NAFLD when simulating inhibition of lipogenesis (26.2-39.0μM->12.3-29.6μM; figure 4.5b). Additionally, plasma FFA concentrations were notably reduced at all stages of NAFLD development (table 4.3), which may reduce lipid build-up in muscle, pancreas, heart and other organs.

The model simulations suggest that pharmacological inhibition of lipogenesis in NAFLD may reduce the mitochondrial stress, ROS production and IR resulting from excess FFAs and excess ETC fluxes, but

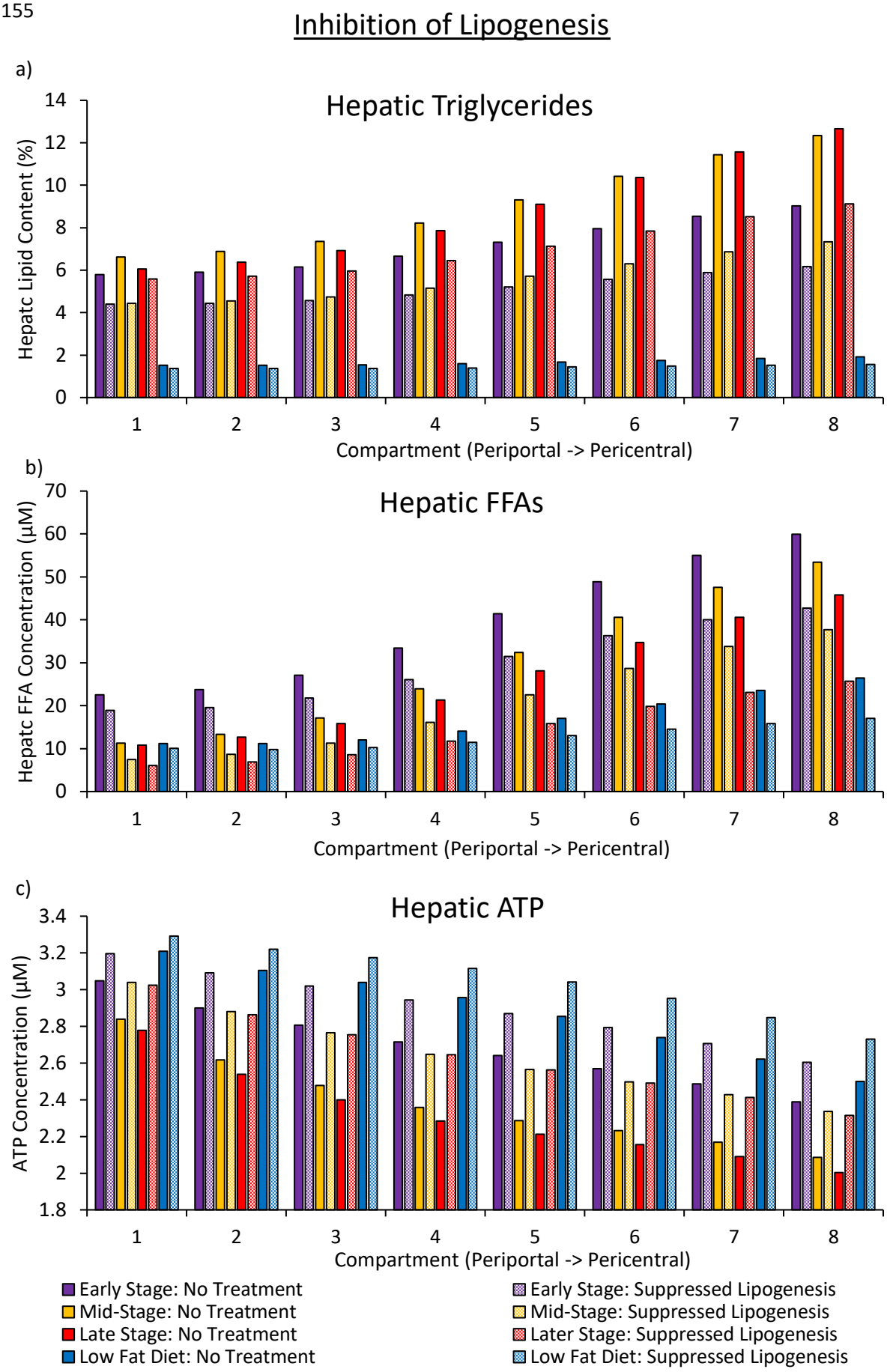

Figure 4.5: Simulating inhibition of lipogenesis. *The simulated effects of complete inhibition of lipogenesis on (a) hepatic lipid content, (b) hepatic FFA concentration and (c) hepatic ATP concentrations when simulating the range of NAFLD stages.*

would fail to reduce overall steatosis, particularly in insulin resistant patients. A treatment targeting lipogenesis, therefore, would not be expected to remove the underlying cause of damage in NAFLD, which would return after the cessation of treatment.

4.2.2.4 β-oxidation

Stimulation of β-oxidation provided a notable improvement to steatosis. The average hepatic lipid content was reduced to below the 5% criteria when simulating all three stages of NAFLD development (figure 4.6a). However, since β-oxidation enzymes have higher expression in periportal cells, the pericentral triglyceride concentration remained greater than 5% when simulated later stage NAFLD. The hepatic FFA concentration was also reduced in all three NAFLD stages (26.9-39.0μM->8.9-17.2μM; figure 4.6b) and plasma FFA and plasma triglyceride levels were notably reduced (table 4.3).

However, when simulating stimulation of β-oxidation, ATP production was disrupted in intermediate and pericentral cells. For later stage NAFLD, the simulated pericentral ATP concentration fell to 1.2mM (figure 4.6c). Stimulation of β-oxidation resulted in cycling between β-oxidation and lipogenesis, both of which consume ATP. Additionally, non-oxidative ATP production was reduced due to the allosteric inhibition of glycolysis by acetyl-CoA derived from increased β-oxidation. Since pericentral cells rely more heavily on glycolysis from energy production, and contain a greater capacity for lipogenesis, the largest fall in ATP concentration was seen in these cells. Furthermore, the rate of oxidative phosphorylation increased further when simulating stimulation of β-oxidation to 10% higher than when simulating metabolically normal individuals (table 4.3).

Based on these simulations, stimulation of β-oxidation alone is not considered to be a suitable treatment for NAFLD. However, to avoid the consumption of ATP in cycling between acetyl-CoA and FAs when stimulating β-oxidation, it may be effective to additionally inhibit lipogenesis. *In vivo*, this could be achieved by reducing the cytoplasmic and mitochondrial malonyl-CoA concentration by targeting the two isoforms of acetyl-CoA carboxylase (ACC1 and ACC2) (chapter 5).

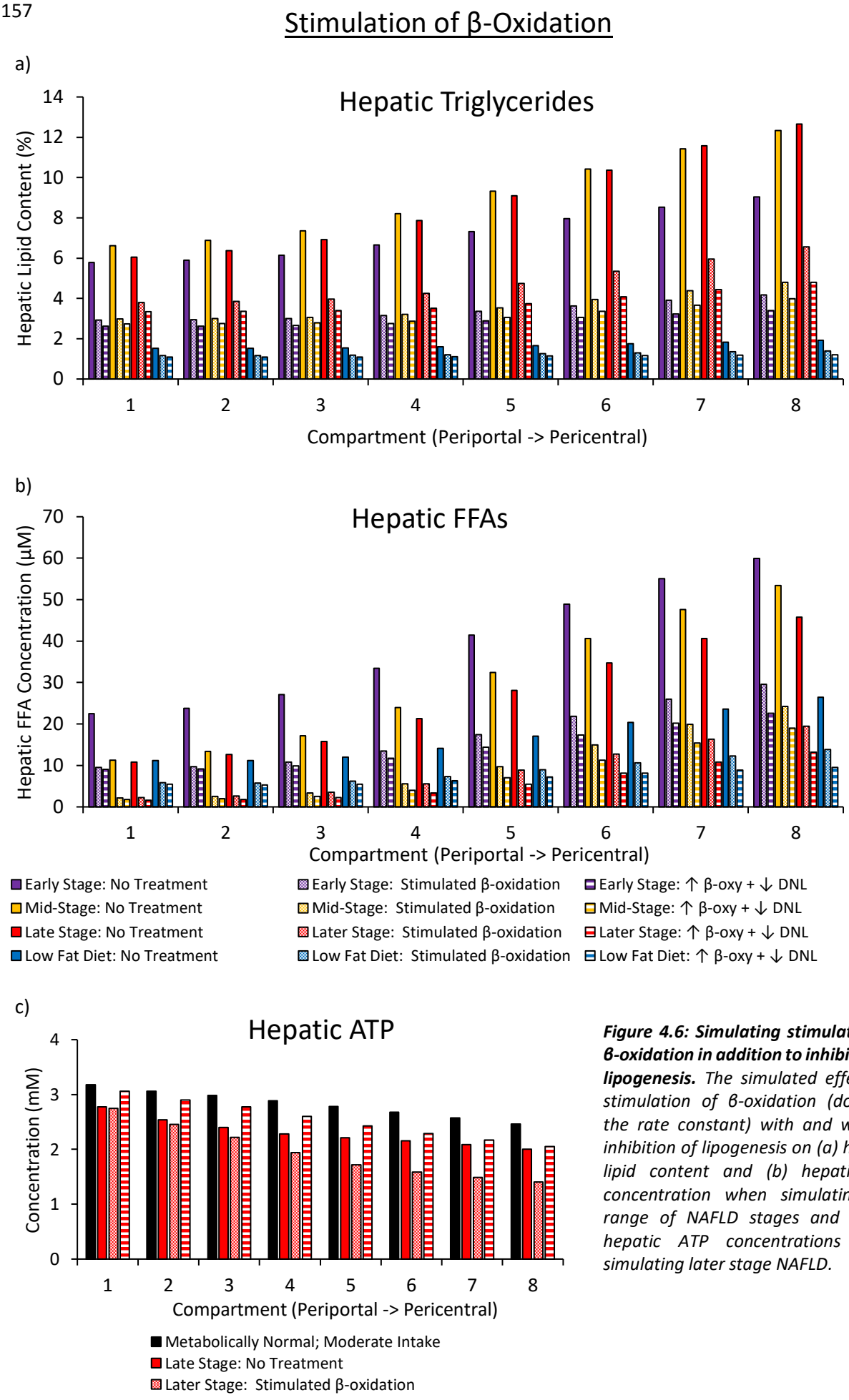

Figure 4.6: Simulating stimulation of β-oxidation in addition to inhibition of lipogenesis. *The simulated effects of stimulation of β-oxidation (doubling the rate constant) with and without inhibition of lipogenesis on (a) hepatic lipid content and (b) hepatic FFA concentration when simulating the range of NAFLD stages and on (c) hepatic ATP concentrations when simulating later stage NAFLD.*

When simulating pharmacological stimulation of β-oxidation (doubling the rate constant) in combination with complete inhibition of lipogenesis, ATP concentrations increased for all NAFLD stages (figure 4.6c). For the later stage of NAFLD, the simulated average concentration increased from 2.2mM to 2.5mM. Furthermore, the rate of oxidative phosphorylation was reduced to near metabolically normal levels, reducing the possibility of ROS production due to excess ETC flux (table 4.3).

Hepatic steatosis was effectively cleared when simulating targeting of both processes (figure 4.6a). The simulated hepatic lipid content was reduced to less than the 5% cut off at which NAFLD is diagnosed for all simulated stages of the disease. Since lipogenesis enzymes show pericentral expression, the additional reduction in lipid content was largest in pericentral cells, whilst stimulation of β-oxidation had a larger effect on the lipid content of periportal cells. As a result, when simulating stimulation of β-oxidation combined with inhibition of lipogenesis, the hepatic lipid content was less than 5% across the sinusoid. The hepatic FFA concentration was also notably reduced (26.2-39.0μM -> 5.8-17.3μM; figure 4.5b).

The plasma glucose concentration increased when simulating the treatment in the mid- and later stages of NAFLD. In these later stages, IR prevents the additional glucose from being stored as glycogen (table 4.3). The average glucose concentration for the later stage NAFLD increased from 6.7mM to 8.8mM. It is therefore important that any treatment based on inhibition of lipogenesis rapidly restores insulin sensitivity through clearing hepatic lipids to avoid hyperglycaemia in insulin resistant patients, or is given in combination with other treatments to reduce the plasma glucose concentration.

4.2.2.5 Triglyceride Synthesis

Blocking triglyceride synthesis had a dramatic effect on simulated hepatic triglyceride levels (figure 4.7a). For all three NAFLD stages, the average concentration was reduced to well below the 5% criteria at which NAFLD is diagnosed in all regions of the sinusoid. Furthermore, plasma triglyceride and FFA concentrations were notably reduced.

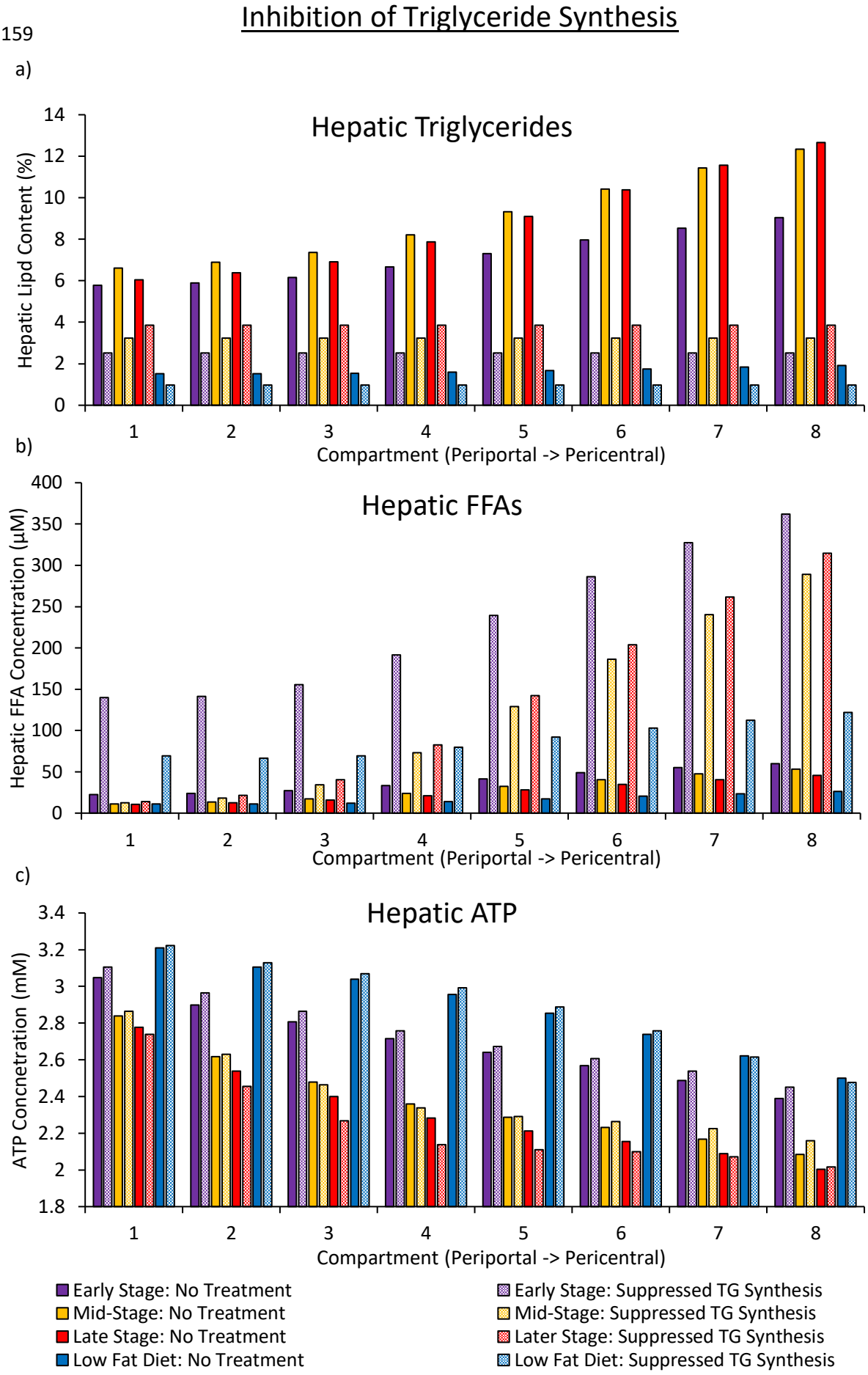

Figure 4.7: Simulating inhibition of triglyceride synthesis. *The simulated effects of complete inhibition of triglyceride synthesis on (a) hepatic lipid content, (b) hepatic FFA concentration and (c) hepatic ATP concentrations when simulating the range of NAFLD stages.*

However, blocking triglyceride synthesis also caused a vast increase in the simulated hepatic FFA concentration (figure 4.7b), which is likely to be far more harmful to the cells than the original triglyceride build-up. When simulating the later stage NAFLD, inhibition of triglyceride synthesis increased the simulated FFA concentration five-fold from 26.2μM to 135.1μM. As discussed, FFAs, along with ceramides and DAGs are thought to promote mitochondrial stress and IR more rapidly than fats stored as triglycerides [8, 146, 247, 248, 253-259]. A large increase in plasma glucose concentration was also predicted as glucose oxidation was replaced with β-oxidation.

No notable change in ATP concentration occurred when simulating inhibition of triglyceride synthesis (figure 4.7c), although the rate of oxidative phosphorylation was marginally increased (table 4.3).

4.2.3 Inter-Individual Variability in Model Simulations

The model simulations suggest that inhibition of lipogenesis in combination with stimulation of β-oxidation would provide an effective mechanism for clearing hepatic steatosis and reducing plasma FFA and triglyceride concentrations without adversely affecting energy metabolism. However, as discussed in the previous section, notable inter-individual variation in metabolism exists between patients and it is important that a treatment is effective across a range of patients. To assess the impact of the treatment across a broader range of patients, inhibition of lipogenesis and stimulation of β-oxidation (doubling the rate constant) was simulated for the 15 patients discussed in section 3.4.3. These example patients have rate constants randomly generated within 10% of the standard parameter value and zonation constants randomly generated within ±0.2 of the standard value (tables 3.2 and 3.3). The effects of the treatment in mid-stage NAFLD were simulated to provide conditions of both IR and high dietary lipid intake. For statistical significance testing in this section, a paired, 2 tailed T-test was performed between the simulated treated and untreated patients with the same parameter values. A p value of 0.05 was considered to represent statistical significance.

Despite a wide variability in the pre-treatment hepatic lipid content across the 15 simulated patients (3.8%-24%), the lipid content in the treated patients was reduced to less than 5% in every case (2.5%-

4.5%; p<0.001) (figure 4.8a). This is consistent with the decrease in lipid content from 9.1% to 2.9% when using the standard parameter values. For most of the simulated patients the hepatic triglyceride content was reduced to less than 5% in all regions of the sinusoid. Three patients showed a hepatic triglyceride content of greater than 5% in the two compartments nearest the central vein (compartments 7 and 8). These were the three simulated patients with the highest zonation constant for ATP synthesis via the citrate cycle (most periportally zonated). Additionally, the Pearson product-moment correlation coefficient between the post-treatment pericentral triglyceride content and ATP synthesis zonation constant was high at 0.823 (p<0.001). Therefore, pericentral oxidative capacity is the most important determinant of the ability for the treatment to fully clear steatosis in all regions the sinusoid.

The simulated plasma and hepatic FFA concentrations were also reduced by the treatment in all patients (figure 4.8b,d), consistent with the predictions when using standard parameter values. Additionally, an increase in ATP concentration occurred for all of the simulated patients after treatment. The average concentration increased by 0.16±0.04mM from 2.29±0.26mM to 2.45±0.25mM (p<0.001) (closer to the simulated metabolically normal range of 2.72±0.20mM) (figure 4.8c).

Therefore, across the range of simulated patients, the treatment reduced hepatic steatosis, reduced FFA levels and increased the hepatic ATP concentration. However, as seen when using standard parameter values, an increase in glucose concentration of 0.39±0.07mM from 6.6±0.1mM to 6.9±0.1mM occurred when simulating the treatment due to defective glycogen storage (p<0.001, figure 4.8e). Therefore, the treatment would have to either rapidly restore insulin sensitivity of glycogenesis, or be accompanied by alternative treatments to prevent hyperglycaemia. The largest increase in glucose concentration was seen for the patients with lower rate constants for oxidative phosphorylation, such that less of the extra acetyl-CoA generated from increased β-oxidation could be metabolised (Pearson's correlation=-0.65; p=0.008).

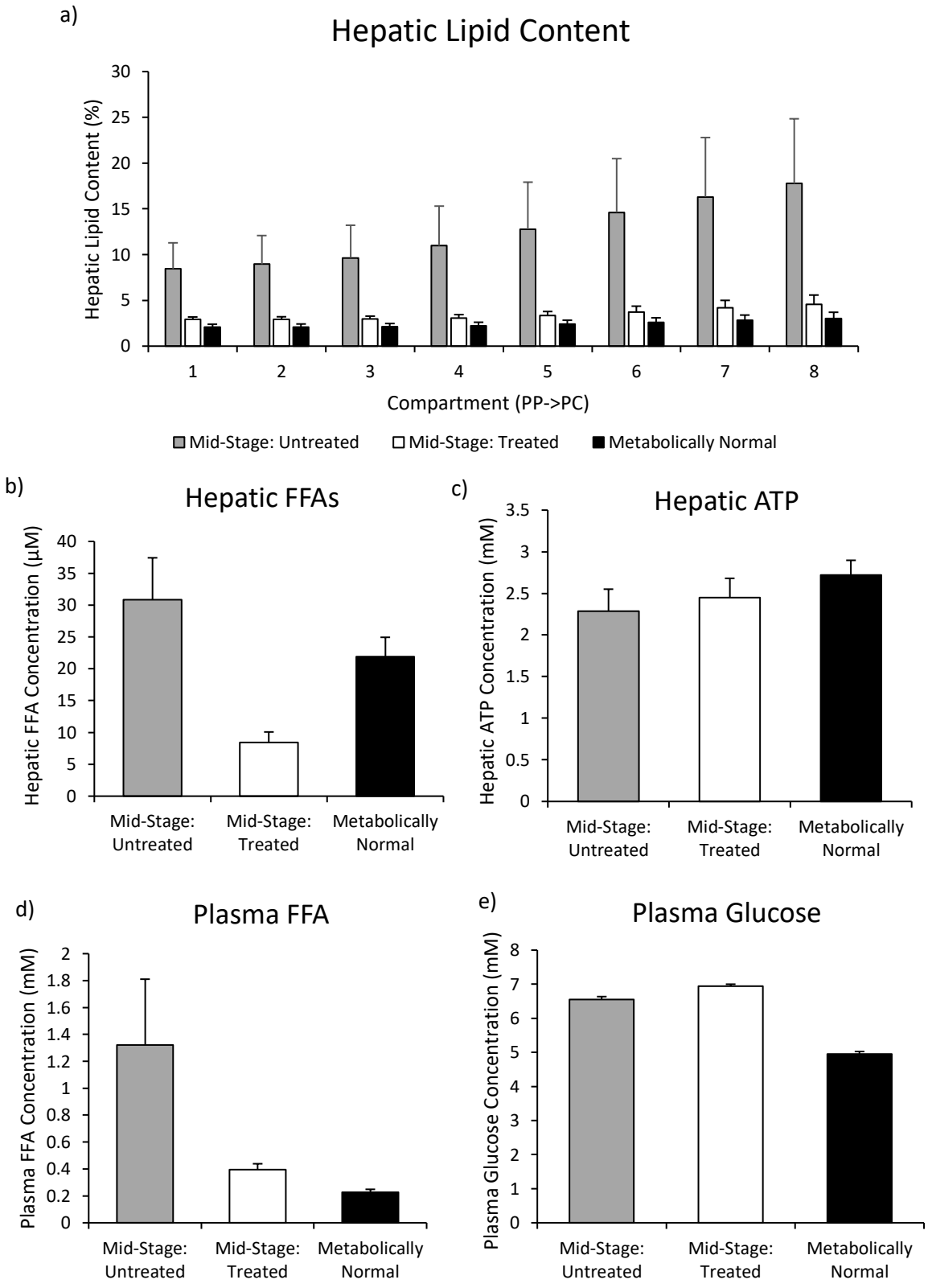

Figure 4.8: Inclusion of inter-individual variability. *The effect of stimulation of β-oxidation in combination with inhibition of lipogenesis in mid-stage NAFLD when simulating using the parameter values for the 15 randomly generated patients discussed in section 3.4.3.*

4.3 Discussion

4.3.1 Adverse effects are predicted when targeting most hepatic processes

The model simulations suggest that most the hepatic processes tested do not provide suitable drug targets for effectively reducing hepatic steatosis without causing adverse effects. Targeting β-oxidation and glycolysis disturbed pericentral energy metabolism in the simulations, whilst targeting pyruvate oxidation caused a reduction in periportal ATP concentration. In reality, cells are likely to adapt and upregulate alternative ATP producing pathways, or downregulate ATP consumption to partially reduce this effect. However, given that ATP concentrations are already significantly depleted in the livers of insulin resistant NAFLD patients, additional large reductions in ATP concentration are likely to be associated with some loss of function. It has been hypothesized that disturbed energy metabolism may be responsible for the progression of NAFLD to NASH [229, 230]. This would be consistent with the observation that fibrosis tends to develop from the pericentral side of the organ where ATP is most depleted [15, 16], highlighting the importance of studying the sinusoid as a whole.

Targeting several processes in the model caused more severe hyperglycaemia in insulin resistant individuals including inhibition of glucose uptake, any stage of glycolysis, pyruvate oxidation and lipogenesis and stimulation of β-oxidation. However, if sufficient fats are removed, it is possible that insulin sensitivity would be improved to a degree where glycogen synthesis is restored (e.g. [531]). Inhibition of pyruvate oxidation also caused severe hyperlactataemia when simulating late stage NAFLD.

When inhibition of the triglyceride synthesis step was simulated, FA concentrations increased markedly. Rather than protecting the cells, this would be expected to expedite cellular damage. As discussed, FFAs, along with closely related molecules including ceramides and DAGs, are known to be particularly potent in promoting mitochondrial stress and IR [8, 146, 247, 248, 253-259].

Numerous potential targets were ineffective at clearing steatosis in the model, particularly when simulating insulin resistant individuals. This includes all of the processes involved in the *de novo* synthesis of FAs from glucose. However, despite not reducing the simulated total hepatic fat content, inhibition of the lipogenesis step (predominantly mediated by ACC and FAS) reduced the hepatic FFA concentration and increased hepatic ATP concentrations. Therefore, despite not removing the underlying cause of the disease, inhibition of lipogenesis may reduce cellular damage and improve IR.

Some of these processes have been targeted in *in vivo* systems previously and the results have largely been consistent with those the simulated data. The increase hepatic FFA concentration seen when simulating inhibition of triglyceride synthesis have been noted in mice along with resulting adverse effects. Yamaguchi *et al.* investigated the effects of inhibiting diglyceride acyltransferase-2 (DGAT-2), one of the enzymes responsible for the addition of a third acyl-CoA to a DAG to form triglycerides, in mice [254]. In this study, hepatic steatosis was reduced. However, the hepatic FFA concentration rose from around 300nMoles/g in NAFLD mice (fed a diet deficient in methionine and choline) to around 1.5µMoles/g in NAFLD mice with inhibited DGAT-2, consistent with the roughly 5-fold increase seen in the simulated data [254]. Furthermore, despite the improved triglyceride levels, Yamaguchi *et al.* showed more severe development of fibrosis in these mice demonstrating that the damage caused by the increased levels of FFAs (or closely related molecules) outweighed any benefits from clearing triglycerides themselves. In model simulations, the most severe adverse effects of the treatment were seen in pericentral cells. Unfortunately, the effects of the treatment on individual regions of the sinusoid were not investigated in the experimental study. Whilst there is conflicting evidence to suggest that IR may or may not be improved if triglyceride synthesis is blocked before the formation of DAG rather than blocking the addition of the final acyl-CoA ([532] vs [533]), it remains likely that sustained severely increased FFA concentrations will cause mitochondrial stress independent of the enzyme targeted. Therefore, triglyceride synthesis is not considered to be a suitable target for drugs aiming to reduce hepatic steatosis. Interestingly, in both the experimental study and the model

simulations, despite a severe rise in hepatic FFA concentration, plasma FFA concentrations fell [254]. In the model this occurred because of a reduction in adipose lipolysis.

Inhibition of pyruvate dehydrogenase has not been widely studied as a treatment for NAFLD *in vivo*. However, consistent with the simulations, genetically inherited system-wide (not liver specific) deficiency of PDH is associated with severe lactate build-up along with neurological problems resulting from reduced cellular energy production [534]. Neurons rely heavily on glucose metabolism substrates rather than lipids as an energy source. Furthermore, heart and muscle specific PDH-knockout mice survive less than 7 days unless kept on a high fat diet [535]. However, more promising results have been published for liver-specific PDH knockout mice. These mice show significant reductions in liver FA synthesis, in body mass and in fat mass [531]. An increase in hepatic glycogen content, rather than plasma glucose concentration was measured due to an improvement in insulin sensitivity. Unfortunately, the plasma lactate concentration was not measured in this study. It therefore remains unknown whether this treatment would cause the hyperlactataemia predicted for insulin resistant NAFLD patients, or if insulin sensitivity would be restored rapidly enough for the additional lactate to be stored as glycogen. Furthermore, no specific test from the minor disruption to periportal ATP concentrations predicted by the model was performed.

The inhibition of *de novo* lipogenesis has been studied experimentally through inhibition of FAS with mixed results. FAS is the main enzyme responsible for adding additional malonyl-CoA molecules to the chain of FAs. System-wide knockout of FAS is lethal in embryo development [536]. Liver-specific deletion of the FAS gene was shown to expedite rather than protect against the development fatty liver in a mouse model of NAFLD. On a normal diet, little difference was seen between the control and FAS knockout mice. However, on a high fat diet, the FAS knockout mice developed more severe steatosis due to a reduction in β-oxidation [537]. This may result from increased allosteric inhibition of β-oxidation by malonyl-CoA, given that the physically separation of lipogenesis and β-oxidation enzymes has been shown to break down under abnormal conditions [538]. On the other hand,

platensimycin, an inhibitor of FAS specific to liver, has been demonstrated to reduce lipid build-up in hepatocytes because of a reduction in lipogenesis [539]. However, these mice were fed a high fructose diet rather than the high fat. In the model simulations, inhibition of lipogenesis was only effective at clearing steatosis when FAs were not readily available in the plasma. Mice lacking FAS in adipose tissue meanwhile, showed a reduction in diet-induced obesity, suggesting that adipose rather than hepatic lipogenesis may provide a pertinent target for reducing hepatic steatosis [540]. The analysis in this study focussed on potential hepatic targets.

4.3.2 Acetyl-CoA carboxylase may provide a pertinent target for NAFLD

Targeting β-oxidation alone caused a fall in the simulated hepatic ATP concentration, particularly in pericentral cells. However, when stimulation of β-oxidation was combined with inhibition of lipogenesis, ATP concentrations were improved relative to untreated NAFLD and steatosis was effectively cleared. The simulated triglyceride content was reduced to a metabolically normal range for all three NAFLD stages. Furthermore, the rate of oxidative phosphorylation was returned to normal values, reducing the chance of damage due to ROS production resulting from excess ETC flux. The simulated hepatic and plasma FFA concentrations also improved which is likely to be associated with an improvement mitochondrial stress and IR [8, 146, 247, 248]. One adverse effect was an increase in plasma glucose concentration when simulating an insulin resistant individual. Therefore, it is important that any treatment targeting β-oxidation and lipogenesis restores insulin sensitivity rapidly such that glycogen synthesis can prevent hyperglycaemia from occurring.

The two forms of acetyl-CoA carboxylase (ACC1 and ACC2) provide a potential target for both inhibiting lipogenesis and stimulating β-oxidation. ACC1 is in the cytosol and produces malonyl-CoA which can be accessed by FAS for lipogenesis. ACC2, meanwhile, is in the mitochondria and produces malonyl-CoA to negatively regulate β-oxidation [462, 541]. Malonyl-CoA synthesized by ACC2 is physically separated from FAS under normal physiological conditions [462]. Therefore, inhibition of

ACC1 provides a target for inhibiting lipogenesis, whilst inhibiting ACC2 will lead to stimulation of β-oxidation.

Some *in vivo* studies have investigated the inhibition of ACC1 and ACC2 either together or separately. Globally knocking out ACC1 in mice is lethal in embryonic development [542]. However, liver specific ACC1 knockout mice have been developed. Mao et al. demonstrated a significant reduction in liver triglycerides, hepatic FA synthesis and serum FFAs despite compensatory up-regulation of ACC2, but no improvement in glucose concentration or resensitization to insulin [543]. In another liver-specific ACC1 knockout, Harada *et al.* found that up-regulation of ACC2 entirely compensated for the reduction in ACC1 expression suggesting that, under these non-physiological conditions, FAS is able to access malonyl-CoA produced by ACC2 [538]. *De novo* lipogenesis was only reduced with the addition of 5-(tetradecyloxyl)-2-furancarboxylic acid (TOFA), an inhibitor of both ACC1 and ACC2.

In another study, Savage et al. used antisense oligonucleotide inhibiters to knock down ACC1 and ACC2 both separately and together in a rat model of NAFLD. Suppression of ACC1 alone caused a reduction in mitochondrial as well as cytoplasmic malonyl-CoA, suggesting some stimulation of β-oxidation in addition to inhibition of lipogenesis [526]. This suppression of lipogenesis combined with partial stimulation of β-oxidation caused reductions in the rate of oleic acid and glycerol incorporation into triglycerides. Knockdown of ACC2 alone caused a larger increase in the rate of β-oxidation than ACC1 knockdown but a smaller reduction in triglyceride synthesis. This suggests that stimulation of β-oxidation alone, without inhibiting lipogenesis, is only moderately effective at treating steatosis. Consistent with model simulations, the largest improvements were seen when both ACC1 and ACC2 were knocked down, leading to a 45% reduction in hepatic triglyceride levels. No adverse changes to energy metabolism were noted after ACC1 and ACC2 inhibition and the plasma ALT concentration, a marker of hepatic injury, was not increased.

When ACC1 and ACC2 were inhibited in a hamster model through feeding with a chow diet containing 0.15% TOFA, their plasma triglyceride concentration reduced by around 50% after 6 days [544]. In the

same study, the intracellular triglyceride concentrations of cultured hamster hepatocytes treated with 20μM TOFA were reduced compared to untreated cells by around 80% when grown in FA-free medium and 40% when cultured in medium containing 1mM oleic acid.

Global suppression of ACC2 has been demonstrated to reduce the risk of development of T2DM, metabolic syndrome and obesity in mice due to upregulation of β-oxidation [523]. ACC2 knockout mice also showed 50% less fat storage in adipose tissue [524, 525]. Neither of these studies reported pericentral centred damage or loss of function. In another study, down-regulation of ChREBP, a key regulator of lipogenic gene transcription (including FAS and ACC), led to improved FFA and triglyceride levels in ob/ob KO mice and offered protection against IR as a result of reduced hepatic lipogenesis [200].

Collectively these data suggest that steatosis is improved when ACC1 and ACC2 are suppressed due to a reduction of lipogenesis and stimulation of β-oxidation, consistent with the model simulations. Furthermore, none of the experimental studies have noted adverse effects in energy metabolism when inhibiting ACC1 and ACC2.

4.4 Conclusions of Chapter

The computational model of hepatic metabolism across the sinusoid was used to assess potential processes which could be targeted to reduce steatosis in NAFLD patients. The model simulates cell across the porto-central axis of the sinusoid allowing the effects of targeting specific processes on both steatosis and energy metabolism in individual regions of the sinusoid to be simulated. Furthermore, by simulating varying dietary intake and degrees of metabolic dysregulation, the effects of each treatment could be studied for a range of NAFLD patients.

Substantial adverse effects were predicted, either in the hepatocytes themselves or through changes in plasma concentrations of lipids, glucose or lactate when targeting most metabolic processes. Many of these adverse effects occurred in specific regions of the sinusoid highlighting the importance of

studying the sinusoid as a whole. Where possible the predicted effects of each treatment were compared with previously published experimental data and were shown to be consistent. However, since experiments in specific regions of the sinusoid are largely missing from the literature, the predictions highlight potential adverse effects which may be missed when performing measurements on bulk liver tissue.

No single hepatic process was predicted to provide a pertinent drug target for clearing steatosis. However, stimulation of β-oxidation combined with inhibition of lipogenesis showed promising results in reducing both hepatic and plasma FFA and triglyceride concentrations. Energy metabolism was not disturbed and ATP levels were slightly improved. This is supported by experimental data from the literature for mice lacking both ACC1 and ACC2 which show improvements in steatosis due to an increased rate of β-oxidation and suppressed lipogenesis.

5 Chapter 5: Experimental Validation of Model Predictions

5.1 Introduction to Chapter

In the previous chapter, the model was used to simulate the effects of pharmacologically targeting various processes in order to clear hepatic steatosis in NAFLD without disrupting energy metabolism. In this chapter, five of these pharmacological interventions are tested experimentally on HepG2 cells, a cell culture line derived from a differentiated hepatocellular carcinoma. These results allow comparison with the model simulations to test the predictive capacity of the model.

Before testing the effects of the pharmacological interventions, it is first necessary to ensure the key changes occurring in NAFLD *in vivo* can be replicated in the cultured cells. This was performed by adding a cocktail of FFAs to the medium of the cells, corresponding to the raised plasma FFA levels in NAFLD *in vivo*. *In vivo*, hepatocytes show increasing steatosis [15], cell damage [545, 546], oxidative stress [501, 512, 514-516, 547, 548], IR [146, 549, 550], reduced ATP levels and reduced mitochondrial function [44, 227, 228, 506, 510-513, 547, 548] as NAFLD develops. It is important that a cell culture model used to validate model predictions also replicates this disease progression. After establishing and describing the cell culture model of NAFLD, the cells were treated with a range of small molecule inhibitors known to target specific metabolic processes (section 5.4). The impact of inhibiting key processes on cell viability and function was studied for FA treated cells and compared with the model simulations.

It should be noted that the cell culture model does not allow testing of zonated effects as seen in the model simulations. However, as discussed below, the HepG2 cells are most similar in metabolism to pericentral cells and most adverse effects occurred in these cells in simulations.

5.1.1 HepG2 cells

HepG2 cells are a perpetual cell line of well-differentiated hepatocellular carcinoma cells derived from a 15 year old Caucasian [551]. Although derived from a liver carcinoma, rather than healthy liver cells,

due to their high level of differentiation, HepG2 cells retain epithelial morphology and continue to perform a wide range of liver cell functions [551]. They also continue to express insulin receptor and insulin-like growth factor II receptor despite showing little glycogen content [552, 553].

Despite retaining many liver cell functions, HepG2 cells show notable differences from healthy primary liver cells. Firstly they contain a higher numbers of chromosomes with some variation (50-56) around a modal number of 55 [551]. Additionally, they contain a high quantity of fat, even when cultured in FA free, normoglycaemic (5mM glucose) medium (see section 5.3.2). The cellular rate of lipogenesis is similar to primary cultures of rat hepatocytes and freshly prepared rat hepatocytes [554]. Instead, the build-up of fat in HepG2 cells is due to reduced secretion of FAs in lipoproteins [554]. They also show increased anaerobic metabolism through glycolysis [555] due to their background as cancer cells [556]. This production of energy through glycolysis followed by lactic acid fermentation rather than oxidative metabolism is known as the Warburg effect. Due to both their high fat content, and dependence on glycolysis for ATP synthesis, HepG2 cells are most similar to pericentral cells which exist in a hypoxic environment and show a higher lipid content.

When treated with saturated FAs, HepG2 cells have previously been shown to reproduce a number of the metabolic changes occurring in *in vivo* hepatocytes in NAFLD [557]. However, due to the differences between HepG2 cells and healthy *in vivo* hepatocytes, the first section of this chapter is dedicated to assessing the suitability of HepG2 cells as a model for steatotic hepatocytes in NAFLD.

5.1.2 Treatments

5.1.2.1 Fatty acids

Five FFAs treatments were tested, either individually or in combination. These were butyric acid (4:0), lauric acid (12:0), palmitic acid (16:0), oleic acid (16:1) and linoleic acid (16:2).

Butyric acid is a short chain, saturated FA found in milk and dairy products predominantly in its triglyceride form. It is additionally produced in the gut. It has been demonstrated to improve insulin

sensitivity and reduce adiposity due to increased energy expenditure in mouse models of diabetes [558, 559].

Lauric acid is a medium chain FA found in human breast milk and cow's milk along with coconut milk, coconut oil (44-52%), laurel oil, and palm kernel oil (40-52%) [560]. It is additionally synthesized in human tissues, although at a lower rate than palmitic and oleic acids. The effects of lauric acid on the liver are debatable since, although it's consumption has been shown to improve the high density lipoprotein (HDL) to low density lipoprotein (LDL) ratio relative to other saturated fats, it is also thought to increase the probability of cardiovascular disease due to an increase in plasma cholesterol [561, 562]. Additionally, any potential benefits of lauric acid may result from an antibacterial effect on the microbiome rather than a direct effect on liver cells. These microbiome effects would not be seen in the cell culture experiments presented here [563, 564].

Palmitic acid is the most common FA in mammals, plants and microorganism. It is a saturated FA present in numerous food types in addition to being synthesized in the body. It accounts for 20-30% of fat stored in adipose tissues [41, 42, 565]. It is linked with an increased probability of developing cardiovascular disease and IR and is thought to increase the LDL content in the blood [566, 567]. It is therefore considered to be one of the more detrimental common FAs found in the diet.

Oleic acid is the second most abundant FA in human tissues, and the most abundant in adipose FA stores (of humans and other mammals) comprising around 45% in these tissues [41, 42, 565]. It is an omega-9 monounsaturated FA. Due to its presence in animal fat, it is abundant (in triglyceride form) in lard. Additionally, it is abundant in olive (65-80%) after which it is named, peanut oil (52-60%), sesame oil (40-50%), sunflower oil (14-35%) and other oils [560, 568]. Oleic acid consumption is linked with reduced cholesterol levels in comparison with lauric and palmitic acids and increases the ratio of HDL to LDL [569]. It also may be responsible for the reduction in blood pressure that results from olive oil consumption [570].

Linoleic acid is an omega-6 polyunsaturated FA. In humans, it is derived exclusively from diet. It is abundant in sunflower seed oil (44-75%), maize oil (34-62%), hemp seed oil (54-56%), poppy seed oil (72%) and other vegetable and nut oils [560]. Compared with saturated acids, linoleic acid consumption is associated with reduced probability of developing coronary heart disease [571]. The effects of linoleic acid supplementation on IR remain unclear, with health benefits of linoleic acid consumption widely reported, but adverse effects also shown in several studies [572-574].

5.1.2.2 Small Molecule Inhibitors

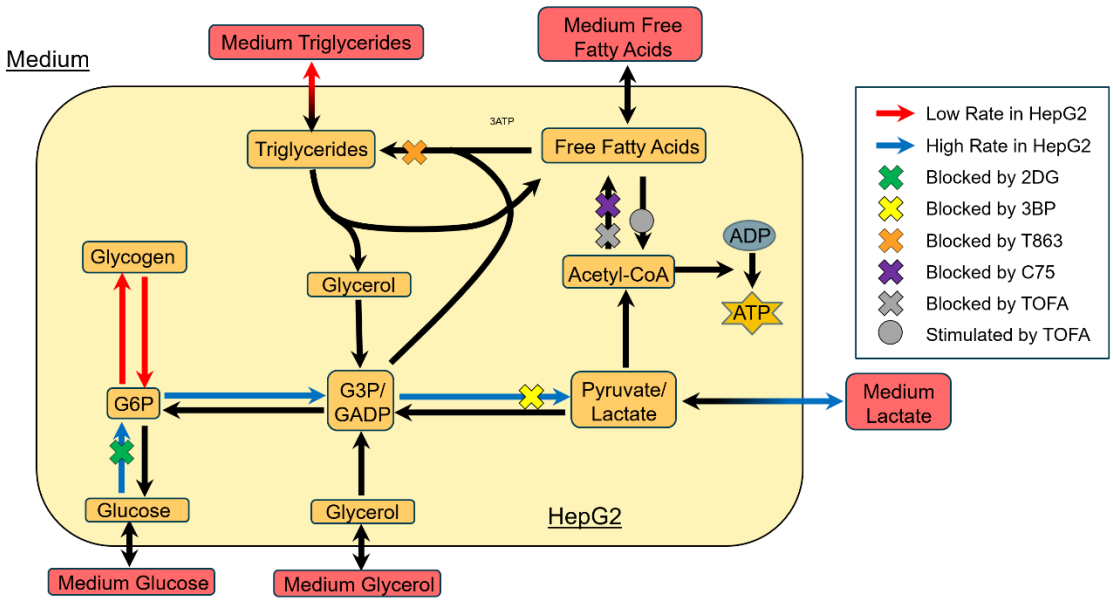

Figure 5.1: The processes (as represented in the model) targeted by the small molecule inhibitors TOFA, C75, T863, 2DG and 3BP in HepG2 cells. *Additionally, the known increase in glycolysis [555] and decrease in glycogen synthesis [553] and triglyceride release [554] in HepG2 relative to hepatocytes are labelled.*

Five inhibitory molecules were studied. These were lipogenesis inhibitor and β-oxidation stimulator 5-(tetradecyloxy)-2-furoic Acid (TOFA), lipogenesis inhibitor 4-Methylene-2-octyl-5-oxotetrahydrofuran -3-carboxylic acid (C75), triglyceride synthesis inhibitor 2-((1,4-trans)-4-(4-(4-Amino-7,7-dimethyl-7H-pyrimido[4,5-b][1,4]oxazin-6-yl)-phenyl)cyclohexyl)acetic acid (T863) and glycolysis inhibitors 3-bromopyruvate (3BP) and 2-deoxy-D-glucose (2DG). The processes targeted by each of these inhibitory molecules are shown in figure 5.1.

Firstly, to test the model predictions for simultaneous inhibition of lipogenesis and stimulation of β-oxidation, TOFA, a potent inhibitor of both forms of acetyl-CoA carboxylase (ACC1 and ACC2), was used [575-578] (figure 5.1). ACC1 produces cytosolic malonyl-CoA accessible to FAS for use in

lipogenesis (figure 5.2) [462, 541]. ACC2 meanwhile is restricted to the mitochondria and produces malonyl-CoA which negatively regulates β-oxidation [462, 541]. Therefore, treatment with TOFA both directly reduces lipogenesis by reducing the malonyl-CoA available to FAS, and reduces the inhibition of β-oxidation by mitochondrial malonyl-CoA.

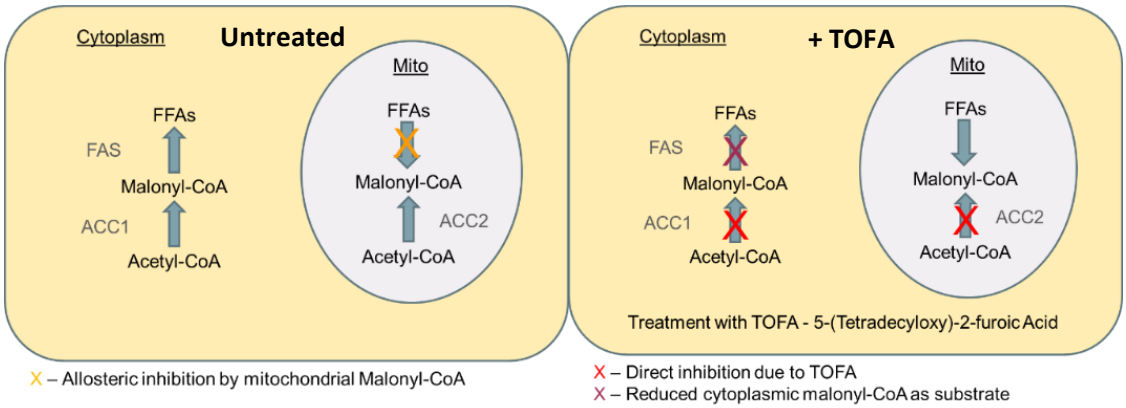

Figure 5.2: The effect of ACC1 and ACC2 inhibition with 5-(tetradecyloxy)-2-furoic Acid (TOFA) on metabolism.

TOFA is converted intracellularly into a CoA analogue which blocks ACC activity [575]. It has been shown to reduce FA synthesis and TG secretion in cell culture models [544, 575, 579] and animal models [544, 580, 581] including rhesus monkeys. It has been suggested that TOFA may additionally have an effect on enzymes involved in the metabolism of long-chain FAs due to its similarity to long chain FAs [581, 582]. However, its predominant site of action is its potent inhibition of ACC. Since only the stimulation of β-oxidation and inhibition of lipogenesis are simulated in the model, the specific enzymes targeted to achieve these effects are of lesser importance. Inhibition of lipogenesis combined with stimulation of β-oxidation was simulated in section 4.2.2.4.

Secondly C75, a potent synthetic inhibitor of FAS was used to directly inhibit lipogenesis [577, 578, 583, 584] (figure 5.1). Since FAS inhibition does not alter mitochondrial malonyl-CoA production, C75 has little effect on the rate of β-oxidation [577, 578, 583, 584]. It should be noted, however, that whilst under normal conditions cytoplasmic and mitochondrial malonyl-CoA are physically separated [462], it is possible that under non-physiological conditions this separation may breakdown [538]. Therefore, some stimulation of β-oxidation may occur with C75 treatment, but this would be notably lower than for TOFA treatment. Inhibition of lipogenesis was simulated in section 4.2.2.3.

T863 was used to inhibit triglyceride synthesis by DGAT1 (figure 5.1). DGAT1 is one of the enzymes which mediates the final binding of a FA (in the form of acyl-CoA) to diacylglycerol molecule to form a triglyceride [585]. Therefore, inhibiting this enzyme leads to the build-up of precursors to triglyceride synthesis including FAs and DAGs. DAGs in particular have been suggested as a major molecule type responsible for the development of hepatic damage and IR in NAFLD [8, 146]. Inhibition of triglyceride synthesis was simulated in section 4.2.2.5.

Finally, two glycolysis inhibitors, 3BP and 2DG were used to assess the impact of inhibiting glycolysis at different stages (figure 5.1). 3BP inhibits the glycolysis enzyme glyceraldehyde-3-phosphate dehydrogenase which takes glyceraldehyde-3-phosphate (GADP) as a substrate and produces 1,3-biphosphoglycerate [586, 587]. 2DG competitively inhibits at the stage of GK and, therefore, prevents the storage of glucose as glycogen in addition to reducing glycolysis [588, 589]. Inhibition of glycolysis at various stages was simulated in section 4.2.2.1.

5.1.3 Properties measured and relationship to model simulations

The first results section of this chapter describes the effects of FA treatment of HepG2 cells on several properties to investigate whether the HepG2 model represents the key features of NAFLD seen both *in vivo* and in the model simulations. The second section, then describes the effects of treating the cells with the five small molecules inhibitors, which correspond to some of the pharmacological interventions simulated in the previous chapter. Treatment with each inhibitor is investigated for whether the adverse effects resulting from FFA treatment are exacerbated or resolved and to investigate whether the results are consistent with the model simulations. In this section, the relationships between the predicted data in the previous chapter and the experimental measurements presented in this chapter are discussed.

5.1.3.1 Steatosis

Hepatic steatosis is the defining feature of NAFLD *in vivo.* When simulating NAFLD resulting from high fat intake, IR and increased SREBP-1c expression in the model (chapter 3), an increase in cellular lipid

content occurred, particularly in pericentral cells, because of both increased uptake and increased *de novo* lipogenesis. In this chapter, to assess the effects of FAs and the various treatments on cellular steatosis in the HepG2 cell culture model, staining for neutral lipids using oil red O (ORO) was performed. By comparing the ratio of stained and unstained regions, the effects of each treatment on lipid content was determined.

5.1.3.2 Glycogen, and Hyperglycaemia and Insulin Resistance

In the previous chapters, defective glycogen storage (particularly in pericentral cells) and hyperglycaemia were seen when simulating insulin resistant NAFLD patients in the model. In the cell culture model, staining for glycogen was performed to assess the content within cells when treating with FAs and the small molecule inhibitors. The glucose concentration in the medium of cells was also measured to assess changes in glucose uptake and release. In the model, insulin sensitivity is set as a parameter, and the pathways mediating exacerbation or resolution of IR are not included. Only the changes in total lipid content and FFA concentration thought affect insulin sensitivity are simulated. However, in the cell culture model, the effects of FAs and of the small molecule inhibitors on IR was assessed by comparing glycogen content and glucose consumption in insulin treated and insulin-free cells.

5.1.3.3 FFAs and β-Oxidation

When simulating NAFLD in the model, the overall increase in lipid content was accompanied by an increase in cellular FFA concentration in pericentral cells. Furthermore, when simulating high intake and IR, notable increases in the rates of β-oxidation and mitochondrial oxidative metabolism occurred. Experimentally, the intracellular FFA concentration is difficult to measure since FFAs are rapidly bound to a CoA molecule and used in glycerolipid synthesis or β-oxidation after entering a cell. Similarly, any potential overactivation of oxidative phosphorylation pathways would be challenging to study directly. However, many of the adverse effects known to occur in NAFLD result from the presence of excess FFAs and excessive β-oxidation [8, 146, 247, 248, 501, 512, 514-516], and these were

investigated in the HepG2 model. These include oxidative stress, cell death, lipotoxicity, reduced mitochondrial function and IR. These measures do not allow direct comparison with the model simulations, but treatments which reduce the hepatic FFA concentration and return the rates of β-oxidation and oxidative phosphorylation to metabolically normal levels would be expected to also improve these measures.

5.1.3.4 Mitochondrial Function

In NAFLD *in vivo*, mitochondrial function is known to be reduced and this is thought to arise due to mitochondrial stress resulting from increased rates of β-oxidation [547, 548, 590, 591]. Mitochondrial function was assessed in the HepG2 cell culture model by measuring the activity of key ETC enzymes. The ETC comprises of a series of enzymes which mediate transfers of electrons between donor and acceptor molecules coupled to the movement of protons from the mitochondrial matrix into the intermembrane space. The resulting proton gradient is used to power ATP synthesis by the enzyme ATP synthase. Complex I (NADH:ubiquinone oxidoreductase) and complex II (succinate dehydrogenase) mediate the transfer of electrons from NADH and succinate (via FAD) respectively to ubiquinone producing ubiquinol. NADH reduction through complex I additionally causes proton transport into the intermembrane space. Complex III (CoQH2-cytochrome c reductase) mediates the transfer of electrons from the resulting ubiquinol to cytochrome c, coupled with the movement of protons into the intermembrane space. Complex IV (cytochrome c oxidase), the final enzyme in the chain, mediates the transfer of electrons from the reduced cytochrome c to molecular oxygen (producing water), and is also coupled with transfer of protons into the intermembrane space. This pathway is fundamental to cellular energy metabolism. Reduced mitochondrial function after FFA treatment would be indicative of stress on mitochondria resulting from lipotoxicity.

5.1.3.5 Intracellular ATP Concentration

In the model simulations, a reduction in intracellular ATP concentration occurred due to increased ATP consumption in lipogenesis, β-oxidation and triglyceride synthesis and reduced non-oxidative ATP

synthesis. *In vivo* larger drops in ATP concentration [548, 591, 592] are seen as a result of reduced mitochondrial function [547, 548, 590, 591]. The ATP concentration was measured directly in the cell culture model after addition of FFAs and the various small molecule inhibitors.

5.1.3.6 ROS Production

Excess FFA concentrations and excess β-oxidation are thought to contribute to oxidative stress and ROS production seen in NAFLD *in vivo* [225, 382, 547, 591, 593]. Increased mitochondrial FA oxidation is seen in NAFLD as an adaptive mechanism to clear excess fats [548]. However, reduced ETC enzyme function and excessive flow of electrons through the ETC can result in ROS production predominantly in the form of superoxide. Most electrons passing through the ETC are eventually combined with molecular oxygen to form water. Even under normal metabolic conditions, a small fraction leak to form the superoxide anion radical before being converted to hydrogen peroxide by manganese superoxide dismutase [548]. The majority of this is then converted to water, removing all but a small residual amount of ROS used for signalling. However, a combination of reduced ETC enzyme activity and increased flow of electrons along the chain results in overproduction of superoxide [548, 591, 594]. Excessive production of ROS can cause oxidative stress in mitochondria by causing oxidative damage to lipids, proteins and nucleic acids as is observed in both NASH and NAFLD [547, 591, 593].

Oxidative stress was assessed experimentally using two techniques. Lipid peroxidation in cell homogenates was measured as a marker of intracellular ROS production. Lipid peroxidation was assayed using a TBARS test to determine the presence of the breakdown products of lipid peroxidation, particularly MDA, in the sample. It should be noted that the assay shows only a moderate specificity for MDA or the products of lipid peroxidation breakdown. To minimise the reaction with other unwanted chemicals in the sample, EDTA was added to chelate heavy metals which catalyse oxidation, and anhydrous sodium sulphate in addition to sodium dodecyl sulphate was included to prevent oxidization of further lipids during heating. However, only large increases in the TBARS reading were considered to correspond to increased lipid peroxidation.

Secondly, the redox potential and antioxidant capacity of the supernatant media were measured as a marker of extracellular ROS release. The redox potential, usually measured in patient blood samples, has been shown to correlate with the degree of oxidative injury in a number of conditions [595-598]. The antioxidant capacity is a measure of the amount of oxidative reserves in the sample which relates to the ability of the patient (or cells) to respond to the injury. An increase in redox potential has been demonstrated in patients with T2DM and the metabolic syndrome [595], although no changes in redox potential or antioxidant capacity were seen in obese individuals [597]. An increase in redox potential is measured in the perfusate after human liver perfusion, an instance in which liver cells are known to produce ROS [599].

5.1.3.7 Cell Viability and Markers of Hepatic Function

The effects of a treatment on the number of viable cells, number of dead cells and proliferation rate per cell were measured to assess the overall beneficial or damaging effects of each treatment to the cells.

5.2 Materials and Methods

5.2.1 Statistics

Throughout this section, where two groups were compared, significance was calculated by an unpaired, unequal variance, 2 tailed T-test. Where multiple treatments were compared against control, an ANOVA was performed to assess statistical significant of variation between the groups before the Holm-Sidak method was used to calculate a t-test adjusted to account the multiple comparisons performed [600]. The tests performed are stated in the legend of each figure and table. The calculations were performed using GraphPad Prism. A p value of less than 0.05 was considered to represent a significant difference.

5.2.2 Maintenance of Cell Cultures

Cells were cultured in Eagles minimum essential medium (EMEM) with Earl's salts, L-glutamine and sodium bicarbonate (Sigma M4655) supplemented with 10% FBS and 1X MEM non-essential amino

acids (Sigma M7145) in T75 culture flasks. For passaging, Dulbecco's Phosphate Buffered Saline (PBS; Sigma D8662) and trypsin-EDTA solution (Sigma T4049) were used. Cells were incubated at 37^{o}C in a sterile environment containing 5% carbon dioxide. The following volumes of medium were used for each container when culturing cells and running experiments: T75 flask – 15ml, T25 flask – 4ml, 6 well plate – 3ml, 24 well plate – 1 ml, 48 well plate – 500µL and 96 well plate – 300µL.

5.2.3 Preparation of Treatments

5.2.3.1 Fatty Acids

To solubilize lauric acid and palmitic acid, they were first dissolved in ethanol at 50µM and 100µM concentrations respectively. These stocks were replaced every 2-4 weeks. The stocks were diluted in medium and sterilized before use. Once diluted in medium, the fatty acid solutions were discarded within 3 days. Oleic, linoleic and butyric acids were diluted directly in medium from pure stocks, then sterilized a using 20µm filter. Fatty acid free medium containing ethanol was prepared to validate that any effects of lauric and palmitic acid additions arose due to the fatty acids themselves and not the ethanol. Additionally, a fatty acid cocktail containing equal molar mass of palmitic, lauric, oleic, linoleic and butyric acids was prepared and sterilized using a 20µm filter. Oleic, linoleic and butyric acids were added directly from pure stocks using multiple dilutions in medium, whilst lauric and palmitic acids were added from the stocks in ethanol. In the final solution, each 100µM of total fatty acid contained 0.06% ethanol. The fatty acid cocktail was replaced every 2-4 days.

5.2.3.2 TOFA

Pure TOFA powders were dissolved in dimethyl sulfoxide (DMSO) to give a 5mg/ml stock solution. This was then diluted in medium to give the desired concentration of 1-40µg/ml before being sterilized using a 20µm filter.

5.2.3.3 C75

Pure C75 powders were dissolved in DMSO to give a 10mg/ml stock solution. This was diluted in medium to give treatment solutions of 0.5-40µg/ml before sterilizing using a 20µm filter.

5.2.3.4 T863

Pure T863 powders were dissolved in DMSO to form a 5mg/ml stock solution. This was diluted in medium to give solutions of 5-400ng/ml before sterilizing using a 20µm filter.

5.2.3.5 3-Bromopyruvate

Pure 3BP powders were dissolved in water to give a 10mg/ml stock solution. This was then diluted in medium to give treatment solutions of 40ng/ml-10µg/ml before sterilizing using a 20µm filter.

5.2.3.6 2-deoxyglucose

Pure 2DG powders were dissolved in DMSO to give a 3mg/ml stock solution. This was then diluted in medium to give treatment solutions of 30ng/ml-3µg/ml before sterilizing using a 20µm filter.

5.2.4 Cellular Viability and Proliferation.

5.2.4.1 MTS assay

To assess viability for a large number of treatments when performing initial dose-response experiments (section S2), an MTS assay was used. The MTS viability assay is based on the reduction of 3-(4,5-dimethylthiazol-2-yl)-5-(3-carboxymethoxyphenyl)-2-(4-sulfophenyl)-2H-tetrazolium (MTS) to generate a formazan product which absorbs light at 490nm. This conversion is largely carried out by mitochondrial NADPH (reduced nicotinamide adenine dinucleotide phosphate) dependent enzymes, and the assay therefore assesses total mitochondrial metabolic activity rather than cell numbers specifically. As well as not specifically measuring cell numbers, the assay tends to be associated with large dispersion in results. However, the assay is rapid and allows many conditions to be assessed, before validation through a trypan blue exclusion assay.

Cells were seeded in 96-well plates at a density of 26000 cells/cm^3 and grown initially in 200µL unaltered MEM (fatty acid-free) medium. After 24 hours, the medium was removed and replaced with medium containing the stated treatment. The treated medium was replaced every 24 hours until the end of the experiment. To take readings, the medium was removed and replaced with 100µL fresh

medium in each well. 20µL of MTS solution (CellTiter Aqueous One Solution) was additionally added to each well. After 1 hour, the absorbance at 490nm was measured using the FLUOstar Omega multi-mode microplate reader.

5.2.4.2 Trypan Blue Exclusion Assay

HepG2 cells were seeded in 6 well plates at a density of 26000 cells/cm^3 and initially grown in 3ml of unaltered MEM (fatty acid free) medium. After 24 hours, the medium was removed and replaced with 3 ml of medium containing the stated treatment. The treated medium was replaced every 24 hours until the end of the experiment. The cells were dissociated by 5-minute incubation at 37^oC with 250µL trypsin-EDTA solution (trypsinization), before adding 750µL medium and syringing to break up clumps. A 10µL sample was used to count in a glass cytometer. 0.4% Trypan Blue (Sigma T8154) was added to distinguish viable and non-viable cells.

5.2.4.3 Culture doubling time

The time constants (doubling times), τ, were calculated for each treatment using the difference between the viable cell counts after 0 hours and 48 hours and assuming exponential growth of the form $N=N_0 2^{t/\tau}$. When cells grown in untreated medium were counted at several time points, this pattern of growth was followed until near confluence was reached. For the studies in this report, the cells seeded at 26000 per cm^2 were far from confluence at the 48-hour time point such that contact inhibition would not be expected to notably influence results.

5.2.4.4 BrDU Incorporation

To measure the division/proliferation rate of the cells, an assay based on the incorporation of marker bromodeoxyuridine (BrDU) into DNA was used. The Roche 'Cell Proliferation ELISA, BrDU (colorimetric)' assay kit was used. BrDU is incorporated into newly synthesized DNA as an analogue of thymidine during the S-phase. Cells were seeded at a density of 26000 per cm^2 in 96 well plates and allowed to attach for 24 hours in 200µL untreated medium. After this time, 200µL of medium containing both the treatments and the BrDU marker was added to the cells. Measurements of

incorporated BrDU were taken after 24 hours using an ELISA (enzyme-linked immunosorbent assay) according to the kit's protocol.

5.2.5 Intracellular Lipid Staining using ORO

5.2.5.1 Experimental Protocol

HepG2 cells were seeded on to sterilized glass cover slips placed in 24 well plates at a density of 26000 cells/cm^3 and initially grown in 1ml unaltered MEM medium. For each set of conditions (and each repeat) two wells were seeded. In one of these both the lipids and the nuclei were stained. In the other only the lipids were stained. After 24 hours, once the cells had adhered to the glass cover slip, the medium was removed from each well and replaced with 1ml of medium containing the stated treatment. This medium was replaced every 24 hours until measurements were taken.

The medium was aspirated and the cells were washed for 5 minutes twice with PBS. To fix the cells, 10% formalin was added to each well for a minimum of 60 minutes. The formalin was removed and the cells were washed twice with diH_2O before incubating for 5 minutes in 60% isopropanol. The cells were then incubated for 20 minutes in Oil Red O (ORO) working solution (0.18% ORO in 60% isopropanol, 40% diH_2O) (Sigma O1391). 2-5 diH_2O washes were performed until the stain was no longer apparent in the water. For each fatty acid preparation, one well was left with the cells in diH_2O and imaged. From the second well the diH_20 was aspirated and one drop of haematoxylin was added to stain the nuclei. This was rapidly washed away (within 10 seconds) with 2-5 diH_2O washes before imaging.

5.2.5.2 Image Analysis

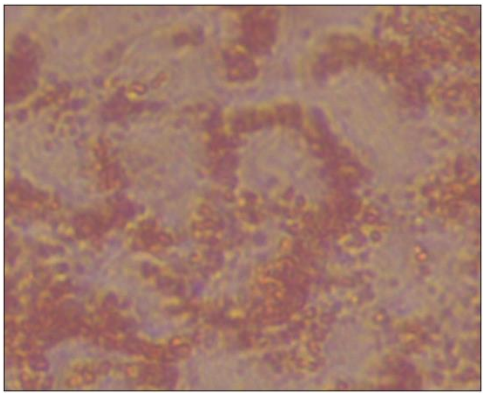

Original Image
Stained regions can clearly be seen by eye, but vary in colour and brightness throughout the image, and between images.

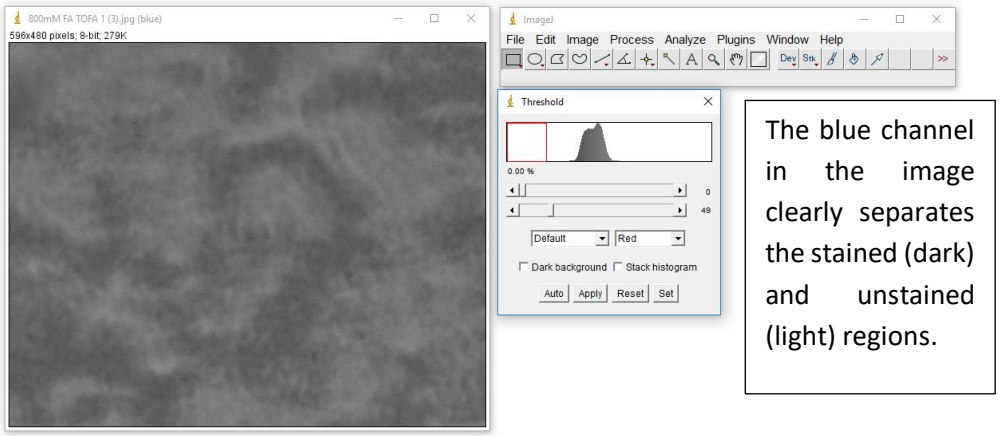

The blue channel in the image clearly separates the stained (dark) and unstained (light) regions.

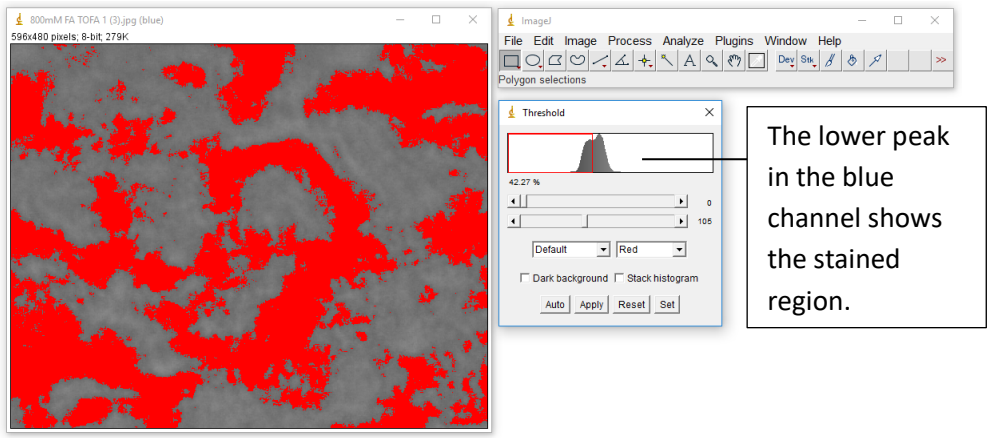

The lower peak in the blue channel shows the stained region.

Previous ORO staining protocols suggested measuring the total lipid content in the sample by breaking up the cells with 100% isopropanol and measuring the change in light absorbance due to the release of ORO. However, since a large number cells were detached from the well plate and during the imaging process (particularly when adding isopropanol), it was impossible to know the number of cells in the plate and, therefore, the quantity of lipid per cell could not be measured in this way. Instead, the percentage of cellular area stained for lipid and the average lipid droplet size were calculated from

the images. Image J was used to perform the image analysis. Since the image analysis performed was only partially automatic, the images were numbered randomly and analysed without knowledge of the treatment to avoid bias. The images were cropped to exclude the areas without cells or where cells had grown on top of one another (often near the edges of the well), leaving only the one-cell-thick regions. To calculate the percentage of area that was stained by ORO, the cropped image regions were separated by into RBG channels. Although the stain is red, numerous areas other than those containing lipid stain also showed up bright in the red channel. Instead, the lipid stained regions were more clearly identified by using the dark regions in the blue channel. Unfortunately, due to post-image capture changes automatically applied by the microscope software, the images varied significantly in brightness and saturation such that no fixed threshold could be set between images to define stained and unstained regions. Instead, the threshold was set manually for each image, with a peak in the low intensity of blue corresponding to stained regions (see image above). Lipid droplet size was determined by manually circling single separate lipid droplets using images at fixed magnification and saving the measured areas. This was again performed using randomly numbered images to avoid bias.

5.2.6 Staining and Quantifying Glycogen Using a Periodic Acid Schiff Stain

Glycogen was stained by treating fixed cells with a periodic acid solution followed by a Schiff solution (PS stain). Since this stains both glycogen and glycoproteins, a second well was treated with diastase followed by periodic acid and Schiff solutions (PSD stain). Diastase breaks down glycogen to maltose such that it is no longer stained. By comparing the two, the amount of glycogen can be calculated.

Cells were seeded at a density of 26’000 per cm^2 on glass slips in 24 well plates in 1ml untreated medium. After 24 hours, 1ml medium containing the stated treatment was added. The cells were grown in the treated medium for 48 hours. Two wells were seeded for each set to allow for both PS and PSD stains to be performed. The cells were washed twice with PBS, then fixed with 10% formalin for a minimum of 1 hour. The PS wells were left in formalin whilst the PSD wells were washed twice with ddH_2O incubated in 0.5% diastase solution for 20 minutes. After this, all wells were washed twice

with ddH_2O and incubated with 1% periodic acid solution for 5 minutes. After two ddH_2O washes, the cells were incubated in Schiff's solution for 15 minutes. 2-5 tap water washes were performed until the water was clear before imaging.

Finally, to quantify total hepatic glycogen, the cells were broken up by the addition of tween-20 in 100% isopropanol with shaking. The absorbance at 550nm minus 650nm was measured using the FLUOstar Omega multi-mode microplate reader. The PSD reading was subtracted from the PS reading to give the absorbance corresponding to glycogen. These readings were compared with visual observation for validation.

5.2.7 Mitochondrial Enzyme Activity Assays

Cells were seeded at a density of 26000 per cm^2 in T25 culture flasks and allowed to attach for 24 hours in 4ml of untreated medium. 4ml of medium containing the stated treatments was added and replaced after 24 hours. After 48 hours, the cells were harvested and stored at -20C in PBS for less than a week. The cell-PBS suspensions were thawed on ice and re-frozen twice to break up the cell membranes. Finally, they were thawed a third time before performing the enzyme activity assays. For all three ETC enzyme measurements, the rates were normalised to citrate synthase activity in the sample to give the activity per total mitochondria as discussed below.

5.2.7.1 Preparation of Cells for Mitochondrial Assays

Cells were grown and treated as described above. To prepare cell homogenates, firstly the medium was removed and, if required, a sample was transferred to an Eppendorf. The cells were then dissociated with 500µL trypsin before resuspending in medium to a total volume of 1.5ml. The suspension was transferred to an Eppendorf and the number of cells was counted using a 10µL sample. Each Eppendorf was centrifuged for 2 minutes at 200RCF (relative centrifugal force). The supernatant was removed before the pellet was resuspended in 1ml of iced PBS. The suspension was centrifuged for 2 minutes at 200RCF and the PBS removed. Finally, the pellet was resuspended to a volume of

0.5mM in iced PBS and rapidly moved to -20^{o}C. The cell suspensions were put through at least three freeze-thaw cycles, defrosting slowly in ice, before use.

A biuret test was used to quantify the presence of peptide bonds and hence the protein content of each sample. To make the biuret working solution 1.5g copper sulphate pentahydrate, 6g sodium potassium tartrate and 30g sodium hydroxide were dissolved in 1 litre of water. To provide reference protein solution, bovine serum albumin was dissolved in PBS at 100mg/ml, 50mg/ml, 25mg/ml, 12.5mg/ml, 6.25mg/ml, 3.125mg/ml, 1.5625mg/ml and 0.78125mg/ml. 150µL of working solution and 20µL of cell solution or reference protein solution were added to each well of a 96 well plate, with at least 2 repeats in each case. After 30-60 minutes, the 550nm absorbance was measured using the FLUOstar Omega multi-mode microplate reader. The FLUOstar Omega data analysis software was used to calculate the concentration of protein in the sample.

5.2.7.2 Citrate Synthase

Firstly, the activity of citrate synthase was measured. As a mitochondrial matrix protein known to be largely unaffected by loss of mitochondrial function, citrate synthase is commonly used as a marker for the amount of mitochondria in a sample (e.g. [601]). The enzyme catalyses the reaction between acetyl-CoA, oxaloacetic acid and water to form citrate along with a CoA molecule with a thiol group (CoA-SH). In the assay, 5,5'-dithiobis-(2-nitrobenzoic acid) (DTNB) is additionally provided which reacts with the thiol group to form 5-thio-2-nitrobenzoic acid (TNB) which absorbs at 412nm. It is this absorbance which is measured. The method used was a slightly modified version of that used previously in HepG2 cells by Garcia-Ruiz [557].

A stock buffer of 200mM k^{+} HEPES (4-(2-hydroxyethyl)-1-piperazineethanesulfonic acid) in ddH_2O was prepared and adjusted to PH8 using a potassium hydroxide (KOH) solution. Stock solution of 5mM oxaloacetate, 2mM DTNB and 10mM acetyl-CoA in ddH_2O were prepared on ice and stored at -20^{o}C.

To perform the assay, the cell suspensions and stock solutions were defrosted slowly on ice. 10µL of cell suspension (containing a total protein concentration of around 4µg/ml) was used in a total volume

of 200µL of solution in a 96 well plate. A solution containing the cell suspension and final concentrations of 100mM k^+ HEPES, 250µL oxaloacetate and 100µL DTNB was prepared in each well. The mixture was briefly incubated at 37°C. Finally, the acetyl-CoA was added to start the reaction at a final concentration of 500µM and the absorbance was read at 412nm minus 640nm for a period of ~4 minutes. The gradient over time was used to measure of citrate synthase activity.

5.2.7.3 Complex 1

Complex 1 catalyses electron transfer from NADH to decylubiquinone (Q10). The reduction in UV absorption of NADH (340nm) was measured in this assay. High concentrations of NADH and Q10 were provided to ensure maximum activity is measured. Complex 4 inhibitor potassium cyanide was added to minimise activity elsewhere in metabolism. To account for any NADH consumption or production by enzymes other than complex 1, measurements were taken with and without the addition of rotenone, a potent complex 1 inhibitor. The protocol used was a slightly modified version of that used previously in HepG2 cells by Garcia-Ruiz [557].

A stock buffer of 50mM potassium phosphate (KPi) in ddH_2O was prepared and adjusted to PH 7.2 using a KOH solution. Stock solutions of 200mM magnesium chloride, 2mM potassium cyanide (in a strongly alkaline solution), 50mg/ml bovine serum albumin (BSA), 2mM NADH, 500µM decylubiquinone and 40mM rotenone were prepared on ice and stored at -20°C.

To perform the assay, the cell suspensions and stock solutions were defrosted slowly on ice. 20µL of cell suspension was used in a total volume of 200µL of solution in a 96 well plate. Two wells were run for each sample allowing measurement of the rate with and without the addition of rotenone. A solution containing the cell suspension and final concentrations of 25mM KPi buffer, 10mM magnesium chloride, 200µM potassium cyanide, 2.5mg/ml BSA, 100µM NADH and 0mM or 2mM rotenone was prepared in each well. The mixture was heated to 30°C. To initiate the reaction, the Q10 was added at a final concentration of 25µM and the absorbance was read at 340nm minus 380nm for

a period of ~60 minutes. The maximum rate over a 20minute period was taken subtracting the value with the addition of rotenone from the value without.

5.2.7.4 Complex 2/3

It is difficult to separate the activities of complexes 2 and 3 experimentally and a combined assay was performed. The rate of production of reduced cytochrome C by complex 3 from complex 2 substrate succinate is measured. The reduction of cytochrome C was measured through a change in its absorbance spectrum. Complex 3 requires ubiquinol (reduced Q10) to reduce cytochrome C, and a high concentration of succinate was provided to stimulate ubiquinol synthesis by complex 2. Sodium azide was provided to prevent the re-oxidation of reduced cytochrome c by complex 4. To compensate for any reduction or oxidation of cytochrome c by other enzymes, the assay was run with and without the addition of antimycin A, a potent complex 3 inhibitor. The protocol used was a slightly modified version of that used previously in HepG2 cells by Garcia-Ruiz [557].

A 322mM KPi buffer was prepared and adjusted to PH7.4 using a KOH solution. Stock solutions of 6mM dipotassium ethylenediaminetetraacetic acid (diK-EDTA), 1mM cytochrome C oxidase, 50mg/ml BSA, 20mM sodium azide, 200mM sodium succinate and 40mM antimycin A were prepared on ice and stored at -20^{o}C.

To perform the assay, the cell suspensions and stock solutions were defrosted slowly on ice. 20µL of cell suspension was used in a total volume of 200µL of solution in a 96 well plate. Two wells were run for each cell suspension allowing measurement of the rate with and without the addition of antimycin A. A solution containing the cell suspension and final concentrations of 166mM KPi buffer, 300µM diK EDTA, 50µM cytochrome c, 2.5mg/ml BSA, 1mM sodium azide, and 0mM or 2mM antimycin A was prepared in each well. The mixture was heated to 30^{o}C. To initiate the reaction, the sodium succinate was added at a final concentration of 10mM and the absorbance was read at 550nm minus 630nm for a period of ~60 minutes. The maximum rate over a 20minute period was taken subtracting the value with the addition of rotenone from the value without.

5.2.7.5 Complex 4

Cytochrome c oxidase (complex 4) is the final enzyme in the electron transport chain. Electrons are taken from reduced cytochrome c oxidase, converting it to its reduced form and moving protons into the intermembrane space in the process. The change in absorption resulting in the oxidation of reduced cytochrome c was measured in this assay. To account for cytochrome c oxidation elsewhere in metabolism, the change in absorbance was measured with and without the addition of potassium cyanide, a potent complex 4 inhibitor. Lauryl maltoside, a detergent, was added to further break up the inner membranes of the cells. The protocol used was a slightly modified version of that used previously in HepG2 cells by Garcia-Ruiz [557].

A 100mM KPi buffer was prepared and adjusted to PH7 using a KOH solution. Stock solutions of 0.3% lauryl maltoside, 600µM reduced cytochrome c and 2mM potassium cyanide were prepared on ice and stored at -20^{o}C. Reduced cytochrome c was produced by adding one or two crystals of sodium dithionite to oxidised cytochrome c and passing through a PD10 column to remove the sodium dithionite. The solution was washed through by a 322mM ph7.4 KP_i buffer (see complex 2/3).

To perform the assay, the cell suspensions and stock solutions were defrosted slowly on ice. 20µL of cell suspension was used in a total volume of 200µL of solution in a 96 well plate. Two wells were run for each cell suspension allowing measurement of the rate with and without the addition of potassium cyanide. A solution containing the cell suspension and final concentrations of 50mM KPi buffer, 0.015% lauryl maltoside, and 0µM or 200µM potassium cyanide was prepared in each well. The mixture was heated to 30^{o}C. To initiate the reaction, the reduced cytochrome c was added at a final concentration of 30µM and the absorbance was read at 550nm minus 630nm for a period of 60 minutes. The maximum rate over a 20minute period was taken, subtracting the value with the addition of rotenone from the value without.

5.2.8 Intracellular ATP Concentrations

A luminescence ATP detection kit (abcam Luminescent ATP Detection Assay Kit (ab113849) was used to quantify the ATP concentration in cultured cells. Cells were seeded at a density of approximately 26000 cells/cm^2 in 96 well plates. After 24 hours, the medium was replaced with fresh medium containing the stated treatment. This was replaced after 24 hours before readings were taken at 48 hours. To take readings, the treated medium was removed and replaced with 100µL of fresh medium. 100µL of medium containing 1µM, 2µM, 5µM, 10µM and 20µM reference concentration of ATP was added to additional wells in triplicate. Following the suggested protocol, 50µL of detergent solution was added to each well before shaking at 800rpm for 5 minutes. Avoiding direct light, 50µL of substrate buffer was added before shaking at 800rpm for 5 minutes in darkness. 100µL of the solution from each well was transferred to a 96 well assay plate avoiding direct light. Luminescence was measured using the FLUOstar Omega multi-mode microplate reader with a gain of 3000 over a period of 10 minutes to ensure no change in emission occurred as a result of any exposure to light. Since no changes were seen in any of the tests run, the average luminescence over the 10 minutes was taken. A linear fit was performed to the reference data and used to quantify the ATP concentration in the 50µL of medium. Finally, the measured concentration was divided by the calculated number of cells to give the µMoles ATP per million cells. The number of cells was calculated based on an initial concentration of 26000 cells and using the measured time constants for exponential growth for each treatment.

5.2.9 Oxidative Stress

Two assays were used to assess oxidative stress in treated cells. The redox potential (measured as the static oxidation reduction potential (ORP)) and antioxidant capacity (measured as the capacity ORP) were measured as markers of extracellular ROS and extracellular antioxidant reserves respectively (using the REDOXSYS system). A Thiobarbituric acid reactive substances (TBARS) assay was performed on cell homogenates to assess for intracellular lipid peroxidation.

Cells were seeded in T25 flasks at a density 26000 per cm^2 in unaltered medium and allowed to attach for 24 hours. After this time, medium containing the stated treatment was added and replaced after 24 hours. After 48 hours, a 1ml sample of medium was taken from each flask, put into an Eppendorf and centrifuged for 2 minutes at 200RCF at 4^oC to remove any floating cells. After centrifugation, the supernatant was transferred into a new Eppendorf and stored at -20^oC for less than 1 week. The cells were harvested as described in section 5.2.7.1 and stored in PBS at -20C for less than a week.

To assess extracellular ROS in the supernatant medium, 20µL of each sample was added to the REDOXSYS and the static ORP and capacity ORP were measured by the REDOXSYS machine. To assess lipid peroxidation, a standard assay was performed to assess the presence thiobarbituric acid reactive substances (TBARS), most notably malondialdehyde, which are produced as degradation products of fats after peroxidation. This assay shows only moderate specificity for lipid peroxidation byproducts, and should be studied with caution, but large increases in readings are thought to signify increased lipid peroxidation.

A reaction mixture was produced with a base containing 1 part each of 0.25 N hydrochloric acid, 15% trichloroacetic acid (TCA) and .375% thiobarbituric acid with 2.5mM butylated hydroxytoluene. To this was added 0.3 parts of sodium dodecyl sulfate. Finally, to the reaction mixture, 0.03 parts of 2.5mM EDTA and 0.03 parts of 1.5mM sodium sulfate were added.

150ml of each cell homogenate sample, along with 150ml PBS for blanks, was added to 300ml of reaction mixture in an Eppendorf and heated for 1 hour at 70 degrees. The Eppendorfs were allowed to cool before 500ml of 1-butanol was added. After vortexing each tube repeatedly to mix, they were next centrifuged at 8000rpm for 1 minute. A 100ml sample was taken from the butanol layer and put in a glass 96 well plate. Absorbance was measured at 532-570nm and black corrected.

5.2.10 Glucose Consumption, Lactate Output and Insulin Sensitivity

The rates of glucose consumption and lactate output were measured through changes in the concentration in the medium. Insulin sensitivity was measured through the change in glucose

consumption resulting from the addition of insulin. Cells were seeded at a density of 26000 per cm^2 in 48 well plates containing 500µL untreated or T25 flasks containing 4ml untreated as stated and allowed to attach for 24 hours. Additional wells containing no cells were used to control for the effects of evaporation on medium concentrations. After this time, medium containing the stated treatments, insulin concentrations and glucagon concentrations was added and replaced after 24 hours. The medium was collected after 48 hours, such that consumption is assessed over the second 24-hour period. 250 µL of medium was harvested from each well and stored at -20C for less than one week. A COBAS machine was used to measure the change in glucose and lactate concentrations. A 200µL sample of medium from each well was added into COBAS tubes (including the cell-free wells) before running automated assays for glucose and lactate using the GLUC3 and LACT2 cartridges. The concentrations measured for each treatment were subtracted from the concentration measured from the cell-free wells to get the rate of consumption/output.

5.3 Results 1: Effects of Fatty acids on Metabolism in HepG2 Cells – Characterisation of the experimental model of NAFLD

5.3.1 Effect of FFAs on cell numbers, cell death and proliferation

Firstly, the effects of FA treatment on cell viability and proliferation rates were assessed to identify the concentrations at which lipotoxicity lead to reduced viability in the cell culture model. This was performed both for the FA cocktail (containing equal molar concentrations of butyric, lauric, palmitic, oleic and linoleic acids) and for each of the FAs individually.

5.3.1.1 Fatty Acid Cocktail

Figure 5.3 shows the effects of increasing concentrations of the FA cocktail up to 800µM on cellular viability after 24 and 48 hours of treatment and on the proliferation rate per cell. Table 5.1 shows the effects of the FA cocktail treatments on the culture doubling time based on the 48 hour counts.

FA treatments were compared with both an unaltered, FA free medium naive control and a vehicle control containing 0.48% EtOH, equal to the amount used to solubilize the 800µM FA treatment. The 0.48% EtOH vehicle control had no significant effect on the percentage of viable cells or total number of viable cells after either 24 hours of 48 hours or on the proliferation rate when compared with the naive control and so only the vehicle control data is presented here.

The percentage of cellular viability was significantly decreased after 48 hours of treatment with 400µM or greater of FA cocktail and after 24 hours with 800µM FA cocktail relative to control. 48 hours of treatment with 800µM caused a notable decreased the percentage of cell viability to 79.3±1.4% relative to the control value of 98.2±0.7% (n=3; p<0.001). Significant increases in the culture doubling times were seen for 400µM FA cocktail or greater (table 5.1). For 400µM, the doubling time of the cultures increased from $2.0^{+0.1}_{-0.1}$ to $2.7^{+0.5}_{-0.3}$ days, whilst almost no increase in viable cell numbers occurred over the 48 hours of treatment with 800µM FA cocktail (n(t=48 hours)/n(t=0)=1.08±0.07, p<<0.001 for both controls). Conversely, no significant difference in the rate of proliferation occurred between the FA free and FA cocktail treated cells (rate for 400µM FA cocktail = 1.01±0.18 times control; p=0.86). Therefore, the measured reduction in viable cell numbers (table 5.1) resulted from reduced viability rather than reduced proliferation.

Table 5.1: the effects of varying FA cocktail concentrations on the doubling time of HepG2 cultures.

Treatment	Doubling time, τ (days)
Control	$2.0^{+0.1}_{-0.1}$ (n=6)
0.48% EtOH	$1.9^{+0.1}_{-0.1}$ (n=3)
200µM FA cocktail	$2.0^{+0.2}_{-0.2}$ (n=6)
400µM FA cocktail	$2.7^{+0.5}_{-0.3}$ (n=6) *
600µM FA cocktail	$4.7^{+1.3}_{-0.8}$ (n=3) *
800µM FA cocktail	$17.3^{+82.0}_{-7.6}$ (n=6) *

*Calculated based on cell counts using a trypan blue exclusion assay at t=0 and t=48 hour counts assuming grown of the form $N=N_0 2^{t/\tau}$. After conversion from measurement of the numbers of viable cells to the time constants, the data is no longer centrally distributed (due to taking the logarithm). To show the equivalent of standard deviation, the upper and lower bounds displayed correspond to the 15.9th and 83.1st percentile. * p<0.05 vs control as assessed by a one-way ANOVA using the 48-hour viable cell count data. The FA cocktail comprised of an equal molar mix of butyric, palmitic, lauric, oleic and linoleic acids.*

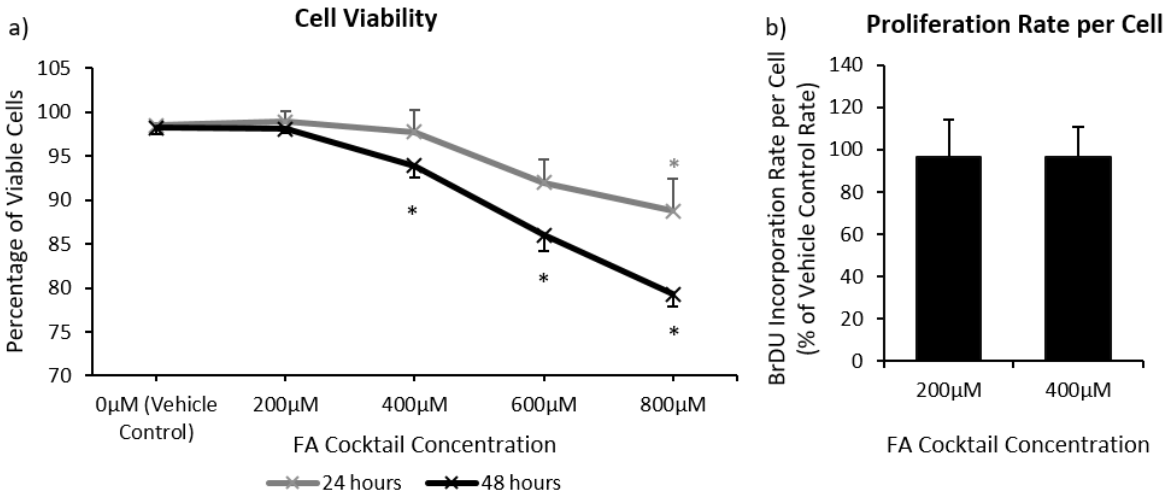

Figure 5.3: The effects of FA treatment on the cellular viability the rate of proliferation per cell. *The effect of treatment with 0-800µM FA cocktail (an equal molar mix of butyric, palmitic, lauric, oleic and linoleic acids) on (a) percentage viability (the number of viable cells divided by the total number of cells) as assessed by a trypan blue exclusion assay and (b) the proliferation rate per cell as assessed by the rate of incorporation of BrDU into cellular DNA. (a) Cells were seeded at 26'000 cells per cm^2 in 6 well plates and allowed to attach for 24 hours before the treatments were added. After the stated treatment time, the cells were dissociated and the number of viable cells and non-viable cells were counted using a trypan blue exclusion assay (section 5.2.4.2). Each data point is the average of 3 independent repeat measurements. A statistically significant effect of both the FA cocktail concentration and the treatment time was first determined using a two-way ANOVA ($p<0.0001$ in both cases) before statistical significance between treated and vehicle control groups was performed using Holm-Sidak adjusted t-tests. * - $p<0.05$ vs both vehicle controls and untreated control. (b) Cells were seeded at 26'000 cells per cm^2 in 96 well plates and allowed to attach for 24 hours before the treatments and BrDU marker were added. Measurements were made after 24 hours of treatment as described in section 5.2.4.4. 3 repeat readings were performed with 2-4 replicates in each case. The bars show the mean the mean and the error bars show the standard deviation (mean ±SD). The vehicle control is the addition 0.48% ethanol equal to the concentration required to solubilize 800µM ethanol. A one-way ANOVA showed no statistical difference between the proliferation rate of FA treated and untreated cells.*

5.3.1.2 Effects of Individual Short, Medium and Long Chain Fatty Acids on Viability

To understand which FAs within the cocktail were causing the reduction in cell viability, HepG2 cultures were next treated with butyric, lauric, oleic, linoleic and palmitic acids individually. Figure 5.4 shows the effects of treatment with individual FAs on cell viability as assessed by a trypan blue exclusion assay.

Treatment with oleic and linoleic acids for 48 hours had no significant effect on cellular viability up to a concentration of 400µM. This suggests that these mono- and poly- unsaturated FAs are not primarily responsible for the decrease in cell numbers resulting from treatment with the FA cocktail. Conversely, the saturated long chain FA palmitic acid caused a notable reduction in cell viability at 200µM or

greater. The percentage viability fell from 98.2±1.1% in control cells to 90.8±2.3 when treated with 200µM palmitic acid (n=3, p=0.022) and 84.1±3.4% when treated with 400µM (n=3; p=0.015). Similarly, treatment with 400µM of the saturated medium chain FA lauric acid caused a significant reduction in cell viability to 86.7±2.1% (n=3; p=0.005) respectively.

Finally, treatment with 400µM of the short chain FA butyric acid caused a significant reduction in cell numbers. This effect was less severe than in the case of palmitic and lauric acids and the percentage viability only reduced to the doubling time of the culture only increased 94.8±0.9% (n=3; p=0.003).

Therefore, the reduction in viable cell numbers resulting from the FA cocktail primarily occurs due to the saturated medium and long chain palmitic and lauric acids, although the saturated short chain butyric acid may also contribute.

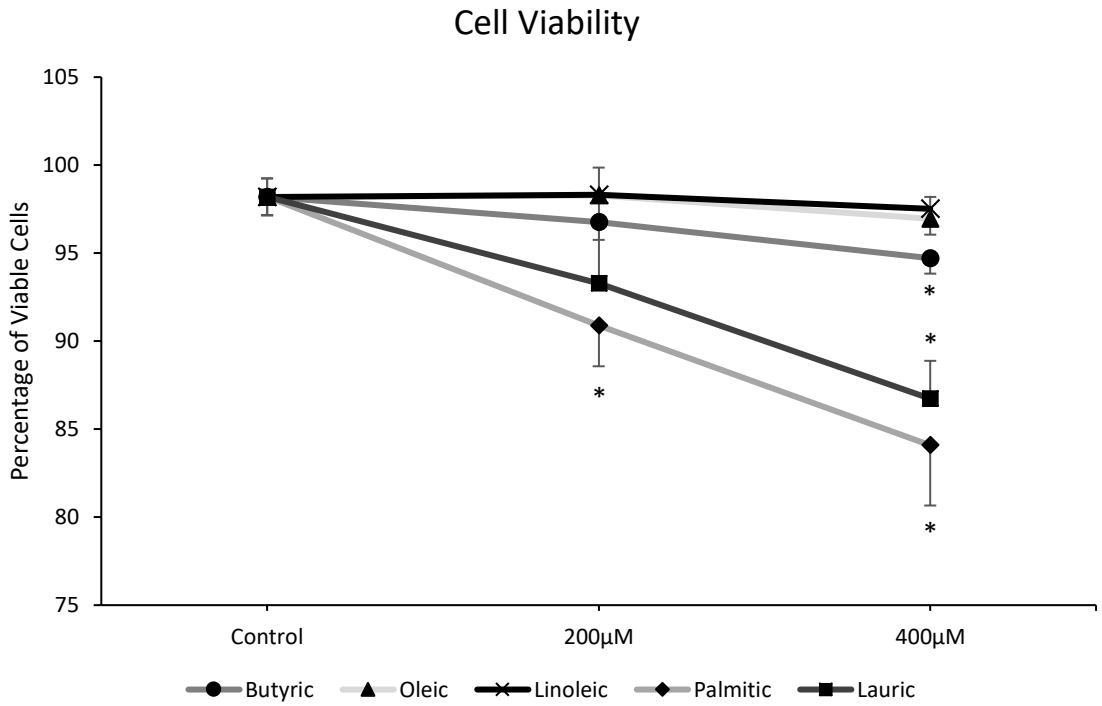

Figure 5.4: The effects of treatment with individual fatty acids on viability. *The effect of 48 hour treatment with individual fatty acids on the percentage viable cells as assessed by a trypan blue exclusion assay. Cells were seeded at 26'000 cells per cm^2 in 6 well plates and allowed to attach for 24 hours before treatments were added. The treated medium was replaced after 24 hours. After 48 hours of treatment the cells were dissociated and counted using a cytometer using trypan blue to identify dead cells. In all cases 3 repeats of 4 replicate counts were performed. The graph shows the mean ±SD. A two-way ANOVA was used to determine significant variation between the groups sets before Holm-Sidak adjusted t-tests were used to calculate significance of each treatment from control at each FA concentration. * - p<0.05 vs control.*

5.3.2 Steatosis

Having established that reduced viability occurs for FA cocktail concentrations of greater than 400µM, the effect of the FA treatments on cellular lipid content was next assessed. Steatosis is the defining feature of NAFLD and severely increased lipid content was seen when simulating high fat intake and IR in the model. It is therefore important that it is seen in the cell culture model.

The effects of treatment for 48 hours with varying concentrations of the FA cocktail and with each FA individually on cellular lipid content are shown in figure 5.5. In the control cells, 20±5% of cellular area was stained by ORO. Although this is a percentage of area in the images rather than a percentage of mass, it is still high relative to the lipid content seen in healthy liver cells *in vivo* and HepG2 cells are known to contain a high lipid content due to reduced secretion of triglycerides [554]. Treatment with a 0.48% ethanol vehicle control, equal to the highest ethanol content used for 800µM FA cocktail, increased the percentage of area stained compared with control to 24±5% ($p<0.01$).

As would be expected, addition of increasing concentrations of FA cocktail to the culture medium caused a significant increase in hepatic lipid concentrations (figure 5.5a). After treatment with 200µM, 400µM, 600µM and 800µM FA cocktail over 48 hours, the percentage of cell area stained for lipid increased to 32±4%, 43±5%, 50±3% and 66±9% respectively ($p<0.05$ compared with both unaltered medium and vehicle controls). In the case of 800µM, the cells were almost entirely full of lipids with only the nuclei remaining unstained (figure 5.5c).

Increasing the concentration of FA cocktail in the medium not only increased the total lipid content of the cells, but also increased the sizes of lipid droplets (figure 5.5b). When treated with 800µM the median lipid droplet area nearly doubled from 83 pixels to 161 pixels whilst the 95th percentile droplet area increased from 133 pixels to 321 pixels.

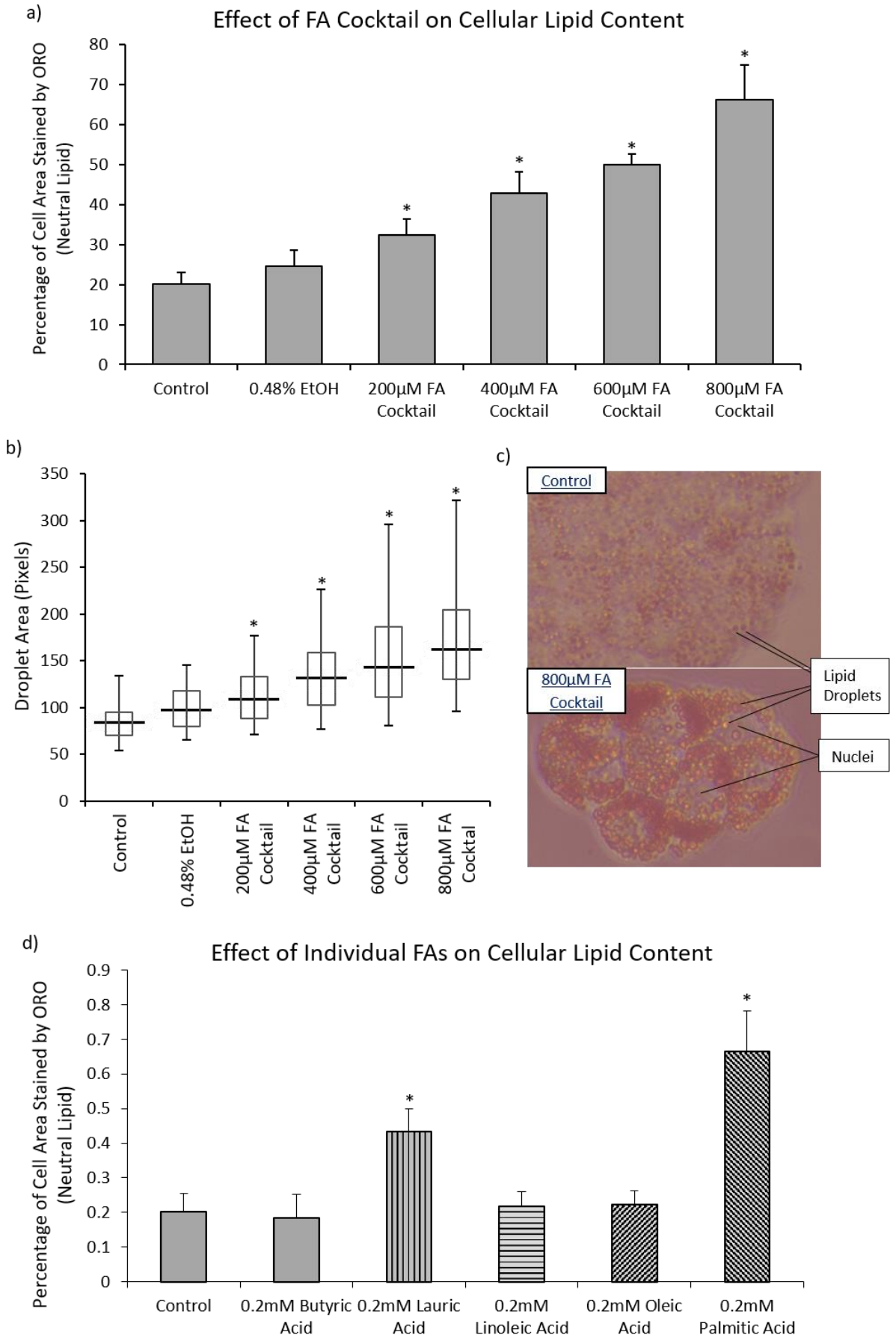
a)
Effect of FA Cocktail on Cellular Lipid Content
Percentage of Cell Area Stained by ORO (Neutral Lipid)
0
10
20
30
40
50
60
70
80
Control
0.48% EtOH
200µM FA Cocktail
400µM FA Cocktail
600µM FA Cocktail
800µM FA Cocktail
b)
Droplet Area (Pixels)
0
50
100
150
200
250
300
350
Control
0.48% EtOH
200µM FA Cocktail
400µM FA Cocktail
600µM FA Cocktail
800µM FA Cocktal
c)
Control
800µM FA Cocktail
Lipid Droplets
Nuclei
d)
Effect of Individual FAs on Cellular Lipid Content
Percentage of Cell Area Stained by ORO (Neutral Lipid)
0
0.1
0.2
0.3
0.4
0.5
0.6
0.7
0.8
0.9
Control
0.2mM Butyric Acid
0.2mM Lauric Acid
0.2mM Linoleic Acid
0.2mM Oleic Acid
0.2mM Palmitic Acid

Figure 5.5: The effect of fatty acid treatment on cellular steatosis. (a) *The effect of the fatty acid cocktail (an equal molar mix of butyric, palmitic, lauric, oleic and linoleic acids) on percentage of cellular area stained for lipid.* ***(b)*** *The effect of the fatty acid cocktail on the distribution of lipid droplet sizes. Horizontal lines represent the average median, boxes represent the average 25th and 75th percentiles and whiskers represent the average 5th and 95th percentiles.* ***(c)*** *Representative images of control and 800µM FA cocktail treated HepG2 cells taken at 40x magnification.* ***(d)*** *The effect of treatment the individual FAs on the percentage of the cellular area stained for lipid. The mean ±SD is presented from a minimum of 3 independent repeats.*
*Cells were seeded at 26'000 cells per cm^2 in 24 well plates containing glass coverslips in untreated medium and allowed to attach. After 24 hours, the untreated medium was aspirated and replaced with medium containing the stated treatment. The treated medium was replaced after 24 hours. The cells were stained with ORO after 48 hours of treatment before imaging. Quantification was performed using Image J as discussed in section 5.2.5. A minimum 3 independent repeats of at least 7 technical replicates were analysed for the fatty acid cocktail treatments and a minimum of 3 independent repeats of 3 technical replicates were analysed for the individual fatty acid treatments. A minimum of 250 droplets were analysed from each independent repeat to calculate the distributions in (b). An ANOVA was used to determine significance between the treatment groups sets before Holm-Sidak adjusted t-tests were used to calculate the significance of the difference between each treatment and both untreated and (EtOH) vehicle controls. *- p<0.05 vs control and vehicle control.*

To investigate which FAs within the cocktail resulted in steatosis, HepG2 cells were treated with 200µM of each individual FA and stained with ORO after 48 hours (figure 5.5d). The percentage area stained for lipid was not significantly increased by treatment with 200µM of butyric acid (18±6%; n=8; p=0.57), oleic acid (22±4%; n=6; p=0.06) or linoleic acid (22±4%; n=11; p=0.07) compared with control (20±5%; n=39). However, a significant increase occurred when the cells were treated with 200µM of either palmitic (43±6%; n=8; p<0.001) or lauric acids (67±12%; n=8; p<0.001).

It should be noted that equal molar concentrations rather than equal masses or volumes of each FA were used as treatments. The four medium and long-chain FAs have similar molar masses in the range 200-300 grams per mole and densities in the range 0.85-0.9g/cm^3 (dependent on the temperature as well as the type of fat). However, the short-chain butyric acid has a much lower molecular mass of 88.1 grams per mole (33.4% of the molar mass of palmitic acid). Therefore, although the same number of molecules were added, the total mass (and volume) of FA in the case of butyric acid was around a third of that for the other FAs. However, since 200µM butyric acid failed to cause even a non-significant increase in hepatic lipid levels, this is unlikely to account for the difference in lipid content between butyric acid and palmitic acid treated cells.

5.3.3 Mitochondrial Function and Oxidative Stress

As discussed above, reduced mitochondrial function and oxidative stress are both known to occur in NAFLD *in vivo* and are thought to arise because of increased hepatic FFA concentrations and increased oxidation of fats. In the model simulations, increases in hepatic FFA concentration and overactivation of oxidative phosphorylation occurred, although the pathways mediating the resulting effects on mitochondria are not currently included in the model. Conversely, experimentally it is possible to measure oxidative stress and mitochondrial function but difficult to measure intracellular FFA concentrations due to their rapid binding to CoA and use in glycerolipid synthesis or β-oxidation. In the next section, the effects of FFA treatment on markers of oxidative stress and mitochondrial function (ETC enzyme activity) are assessed in the cell culture model.

5.3.3.1 Electron Transport Chain Activities and ATP levels

Figure 5.6 shows the effects of 48-hour treatment with different concentrations of the FA cocktail on the activity of citrate synthase per million cells as a marker of the mitochondria per cell, on the activities of ETC enzymes complex I-IV per mitochondria and on intracellular ATP concentrations.

Treatment with 200µM of the FA cocktail had no effect on citrate synthase activity ($1.4\pm0.4x10^{-3}$ absorbance units per second per million cells (au s^{-1} mc^{-1}) (n=4) compared with control: $1.4\pm0.2x10^{-3}$ au s^{-1} mc^{-1} (n=4)) (figure 5.6a). However, 400µM and 800µM FA cocktail significantly increased citrate synthase activity to 1.9±0.3 au s^{-1} mc^{-1} (n=4; p=0.007) and $3.0\pm0.6x10^{-3}$ au s^{-1} mc^{-1} (n=4; p<0.001) respectively. Therefore, the total mitochondrial level was increased in the FA treated cells. The increase in activity failed to reach significance for cells treated with 600µM FA cocktail (1.6±0.3 au s^{-1} mc^{-1}; n=4; p=0.21).

Treatment with 400µM or greater of the FA cocktail significantly decreased both the activity of complex I (figure 5.6b) and the combined activities of complexes II and III (figure 5.6c). Treatment with 600µM or greater also significantly reduced complex IV activity (figure 5.6d). This demonstrates reduced mitochondrial function after 48-hour FA treatment.

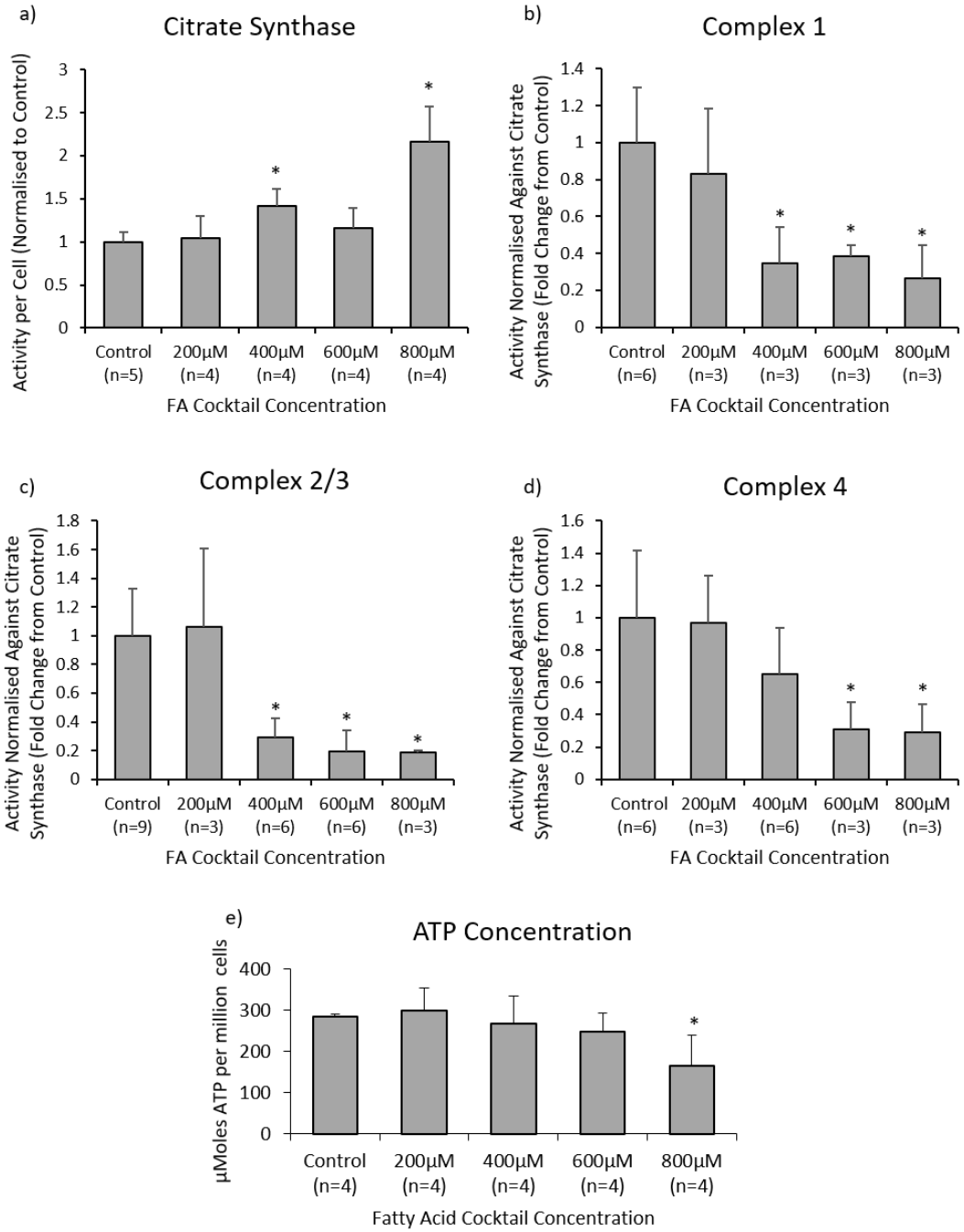

Figure 5.6: The effect of FA treatment on mitochondrial function. *The effect of 48-hour treatment with varying concentrations of FA cocktail (an equal molar mix of butyric, palmitic, lauric, oleic and linoleic acids) on (a) the activity of citrate synthase as a marker for total mitochondrial level, (b) the activity of complex I, (c) the combined activities of complexes II and III, (d) the activity of complex IV and (e) the intracellular ATP concentration. Cells were seeded at 26'000 cells per cm^2 in (a-d) T25 culture flasks and (e) 96 well plates in untreated medium and allowed to attach. After 24 hours, the untreated medium was aspirated and medium containing the stated treatment was added. The treated medium was replaced after 24 hours. The cells were harvested and measurements performed after 48 hours of treatment. Numbers of independent repeats performed are stated in the axes. For (a-d) each independent repeat is based on two replicate reaction rate measurements. For (e) each independent repeat is based on 3-7 replicate measurements. (a,e) Normalised to the number of cells. (b-d) Normalised against citrate synthase to give activity per total mitochondria. The mean ±SD is shown. A one-way ANOVA was used to determine significant variation between the treatment groups before t-tests were used to calculate the significance of the differences between each FA treatment and the control. * p<0.05 vs control.*

The measured increase in citrate synthase activity, and hence total mitochondria, may partially compensate for the reduced mitochondrial function. For example, the complex I, II/III and IV activities in cells treated with 800µM FA cocktail were reduced to 26±18%, 19±2% and 29±17% of their activities in control cells respectively when normalised per mitochondria. However, when the increase in the amount of mitochondria (activity of citrate synthase) per cell is accounted for, the calculated total complex I, II/III and IV activities per cell were 57±40%, 41±8% and 63±40% of their activities in control cells respectively.

Figure 5.6e shows the intracellular ATP concentration in cells treated with varying FA cocktail concentrations for 48 hours. Treatment with 800µM of the FA cocktail significantly reduced the ATP concentration to roughly 60% of that measured in control cells (p=0.046). No significant change in ATP concentration occurred in cells treated with 200µM, 400µM or 600µM FA cocktail. Therefore, reduced ATP levels result from FA treatment of HepG2 cells, but a higher FA concentration is required than for the development of mitochondrial dysfunction.

5.3.3.2 Oxidative Stress

Oxidative stress is known to result from excess FA oxidation and increased FFA levels, particularly in the context of reduced mitochondrial function. Figure 5.7 shows the effects of treatment for 48 hours with the FA cocktail on the redox potential and antioxidant reserves in the supernatant medium and on lipid peroxidation as assessed by a TBARS assay in the cell homogenates.

Figures 5.7 a and b shows the effects of varying concentrations of FA cocktail on the redox potential and antioxidant capacity in the medium of cells which had been treated with varying concentrations of the FA cocktail. The redox potential (measured as the static ORP (section 5.2.9)) increased significantly when cells were treated with 400µM (228±3mV; n=3; p=0.001), 600µM (230±8mV; n=3; p=0.03) and 800µM (224±4mV; n=3; p=0.005) of the FA cocktail compared to control (206±2mV; n=3). Although the differences in redox potential are small relative to the absolute values, they lie within a similar range to the values measured in the blood of type 2 diabetic and control patients [595]. The

antioxidant capacity (measured as the capacity ORP (section 5.2.9)), meanwhile, decreased significantly for FA cocktail concentrations of 600µM (0.18±0.02µC vs control 0.24±0.01µC; n=3; p=0.016) and 800µM (0.19±0.01µC; n=3; p=0.003). This data shows that, in the medium of cells treated with high FA cocktail concentrations, oxidative stress was increased whilst antioxidant reserves were depleted.

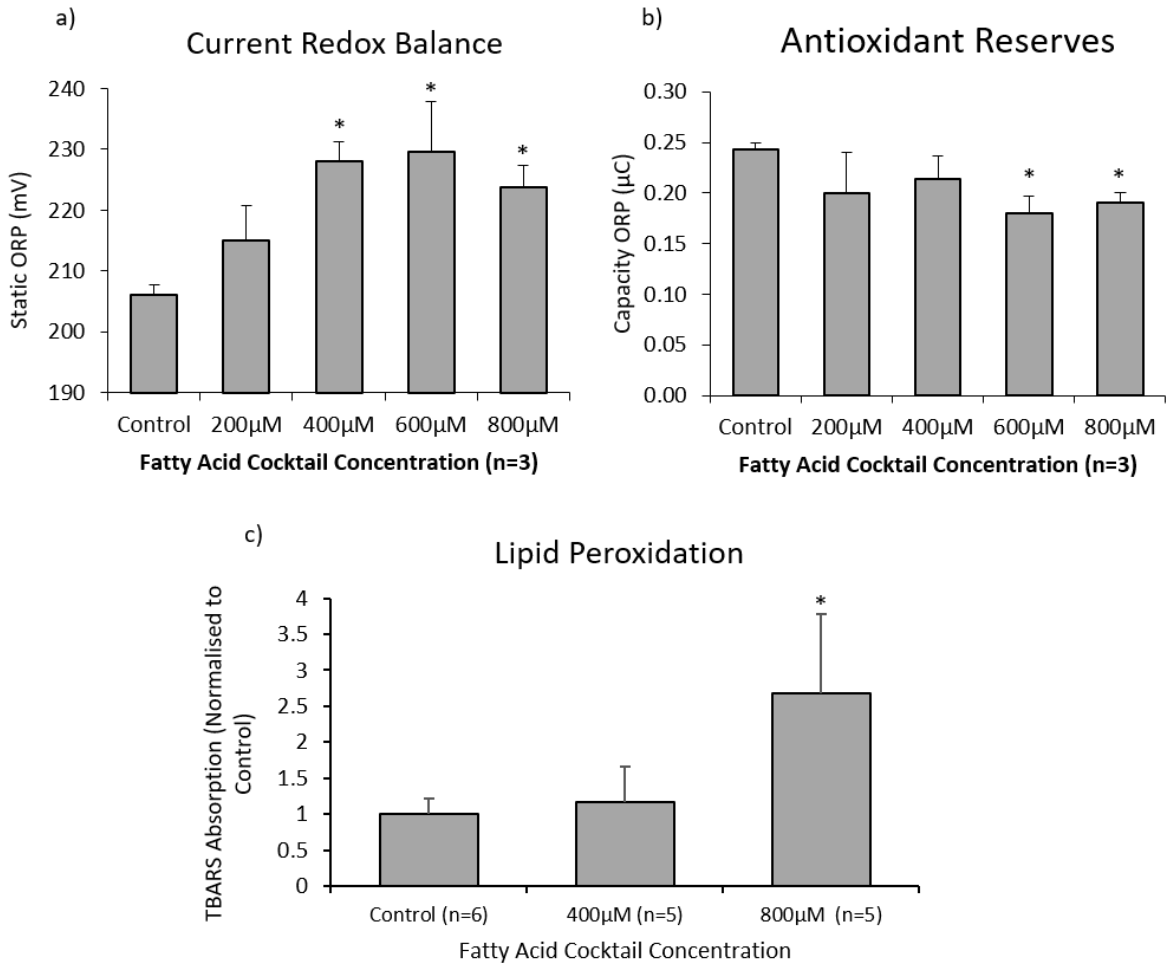

Figure 5.7: The effect of FA treatment on oxidative stress. *The effect of varying concentrations of a FA cocktail (an equal molar mix of butyric, palmitic, lauric, oleic and linoleic acids) on (a) the redox potential in the supernatant medium, (b) the antioxidant capacity in the supernatant medium and (c) lipid peroxidation as assessed by a TBARS assay in the cell homogenates.*
*Cells seeded at 26'000 cells per cm^2 in T25 flasks plates in untreated medium and allowed to attach. After 24 hours, the untreated medium was aspirated and medium containing the stated treatment was added. The treated medium was replaced after 24 hours. The supernatant medium and cells were harvested after 48 hours of treatment. The tested supernatant medium had been in contact with the cells from the 24^{th} to the 48^{th} hour of treatment. The medium was measured for redox capacity and antioxidant reserves whilst the cells were homogenised and assessed for lipid peroxidation (section 5.2.9). The graphs show the mean ±SD based on the numbers of independent repeats shown on the axes of the graphs. A one-way ANOVA was used to determine significant variation between the treatment groups before t-tests were used to calculate the significance of the difference between each FA treatment and the control. * - p<0.05 relative to control.*

Figures 5.7c shows the presence of lipid peroxidation as assessed by a TBARS assay in cell homogenates after 48 hours of treatment with varying concentrations of the FA cocktail. No significant change in TBARS occurred when the cells were treated with 400µM FA cocktail (1.2±0.5 $cell^{-1}$ (n=5) vs 1.0±0.2 $cell^{-1}$ (n=6); p=0.51). However, when treated with 800µM, TBARS increased significantly to almost three times the value in control cells (2.7±1.1 $cell^{-1}$ (n=5); p<0.01). An increase in TBARS measurement this large is strongly indicative of the presence of lipid peroxidation.

5.3.4 Glucose Consumption and Insulin Sensitivity

In vivo, NAFLD is often associated with IR, defective glycogen storage and hyperglycaemia. This is caused by increased intracellular concentrations of FFAs and closely related ceramides and DAGs [8, 146, 247, 248]. In the following sections, the effects of FFAs on glucose consumption and insulin sensitivity are assessed.

Figure 5.8 compares the rates of glucose consumption by cells grown in medium containing varying FA cocktail and insulin concentrations. Cells were treated for a total of 48 hours, with the medium replaced after 24 hours. The medium provided to the cells contained 5mM glucose equivalent to normoglycaemia. In each repeat, the rate of glucose consumption was calculated by subtracting the measured glucose concentration in the supernatant medium of each well after the 48 hours from the concentration measured in a blank (cell-free). This gives the blank corrected change in medium glucose concentration over the second 24-hour period. Since some medium evaporates occurs over 24 hours, the measured average glucose concentration in the blank wells was slightly higher at 5.45mM.

In the absence of insulin, the glucose consumption over 24 hours was notably larger for cells treated with 200µM FA cocktail compared with FA free control cells (3.28±0.18 vs 2.27±0.23mM; p=0.012) (figure 5.8a). When treated with 400µM fatty acid, glucose consumption returned to a rate close to that seen in cells grown in control medium (2.36±0.75mM; p=0.85) (figure 5.8a).

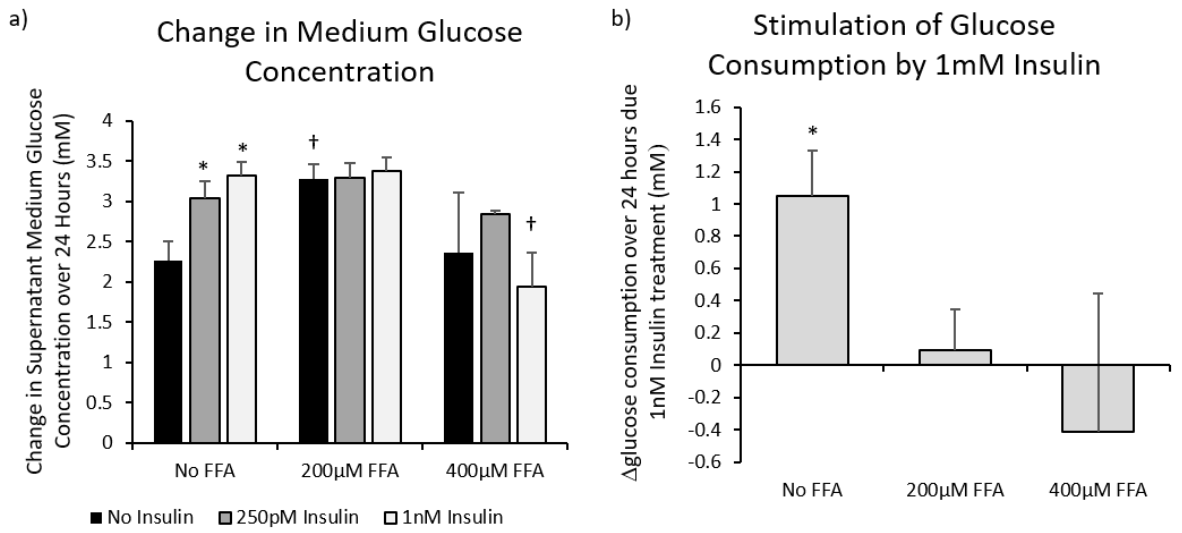

Figure 5.8: The effects of 48-hour treatment with insulin and FA cocktail on the rate of glucose consumption*. (a) The change in supernatant medium glucose concentration (as a measurement of the rate of glucose consumption) when treated with varying FA cocktail concentrations (an equal molar mix of butyric, palmitic, lauric, oleic and linoleic acids) along with the addition of either no insulin, a moderate insulin concentration (250pM) or a high insulin concentration (1nM) in normoglycaemic medium (5mM). (b) The change in glucose consumption as a result of the addition of 1nM insulin in cells treated with varying FA cocktail concentrations.*
Cells were seeded at 26'000 per cm^2 in 48 well plates *in untreated medium containing 5mM glucose and allowed to attach. After 24 hours, the untreated medium was aspirated and medium containing the stated treatment was added. The treated medium was replaced after 24 hours. The supernatant medium was collected and analysed* after 48 hours of treatment as described in section 5.2.10. In each case, the data is based on 3 repeats of 2-7 replicate measurements. *A two-way ANOVA was used to determine significant variation between the FFA and insulin treatment groups sets before Holm-Sidak adjusted t-tests were used to calculate significance of the difference between each FA cocktail treatment and the FFA free value for the same insulin concentration in addition to the significance of the difference between each insulin treatment and the insulin free measurement for the same FA cocktail concentration. * p<0.05 when treated with insulin vs corresponding FA cocktail concentration without insulin. † p<0.05 when treated with FA vs corresponding insulin concentration without FA. Bars show mean ±SD.*

Cells grown in FA free medium showed a statistically significant increase in glucose consumption when treated with 1nM insulin (3.22±0.29mM; p=0.034) and a non-significant increase when treated with 250pM insulin (2.95±0.30mM; p=0.011) and compared with those grown in the absence of insulin (2.27±0.23mM) (figure 5.8b). However, cells treated with 200µM or 400µM FA cocktail, showed no increase in glucose consumption with the addition of 1nM insulin (figures 5.8b). This shows that low concentrations of the FA cocktail cause a complete loss of insulin sensitivity in glucose consumption in HepG2 cells.

When a Schiff stain was performed to assess the glycogen content in cells treated with a high insulin concentration, no glycogen was observed irrespective of the FA concentration. This was assessed both

through simple observation in the images and through the absorbance spectra at 550nm. The measured absorption after adding diastase (which breaks down glycogen to simple sugars) was subtracted from the absorption measured in the absence of diastase to give the glycogen-specific absorption. For control cells the glycogen specific absorption was -2.1±1.8 mOD per million cells (n=3) whilst for cells treated with 400µM FA cocktail it was 0.3±0.6 mOD per million cells (n=3). Therefore, although the control cells showed insulin sensitivity in glucose consumption, the glucose is not used in glycogen synthesis.

5.4 Results 2: Treatment with inhibitory molecules

The data in the previous section show that several metabolic changes result from FA treatment in HepG2 cells. These include reduced cell viability due to increased cell death, the development of steatosis, reduced mitochondrial function, reduced ATP concentrations oxidative stress and IR. As discussed below, these data are corroborated by numerous previous observations of changes in cellular metabolism in NAFLD and, although in some cases not directly comparable, are consistent with the model simulations. In the following section, 5 small molecule inhibitors (TOFA, C75, T863, 2DG and 3BP) were used to test the effects of inhibiting specific processes in HepG2 cells when grown in medium containing varying concentrations of FAs.

A range of concentrations of each inhibitor were first tested for their effect on cell viability to determine treatment concentrations which were not toxic to the cells when grown in FA free medium. This data is presented in supplementary material S2. It should be noted that HepG2 cells are derived from hepatocellular carcinoma, and cancer cells are known to rely on upregulated glycolysis and lipogenesis to permit rapid proliferation under conditions of reduced blood supply [555, 556]. HepG2 cells are therefore susceptible to damage as a result of inhibitions preventing glycolysis and lipogenesis than primary cells. Inhibiting lipogenesis by targeting FAS or ACC1 as well as targeting glycolysis using 2DG or 3BP have been suggested as potential cancer treatments in the literature [602-605]. Therefore, rather than adding the inhibitors at high concentration to fully inhibit each process,

we instead investigated whether low concentrations of the inhibitors (at which they do not cause reduced viable cells numbers when grown in control medium), ameliorate or exacerbate the mitochondrial damage and cell death resulting from FA treatment. Both in the model simulations described in the previous chapters, and when studied *in vivo* [15-17, 377], the majority of adverse effects in NAFLD occur in pericentral cells. Since pericentral cells also rely heavily on glycolysis for energy production and are the most lipogenic group of hepatocytes, the HepG2 model can be thought to most closely resemble these cells. Based on the data, treatment concentrations of 2µg/ml TOFA, 2µg/ml C75, 200ng/ml T863, 500ng/ml 2DG and 2µg/ml 3BP were chosen.

5.4.1 Viability and Steatosis

Figure 5.9 shows the effect of the various inhibitors on cell viability and steatosis for cells grown in medium containing a range of FA cocktail concentrations. Additionally, figure 5.9c shows the effect of TOFA on the distribution of droplet sizes in the cells.

Treatment with 2µg/ml TOFA significantly increased cell viability in for cells grown in medium containing 800µM FA cocktail 79.1±1.3% to 86.1±3.0% (figure 5.9a) ($p=0.007$). The gradient of reducing viability with increasing FA cocktail concentration was significantly reduced by TOFA treatment (TOFA: 15±2%/µM vs control: 25±2%/µM; $p<0.01$). Viability was unchanged by TOFA treatment in control cells (98.1±0.4% vs 97.5±0.4%; $p=0.56$).

TOFA treatment significantly reduced the lipid content of cells grown in medium containing FA concentrations of 400-800µM by 40-50% (figure 5.9b) ($p<<0.05$) and significantly reduced the gradient between cellular lipid content and FA cocktail treatment concentration (TOFA: 31±2%/mg vs control: 55±2%/mg; $p<0.01$). For control, 0.48% EtOH and 200µM FA cocktail treated cells, the reduction in steatosis as a result of TOFA treatment was near significance ($0.05<p<0.08$). For cells grown in medium containing a FA cocktail concentration of 400µM or greater, the addition of 2µg/ml TOFA also caused a significant decrease in the median droplet size ($p<0.05$), giving a lipid droplet distribution more similar to that of control cells (figure 5.9c).

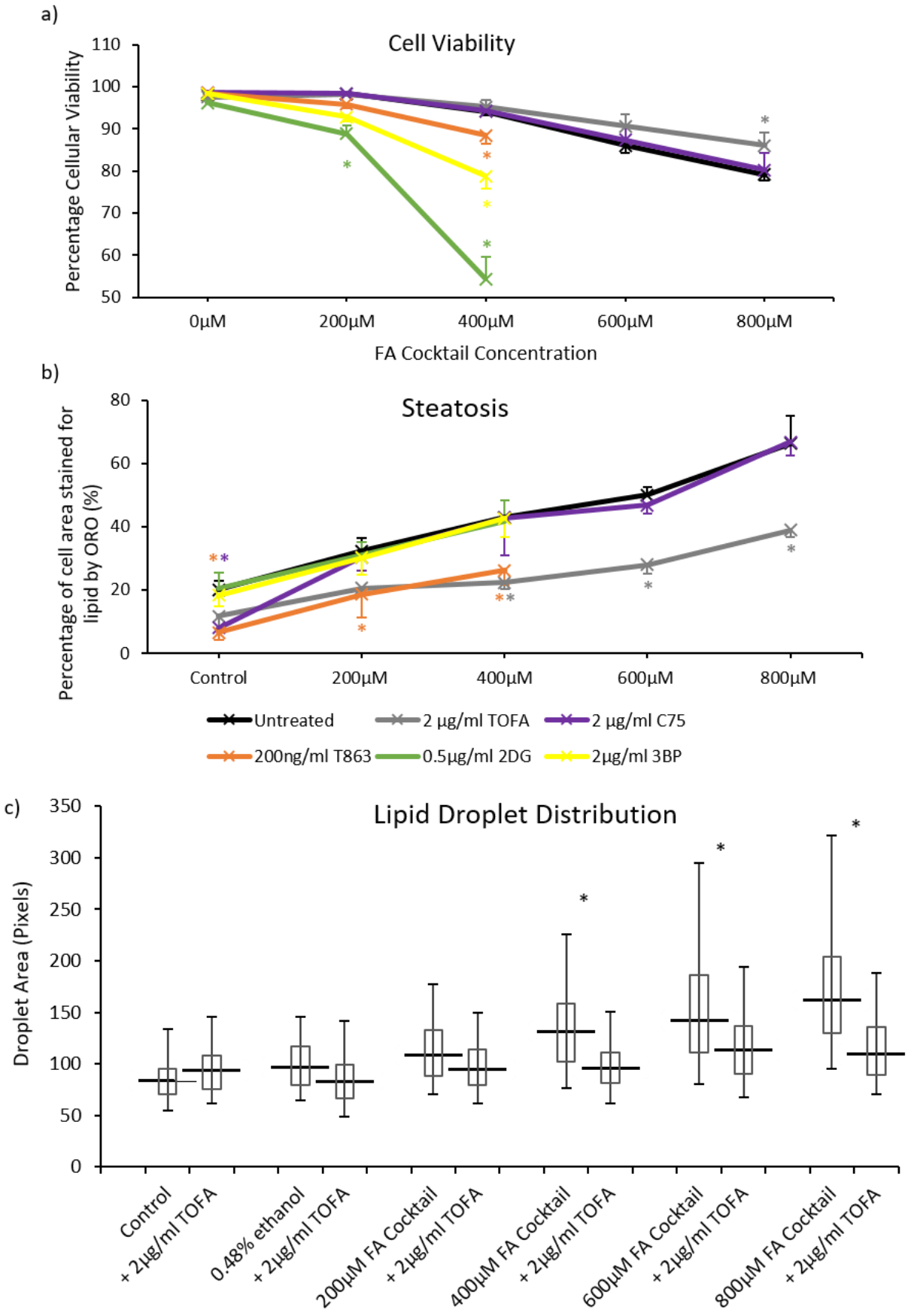
a)
Cell Viability
Percentage Cellular Viability
110
100
90
80
70
60
50
0μM
200μM
400μM
600μM
800μM
FA Cocktail Concentration
b)
Steatosis
Percentage of cell area stained for lipid by ORO (%)
80
60
40
20
0
Control
200μM
400μM
600μM
800μM
Untreated
2 μg/ml TOFA
2 μg/ml C75
200ng/ml T863
0.5μg/ml 2DG
2μg/ml 3BP
c)
Lipid Droplet Distribution
Droplet Area (Pixels)
350
300
250
200
150
100
50
0
Control
+ 2μg/ml TOFA
0.48% ethanol
+ 2μg/ml TOFA
200μM FA Cocktail
+ 2μg/ml TOFA
400μM FA Cocktail
+ 2μg/ml TOFA
600μM FA Cocktail
+ 2μg/ml TOFA
800μM FA Cocktail
+ 2μg/ml TOFA

Figure 5.9: Effect of 48-hour treatment with the various inhibitors on viability and steatosis. *The effects of 2µg/ml TOFA, 2µg/ml C75, 200ng/ml T863, 0.5µg/ml 2DG and 2µg/ml 2BP on (a) cell viability (the number of living cells divided by the total number of cells) as assessed by a trypan blue exclusion assay and (b) the percentage of cell area stained for lipid by ORO in cells grown at a range of FA cocktail concentration (an equal molar mix of butyric, palmitic, lauric, oleic and linoleic acids). (c) The effect of 2µg/ml TOFA on the distribution of lipid droplet sizes in cells grown at a range of FA cocktail concentration. (a) Cells were seeded at a density of 26'000 per cm^2 in 6 well plates and allowed to attach in untreated medium for 24 hours. The treated medium was added and replaced after 24 hours before counting after 48 hours, using trypan blue to identify dead cells. The graph shows the means ± SD based on 3 independent repeats of 4 replicate counts except for the untreated curve which is based on 6 independent repeats. (b, c) Cells were seeded at a density 26000 per cm^2 on glass cover slips in 24 well plates and allowed to attach for 24 hours in untreated medium. After the cells had attached, medium containing the stated treatment was added. This was replaced after 24 hours before the cells were stained and imaged after 48 hours of treatment. Image J was used to quantify the lipid content and droplet sizes. The graphs are based on analysis of at least 3 replicates form 3-4 independent repeat. The box and whisker plots show the average means, average 25^{th} and 75^{th} percentiles and average 5^{th} and 95^{th} percentiles from 3 repeat experiments in which a minimum of 250 droplets were analysed.*
*A statistically significant effect of both the FA cocktail concentration and the treatments was first determined using a two-way ANOVA before statistical significance of the differences between each treated group and the control group were calculated using Holm-Sidak adjusted t-tests. * $p<0.05$ vs untreated for same FA concentration.*

Treatment with FAS inhibitor C75 had no effect on cell viability (figure 5.9a) when tested across the range of FA cocktail concentrations (0-800µM). Therefore, the C75 treatment neither improved nor exacerbated FA induced cell death. C75 treatment also had little effect on cellular steatosis (figure 5.9b). Treating with 2µg/ml C75 only caused a significant reduction in cellular lipid levels for cells grown in FA free medium (2µg/ml C75: 8±4% vs control: 20±5%; p=0.023). In FA free medium all lipids must arise through *de novo* lipogenesis so it is expected that inhibition of the process would reduce the hepatic lipid concentration. However, when cells were grown in medium containing 200-800µM FA cocktail, inhibition of lipogenesis with C75 had no effect on hepatic lipid levels. Since raised plasma lipid concentrations are seen in NAFLD patients, these results suggest the treatment would not be effective at clearing steatosis in NAFLD patients.

Partial inhibition of triglyceride synthesis using T863 in HepG2 cells caused a reduction in cellular lipid levels for all FA cocktail concentrations (0-400µM) (figure 5.9a). For cells grown in medium containing 400µM cocktail, the area stained for steatosis was reduced by nearly 40% (26±5% vs 42±5%; p=0.015) and for cells grown in FA free medium, the percentage decrease was even larger (6±2% vs 20±3%; p=0.003). However, despite the reduction in steatosis, treatment with 200ng/ml T863 of cells grown in medium containing 200µM or 400µM FA cocktail caused a reduction in cell viability (figure 5.9a)

($p<0.05$). T863 treatment did not alter cell viability when the cells were grown in FA free medium. Therefore, despite clearing steatosis, T863 treatment exacerbated rather than improved FA-induced cell death.

Treatment with 500ng/ml 2DG notably decreased the number of viable cells when grown in medium containing 200µM and 400µM FA cocktail (figure 5.9a). Similarly, treatment with 2µg/ml 3BP caused a significant reduction in the number of viable cells for 400µM FA cocktail and a non-significant reduction for 200µM. Glycolysis inhibition by both 2DG and 3BP has previously been shown to cause apoptosis in cancer cells. However, the low 2DG and 3BP treatment concentrations used in this study did not cause significant decreases in the number of viable cells when added to the medium of cells cultured in FA free conditions, as discussed in supplementary material S2. Instead, the results in figure 5.9a show that the low concentrations of 2DG and 3BP acted to exacerbate the cell death resulting from FA treatment.

Neither of the glycolysis inhibitors tested had any effect on the lipid content (figure 5.9b). This suggests that inhibition of glycolysis at either stage (GK or glyceraldehyde-3-phosphate dehydrogenase) has toxic effects on metabolism at concentrations below those at which it reduces lipid levels.

To assess the extent to which glycolysis was inhibited by 3BP and 2DG, the rates of glucose uptake and lactate output were measured for cells grown in either FA free medium or medium containing 400µM FA cocktail with the addition of either no treatment, the 1µg/ml BP, 2µg/ml 3BP, 250ng/ml DG or 500ng/ml 2DG treatments (figure 5.10). For both FA free and FA cocktail treated cells, 1µg/ml and 2µg/ml BP reduced the rates of glucose uptake and lactate output, and hence the rate of glycolysis, by approximately 5-15% and 10-25% respectively. 250ng/ml and 500ng/ml 2DG meanwhile reduced the rates by 25-35% and 40-50% respectively. Therefore, in the case of the high 2DG concentration, even with 40-50% inhibition of glycolysis no change in cellular lipid content occurred. Conversely, in

the case of the low 3BP concentration, resulting in only 5-15% inhibition of glycolysis, increased FA induced cell death occurred.

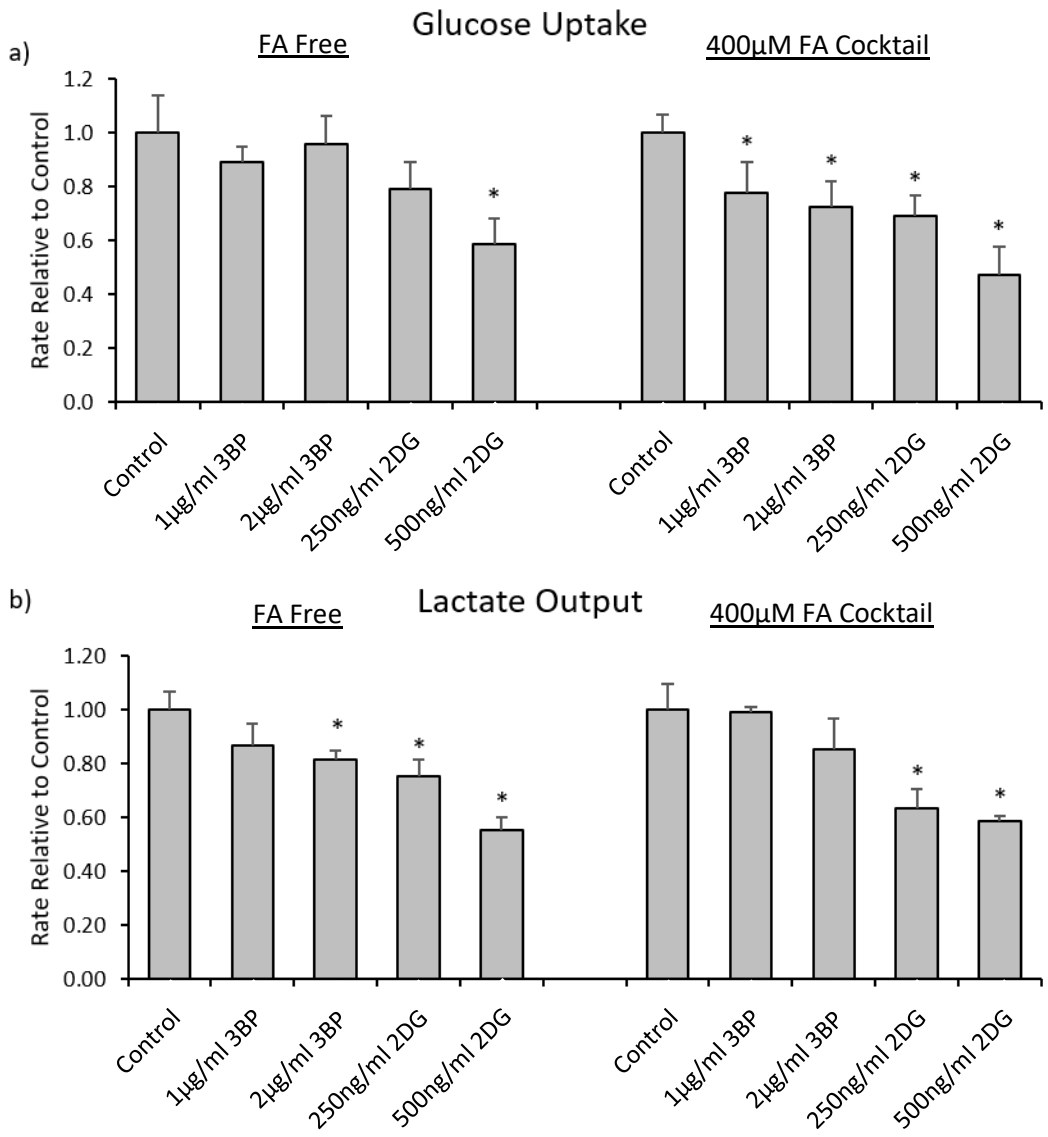

Figure 5.10: The effect of 2DG and 3BP on glucose uptake and lactate output. *The effects of 1µg/ml 3BP, 2µg/ml 3BP, 250ng/ml 2DG and 500ng/ml 2DG on (a) glucose uptake per cell and (b) lactate output per cell for HepG2 cells grown in FA free medium or medium containing 400µM FA cocktail (an equal molar mix of butyric, palmitic, lauric, oleic and linoleic acids). Cells were seeded at 26'000 per cm^2 in T25 culture flasks in untreated medium and allowed to attach for 24 hours. After the cells had attached, the untreated medium was aspirated and medium containing the stated treatment was added. The treated medium was replaced after 24 hours. After 48 hours of treatment, the supernatant medium was collected and analysed (section 5.2.10). n=4 for all measurements. A statistically significant effect of the treatments was first determined using an ANOVA before the statistical significance of the differences between each treated group and the control group were calculated using Holm-Sidak adjusted t-tests. * p<0.05 vs untreated for same FA concentration.*

5.4.2 Oxidative Stress

Next the effect of the various inhibitors on the redox balance and antioxidant reserves in the medium were measured as markers of oxidative stress (figure 5.11). The effects of TOFA on lipid peroxidation were also assessed (figure 5.11c).

2µg/ml TOFA treatment caused a significant decrease in redox potential for cells grown in medium containing 400µM FA cocktail (TOFA: 216±7mV (n=6) vs control 228±3mV (n=3); p=0.025), returning the marker of oxidative stress to nearer control levels (206±2mV (n=3)) (figure 5.11a). For all other FA cocktail concentrations, a non-significant decrease in redox potential was measured. Furthermore, other than in FA free medium, addition of 2µg/ml TOFA caused a non-significant increase in the antioxidant capacity compared with control suggesting that TOFA may also improving the cells' capacity to recover from oxidative injury (figure 5.11b). Treatment with TOFA also caused a significant decrease in lipid peroxidation for cells grown in FA free medium (0.21±0.07mOD.10^{-3}cells vs 0.41±0.07mOD.10^{-3} cells; n=6; p<0.01) and medium containing 800µM FA cocktail (0.3±0.2mOD.10^{-3} cells (n=3) vs 1.1±0.5mOD.10^{-3} cells (n=5); p=0.036) (figure 5.11c). Despite the lack of specificity in the TBARS assay, the large reduction in reading for cells grown in 800µM FA cocktail after treatment with 2µg/ml TOFA is strongly indicative of a reduction in intracellular lipid peroxidation. Together, these data show that TOFA treatment reduces FA induced oxidative stress in HepG2 cells.

Despite not improving cell viability or steatosis, treatment with 2µg/ml C75 caused a significant reduction in redox potential for cells grown in medium containing 400µM FA cocktail (215±2mV vs 228±3mV; n=3; p=0.016) (figure 5.11a) and non-significant reductions at all other FA cocktail concentrations. Therefore, the treatment reduced the mitochondrial stress resulting from FA treatment. No significant change in antioxidant capacity resulted from C75 treatment for any of the FA cocktail concentrations (figure 5.11b).

Treatment with 200ng/ml T863 caused a significant increase in redox potential for cells grown in FA free medium (220±5mV vs 206±2mV; n=3; p=0.006) (figure 5.11a). A non-significant increase in redox

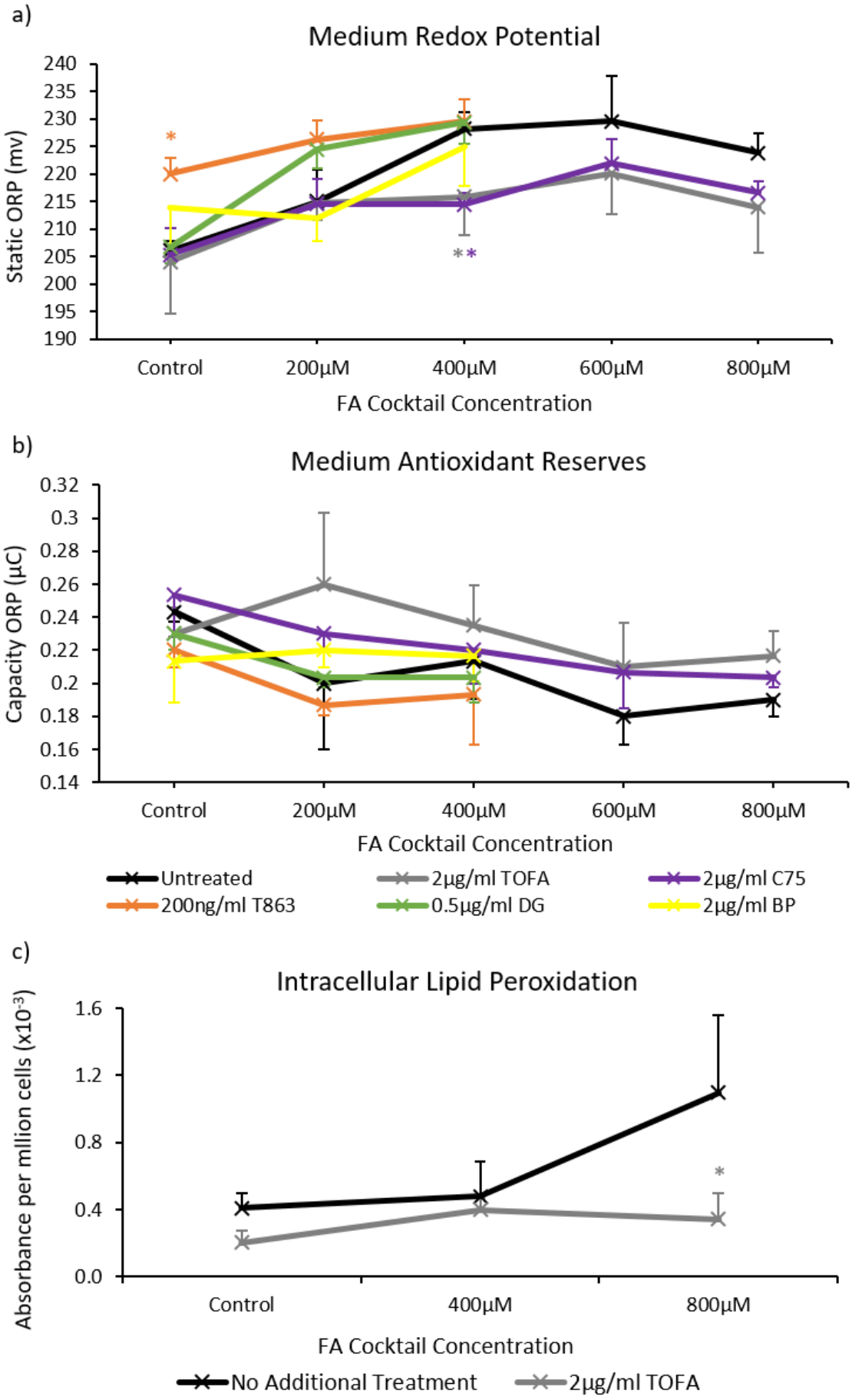
a)
Medium Redox Potential
Static ORP (mv)
240
235
230
225
220
215
210
205
200
195
190
Control
200µM
400µM
600µM
800µM
FA Cocktail Concentration
b)
Medium Antioxidant Reserves
Capacity ORP (µC)
0.32
0.3
0.28
0.26
0.24
0.22
0.2
0.18
0.16
0.14
Control
200µM
400µM
600µM
800µM
FA Cocktail Concentration
Untreated
2µg/ml TOFA
2µg/ml C75
200ng/ml T863
0.5µg/ml DG
2µg/ml BP
c)
Intracellular Lipid Peroxidation
Absorbance per million cells (x10-3)
1.6
1.2
0.8
0.4
0.0
Control
400µM
800µM
FA Cocktail Concentration
No Additional Treatment
2µg/ml TOFA

Figure 5.11: The effect of the various inhibitors on fatty acid induced oxidative stress. *The effect of 48 hour treatment with 2µg/ml TOFA, 2µg/ml C75, 200ng/ml T863, 0.5µg/ml 2DG and 2µg/ml 3BP on (a) the redox potential and (b) antioxidant reserves in the supernatant medium of cells treated with 0-800µM FA cocktail (an equal molar mix of butyric, palmitic, lauric, oleic and linoleic acids). (c) The effect of 48 hour treatment with 2µg/ml TOFA on lipid peroxidation as assessed by a TBARS assay on HepG2 cells grown in medium containing 0-800µM FA cocktail.Cells were seeded at 26'000 cells per cm^2 in T25 culture flasks in untreated medium and allowed to attach. After 24 hours, the untreated medium was aspirated and medium containing the stated treatment was added. The treated medium was replaced after 24 hours. The supernatant medium and cells were harvested after 48 hours of treatment. The tested supernatant medium had been in contact with the cells from the 24^{th} to the 48^{th} hour of treatment. The medium was measured for redox capacity and antioxidant reserves whilst the cells were homogenised and assessed for lipid peroxidation (section 5.2.9). 3 independent repeats were performed in each case other than the ORP measurements for control + TOFA and 400µM FA + TOFA where 6 repeats were performed. A statistically significant effect of the treatments was first determined using a two-way ANOVA before the statistical significance of the differences between each treated group and the control group were calculated using Holm-Sidak adjusted t-tests. * p<0.05 vs untreated for same FA concentration. Bars show mean ±SD.*

potential was measured after T863 treatment for 200µM FA cocktail (226±3mV vs 215±6mV; n=3; p=0.087) and no notable change after treatment with 400µM FA cocktail (230±14mV vs 228±3mV; n=3; p=0.65). Similarly, a significant decrease in antioxidant capacity was measured after T863 treatment for cells grown in FA free medium (0.22±0.01µC vs 0.24±0.01µC; n=3; p=0.047), but no significant change was measured in medium supplemented with 200µM and 400µM FA cocktail (figure 5.11b). Therefore, although no decrease in viability resulted from treatment with 200ng/ml T863 for cells grown FA free medium, it was associated with an increase in oxidative stress and a decrease in antioxidant reserves.

No significant change in redox potential or antioxidant capacity was measured for either 2DG or 3BP across the range of FA cocktail concentrations (figure 5.11). Therefore, although glycolysis inhibition resulted in reduced viability (figure 5.9), it was not shown to result in the release of additional ROS.

5.4.3 Mitochondrial Function

Figure 5.12 shows the effects of 2µg/ml TOFA on the activity of complexes I-IV, the activity of citrate synthase and the ATP concentration for cells grown in medium containing a range of FA cocktail concentrations. Additionally, the effect of 2µg/ml C75, 200ng/ml T863, 0.5µg/ml 2DG and 2µg/ml 3BP on ATP concentrations are shown (figure 5.12e). 2µg/ml TOFA treatment caused near-significant

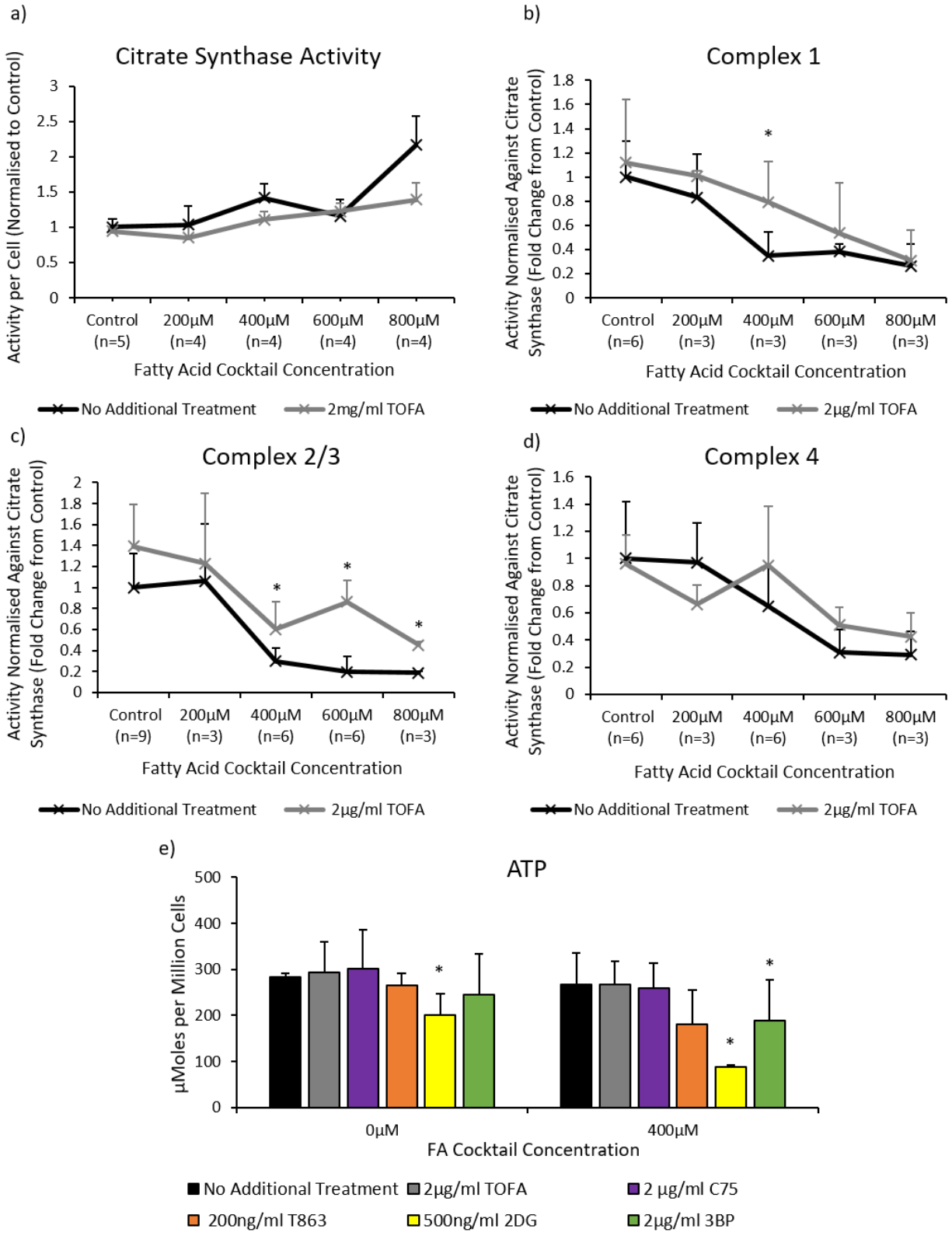
a)
Citrate Synthase Activity
Activity per Cell (Normalised to Control)
3
2.5
2
1.5
1
0.5
0
Control (n=5)
200µM (n=4)
400µM (n=4)
600µM (n=4)
800µM (n=4)
Fatty Acid Cocktail Concentration
No Additional Treatment
2mg/ml TOFA
b)
Complex 1
Activity Normalised Against Citrate Synthase (Fold Change from Control)
1.8
1.6
1.4
1.2
1
0.8
0.6
0.4
0.2
0
*
Control (n=6)
200µM (n=3)
400µM (n=3)
600µM (n=3)
800µM (n=3)
Fatty Acid Cocktail Concentration
No Additional Treatment
2µg/ml TOFA
c)
Complex 2/3
Activity Normalised Against Citrate Synthase (Fold Change from Control)
2
1.8
1.6
1.4
1.2
1
0.8
0.6
0.4
0.2
0
*
*
*
Control (n=9)
200µM (n=3)
400µM (n=6)
600µM (n=6)
800µM (n=3)
Fatty Acid Cocktail Concentration
No Additional Treatment
2µg/ml TOFA
d)
Complex 4
Activity Normalised Against Citrate Synthase (Fold Change from Control)
1.6
1.4
1.2
1
0.8
0.6
0.4
0.2
0
Control (n=6)
200µM (n=3)
400µM (n=6)
600µM (n=3)
800µM (n=3)
Fatty Acid Cocktail Concentration
No Additional Treatment
2µg/ml TOFA
e)
ATP
µMoles per Million Cells
500
400
300
200
100
0
*
*
*
0µM
400µM
FA Cocktail Concentration
No Additional Treatment
2µg/ml TOFA
2 µg/ml C75
200ng/ml T863
500ng/ml 2DG
2µg/ml 3BP

Figure 5.12: The effect of TOFA treatment on mitochondrial function. *The effects of treatment for 48 hours with 2µg/ml TOFA on (a) the activity of citrate synthase, (b) the activity of complex I, (c) the combined activities of complexes II and III and (d) the activity of complex IV and (e) the effects of treatment for 48 hours with 2µg/ml TOFA, 2µg/ml C75, 200ng/ml T863, 0.5µg/ml 2DG and 2µg/ml 3BP on the intracellular ATP concentration in HepG2 cultures treated with varying concentrations of FA cocktail (an equal molar mix of butyric, palmitic, lauric, oleic and linoleic acids). Cells were seeded at 26'000 cells per cm^2 in (a-d) T25 culture flasks and (e) 96 well plates in untreated medium and allowed to attach. After 24 hours, the untreated medium was aspirated and medium containing the stated treatment was added. The treated medium was replaced after 24 hours. The cells were harvested and measurements performed after 48 hours of treatment. The data in (a) and (e) was normalised to the number of cells whilst the data in (b-d) was normalised against citrate synthase to give activity per total mitochondria. For graphs (a-d) the data is based on the numbers of independent repeats stated in the axes and for (e) it is based on 3 repeats of 2-7 replicates. Cells were seeded at 26'000 cells per cm^2 in T25 culture flasks in untreated medium and allowed to attach. After 24 hours, the untreated medium was aspirated and medium containing the stated treatment was added. The treated medium was replaced after 24 hours. The supernatant medium and cells were harvested after 48 hours of treatment. The tested supernatant medium had been in contact with the cells from the 24^{th} to the 48^{th} hour of treatment. The medium was measured for redox capacity and antioxidant reserves whilst the cells were homogenised and assessed for lipid peroxidation (section 5.2.9). 3 independent repeats were performed in each case other than the ORP measurements for control + TOFA and 400µM FA + TOFA where 6 repeats were performed. A statistically significant effect of the treatments was first determined using a two-way ANOVA before the statistical significance of the differences between each treated group and the control group were calculated using Holm-Sidak adjusted T-Tests. * p<0.05 vs untreated for same FA concentration. The mean ±SD is presented.*

decreases in citrate synthase activity (a marker for total mitochondria) in cells grown in medium containing 400µM and 800µM FA cocktail (figure 5.12a). Furthermore, a significant reduction in the gradient between citrate synthase activity and FA cocktail treatment concentration was measured with TOFA treatment, demonstrating that the treatment lessened the FA induced increase in citrate synthase activity ($p<0.01$).

Treatment with 2µg/ml TOFA significantly restored complex II/III activity for cells grown in medium containing 400-800µM of FA cocktail (figure 5.12c) and significantly restored complex I activity for cells grown in medium containing 400µM FA cocktail (figure 5.12b). Non-significant increases in complex I activity were measured after TOFA treatment at all other FA cocktail concentrations. No significant changes in complex IV activity were seen with TOFA treatment across the range of FA cocktail concentrations (figure 5.12d). These data suggest that treatment with 2µg/ml TOFA has the potential to partially restore mitochondrial dysfunction in steatotic hepatocytes through both complex I and complexes II/III. Furthermore, no adverse changes to mitochondrial function occurred in non-steatotic cells grown in control medium after TOFA treatment.

Treatment with either 2µg/ml TOFA or 2µg/ml C75 did not significantly change intracellular ATP concentrations in either FA free or 400µM FA cocktail treated cells (figure 5.12e). Since ATP concentrations were not significantly reduced after treatment with 400µM FA cocktail (despite the reduction in ETC enzyme activities), no increase in concentration would be expected. However, these data show that ATP concentrations were not detrimentally affected by the treatments.

Treatment with T863, however, caused a significant decrease in intracellular ATP concentration for FA treated cells (400µM FA cocktail: treated - 142±106 (n=10) vs untreated - 242±80 (n=14); p=0.004) but no change for cells grown in FA free medium (figure 5.12e). This shows that, when excess FAs are present, inhibition of triglyceride synthesis disrupts energy metabolism in the cells.

Treatment with 2µg/ml 3BP also caused a significant reduction in intracellular ATP concentration for cells grown in medium containing 400µM FA cocktail (treated: 177±100 (n=10) vs untreated: 242±80 (n=14); p=0.024), but no significant change in concentration for cells grown in FA free medium (figure 5.12e). This suggests that the duel effects of the 10-25% decrease in glycolysis resulting from 3BP treatment (figure 5.10) combined with the decreased mitochondrial function resulting from 400µM FA cocktail treatment resulted in decreased cellular ATP concentrations.

Treatment with 500ng/ml 2DG resulted in a severely reduced ATP concentration in both control and 400µM FA cocktail treated cells (figure 5.12e). For 400µM FA cocktail, almost no ATP was present, showing that the majority of cells were no longer viable. Therefore, reducing glycolysis by 40-50% through treatment with 500ng/ml 2DG caused a decrease in cellular ATP concentration in HepG2 cells and, when combined with reduced mitochondrial function resulting from FA treatment, complete disruption of energy metabolism.

5.4.4 Glucose Consumption

Figure 5.13 shows the effect of TOFA and C75 on glucose consumption and insulin stimulation of glucose consumption for cells grown in a range of FA cocktail concentrations. Based on the simulated data in chapter 4, a decrease in glucose would be expected to result from both treatments due to

reduced use of glucose in lipogenesis and increased β-oxidation. However, if the treatments reduce steatosis or the toxic effects resulting from excess fat build-up, an improvement in insulin stimulation of fatty acid uptake might be expected in fatty acid treated cells.

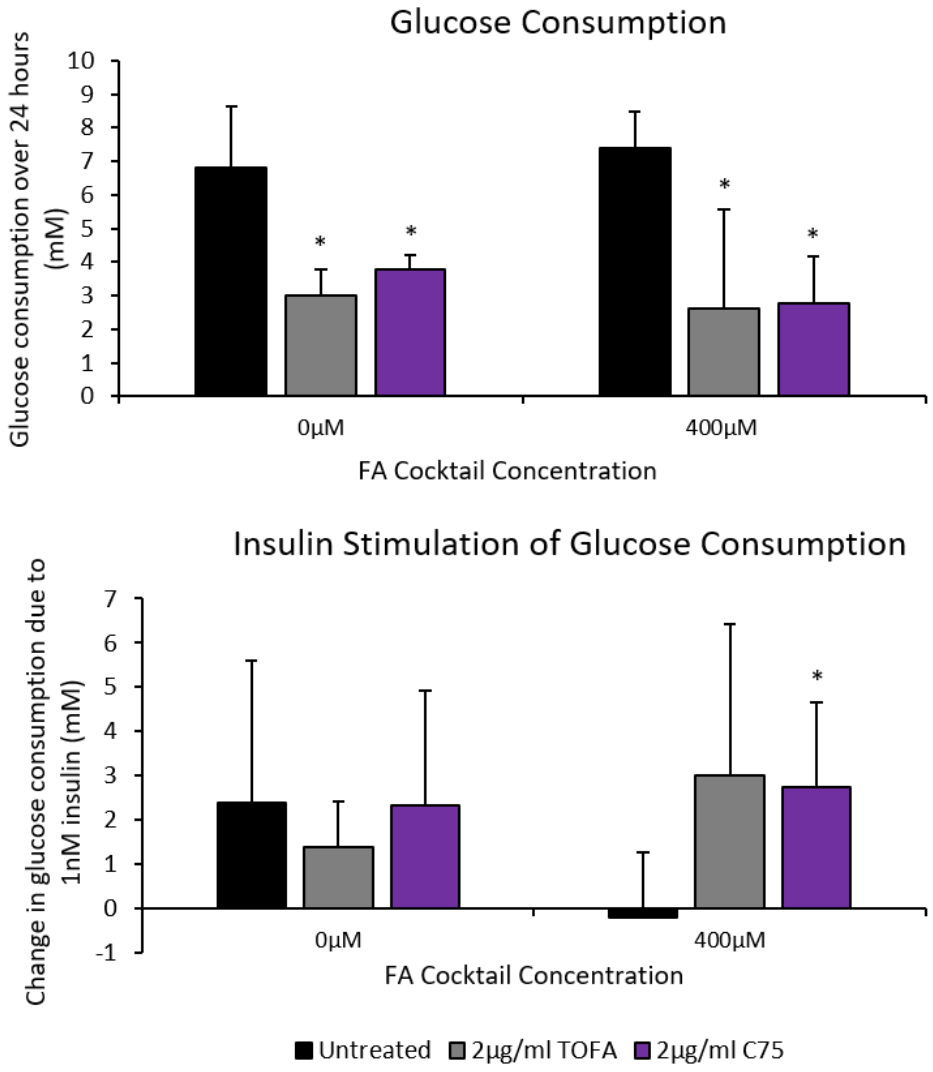

Figure 5.13: The effects of with TOFA and C75 on the rate of glucose consumption*. (a) The change in supernatant medium glucose concentration (as a measurement of the rate of glucose consumption) when treated with varying FA cocktail concentrations along with the addition of either C75 or TOFA in hyperglycaemic medium (15mM). (b) The change in glucose consumption as a result of the addition of 1nM insulin in cells treated with varying FA cocktail concentrations along with the addition of either C75 or TOFA in hyperglycaemic medium (15mM).* Cells were seeded at 26'000 per cm^2 in 48 well plates *in untreated medium containing 15mM glucose and allowed to attach. After 24 hours, the untreated medium was aspirated and medium containing the stated treatment was added. The treated medium was replaced after 24 hours. The supernatant medium was collected and analysed* after 48 hours of treatment as described in section 5.2.10. In each case, the data is based on 3 repeats of 2-7 replicate measurements. *A two-way ANOVA was used to determine significant variation between the FFA and treatment groups sets before Holm-Sidak adjusted t-tests were used to calculate significance of the difference between each treated and control group. * p<0.05 vs untreated for same FA concentration. The mean ±SD is presented.*

Consistent with the model predictions both TOFA and C75 caused significant decreases in glucose consumption in cells cultured in both FA free medium and medium containing 400µM FA cocktail (figure 5.13a). However, insulin sensitivity in the consumption of glucose was significantly improved when cells grown in medium containing 400µM FA cocktail were treated with 2µg/ml C75 (27.3±19.3µMoles Vs -2.1±14.9µMoles; n≥4; p=0.032) (figure 5.13b). TOFA treatment of cells grown in medium supplemented with 400µM FA also appeared to cause an increase in the additional glucose caused by the addition of 1nM insulin but this failed to reach significance (TOFA: 30±34µMoles (n=5) vs control: -2±15 µMoles (n=5); p=0.090).

5.5 Discussion

5.5.1 Fatty acid treated HepG2 cells show steatosis, reduced mitochondrial function, oxidative stress and insulin resistance consistent with *in vivo* NAFLD

In the first section of this chapter HepG2 cells, a cell culture line derived from a well-differentiated hepatoma, were treated with varying concentrations of a FA cocktail (an equal molar mix of palmitic, lauric, oleic, linoleic and butyric acids) in order to provide a cell culture model of steatotic hepatocytes in NAFLD. The effects of the FAs on viability, steatosis, mitochondrial function, oxidative stress and metabolism in these cells were analysed to assess their utility as a model of *in vivo* NAFLD.

Firstly, a cell culture model of hepatocytes in NAFLD should develop steatosis and cell damage dependent on the medium FA concentrations. Even when grown in control medium (FA free, 5mM glucose), HepG2 cells show a high lipid content. This has previously been shown to result from reduced output of fats in lipoproteins rather than excess *de novo* lipogenesis [554]. In addition to a higher baseline lipid content, the cells showed higher susceptibility to FA treatment than would be expected for *in vivo* hepatocytes. When treated with 400µM of the FA cocktail, which represents a normal pre-prandial plasma FFA concentration, a notable increase in steatosis occurred accompanied by increased cell death. When treated with 800µM of the FA cocktail, towards the high end of plasma FFA concentrations seen in NAFLD patients [139, 435, 466], severe steatosis and cell death occurred.

Therefore, HepG2 cells are damaged by increased medium FA concentrations and have an intracellular lipid content dependent on the medium concentration, consistent with *in vivo* cells. However, they show a lower tolerance to raised FFA concentrations and a higher baseline lipid content compared with *in vivo* hepatocytes.

When the cells were treated with each FA individually, the saturated long chain FA palmitic acid and saturated medium chain FA lauric acid had the largest effect on cell viability and cellular steatosis. 200µM of long chain, monounsaturated FA oleic acid and long chain, polyunsaturated FA linoleic acid caused no change in viability or lipid content of cells, whilst 200µM saturated, short chain FA butyric acid only caused a small decrease in viability. These results are consistent with the data published by Garcia-Ruiz *et al.* which showed a number of adverse effects including mitochondrial dysfunction and increased ROS when HepG2 cells were treated with 200µM of saturated palmitic and stearic FAs, but not when treated with 200µM of unsaturated oleic acid [557].

When assayed using a diastase corrected PAS-Schiff stain, the cells showed almost no glycogen content, even in FA free medium containing insulin. This observation has been made previously in the literature [553]. Therefore, it is not possible to study the effects of FAs or other treatments on glycogen storage using these cells. However, insulin stimulation of both glucose consumption was seen in cells grown in FA free medium but not in medium treated with 400µM FA cocktail. Palmitate has previously been shown to cause IR in HepG2 cells [606-608].

Hepatocytes in NAFLD *in vivo* are known to show reduced mitochondrial function and reduced ATP production [547, 548, 591, 592] and it has been suggested that this disruption to energy metabolism may account for the progression from NAFLD to NASH [229, 230]. When treated with the FA cocktail, the HepG2 cells showed reduced activity of complex I, complexes II and III combined and complex IV. As with the development of steatosis in HepG2 cells, this occurred at lower medium FA concentrations (400-800µM) than would be expected *in vivo*. For 400µM and 600µM concentrations of the FA cocktail, the reductions in ETC enzyme activities were not accompanied by a reduction in ATP concentration,

suggesting that the cells either contain excess ETC capacity or were able to compensate for reduced oxidative phosphorylation. Increased total mitochondria was measured in FA treated cells and is seen under conditions of excess fat availability *in vivo* [590], which may partially compensate for reduced mitochondrial function. However, when the cells were treated 800µM FA cocktail, a reduction in ATP concentration was measured, consistent with the severe increase in cell death measured for this concentration.

The results are consistent with the data published by Garcia-Ruiz *et al.* showing reduced activities of complexes I-IV and of ATP synthase along with reduced ATP concentrations in HepG2 cells treated with 200µM palmitic acid or stearic acid [557]. In the study by Garcia-Ruiz *et al.*, no change in ETC activity was seen after treatment with 200µM oleic acid, suggesting that the saturated FAs in the cocktail, particularly palmitic acid, are likely to drive the decrease in ETC activity.

In addition to a loss of mitochondrial function, NAFLD patients show increased hepatic oxidative stress. In the cell culture model, oxidative stress was assessed through two indirect methods. Firstly, the redox potential of the culture medium was measured to detect extracellular ROS. Secondly, a TBARS test for lipid peroxidation was performed on cell homogenates. In FA treated cells, increases in both the redox potential and in lipid peroxidation products were measured. Consistent with this, Garcia-Ruiz *et al.* showed that treatment with 200µM of the saturated FAs palmitic acid and stearic acid, but not with 200µM of the unsaturated FA oleic acid, resulted in an increase in lipid peroxidation [557]. This is consistent with the reduced cell viability seen when treating with palmitic acid (and the other saturated FAs lauric and butyric acids) but not when treating with equivalent concentrations of the unsaturated oleic and linoleic acids. Additionally, Soardo *et al.* showed increases in several mediators of oxidative stress including glutathione, malondialdehyde and nitric oxide when treating HepG2 cells with a cocktail of FAs [609]. In NAFLD patients, oxidative stress and lipid peroxidation have been also shown to occur [225, 382, 547, 591, 593], particularly in pericentral cells. Combined, these data show

that increased oxidative stress accompanies the reduction in mitochondrial function measured in FA treated HepG2 cells.

The cells can therefore be used to test the ability of potential treatments to resolve FA induced cell death, steatosis, oxidative stress, loss of mitochondrial function, ATP depletion and loss of insulin sensitivity in glycolysis. These results can be compared to the model simulations.

However, HepG2 cells show several differences to *in vivo* hepatocytes, as would be expected for an immortalized line derived from a liver cancer. Firstly, they are constantly proliferating with a doubling time of 2 days. Additionally, cancer cells are heavily reliant on glycolysis for ATP synthesis. Given that two of the treatments studied were direct glycolysis inhibitors and two inhibit lipogenesis causing allosteric inhibition of glycolysis, the background of HepG2 cells as cancer cells must be remembered whilst interpreting the results. However, the majority of adverse effects in NAFLD occur in pericentral cells (both in the model simulations and experimentally [15-17, 377]), which are reliant on glycolysis due to their low oxygen environment. The HepG2 model can therefore be considered to most closely resemble these cells.

5.5.2 Validation of the model predictions for targeting specific processes in pericentral cells.

In the chapter 4, the computational model was used to simulate the effects of targeting several different processes on cells across the sinusoid for individuals with NAFLD resulting from high intake and IR. In this chapter, HepG2 cells grown in medium containing FAs were treated with small molecule inhibitors to provide validation of the model's predictions. In particular, due to the reliance of HepG2 cells on glycolysis for energy production, the measurements from the cell culture model are most comparable to the predictions for hypoxic pericentral cells [553]. Five inhibitors were used, which are known to act on specific enzymes. The corresponding targeted processes within the model for each treatment are shown in figure 5.1. The simulated treatments are shown in figure 4.2.

Glycolysis

When partial inhibition of glycolysis was simulated in the model, severely reduced pericentral ATP concentrations were predicted without any notable decrease in steatosis for insulin resistant individuals. This was seen when glycolysis was inhibited at either the conversion of glucose to G6P, the conversion of G6P to GADP or the conversion of GADP to pyruvate. Additionally, when inhibition of glycolysis was simulated at the stage of GK, glycogen synthesis was reduced in the cells leading to plasma hyperglycaemia. Based on these simulations, reduced cellular viability resulting from defective energy metabolism would be expected when inhibiting any of the enzymes in the glycolysis pathway in cell culture.

When studied in HepG2 cells, partial inhibition of glycolysis through either inhibiting GK using 2DG or inhibiting the conversion of GADP to pyruvate using 3BP caused reduced ATP concentrations and FA induced cell death without any notable change in steatosis consistent with the model predictions. Due to the lack of glycogen synthesis in untreated HepG2 cells, the effects of the treatment on glycogen synthesis could not be studied. However, both the model predictions and cell culture experiments show that partial inhibition of glycolysis disrupts energy metabolism without notably improving steatosis. It remains unknown whether glycolysis inhibition causes increased apoptosis in cancer cells specifically due to the blocking of ATP production through glycolysis alone, or whether additional factors contribute [610]. Given that mitochondrial dysfunction was shown to result from FA treatment, it is possible that a duel hit of reduced mitochondrial function and reduced ATP production from glycolysis caused the increase in cell death.

Triglyceride Synthesis

When inhibition of triglyceride synthesis was simulated in the model in chapter 4, steatosis was cleared effectively by the treatment. However, vast increases in hepatic FFA concentration were predicted to occur. FFAs and closely related molecules including DAGs and ceramides are particularly

potent in promoting mitochondrial stress and IR [8, 146, 247, 248]. Based on these simulations, increased mitochondrial stress and FFA induced cell damage would be expected despite the clearance of steatosis when inhibiting triglyceride synthesis in cell culture.

Experimentally, partial inhibition of triglyceride synthesis with the DGAT1 inhibitor T863 significantly reduced the cellular lipid content of the HepG2 cells consistent with model predictions. However, despite reducing steatosis, the treatment exacerbated FA-induced cell death. In control cells viability was unchanged, but after the addition of FAs, treatment with T863 caused reduced viability. Additionally, T863 treatment caused a reduction in ATP concentrations in FA treated but not control cells. This suggests that, when grown in in FA free medium, insufficient FAs are produced for the inhibition of triglyceride synthesis to damage the cells. However, when excess FFAs are present, inhibition of triglyceride synthesis forces lipids to remain in forms which are more potent than triglycerides in causing mitochondrial dysfunction. Previously published i*n vivo* studies have linked inhibition of DGAT2, which performs the same function as DGAT1, with increased liver damage in mice despite a reduction in steatosis [254].

The cell culture data are therefore consistent with the model predictions, although only a vast increase in triglyceride synthesis precursors is predicted by the model and the mechanisms responsible for the effects of FA on mitochondrial function are not included.

Lipogenesis

In model simulations, inhibition of lipogenesis reduced the hepatic lipid content in insulin sensitive individuals, but had little effect when simulating insulin resistant NAFLD where most FFAs are derived from plasma. However, the simulated hepatic FFA concentration and rate of FA oxidation were decreased when lipogenesis was inhibited, and simulated ATP concentrations increased to nearer metabolically normal levels. Therefore, based on the model simulations, improvements in mitochondrial function, oxidative stress and insulin sensitivity would be expected to occur in the cell

culture model despite little improvement in steatosis. Increased plasma glucose concentrations arose in simulations as a result of the inhibition of lipogenesis when simulating insulin resistant individuals. However, this excess was stored as glycogen when simulating insulin sensitive individuals.

Total inhibition of lipogenesis could not be tested experimentally due to the known toxic effect of lipogenesis inhibition of cancer derived cells. Instead, lipogenesis inhibitor C75 was added at a lower concentration such that lipogenesis was only partially inhibited and cell viability was unaffected in FA-free medium.

Partial inhibition of lipogenesis had no effect on the cellular lipid content of cells grown in medium containing FA cocktail. This consistent with the model predictions when simulating insulin resistant NAFLD in which most FFAs are derived from plasma. Additionally, C75 treatment had no effect on FA-induced cell death. However, a fall in the redox potential was measured in the supernatant medium of cells treated with C75 suggesting a reduction in mitochondrial stress. Additionally, a significant increase in insulin stimulation of glucose consumption was measured when cells grown in medium containing the FA cocktail were treated with C75, showing re-sensitisation to insulin. These results are consistent with the predicted reduction in hepatic FFA concentration when inhibition of lipogenesis was simulated in the model.

Lipogenesis and β-oxidation

When inhibition of lipogenesis in addition to stimulation of β-oxidation was simulated in the model, steatosis was resolved and ATP concentrations increased to nearer metabolically normal levels. Furthermore, decreases in intracellular FFA concentrations and the rate of FA oxidation were predicted, both of which are thought to be causes of disrupted mitochondrial function and mitochondrial stress. As an adverse effect, when simulating inhibition of lipogenesis in addition to stimulation of β-oxidation in insulin resistant individuals an increased plasma glucose concentration

occurred. However, when simulating insulin sensitive individuals, increased glycogen synthesis occurred instead.

Stimulation of β-oxidation in combination with inhibition of lipogenesis was tested experimentally through the inhibition of ACC1 and ACC2 using TOFA. As with C75, only partial inhibition by TOFA could be tested due to the known toxic effect of lipogenesis inhibition on HepG2 cells. Treatment with TOFA caused a notable decrease in cellular lipid levels across the range of treatments consistent with the model predictions. Furthermore, this was accompanied by an improvement in viability and mitochondrial function and a reduction in oxidative stress.

In the model predictions, a reduction in glycolysis was predicted resulting in either increased glycogenesis in insulin sensitive individuals or hyperglycaemia in insulin resistant individuals. It is therefore important that any treatment rapidly restores insulin sensitivity whilst clearing steatosis in insulin resistant NAFLD individuals. Since HepG2 cells do not synthesize glycogen even when grown in FA free medium containing insulin, the effects of TOFA treatment on glycogen storage could not be tested experimentally. However, a reduction in glucose consumption was measured consistent with model predictions. Furthermore, an increase in the insulin stimulation of glycolysis approached but failed to reach significant in FA-treated cells when treated with TOFA, suggesting that improved insulin sensitivity may occur.

It should be noted that, in the literature, TOFA has been extensively shown to cause cell death in cancer cell derived lines such as HepG2 [579, 611-613]. This is consistent with the results in supplementary material S2 showing that, for higher TOFA concentrations (10-20μg/ml or greater), reduced cell viability was measured. In human lung and prostate cancer cells, TOFA has been shown to cause a reduction in the number of viable cells even at 1μg/ml [614]. However, the results presented in this report show that, at a concentration below its toxicity threshold, TOFA reduces the cell death and oxidative stress caused by FA treatment. Interestingly, a previous study has shown that addition of palmitate reduces the cell death caused by higher TOFA concentrations in HepG2 cells

[614]. In another study, treatment with TOFA, in contrast to C75 and [6]-gingerol (an additional lipogenesis inhibitor), was shown to inhibit lipogenesis without promoting apoptosis in HepG2 cells [615]. TOFA treatment was additionally shown to reduce the apoptosis after treatment with [6]-gingerol [615]. In non-cancer cells, which are less reliant on glycolysis and lipogenesis, ACC inhibition would be expected to be less damaging to hepatocytes than in cancer cells.

5.6 Conclusions of Chapter

The *in vitro* data in this chapter demonstrates reduced steatosis, improved mitochondrial function and reduced oxidative stress when both stimulating β-oxidation and inhibiting lipogenesis with TOFA. The data also suggest that inhibition of lipogenesis alone may reduce the oxidative stress and IR caused by steatosis without clearing the underlying steatosis. Finally, the experimental data provides validation of the adverse effects predicted when inhibiting triglyceride synthesis or glycolysis as potential treatments for steatosis. These findings are consistent with the model simulations when inhibiting these processes in chapter 4.

6 Conclusions and Future Work

6.1 A Computational Model of Hepatic Metabolism across the Liver Sinusoid

The first objective of this study was to build a computational model of hepatic glucose and lipid metabolisms capable of representing differences in metabolism across the sinusoid. A model containing the major pathways in glucose regulation, lipid storage and ATP synthesis was developed with hepatocytes split into compartments across the sinusoid and with zonation of key enzymes included based on previously published periportal to pericentral ratios.

The model gives realistic values for average plasma and hepatic concentrations and for changes in concentrations of key molecules under known feeding concentrations when compared with

experimental data. It also produces realistic average hepatic rates of processes and relative rates in different regions of the sinusoid. The simulated data was consistent with *in vivo* measurements for both healthy and insulin resistant individuals.

A model of glucose and lipid metabolisms which includes zonation across the sinusoid was previously lacking from the literature and the model presented here may be applicable to study the development and treatment of a range of metabolic liver diseases in addition to NAFLD. Furthermore, since zonated damage is seen in almost all liver diseases and mitochondrial metabolism is involved in the progression of a wide range of these, the model may be useful for studying zonated effects in other conditions. For example, the mechanisms by which alcohol poisoning damages the liver are closely related to those occurring in NAFLD and with some modification, the model could be adapted to study zonation in the damage resulting from metabolism of ethanol. This would require inclusion of the pathways converting ethanol to acetyl-CoA (three enzymes) along with a full representation of NAD/NADH (where they are only represented through their effects on ATP levels in the current model) due to the known importance of the NAD/NADH ratio in causing steatosis after excess ethanol consumption.

6.2 The Development of Zonated Steatosis

The second objective of the project was to study in detail the build-up of fats in different regions of the sinusoid when simulating conditions leading to NAFLD in the model. The tendency for pericentral cells to show more severe steatosis and damage is widely referred to in the literature, but not fully understood due to the experimental difficulty of taking measurements in each region of the sinusoid and the large number of potential variables. Combining existing knowledge of metabolism and zonation into a model, and simulating conditions leading steatosis allowed detailed study of the changes occurring across the sinusoid in the model.

By studying the resulting simulated metabolic flux and metabolite concentration changes, it was demonstrated that, whilst pericentral steatosis arose because of high fat intake and the direct effects or IR alone, increased SREBP-1c expression seen *in vivo* was additionally required to fully replicate the

metabolic changes seen in NAFLD patients. When high fat intake, IR and increased SREBP-1c expression were simulated, pericentral centred triglyceride synthesis arose due to an increased pericentral concentrations of both substrates for triglycerides synthesis, G3P and FFAs. Disrupted glycogen synthesis caused a build-up of glucose intermediates including G3P. Due to the periportal zonation of glycogen synthase and phosphorylation, the loss of glycogenesis was most severe in pericentral cells. Additionally, pericentral cells undergo glucose oxidation at a slower rate, causing reduced clearance of excess glucose metabolism intermediates in these cells.

Changes in FA uptake, β-oxidation and lipogenesis all contribute to an increase in pericentral FFA availability for triglyceride synthesis. Most additional FFAs arose from uptake. Although fatty acid scavenging enzymes are known to show periportal zonation, the switch from insulin stimulated active fatty acid uptake when simulating insulin sensitive individual with low plasma fatty acid concentrations (metabolically normal) to passive facilitated diffusion in an insulin resistant individual with a high plasma fatty acid concentration (NAFLD) partially reduced the effects of the zonated expression. The switch from glucose oxidation to additional fatty acid oxidation, which occurs both in the model and experimentally, cleared a large percentage of the additional fatty acids in periportal cells, which have a high oxidative capacity, but not in pericentral cells which inhabit a hypoxic environment. Finally, increased SREBP-1c expression caused increased lipogenesis which occurs predominantly in pericentral cells due to the pericentral zonation of lipogenesis enzymes.

These changes in metabolic rates in the model will allow targeted future *in vivo* validation, reducing the number of experimentally challenging measurements in individual regions of the sinusoid required to understand zonated damage in NAFLD. As discussed in chapter 3, experimental validation of these simulated data could be performed through the addition of radiolabelled substrates to measure the rates of conversion within individual regions of the sinusoid or through assessing the change in overall metabolism after ablation of particular cell types [518].

6.3 Predicting Inter-Individual Susceptibility to Steatosis

The third objective was to assess the hepatic metabolic variations which had the largest effects on susceptibility to developing steatosis and on the pattern of steatosis development. Experimentally, this would require comparison of enzyme activity and distribution with liver fat content and distribution for many different enzymes involved in various processes for a large number of individuals, whilst accounting for potential confounding factors. In the model, by simulating small variations in the rate constants of each process in the model, we can establish the effects of realistic variations in activity on metabolism.

Two methods of analysis were used. Firstly, sensitivity analysis was used to assess the impact of altering the rate and zonation constants for each process in isolation. Secondly, patients with rate constants randomly generated within realistic bounds were simulated to investigate the effects of variations in each rate constant within the context of overall inter-individual variability.

In both data sets, the hepatic lipid content was most sensitive to inter-individual variations in the capacity for FFA oxidation, either through differences in the overall capacity oxidation of acetyl-CoA or through differences in the FFA oxidation to glucose oxidation ratio. Due to the increasing prevalence of NAFLD and the related conditions, research improving our ability predict an individual's risk of developing the disease at an early stage is vital. As discussed in chapter 3, some evidence exists in the literature to support the prediction that mitochondrial capacity is an important determinant of liver fat *in vivo*. The predominant location of steatosis across the sinusoid, meanwhile, was most sensitive to changes in the zonation of proteins mediating FFA uptake or VLDL synthesis and release in the model, although it also showed moderate sensitivity to the zonation of enzymes mediating FA oxidation. This simulated data will allow for targeted future experimental validation, in which a smaller number of measurements would be required by focussing on the processes predicted to be most important.

6.4 ACC Inhibition as a Potential Drug Target and Future *Work*

The final objectives of the project were to use the model to assess the impact of targeting various hepatic processes on lipid content and energy metabolism across the sinusoid before, where possible, validating these predictions in a cell culture model. Simulations were run for steatosis arising from high fat intake alone, developing IR in addition to high fat intake and severe IR in addition to increased SREBP-1c expression to assess the impact of potential drug targets across a range of patients. Experimental validation was performed in HepG2 cells, ensuring to consider their cancer cell background when interpreting results.

The model simulations suggest that stimulation in β-oxidation in combination with inhibition of lipogenesis provides an effective method of clearing steatosis without causing disruptions to energy metabolism. In the model, hepatic steatosis was reduced, hepatic FFA concentrations (which, along with closely related DAGs and ceramides, are particularly potent in promoting oxidative stress and IR [8, 146, 247, 248]) were reduced and ATP concentrations were increased. Furthermore, the cells become less reliant on overactive oxidative phosphorylation. Numerous zone-specific effects were noted when simulating various treatments highlighting the importance of studying the sinusoid, rather than treating the liver as a homogenous mass of cells.

The effects of inhibition of lipogenesis in combination with stimulation of β-oxidation were validated in HepG2 cells experimentally by inhibiting ACC1 and ACC2 using TOFA. A cell culture system does not allow validation of predicted zone specific effects, which is left for future rodent experiments. However, HepG2 metabolism most closely resemble that of pericentral hepatocytes, in which most adverse effects were centred. When treated with TOFA, both steatosis and FFA-induced cell death were reduced consistent with the model simulations. Mitochondrial function was improved by the treatment as evidenced by restoration of ETC enzyme activity. Oxidative stress, indirectly measured by both the medium oxidation-reduction potential and a TBARS assay for lipid peroxidation, was reduced. An increase in medium (corresponding to plasma) glucose concentration was measured,

consistent with the model simulations for the treatment in insulin resistant individuals. However, if insulin signalling were sufficiently restored in *in vivo* hepatocytes which, unlike HepG2 cells, are capable of glycogenesis, increased glycogen concentrations would be expected rather than hyperglycaemia.

Future work should further validate these results in an *in vivo* model. Firstly, an appropriate *in vivo* model (e.g. rodent) which develops steatosis and the resulting IR, mitochondrial stress and fibrosis across the sinusoid in a reasonable time frame should be identified and characterised. This should then be used to study the effects of either genetically or pharmacologically inhibiting ACC when considering all sets of hepatocytes across the sinusoid. It is vital to account for differences between rapidly developing NAFLD in a rodent model and the development of the disease over decades in humans when interpreting results from these *in vivo* experiments.

There is additionally scope for expanding the model in future work to increase its scope. At present, the model has been shown to provide realistic predictions for the effects of suppressing or stimulating overall hepatic processes across the sinusoid without considering the drug used to achieve this effect. Whilst this is an important step in attempting to predict drug behaviour, a more detailed model may further aid drug development. Firstly, by including each individual enzyme within the pathways currently represented by the overall processes, the model may be able to highlight the most pertinent individual enzymes to target. The model could also be expanded to include the action, metabolism and degradation of drugs known to target each enzyme to provide predictions for optimal dosing. Furthermore, the representation outside of metabolism could be expanded to investigate the effects of targeting processes outside of liver and to further study the interactions between targeting of hepatic processes and peripheral organs.

The model could be additionally expanded to include the pathways leading to oxidative stress as a result of increased FFA concentrations and β-oxidation. At present increased FFA concentrations, increased β-oxidation and reduced ATP concentrations are used as markers to predict oxidative stress.

Including the subsequent pathways would further elucidate the mechanisms leading to oxidative stress and improve comparison between simulated and experimentally measured data. Furthermore, there is evidence that different fatty acids are more or less potent in causing oxidative stress than others and some of the major genetic variations known to be associated with susceptibility to NAFLD such as PNPLA3 are thought to affect the fatty acid profile within cells [194]. Therefore, the model could be expanded to allow prediction of the concentrations of individual FAs and triglycerides within the cells. The limiting factor within this would be the availability of data for the various enzyme kinetics when using each fatty acid as a substrate and for any possible interactions between the different fatty acids with the enzymes along with a vast increase in the number of fitted parameters. However, as the system becomes better characterised experimentally, the expansion of the model to include the individual FAs would allow for prediction of the heterogeneous effects resulting from fats of different chain lengths and saturations.

S1 Supplementary Material 1: Comparisons of Model Simulations with Experimental Data

In the following sections, data produced by the model are compared with several sources of experimental data. This validation focusses on model predictions for hepatic and plasma concentrations and hepatic metabolic rates when simulating metabolically normal and insulin resistant individuals. Additional comparison the simulated data with experimental data related to the development of NAFLD is performed in chapter 3 when establishing a representation of the disease in the model.

In section S1.1, the model simulations are compared with experimental data for metabolically normal individuals. Firstly, the average concentrations of the various hepatic molecules over a moderate dietary intake cycle are compared with experimental data from a range of sources (section S1.1.1). Next, the change in hepatic glycogen concentration, along with plasma glucose and FFA concentrations after a mixed meal is compared with data published by Taylor *et al.* [428] (section S1.1.2). In section S1.1.3, the rate at which various metabolic processes occur under conditions leading to hepatic glucose production and to hepatic glucose clearance are compared with experimental data from Ainscow and Brand [444], Edgerton et al. [443] and Mandarino et al. [431]. In section S1.1.4, the effects of a daily intake/use cycle on plasma concentrations of glucose, lactate, FFAs, triglycerides and insulin are compared with experimental data from Daly *et al*. In section S1.1.5, the heterogeneity in the rates of various processes across the sinusoid in the model are compared with experimental data from a range of sources. Very little data regarding the concentrations of molecules in different regions of the sinusoid have been published. Instead the variation in rates of different glucose and lipid metabolism processes are compared with experimental data.

In section S1.2, the effects of IR on plasma variables are validated against experimental data from a range of sources. Firstly, the average concentrations of various plasma molecules are compared with experimental data for insulin resistant and metabolically normal individuals (section S1.2.1). Secondly,

the changes in glucose and lactate concentrations after intake of a glucose load in insulin resistant and metabolically normal individuals are compared with experimental data (section S1.2.2). The relative contributions of various sources of fatty acids to hepatic steatosis are compared with experimental data for NAFLD patients in section S1.2.3.

Finally, in section S1.3, the simulated post-prandial changes in the relative rates of glucose oxidation and β-oxidation are compared with experimental data from Daly *et al.* [452] and Seal *et al*. [453] when simulating metabolically normal and insulin resistant individuals.

S1.1 Validation of Liver Metabolism in Healthy Patients

S1.1.1 Concentrations of intermediates and of the energy molecule

In table S1.1, the average concentrations of the various hepatic metabolism intermediates and the mono-, di-, and tri-phosphate molecules (when simulating the 4-hour moderate intake cycle discussed in section 2.2.4.2) are compared with experimentally measured values. It is important that, when simulating normal physiological conditions, the simulated concentrations remain in a realistic range. The values are the average over the 4-hour cycle. For hepatic molecules, the average concentration across the hepatic compartments is shown. For plasma molecules, the concentration in the body compartment is shown.

The simulated average values for hepatic glucose and triglycerides along with glucose metabolism intermediates G6P, G3P and acetyl-CoA are within the experimentally measured ranges. Similarly, the simulated average concentrations for inorganic phosphate, ATP, ADP, AMP, GTP and GDP are all within the experimentally measured confidence intervals. This shows that, when an input approximating a daily meal cycle is provided, the model gives realistic values for the average values of key intermediates of glucose and lipid metabolism in hepatocytes, along with the adenosine and guanine phosphate molecules.

Table S1.1: The concentration of various hepatic metabolism intermediates and of the mono-, di-, and tri-phosphate molecules included in the model when simulating a mixed meal.

Protein	Average Value (Low-high over intake cycle) – Model (mM)	Average Value (Confidence Interval) – Experimental (mM)
Inorganic Phosphate	3.96 (3.871-4.011)	4.07 (3.55-4.07) [429]
ATP	2.82 (2.64-2.96)	2.78 (2.71-2.85) [429]
ADP	0.832 (0.765-0.926)	0.885 (0.794-0.976) [486]
AMP	0.269 (0.223-0.337)	0.237 (0.200-0.272) [429]
UTP	0.324 (0.205-0.365)	0.285 (.255-.315) [486]
UDP	0.069 (0.031-0.188)	0.108 (0.096-0.120) [486]
GTP	0.274 (0.271-0.275)	0.277 (0.266-0.288) [486]
GDP	0.101 (.100-.104)	0.098 (0.091-0.105) [427, 486]
Hepatic Glucose	8.24 (7.28-10.0)	9.86-10.20 [426, 427],[616]
G6P	0.085 (0.031-0.126)	0.071 ± 0.004mM – starved rats, 0.133 ± 0.010mM – well fed rats [429]
GADP	0.236 (0.195-0.312)	0.2-1.0 [426]
Acetyl-CoA	0.046 (0.035-0.058)	0.039 [426]
Glycogen	~200mM of glucose (0 – 500mM of glucose depending on previous feeding conditions)	Since glycogen is used for glucose storage, the liver glycogen concentration is strongly dependent on previous feeding conditions. See section S1.1.2 for comparison with Taylor *et al.* [428].
Hepatic Triglyceride	Average: 38.1mM (37.6-38.4mM) ➔ 2.31% (2.28-2.33%) Periportal: 33.6mM (33.1-34.0mM) ➔ 2.05% (2.01-2.07%) Pericentral: 45.5mM (45.0-45.7mM) ➔ 2.75% (2.72-2.76%)	Model values are slightly lower than the average but within the 90th percentile of liver triglyceride concentrations measured in the population by Szczepaniak *et al.* consistent with simulating a healthy diet [211]. The change across the sinusoid is consistent with the values of 59.2±5.8nmol/mg of protein and 65.7±4.0nmol/mg in isolated periportal and pericentral cells respectively measured by Guzman *et al.* [487].

Average values when simulating a moderate intake diet of 70% carbohydrate: 30% FFA, averaged over each 4-hour input cycle.

Only the simulated UTP and UDP concentrations are outside of the experimentally measured confidence intervals. The simulated average UTP concentration is 13% higher (+39µM) than the value measured experimentally, whilst the UDP concentration is 39µM lower, suggesting that the activity of NDKU in converting UDP to UTP is overestimated in the model. Therefore, a potential solution to return these concentrations to the experimentally measured range would be to reduce the rate constant for NDKU in the model. However, due to the strong dependence of the UTP concentration on feeding state in the model, if the rate constant for NDKU is reduced by more than around 20% from its value in the model, the simulated UTP concentration in periportal cells falls to near zero during periods of high glycogenesis. This disrupts the storage of glucose as glycogen in these cells after feeding. On the other hand, since the Michaelis-Menten constant for UTP in glycogen synthase is low (48µM) relative to the average UTP concentration (285µM experimental/324µM simulated), the small increase in simulated average UTP concentration has little effect on overall metabolism. It is possible that NDK shows zonated expression *in vivo* with higher activity in the periportal zone to match the increased glycogenesis in this region of the sinusoid.

The relative concentrations of hepatic molecules are also consistent with concentrations measured in other experimental studies Faupel *et al.* [430] and Saggerson *et al.* [467]. However, since the Faupel *et al.* data was normalised against DNA weight rather than total protein or cell volume and the Saggerson *et al.* data was measured in adipose tissue, absolute comparison was not possible in either case and these relative comparisons are not presented.

S1.1.2 Glycogen Synthesis after a mixed meal

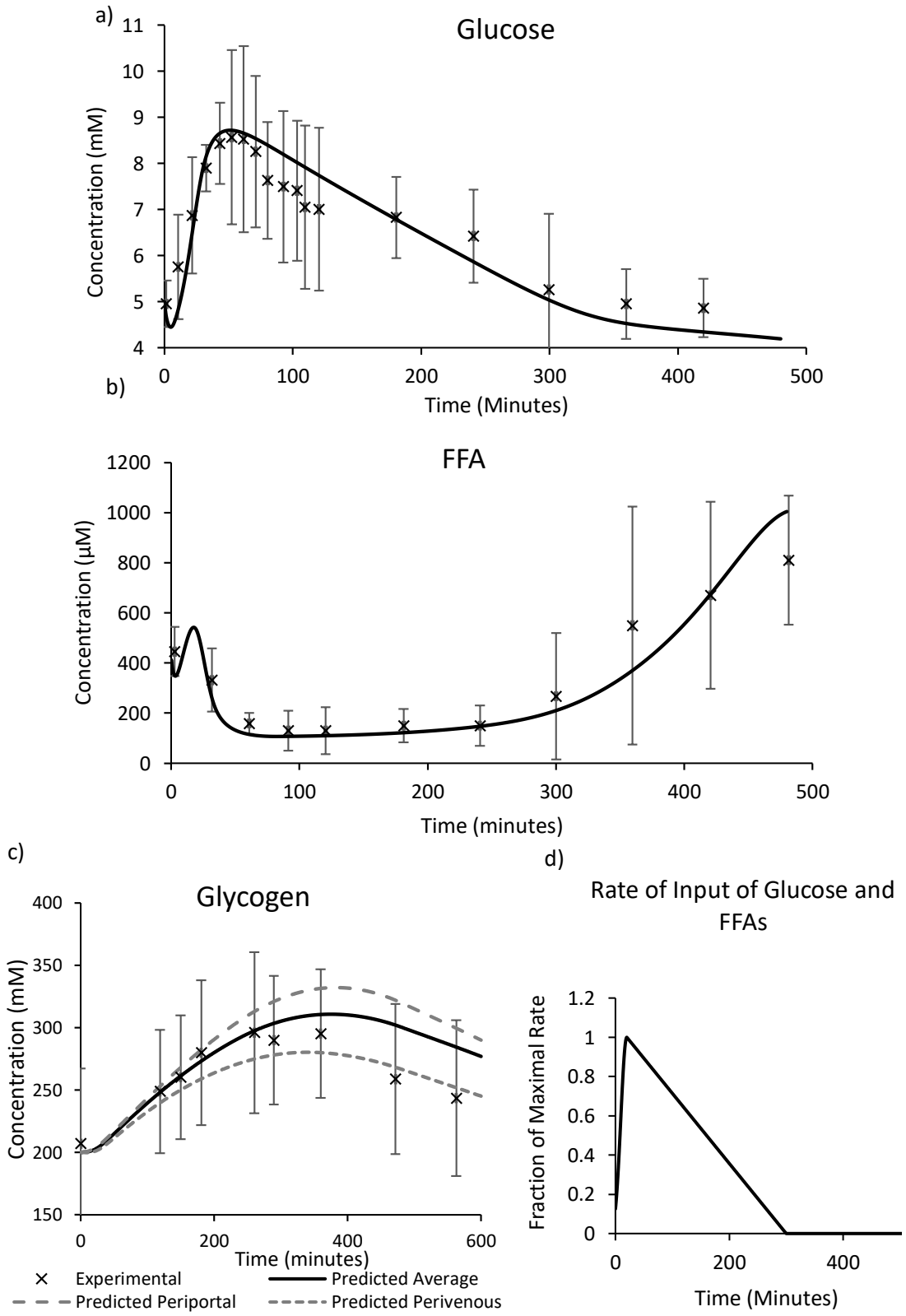

Figure S1.1: Comparison of simulated and experimental data for glycogen synthesis after a mixed meal. *(a) The glucose and FFA input used to represent the mixed meal and the* simulated *concentrations of (b) glucose, (c) FFA and (d) glycogen concentrations after input of a mixed meal in which 62% of the energy comes from carbohydrate and 38% from lipid compared with experimental data from Taylor et al. [428]. Experimental data approximated from the graphs provided using Image J to determine the position of each point relative to the x and y axes. The error bars on the experimental data are the SD based on the SEM provided.*

In addition to providing realistic values for average concentrations, the model outputs must also match experimental data for the change in plasma and hepatic concentrations under conditions of known intake. The liver is the major tissue responsible for the storage of glucose as glycogen. Therefore, the model must give reasonable values for the change in glycogen storage, along with plasma glucose and FFA concentrations under conditions in which known quantities of glucose and fat are consumed. The simulated data were compared with experimental data published by Taylor *et al.* [428] for glucose, FFA and glycogen concentrations after intake of a mixed meal in which 62% of the energy comes from carbohydrate and 38% from lipid (neglecting the protein content of the meal provided experimentally) [428] (figure S1.1). Since the exact rates at which glucose and FFAs enter the blood stream are unknown, as an approximation, inputs with an initial spike followed by a slow linear decrease were used (figure S1.1a).

The average differences between the simulated and measured glucose and FFA curves over the first 5 hours (excluding t=0) are 0.3 standard deviations (420μM) and 0.51 standard deviations (34μM) respectively. After 6 hours, the simulated glucose concentration falls to a slightly lower baseline value than the experimental data, whilst the simulated increase in FFA concentration is delayed relative to the experimental data. However, in both cases the simulated data remain within one standard deviation of the experimental data, and the shape of the simulated curves remains consistent with the experimental data.

The simulated average glycogen concentration is on average less than 0.1 standard deviations from the experimentally measured mean concentrations for the first 6 hours after the mixed meal. This shows that the model is able to accurately represent the storage of glucose as glycogen after intake

of a mixed meal. After 6 hours, the fall in glycogen concentration was larger in the experimental data than in the simulated data, but the difference between the two curves remains well within one standard deviation. Over a period of longer than 6 hours, numerous factors may explain the more rapid fall in the experimental curve compared with the simulated data. For example, the model does not account for any variation in the activity of the patient and energy is consumed at a roughly constant rate (dependent on plasma concentrations of hormones, FFA and glucose).

The simulated compartment 1 (proximal periportal) and compartment 8 (distal pericentral) concentrations are also plotted to show the difference in glycogen storage across the sinusoid. Both *in vivo* [45] and in the simulated data, a higher rate of glycogen synthesis is seen in periportal cells post-prandially.

S1.1.3 Metabolic Rates

The data in the previous sections provide validation of the simulated concentrations of molecules in hepatocytes. However, the model must also produce realistic data for the rates of various processes occurring within hepatocytes. In the following sections, the relative rates of various hepatic processes are compared with experimental data during glycogen breakdown and glycogen synthesis. Further validation of the rates of oxidation in both insulin resistant and metabolically normal individuals is provided in section S1.3.

S1.1.3.1 During glycogen breakdown

The simulated rates of various metabolic processes were next compared with experimental data presented by Ainscow and Brand under conditions of hepatic glucose production [444]. Rather than simulating Glucose and FFA inputs as in the previous sections, to allow comparison with the experimental data, the plasma fatty acid, glucose, lactate, glycerol, insulin and glucagon concentrations were set to fixed values of 0.4mM, 5mM, 0.45mM, 0.04mM, 0pM and 31.5pM in the simulations. Rates were taken after 2000s, once they had reached equilibrium.

Table S1.2: Simulated Hepatic metabolic rates compared with experimental data under conditions of glycogen breakdown.

Process	Simulated % of Glycogen Breakdown (mM/s)	Experimental % of Glycogen Breakdown ($nmol.mg^{-1}.min^{-1}$) [444]
Glycogen Breakdown	100% (5.63 [Glucose])	100% (8.67 [Glucose])
Glucose Production	54.7% (3.08 [Glucose])	54.4% (4.72 [Glucose])
Glycolysis	45.3% (2.55 [Glucose])	45.7% (3.96 [Glucose])
Lactate Release	31.3% (1.76 [Glucose]*)	35.6% (3.09 [Glucose]*)
Pyruvate Oxidation	24.3% (1.37 [Glucose]*)	~20.1% (8.72 [Ox])
Lipogenesis	3.3% (0.19 [Glucose]*)	~0
Mitochondrial Oxidation	115 [ATP]	18.01 [ATP]
ATP Consumption	199 [ATP]	31.63 [ATP]

*Simulated hepatic metabolic rates compared with experimental data from Ainscow and Brand under conditions of glycogen breakdown [444]. To simulate conditions of constant glycogen breakdown, the plasma fatty acid, glucose, lactate, insulin and glucagon concentrations were set to fixed values of 0.4mM, 5mM, 0.45mM, 0mM and 31.5pM. Rates were taken after 2000s, once they had reached equilibrium. * equivalents of glucose.*

Although comparison of the absolute values is not possible due to the different units in the two data sets, the relative rates of all of the processes provide a reasonable approximation to the experimental data (table S1.2). In both the simulated and experimental data, approximately 55% of G6P derived from glycogen breakdown was converted to glucose, whilst 45% underwent glycolysis. 31.3% of the G6P was released as lactate in the model compared with 35.6% experimentally. 24.3% underwent oxidation to acetyl-CoA compared with 20.1% experimentally. Therefore, a slightly higher relative rate of pyruvate oxidation occurred in the model than is seen experimentally, but the values remain well within a range which could be accounted for by small differences in plasma and hepatic metabolite concentrations. Only a very low rate of lipogenesis occurred when simulating the presence of glucagon but not insulin, consistent with the experimental study. The ratio of ATP consumption to mitochondrial oxidation (1.73:1) is within 2% of the experimentally measured ratio (1.75:1). However absolute comparison is not possible since the experimental data is provided in units of moles per milligram of tissue rather than moles per litre. These results demonstrate that the model provides realistic relative metabolic rates under conditions of glycogen breakdown.

S1.1.3.2 During glycogen synthesis.

A similar study under conditions of glycogen synthesis was not available. However, the relative effects of basal and high insulin concentrations on glucose removal and gluconeogenesis are consistent with experimentally measured values for canine livers from Edgerton *et al.* [443]. For comparison, simulations were run using 3 fixed plasma insulin concentrations, a fixed plasma glucagon concentrations of 93.75pM and fixed plasma glucose, lactate and FFA concentrations at the values measured experimentally. Absolute comparison was not possible since the experimental data were measured in mg/kg/min. However, the relative rates after addition of insulin (leading to a plasma concentration of 700pM and 173pM) in comparison with no addition (basal) were compared between the data sets (tables S1.3 and S1.4). 700pM insulin caused the simulated rate of glucose storage as glycogen to fall to -1.01 times the rate of clearance at basal insulin, showing a switch from glucose clearance to production (table S1.3). The experimental data is presented for the rate of glucose uptake and the rate of glycogenesis separately. In this case, 700pM caused the experimentally measured rates of glucose uptake and for glycogen synthesis to fall to -0.69 and -1.67 of the basal rates, consistent with the simulated data. In both cases gluconeogenesis was heavily stimulated by 700pM insulin (table S1.4).

The relative effects of moderate to high insulin perfusion on the system are similar in the simulated and experimental data. The change in rate due to 173pM insulin was roughly 80% of that due to 700pM Insulin in both the simulated data and the experimental data sets for both glucose removal and glycogen synthesis. At the moderate insulin concentration, the suppression of gluconeogenesis was approximately 20% of the change for the high insulin concentration in both the simulated and experimental data.

Additional validation of the model simulations for the rates of glucose and fatty acid oxidation under conditions of glucose storage is presented in section S1.3.

Tables S1.3: Comparison of the simulated effects of insulin stimulation on hepatic glucose clearance with experimentally measured values.

Hepatic Glucose Clearance	**Basal**	**Moderate Insulin (173pM)**	**High Insulin (700pM)**
Simulated Glucose Storage as Glycogen: µmol/L/s (fold change from basal)	11.3 (1.00 basal)	-7.1 (-0.62 basal)	-11.4 (-1.01 basal)
Experimental Glucose Uptake: mg/kg/min (fold change from basal)	1.3±0.4 (1.00 basal)	-0.2±0.2 (-0.15 basal)	-0.9±.7 (-0.69 basal)
Experimental Glycogen Synthesis: mg/kg/min (fold change from basal)	0.9±0.4 (1.00 basal)	-1±0.4 (-1.11 basal)	-1.5±0.5 (-1.67 basal)

Table S1.4: Comparison of the simulated effects of insulin stimulation on gluconeogenesis with experimentally measured values.

Gluconeogenesis	**Basal Insulin**	**Moderate Insulin (173pM)**	**High Insulin (700pM)**
Simulated: Change in Gluconeogenesis	0 µmol/L/s	-1.2 µmol/L/s	-4.7 µmol/L/s
Simulated: Change in Net Gluconeogenesis	0 µmol/L/s	-0.56 µmol/L/s	-3.4 µmol/L/s
Experimental: Change in Flux to G6P	0±0.4 mg/kg/min	-0.1±0.7 mg/kg/min	-0.5±0.7 mg/kg/min

Tables S1.3 and S1.4: Comparison of the simulated effects of insulin stimulation on hepatic glucose production and storage with experimentally measured values for canine livers [443]. Simulated using a fixed plasma glucagon concentrations of 93.75pM and fixed plasma glucose, lactate, insulin and FFA concentrations at the values measured experimentally.

S1.1.4 Plasma Concentrations throughout the day

The data in the previous sections focussed on hepatic concentrations and rates. However, the model additionally aims to produce realistic data for plasma concentrations under conditions of known dietary intake. Figure S1.2 compares the simulated plasma glucose, FFA, insulin and triglyceride concentrations (red) plotted with experimental data measured by Daly *et al.* (blue) throughout a daily meal cycle [17]. The model was provided with an equal spiked input every four hours and twenty minutes roughly corresponding to the food intake provided experimentally (as discussed in section 2.2.4.2). The glucose and FFA inputs were matched to the average values provided per meal experimentally. However, in the experimental study, the meals were not equally spaced and differed in size through the day.

Since the spiked periodic input provided is only a crude approximation to the rate of intake of glucose and fatty acids, it was considered inappropriate to base the comparison of the simulated and experimental curves on a simple calculation of the squared difference between the curves. When this analysis was performed, the differences in food intake times meant that, whilst the differences between the simulated (χ) and experimental (x) curves remained low for most time points, high errors were seen around meal times (e.g. 13:00-14:00). This was particularly true for glucose and lactate, for which the summed error (difference from experimental data) over variance (in the experimental data) for glucose and lactate were 1.30 and 1.08 respectively (calculated as $\frac{\sum_{i=1}^{i=n}\frac{|x(i)-\chi(i)|}{\sigma(i)}}{n}$, where $i = 1{:}\, n$ are times at which experimental data points were available). The summed error over variance for triglyceride was also large at 1.59.

Instead, to give a more representative quantitative comparison of simulated and experimental data, table S1.5 compares the peak, trough and average concentrations for each variable along with the offset in the peak time from the glucose peak. Values for lactate and glycerol are additionally included in this table. These measures are less dependent on the differences in meal time and size between the two data sets. Since data points were taken at 30 minute intervals in the data, there is a 30-minute uncertainty in the time at which peaks occurred in the experimental study.

The simulated glucose, insulin and FFAs concentrations replicate the key features of experimental data. In both the simulated and experimentally measured data, the glucose and insulin concentrations show sharp post-prandial peaks followed by broad troughs between meals. The FFA concentration gradually rises between meals before falling rapidly postprandially in both data sets.

The simulated peak concentrations are equal in magnitude because equal meal sizes were simulated, whilst the experimental peaks increase throughout the day due to increases in the size of the meal. As a result, the final peak matched the experimental data well, but the simulated first and second post-prandial glucose peaks were 1.09 and 0.74 standard deviations higher than measured

respectively. The simulated peak concentrations were 0.79 standard deviations higher than the average peak in the experimental data. However, since readings were taken at 30 minute intervals in the experimental study, and the peaks in glucose concentration are very sharp, the true peak concentration is likely to be higher than the experimentally measured peak.

The simulated average peak insulin concentration closely matches the experimentally measured value (0.27 standard deviations). However, the simulated plasma concentration falls to effectively zero between meals whilst the experimentally measured value only falls to at 29±24pM. This is because no insulin release occurs between meals in the model, where some release would be expected *in vivo*. A concentration this small is unlikely to have a large effect on metabolism and will be dwarfed by the effects of the raised glucagon concentration.

The simulated FFA concentration curve matches the experimental data well. Sharp pre-prandial peaks in concentration occurred in the simulated data. This would not be seen experimentally because the experimental data provides an average over several patients with readings taken at half hour intervals. Therefore, comparison of this aspect of the simulated data with the experimental data is not possible.

In both the simulated and experimental data, the lactate concentration follows a similar pattern to the glucose concentration but with a slightly delayed peak. The simulated peak concentrations match the experimental data well in both magnitude and time relative to the peak in glucose concentration. However, the simulated concentration only fell to 0.82mM between meals in the model, compared with 0.52±0.15mM experimentally.

The triglyceride and glycerol concentrations show stronger periodic behaviour in the model simulations than in the experimental data. This difference occurs because adipose tissue storage of triglycerides is not included in the model. Since the focus of the study is on hepatic metabolism a separate adipose compartment allowing adipose triglyceride storage was not included. However, hepatic uptake of triglycerides from plasma is slow, such that the hepatic triglyceride concentration is

more strongly dependent on the longer-term average plasma concentration than on short-term fluctuations. Once equilibrium is reached, less than a 5% variation is seen in hepatic triglyceride concentration throughout a meal cycle, and most of this results from variation in hepatic synthesis. Additionally, very little lipolysis occurs in hepatocytes such that variations in hepatic triglyceride concentration only very weakly feed back into the rest of hepatic metabolism. Therefore, in developing a model to study hepatic metabolism, it is more important that the longer-term average triglyceride concentration remains in the experimentally measured range. From figure S1.2 and table S1.5, it can be seen that the simulated triglyceride concentration remains in the same range as the experimental data. It is also important that the experimentally measured changes in average triglyceride concentration under conditions of insulin resistance are reproduced in the simulated data as discussed in section S1.1.5.3.

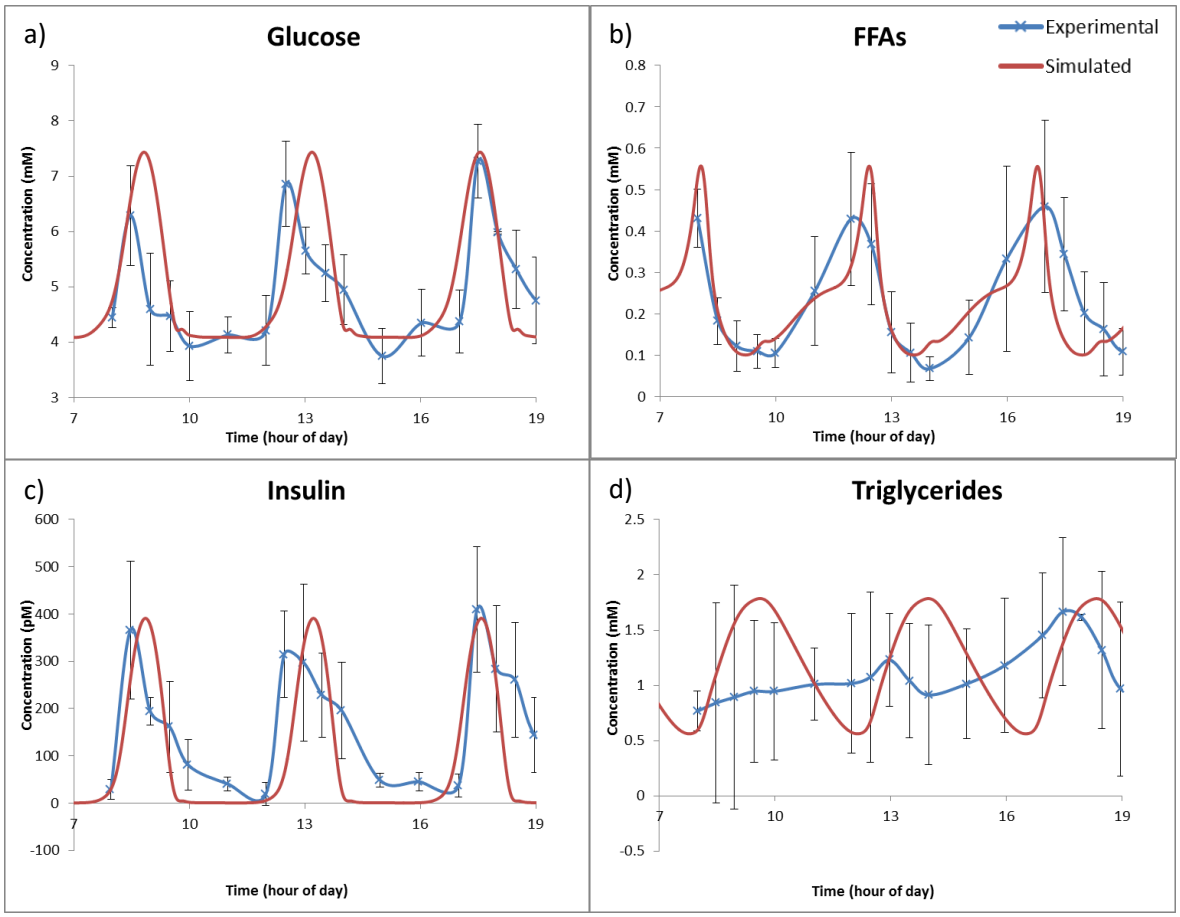

Figure S1.2: Comparison of the model predictions for plasma concentrations over a daily meal cycle with experimental data. *Comparison of the model simulations (red) for plasma glucose, FFA, lactate, insulin, triglycerides and glycerol throughout a daily feeding cycle with experimental data from Daly et al. [17] (blue). Experimental data approximated from the graphs provided using Image J.*

Table S1.5: Comparison of the simulated peak, trough and average concentrations and peak times with experimental data for plasma concentrations throughout a daily feeding cycle.

	Peak Concentrations	Trough Concentrations	Average Concentration	Difference in peak time from peak glucose
Glucose				
Simulated	**7.43mM**	**4.08mM**	**4.92mM**	-
Experimental	**Av.) 6.81±0.78mM (Δ = 0.79 σ)** 1) 7.27±0.67mM (0.24 σ) 2) 6.86±0.77mM (0.74 σ) 3) 6.29±0.90mM (1.09 σ)	**Av.) 3.84±0.56mM (Δ = 0.43 σ)** 1) 3.75±0.50mM (0.66 σ) 2) 3.93±0.62mM (0.24 σ)	**4.59±0.65mM (Δ = 0.51 σ)**	-
FFAs				
Simulated	**557µM**	**100µM**	**229µM**	**-45.6 mins**
Experimental	**Av.) 445±186µM (Δ = 0.60 σ)** 1) 460 ± 208 (0.47 σ) 2) 429 ± 161 (.80 σ)	**Av.) 86±32µM (Δ =0.44 σ)** 1)104±35 (0.11 σ) 2) 67±29 (1.14 σ)	**234±93µM (Δ =0.05 σ)**	**-30 mins (-60<t<0 mins)**
Triglycerides				
Simulated	**1.79mM**	**0.56mM**	**1.19mM**	**47.64 Minutes**
Experimental	**-No peaks or troughs following intake, but an increase from 0.77mM increase to 1.66mM throughout the day.**		**1.08±0.30mM (Δ =0.37 σ)**	-
Lactate				
Simulated	**2.70 mM**	**0.82 mM**	**1.23mM**	**19.7minutes**
Experimental	**Av.) 2.29 ± 0.92 mM (Δ =0.45σ)** 2.11 ± 0.63mM 2.39 ± 1.20mM 2.38 ± 0.93mM	**Av.) 0.52 ± 0.15mM (Δ =2σ)** 0.52±0.17 mM 0.52±0.13 mM	**1.21 ± 0.55mM (Δ =0.04 σ)**	**30 mins (0<t<60 mins)**
Insulin				
Simulated	**391pM**	**1pM**	**89pM**	**2.3 mins**
Experimental	**Av.) 363 ± 123 pM (Δ =0.23σ)** 366 ± 146 pM 315 ± 91 pM 409 ± 133 pM	**Av.) 29±24pM (Δ =1.17σ)** 19±24pM 38±24pM	**118 ± 90pM (Δ = 0.32 σ)**	**0 mins (-30<t<30 mins)**
Glycerol				
Simulated	**39µM**	**21µM**	**30 µM**	**2.0 hours**
Experimental	**39±19µM **Not periodic with meal cycle**	**22±10µM ** Not periodic with meal cycle**	**32±15 µM (Δ =.13 σ)**	**3.5±0.5, 4.5±0.5 hours**

Comparison of the simulated peak, trough and average concentrations and peak times relative to the glucose peak for plasma glucose, FFA, lactate, insulin, triglycerides and glycerol throughout a daily feeding cycle with experimental data from Daly et al. [17]. Experimental data approximated from the graphs provided using Image J.

S1.1.5 Validation of Zonation

A major aim of this study was to develop a model which is able to represent the zonation of processes across the sinusoid. To achieve this, the zonation in the rate constants of processes across the sinusoid was based on experimental data for differences in the activities of key enzymes (section 2.2.6). In the following section, simulated data within different zones of the sinusoid are compared with experimental data.

S1.1.5.1 ATP across sinusoid

Data measuring the concentrations of molecules in specific regions of the sinusoid are relatively few. As a result, hepatic heterogeneity in the model was largely validated against measurements of the relative rates of various processes occurring in different regions of the sinusoid. However, Nauck *et al.* approximated the change in ATP concentration across the sinusoid in an *in vitro* experiment by comparing cells grown in culture conditions similar those seen by periportal and pericentral cells *in vivo* [69]. Cells cultured in periportal oxygen and hormone concentrations had an ATP concentration of 2.9±0.2mM whilst those grown in pericentral conditions had a concentration of 2.5±0.2mM [69].

When simulating a moderate diet in a metabolically normal individual (section 2.2.4.2), the ATP concentration falls from 3.0mM in the periportal half of the sinusoid to 2.6mM in the pericentral side. Therefore, as well as the average values matching those measured *in vivo* [429], the change in ATP concentration across the sinusoid matches that measured between isolated periportal and pericentral cells [69]. It is important that the energetics are represented properly since the inability of pericentral cells to produce sufficient ATP through oxidative phosphorylation is the primary motivation for zonation. Unfortunately, data was not available for the relative contribution of oxidative phosphorylation and glycolysis across the sinusoid. However the relative rates of gluconeogenesis and glycolysis across the sinusoid are compared with experimental data in section S1.1.5.2, whilst the energetic benefit resulting from zonated enzyme expression is demonstrated in section S1.1.5.3.

S1.1.5.2 Processes

Although the zonation of enzymes in the model was based upon experimental data, the relative rates of processes across the sinusoid are also determined by other factors such as substrate concentrations and allosteric regulation. In this section, the relative rates of some of the key processes in the model are compared with experimental data to validate the representation of zonation in the model. In each case, model values are the average when the model was provided with an input cycle representing a moderate diet as discussed in section 2.2.4.2.

S1.1.5.2.1 β-oxidation

In two studies, Guzman *et al.* measured the rate of β-oxidation to be 1.2±0.3, and 1.4±0.3 times higher in periportal than in pericentral cells in fed animals [83, 86, 87]. Consistent with these studies, the simulated rate of β-oxidation is 1.25 times higher in the periportal half of the sinusoid than the periportal half. The simulated rate is 1.47 times higher in the proximal periportal compartment (compartment 1) compared to the distal pericentral compartment (compartment 8).

S1.1.5.2.2 Triglyceride synthesis, storage and release as very low density lipoproteins (VLDL)

In two different *in vivo* studies by Guzman *et al.*, pericentral cells were measured to synthesize triglycerides at 1.6±0.4 and 1.3±0.3 times the rate of periportal cells, and release triglycerides as VLDL at 1.5±0.5 and 1.3±0.3 times the periportal rate [83] [86]. In the model, triglycerides are synthesized in pericentral cells at 1.64 times the rate in periportal cells.

Guzman *et al.* also measured an 11% increase in triglyceride concentration between periportal and pericentral hepatocytes, although this was not statistically significant [86]. In the model, the average triglyceride concentration in the pericentral half of the sinusoid is 22% larger than in the periportal half, slightly overestimating this difference. However, this is strongly dependent on the glucose and FFA inputs. A higher glucose to FFA ratio gives more evenly distributed triglyceride levels.

S1.1.5.2.3 Fatty acid uptake

Using fluorescently tagged fatty acids, Fitz *et al.* measured higher fatty acid uptake in periportal cells [92]. However, no quantitative comparison was made. In the model, the rate of fatty acid uptake in the periportal half of the sinusoid was 1.21 times higher than in pericentral cells.

S1.1.5.2.4 Lipogenesis

When measured *in vivo* by Guzman *et al.* in two studies, the pericentral rate of lipogenesis was measured to be 1.6±0.4 and 1.7±0.5 times that in periportal cells [83, 86]. When simulated in the model, the pericentral rate of lipogenesis was 1.9 times higher than the periportal rate. This is within one standard deviation of the experimental data but slightly higher than the average. However, the relative rates of lipogenesis across the sinusoid are dependent on the ratio of glucose to FFA input.

S1.1.5.2.5 Gluconeogenesis and glycolysis

Wolfe *et al.* performed an *in vitro* study in which they measured the relative rates of gluconeogenesis and glycolysis in cells cultured in periportal or pericentral oxygen and hormone concentrations [77]. Their results show that glycolysis is 1.5-2.5 times more rapid in pericentral-like cells whilst gluconeogenesis is 1.5-2.5 times more rapid in periportal-like cells [77]. When simulating a moderate diet in the model, glycolysis occurs 1.7 times more rapidly in pericentral cells whilst gluconeogenesis occurs 2.3 times as quickly in periportal cells consistent with the *in vitro* data.

Both the simulated data and the results of this *in vitro* study are consistent with the idea of glucose-lactate cycling known to occur *in vivo* [50]. In glucose-lactate cycling, hypoxic pericentral cells undergo glycolysis to supplement ATP production from oxidative phosphorylation. This produces lactate which cycles around the body and is converted back to glucose by the oxygen rich periportal cells. Due to their higher oxygen environment, periportal hepatocytes can produce sufficient ATP through oxidative phosphorylation to survive and to fuel the additional gluconeogenesis, largely using fatty acids.

S1.1.5.3 Validating the role of zonation in hepatic energy metabolism

The low oxygen concentration of pericentral cells is major motivation for the presence of zonation in energy metabolism (see chapter 1). In the absence of sufficient oxygen, pericentral cells are unable to produce sufficient ATP through oxidative phosphorylation and are forced to upregulate glycolysis, whilst suppressing ATP consumption in gluconeogenesis. To ensure that zonation in energy metabolism is properly represented in the model, simulations were next used run with both zonated enzyme expression and with homogenous enzyme expression. The simulated data in these two cases were compared to ensure that zonated enzyme expression leads to increased ATP concentrations across the sinusoid.

In figure S1.3, the average rates of glycolysis, gluconeogenesis and average ATP concentrations when simulating a moderate intake diet of the form discussed in section 2.2.4.2 are compared when running simulations with zonated and homogenous enzyme expression.

Removing the zonation in glucose and lipid metabolism enzymes caused severely reduced pericentral ATP concentrations (figure S1.3a) because of higher gluconeogenesis (figure S1.3b) and lower glycolysis (figure S1.3c) in these cells. The ATP concentration in the most pericentral compartment fell to below 1.2mM when simulating homogenous enzyme expression. ATP is required for most cellular processes and concentrations this low would cause loss of function or cell death. A slight increase in ATP concentration was seen in periportal cells when simulating homogenous enzyme expression relative to zonated expression due to reduced gluconeogenesis in these cells. However, zonated enzyme expression increased the average ATP concentration across the sinusoid (zonated enzyme expression: 2.81mM, heterogeneous enzyme expression 2.57mM) and resulted in a much more even distribution across the sinusoid. Therefore, a clear increase in fitness is results from zonation in the model.

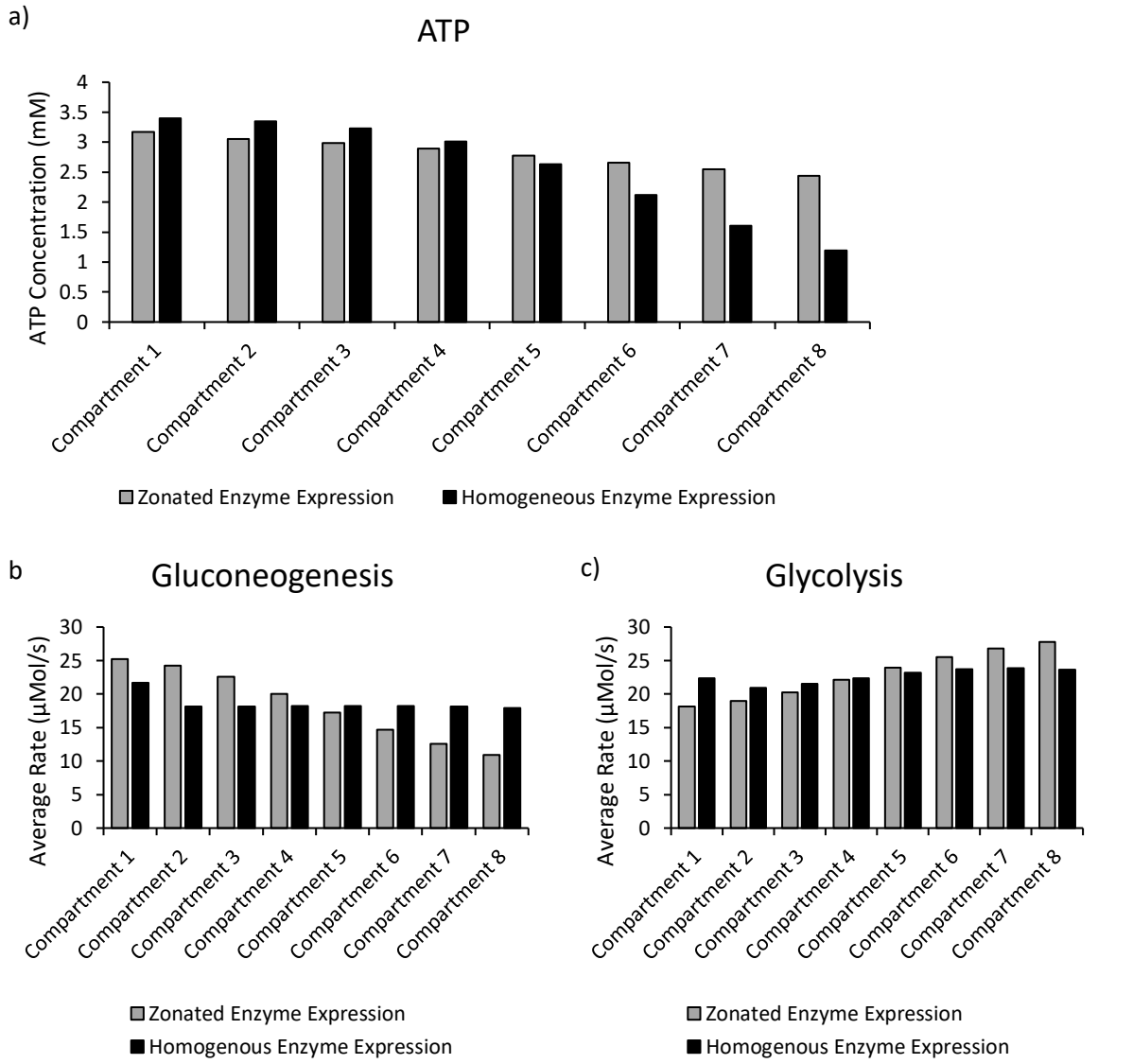

Figure S1.3: The effects of simulating zonated and homogenous enzyme expression on energy metabolism. *The effects of zonated enzyme expression on a) the ATP concentration b) the rate of gluconeogenesis and c) the rate of glycolysis. The average concentration is shown when simulating a moderate intake 70% carbohydrate 30% lipid diet with (grey) homogenous enzyme expression or (black) zonated enzyme expression.*

S1.2 Validation of Simulated Data for Insulin Resistant Patients

Having shown that the model is able to produce realistic data for the average concentrations of hepatic molecules, for plasma concentrations of key variables during a daily feeding cycle and after a mixed meal, for glycogen storage after a mixed meal, for the rates of key metabolic processes during periods of glycogen synthesis and breakdown and for the zonation of key metabolic processes in metabolically normal individuals, the model outputs were next compared with experimental data when simulating insulin resistance. Insulin resistance is simulated in the model by multiplying the

detected insulin by a constant $0 \leq K_{IR} < 1$ where $K_{IR}=0$ would correspond to total insulin resistance and KIR=1 would correspond to normal insulin sensitivity.

S1.2.1 Average plasma values in metabolically normal and insulin resistant individuals

Firstly, the average plasma values of triglycerides, glucose and FFAs are compared with experimental data when simulating metabolically normal and insulin resistant individuals. The simulated average plasma concentrations are dependent on the inputs provided and on the severity of IR. To provide the data for table S1.6, simulations were run with the moderate diet intake cycle discussed in section 2.2.4.2 with two severities of IR. Developing and severe IR were simulated by reducing the detected insulin concentration to 5% and 1.5% respectively.

Table S1.6: The simulated and experimentally measured average triglyceride, glucose and FFA concentrations in metabolically normal and insulin resistant patients.

	Simulated	Experimental
Average Triglyceride (mM)		
Metabolically Normal	1.2±0.4	0.9±0.4[a]
Insulin Resistant	Developing: 2.1±0.8 Severe: 3.7±0.9	2.6±0.5[a]
Average Glucose (mM)		
Metabolically Normal	4.9±1.1	4.7±0.7[a], 5.3±1.5 (4.5 - 6.8) [d]
Insulin Resistant	Developing: 6.3±2.4 Severe: 8.1±3.9	9.0±2.2[a] Low TG group (less severe): 6.3±0.5 [c] High TG group (more severe): 6.8±0.5 [c] Mild NIDDM: 8.0±2.7 (6.7 - 10.9) [d] Severe NIDDM: 19.6±5.3 (16.9 - 23.7) [d]
Average FFA (mM)		
Metabolically Normal	0.23±0.12	0.3±0.1[b], 0.3±0.1 (0.16 - 0.52) [d]
Insulin Resistant	Developing: 0.48±0.16 Severe: 0.84±0.70	0.6±0.1[b] Low TG group (less severe): 0.54±0.07 [c] High TG group (more severe): 0.81±0.07 [c] Mild T2DM: 0.4±0.1 (0.19 - 0.59) [d] Severe T2DM: 0.6±0.1 (0.37 - 0.75) [d]

Experimental data from: [a] – Sindelka et al. [141], [b] – Berndt et al. [435], [c] – Monti et al. [466], [d] – Reavan et al. [139] ([a,b] standard deviations calculated based on the SEM provided, [d] – averages, ranges and error bars taken from the graphs provided using Image J). Simulated data are averages ± the average deviation from the mean value over each feeding cycle.

For metabolically normal individuals, the simulated data are within one standard deviation of the experimental data for glucose, FFAs and triglycerides further validating the ability of the model to give realistic data for non-insulin resistant patients (table S1.6).

The FFA and triglycerides concentrations measured by Sindelka *et al.* [141] and Berndt *et al.* [435] in insulin resistant individuals lie between the simulated values for developing IR and for severe IR (table S1.6). This is consistent with the experimental groups containing individuals with a range of severities of IR. Monti *et al.* measured FFA levels in T2DM individuals grouped according to their plasma triglyceride levels [466]. The measured concentrations in the low and high triglyceride concentration groups match the simulated data for developing and severe IR respectively. Reavan *et al.* meanwhile measured slightly lower average FFA concentrations in mild and severe T2DM than the simulated data [139].

Large heterogeneity was seen in the experimental measurements of glucose concentrations in insulin resistant individuals. The mean concentration measured by Sindelka *et al.* in insulin resistant individuals is slightly higher than the simulated value when simulating severe IR (0.4 standard deviations) [141]. Conversely the concentrations measured in both groups by Monti *et al.* are several standard deviations lower than the simulated concentration for severe IR. Meanwhile, the glucose concentration measured in mild T2DM by Reavan *et al*. matches that when simulating severe insulin resistance (0.03 standard deviations), whilst the concentration measured in severe T2DM is more than double this [139].

This variation is likely to result from differences in the severity of IR within the group and differences in feeding. When simulating severely insulin resistant patients on a moderate diet, hyperglycaemia is seen post-prandially due to reduced glycogenesis. However, between meals the blood glucose concentration becomes hypoglycaemic because there are no glycogen stores to break down. It is because of this that the average glucose concentration to show only a modest increase. When simulating a high intake diet, sustained hyperglycaemia occurs in IR patients more consistent with the measurements of Reavan *et al*. [139].

S1.2.2 Change in glucose and lactate concentrations after a glucose load

Having shown that the model provides reasonable values for average plasma concentrations in both metabolically normal and insulin resistant individuals, it was next compared with data for the change in plasma glucose and lactate concentrations after an oral glucose load. Table S1.7 shows the simulated and experimental data for the change in plasma lactate and glucose concentrations after intake of an 100g glucose load [434]. Since the rate at which the oral glucose load glucose entered the blood stream in the experimental study is unknown, as an approximation a spiked input of the form $\sin^6(t)$, starting from zero input at t=0 and reaching peak input at 30 minutes was used. However, to account for the possibility that the sugars may enter the blood stream more or less rapidly than this, two additional input functions were used of the same form and with the same total input, but with peak inputs at 20 minutes (rapid intake) and 45 minutes (slow intake). The simulated data in these two cases are shown by the upper and lower error bars respectively. In all three cases, the total glucose input was equal to that in the experimental study (assuming 5L of blood in the body). Severe IR was simulated using an IR constant, K_{IR}, of 0.015.

For both metabolically normal and insulin resistant individuals, the experimentally measured and simulated changes in glucose and lactate concentrations are well within one standard deviation of the experimental data. This shows that the model can accurately represent the changes in hepatic glycogenesis and glycolysis resulting from IR after a glucose load.

Table S1.7: The simulated change in glucose and lactate concentrations after a 100g glucose load in metabolically normal and insulin resistant individuals compared with experimental data.

Change in Glucose	Metabolically Normal	Insulin Resistant
Simulated	$2.1^{+1.0}_{-1.0}$	$8.5^{+2.1}_{-3.6}$
Experimental	2.8 ± 2.0	9.7 ± 4.6
Change in Lactate	Metabolically Normal	Insulin Resistant
Simulated	$0.46^{+1.50}_{-0.29}$	$0.40^{+0.09}_{-0.12}$
Experimental	0.46 ± 0.12	0.31 ± 0.13

The simulated change in glucose and lactate concentrations after a 100g glucose load in metabolically normal and insulin resistant individuals compared with experimental data from Prando et al. [434]. Experimental data approximated from the graph presented using Image J.

S1.2.3 Contribution of lipogenesis, FFA uptake and diet to hepatic triglycerides across the sinusoid

Table S1.8: The simulated contribution of hepatic de novo lipogenesis, FFA uptake and dietary triglycerides to hepatic steatosis compared with experimental data.

Metabolically Normal, Moderate Intake		
	Simulated	Experimental
Plasma FFA	54.0%	-
Hepatic DNL	12.0%	-
Dietary Triglycerides	34.0%	-
Severe IR + Raised SREBP-1c expression (NAFLD)		
	Simulated (Liver & VLDL)	Experimental - NAFLD
Plasma FFAs	60.0%	Liver: 59.0±9.9% VLDL: 62.4±11.7%
Hepatic DNL	20.2%	Liver: 26.1±6.7% VLDL: 22.9±6.2%
Dietary Triglycerides	19.8%	Liver: 14.9±7.0% VLDL: 14.7±8.5%

The simulated contribution of hepatic de novo lipogenesis, FFA uptake and dietary triglycerides to hepatic steatosis compared with experimental data from Donnelly et al. [26].

Table S1.8 compares the contribution of plasma FFAs, hepatic *de novo* lipogenesis and uptake of dietary triglycerides to overall hepatic triglyceride levels (averaged across the sinusoid) when simulating severe IR combined with increased SREBP-1c expression (as seen in NAFLD; see chapter 3) with the contributions measured experimentally by Donnelly *et al*. in NAFLD patients [26]. Donnelly *et al.* measured the contribution of these three sources to both liver triglycerides and VLDL. However, in the model, the composition of VLDL is solely determined by the composition of liver triglycerides such that the two are equal. Additionally, the contributions when simulating a metabolically normal individual are shown.

The contributions of each source of FAs to both liver triglycerides and VLDL are all within one standard deviation of the values measured by Donnelly *et al*. when simulating NAFLD [26]. The contribution of dietary triglycerides is towards the high end of the measured values suggesting this may be slightly overestimated. However, this component is the most susceptible to changes in dietary input, and the simulated values remain in the correct range.

Experimental data comparing the contributions of different sources to FA levels in individuals without excessive liver fat was not available. However, the simulated contribution of plasma FFAs was slightly higher when simulating NAFLD than for metabolically normal individuals (60.0% vs 54.0%). The simulated contribution of dietary triglycerides was lower when simulating NAFLD compared with metabolically normal individuals on the same diet (19.8% vs 34.0%). If higher dietary intake was additionally simulated, as is often seen in NAFLD patients *in vivo,* this difference would be expected to fall. The percentage of hepatic triglycerides arising from de novo lipogenesis was higher when simulating NAFLD (20.2% vs 12.0%).

S1.3 Validation of the relative contributions of lipids and carbohydrates to oxidative phosphorylation

Finally, to properly integrate hepatic glucose and lipid metabolisms, it is important that the model can produce realistic values for the rates at which fatty acids and glucose are oxidised before and after dietary intake. Relatively little time series data exists investigating the rates of oxidation in liver. However, in the following sections the model simulations for the rates in liver are compared with experimental data for the rates in the whole body. Experimental and simulated rates are compared after a mixed meal in metabolically normal individuals (section S1.3.1) and after the intake of starch with either slow or fast hydrolysis rates in metabolically normal and T2DM individuals (section S1.3.2).

S1.3.1 Energy production after a mixed meal

Daly *et al.* measured the rates of carbohydrate and fatty acid oxidation after a high sucrose/low starch meal with 65% of energy as carbohydrate and 26% as fat (2.5:1) [452]. Using the number of ATP molecules produced per glucose and per palmitate in the model, this corresponds to 6.9 moles of glucose per mole of palmitate (or 4.85 grams of glucose per gram of palmitate). The model was provided with glucose and FFA inputs with the total magnitude to match the inputted carbohydrate (high sugar/low starch) and fat in the meal. The meal was inputted in the form of a single $\sin^6(t)$ spike rising from 0 at t=0 to a peak input at 30 minutes. The simulated FFA and glucose concentrations are

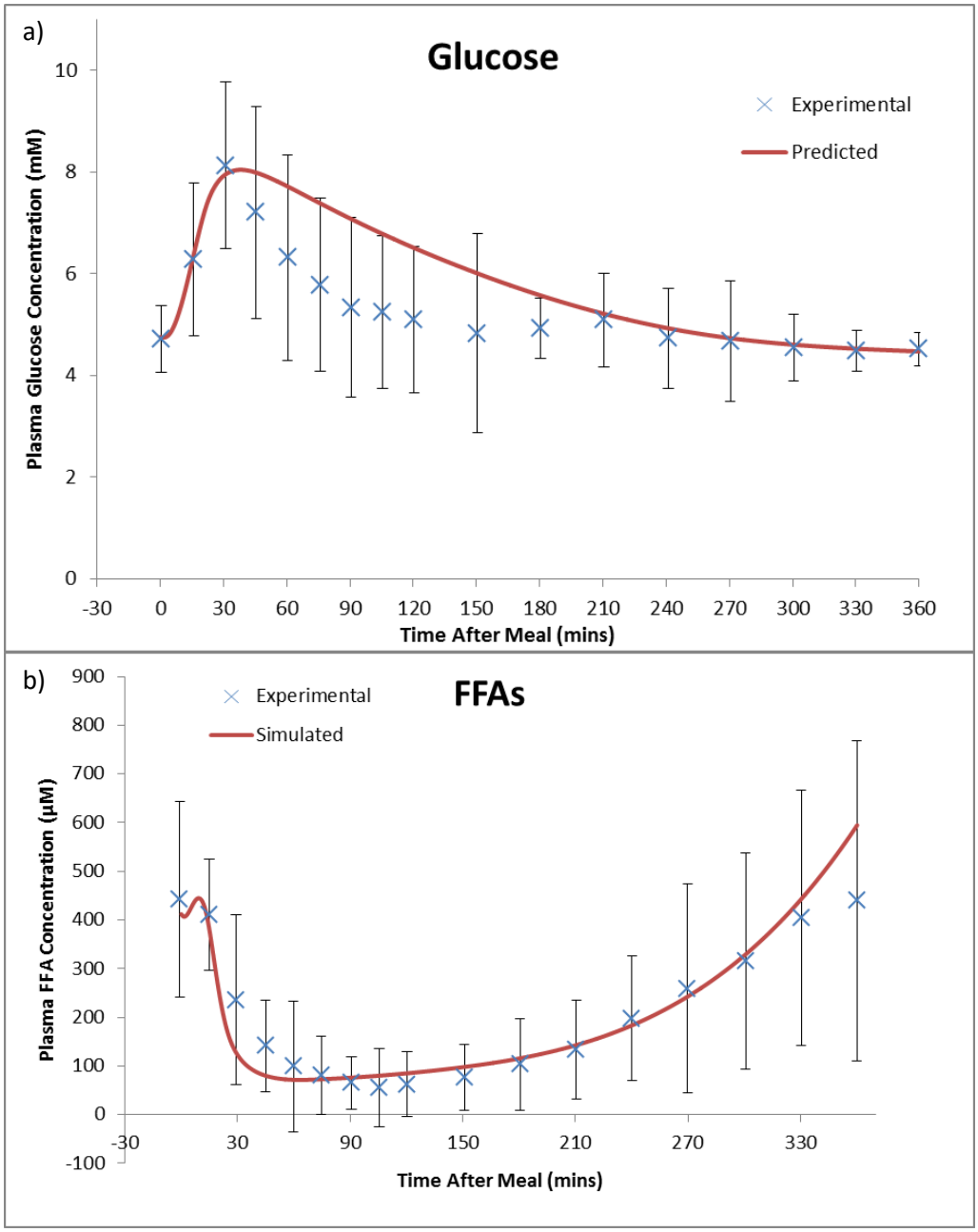

Figure S1.4: Comparison of the simulated plasma glucose and fatty acid concentration after intake of a mixed meal with data measured experimentally. *Experimental data from Daly et al. [452]. The model was provided with glucose and FFA inputs with the total magnitude to match the inputted carbohydrate (high sugar/low starch) and fat in the meal. The meal was inputted in the form of a single sin6(t) spike rising from 0 at t=0 to a peak input at 30 minutes.*

well within one standard deviation of the experimental data at all time points when this input was simulated in the model (figure S1.4a,b), although the simulated glucose concentration has a less sharp peak and shows a slower decrease initially after the peak concentration. This suggests that the simulated input provides a reasonable approximation to the meal provided experimentally.

In the experimental study, the rates of carbohydrate and lipid oxidation were measured in grams per minute in the body as a whole (figure S1.5a,c). These results cannot be compared quantitatively with the simulated data for the rate of pyruvate oxidation and β-oxidation in liver alone calculated in moles per minute (figure S1.5b,d). However, qualitative comparison of the changes occurring postprandially can be made.

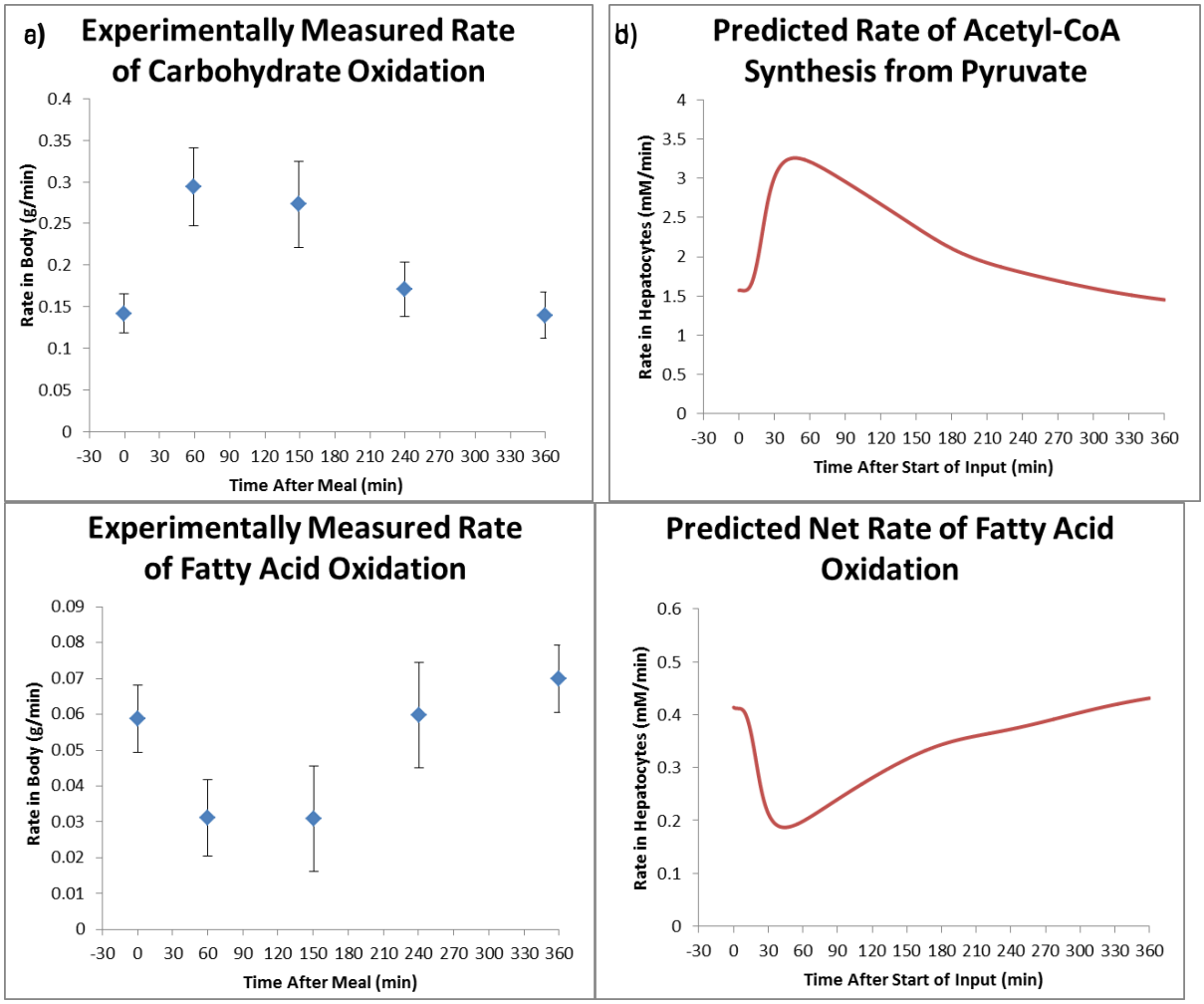

Figure S1.5: Comparison of simulated fatty acid and glucose oxidation rates with experimental data. *The rates of oxidation of (a,b) glucose and (c,d) fatty acids and when (a,c) measured experimentally in the body as a whole by Daly et al. [452] and (b,d) simulated in liver alone after intake of a mixed meal as discussed in the text.*

The simulated curves for the rates of fatty acid and carbohydrate oxidation follow a similar shape over the 6 hours to those measured experimentally. The rate of carbohydrate oxidation doubles postprandially before falling back to its initial value in both the simulated and experimental data. Similarly, in both cases the rate of fatty acid oxidation falls by half before rising to slightly above its

initial value. The peak in carbohydrate oxidation and the trough in lipid oxidation appear sharper and occur more rapidly after intake in the simulated data than experimentally. This may be because only the liver is simulated, rather than the body as a whole. Due to the role of liver in the storage of glucose, and the large quantities of blood that pass through the organ, hepatocytes would be expected to react particularly quickly to changes in plasma insulin and glucagon levels. When considering the body as a whole, less responsive organs would slow this effect.

S1.3.2 Comparison of energy production in metabolically normal and diabetic individuals

Seal *et al.* compared the rates of carbohydrate and lipid oxidation in metabolically normal and T2DM patients fed 50g of rapidly or slowly hydrolysed starch [453]. In this study, the rates at which the two starches were broken down to sugars were also measured, allowing a more accurate approximation of the rate at which glucose entered the blood stream. To validate the models simulations for energy metabolism in insulin resistant individuals, the model was provided with glucose inputs set to match the rates at which carbohydrates were broken down *in vivo*. For the fast release starch, an input was provided with a sharp peak at 30 minutes before falling rapidly to zero (figure S1.6). For slow release starch an input with a smaller peak centred after an hour was used before falling more slowly, such that the rate of input remained at 17% of its peak rate after 6 hours (as measured experimentally) (figure S1.6). Experimentally, only 70% of the slowly hydrolysed starch was broken down over the 6 hours compared to 96% for the rapidly hydrolysed starch. As a result, the total glucose inputted to the model was larger when simulating the rapidly hydrolysed starch to match these values. In both cases, the model was run for 1.5 hours with no input before the starch intake to allow variables to equilibrate.

IR was simulated by multiplying the detected insulin concentration by a constant (K_{IR}) smaller than one. Three severities of IR were simulated to account for variability in the degree of insulin sensitivity

between T2DM individuals. Mild, moderate and severe IR correspond to 90%, 95% and 98.5% de-sensitivity respectively in the graphs.

For the metabolically normal individuals, the simulated glucose concentrations match the experimental data closely with the average difference between the simulated and experimental curves well within one standard deviation. This provides further validation of the simulated data for the plasma glucose concentration under conditions where the rate of input is known (figure S1.7).

The simulated data for the glucose concentration in insulin resistant individuals match the experimental data through the initial postprandial rise and initial subsequent fall (figure S1.7). The experimentally measured concentration remains within one standard deviation of the simulated data for moderate IR and between the simulated data for mild and severe IR over the first 4-5 hours. However, around 4 hours after the intake of fast release starch and 5 hours after the intake of slow release starch, a drop of glucose concentration to well below the pre-prandial value was measured experimentally but not seen in the simulated data. This was, accompanied by a widening of the error bars in the experimental data. When simulating IR, the only change that was made was to multiply the detected insulin concentration by an IR constant less than 1 to allow direct comparison. However, *in vivo*, diabetics additionally show severely depleted glycogen stores reducing their capacity to provide glucose to the blood when plasma concentrations fall. Therefore, the difference between the simulated and experimental data is likely to arise because in the simulations the initial glycogen stores were set to 200mM for both insulin resistant and metabolically normal individuals. Due to this difference in plasma concentrations after 4-5 hours, the rates of oxidation are only compared for the first 300 minutes.

As with section S1.3.1, the model simulates the rates of pyruvate oxidation and fatty acids in liver and so cannot be compared quantitatively with the experimentally measured rates of carbohydrate and lipid oxidation in the body as a whole (figures S1.8 and S1.9). However, the change in the rates of these

processes occurring postprandially in the liver should be qualitatively similar to those for the body as a whole.

Over the 360 minutes, the changes in the rates of oxidation relative to baseline match the experimental data closely with an upregulation of carbohydrate oxidation and reduction in lipid oxidation occurring. In the case of fast release starch, a slightly larger increase in carbohydrate oxidation and reduction in lipid oxidation is seen in T2DM than metabolically normal individuals after the intake of fast release starch in both the simulated and experimental data (figures S1.8). In the case of slow release starch the change in the rate of fatty acid oxidation was roughly the same for T2DM and insulin sensitive individuals in both the simulated and experimental data (figure S1.9). A slightly lower increase in carbohydrate oxidation was seen for T2DM individuals experimentally, perhaps due to depleted glycogen stores.

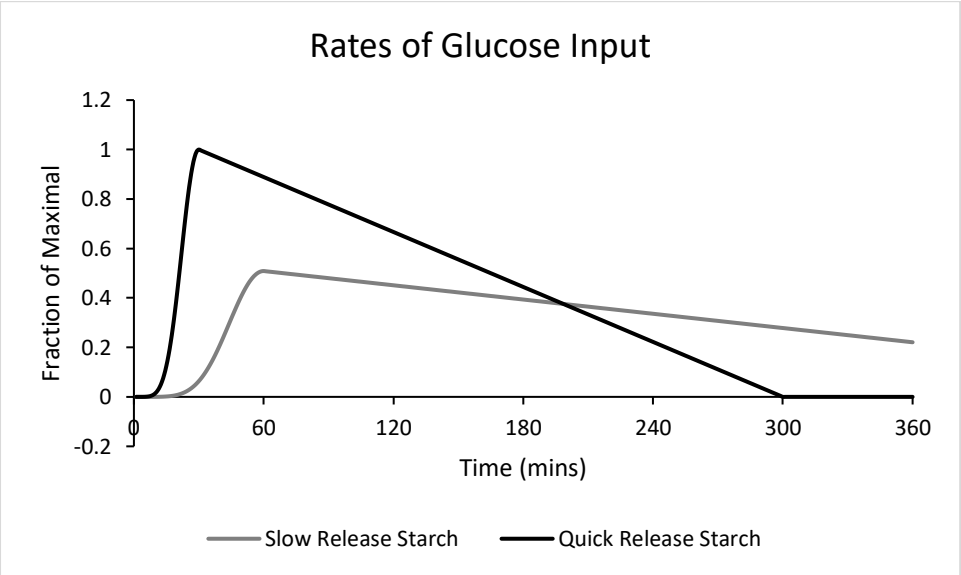

Figure S1.6: The rates of glucose input used when simualting the intake of 50g of rapidly and slowly hydrolysing starch. *When simulating quick release starch 100% of the 50g was inputted to the blood stream over the 6 hours whilst for slow release starch, 83% entered the blood stream for consistency with the experimental data.*

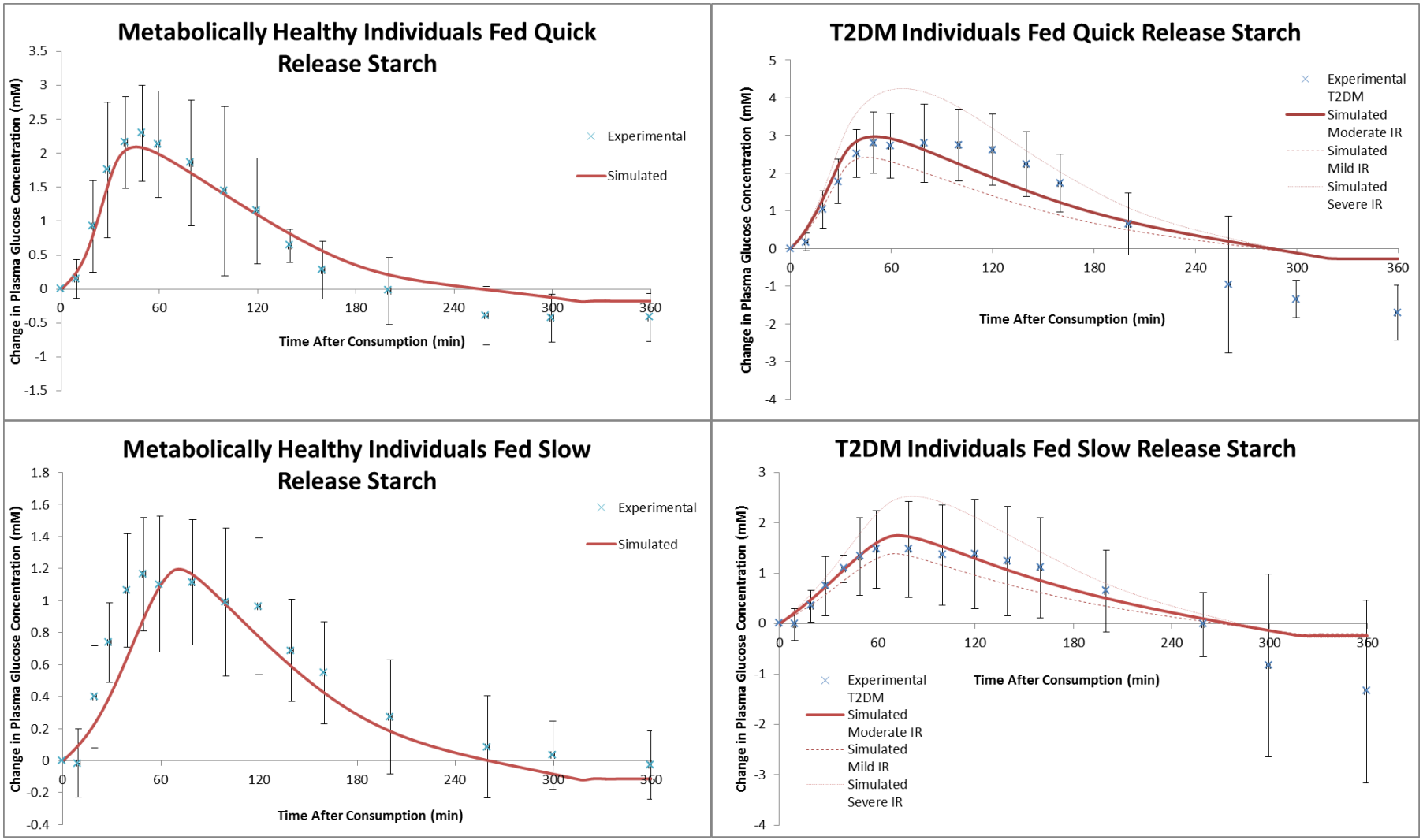

Figure S1.7: Comparison of simulated and experimentally measured glucose concentrations after slow and fast release starch intake. *The glucose concentration after intake of a (top) 50g of quick release starch and (bottom) 50g of slow release starch when measured experimentally by Seal et al. [453] and simulated by the model in (left) metabolically normal and (right) T2DM individuals.*

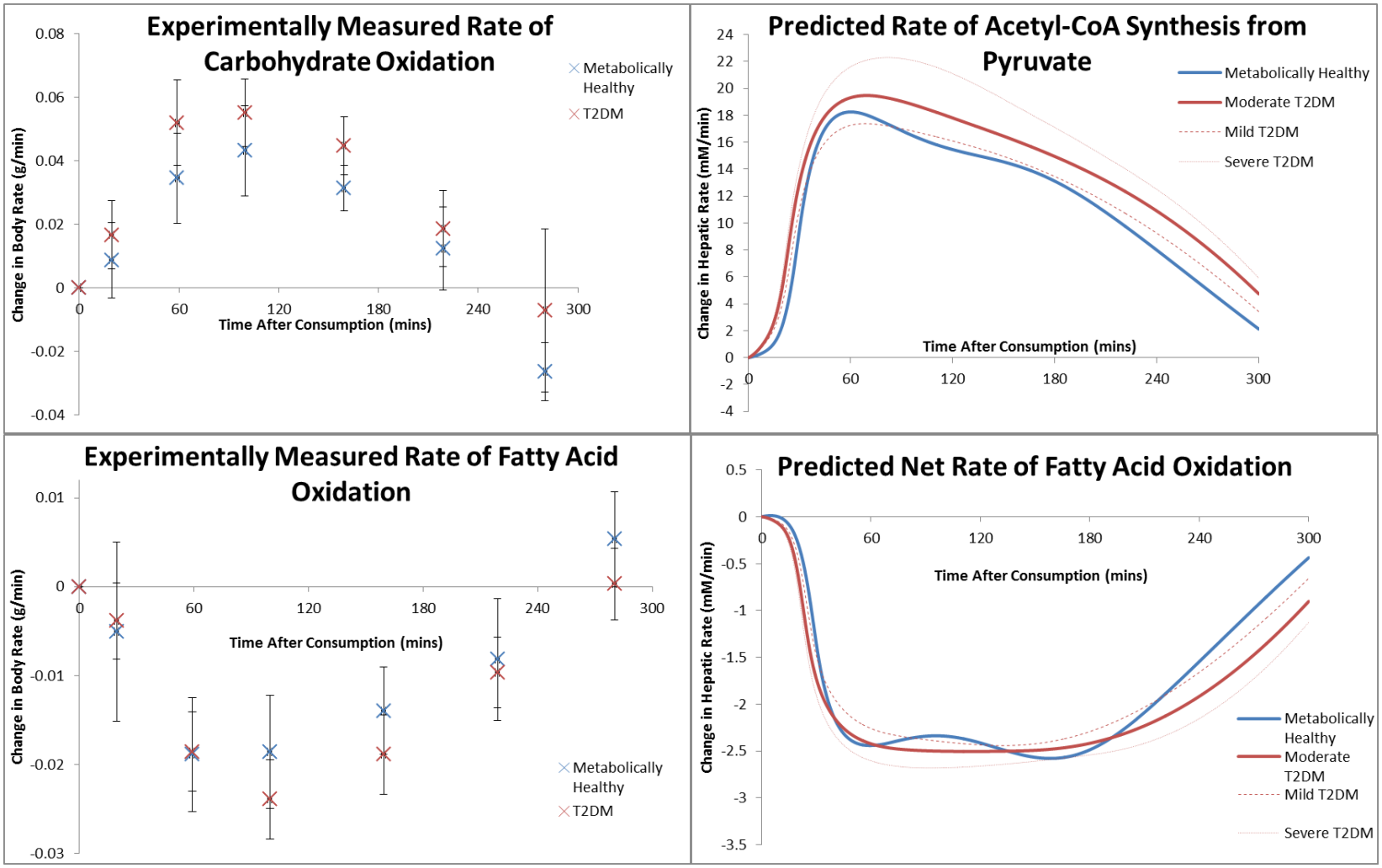

Figure S1.8: Simulated and experimentally measured rates of carbohydrate and fatty acid oxidation after intake of quick release carbohydrate. *The rates of oxidation of fatty acids and glucose in metabolically normal and T2DM individuals when (left) measured experimentally in the body as a whole by Seal et al. [453] and (right) when simulated in liver alone after intake of 50g of quick release starch as discussed in the text.*

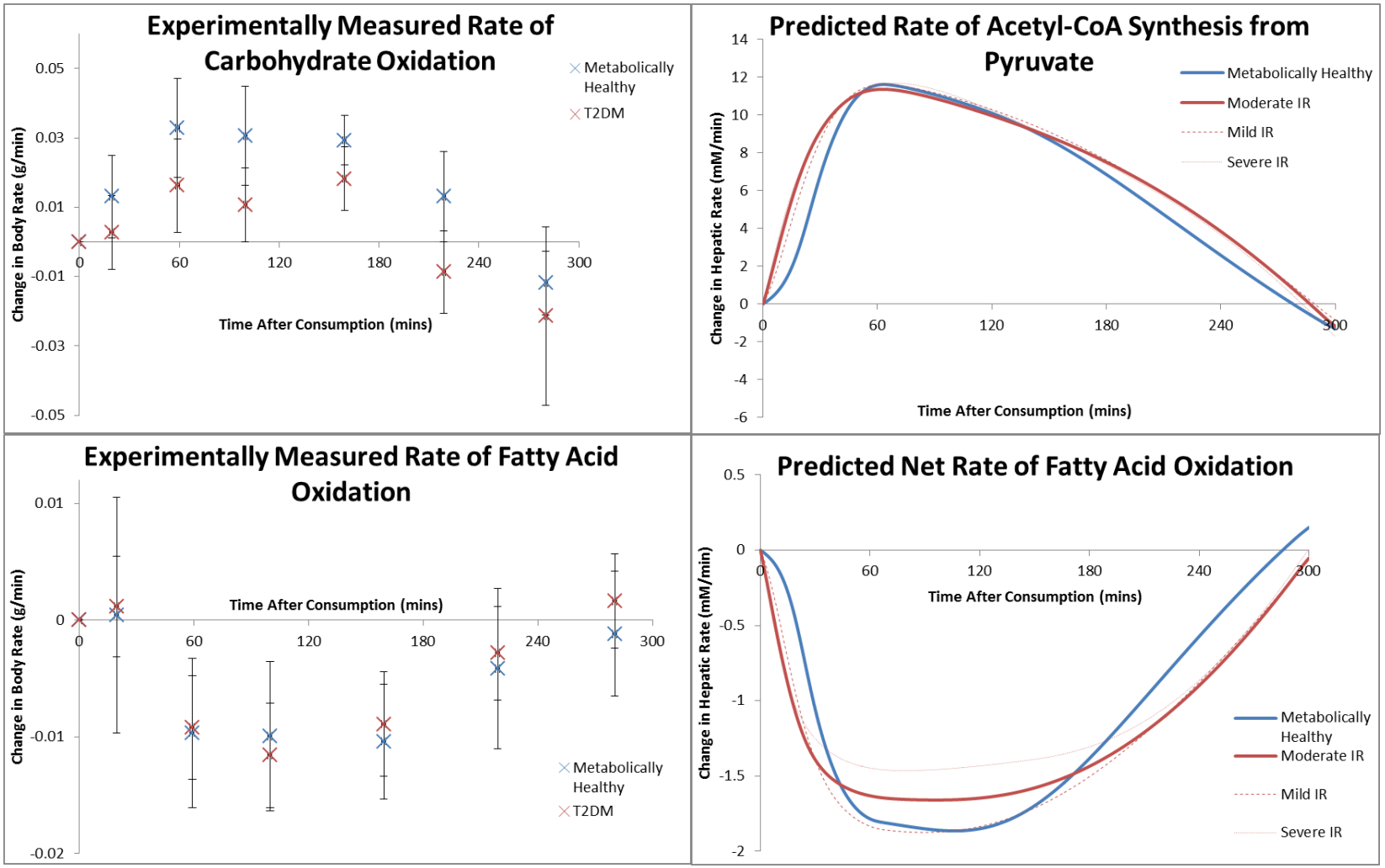

Figure S1.9: Simulated and experimentally measured rates of carbohydrate and fatty acid oxidation after intake of slow release carbohydrate. *The rates of oxidation of fatty acids and glucose in metabolically normal and T2DM individuals when (left) measured experimentally in the body as a whole by Seal et al. [453] and (right) when simulated in liver alone after intake of 50g of slow release starch as discussed in the text. Error bars in experimental data are SEM rather than SD with n=8 for metabolically normal and n=13 for T2DM.*

S2 Determining Treatment Concentrations

S2.1 Assessing treatment concentration ranges using an MTS assay

To determine an approximate range of appropriate treatment concentrations, an MTS assay was used to assess the effects of a range of concentrations on cell viability after 48 hours. The MTS assay allows rapid measurement of viability for a range of different treatments, but is associated with fairly large variation in the readings. Note also that only one independent repeat of this experiment was performed and the numbers stated in the graphs are for technical replicates (in this section only). As a result, the statistical significances presented in this section are only applicable to the particular cells used under the exact conditions tested. Therefore, once appropriate treatment concentrations were determined through the MTS assay, the effect of these treatments on viability were validated with a trypan blue exclusion assay (see section S2.2). The tested ranges were based on ranges of effect and toxicity published in the literature (TOFA [579, 611-613], C75 [617-619], T863 [585, 620], 2DG [603, 621], 3BP [622, 623]).

20µg/ml and 40µg/ml TOFA significantly reduced cell viability whilst 10µg/ml caused non-significant decrease (figure S2.1a). No significant changes in cell numbers were seen for concentrations of 5µg/ml or lower. This suggest that TOFA is less toxic to HepG2 cells than other cancer derived lines such as lung and colon cancer cells in which 1µg/ml of TOFA caused cell death [614]. Similarly, treatment with 20µg/ml or higher caused a significant decrease in cell viability whilst 10µg/ml C75 caused a non-significant decrease (figure S2.1b). No significant change in viability was noted for lower concentrations.

a)

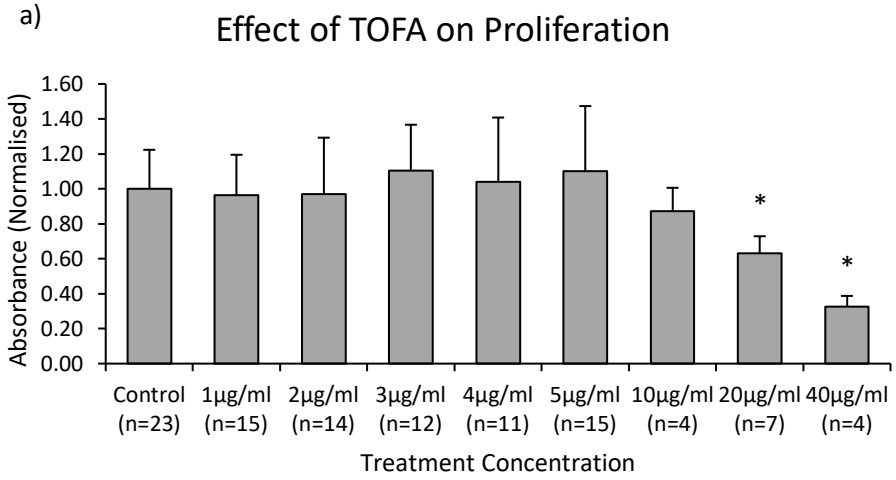
Effect of TOFA on Proliferation
Absorbance (Normalised)
1.60
1.40
1.20
1.00
0.80
0.60
0.40
0.20
0.00
*
*
Control (n=23)
1µg/ml (n=15)
2µg/ml (n=14)
3µg/ml (n=12)
4µg/ml (n=11)
5µg/ml (n=15)
10µg/ml (n=4)
20µg/ml (n=7)
40µg/ml (n=4)
Treatment Concentration

b)

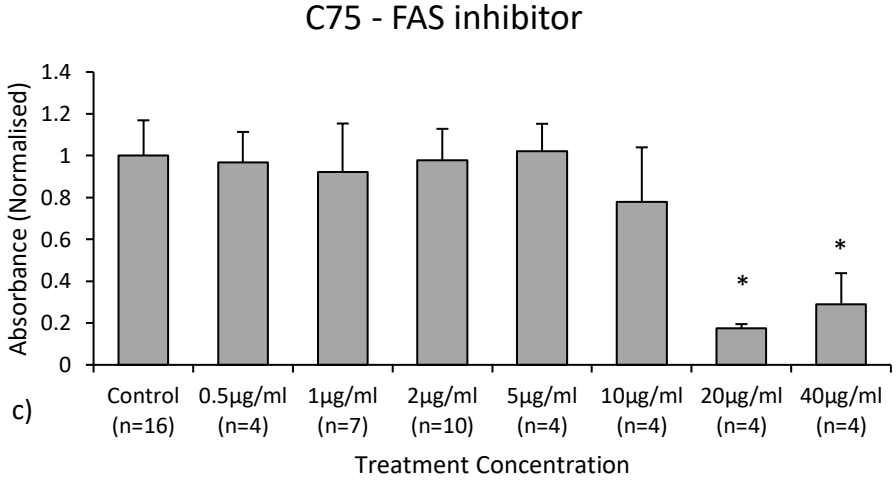
C75 - FAS inhibitor
Absorbance (Normalised)
1.4
1.2
1
0.8
0.6
0.4
0.2
0
*
*
Control (n=16)
0.5µg/ml (n=4)
1µg/ml (n=7)
2µg/ml (n=10)
5µg/ml (n=4)
10µg/ml (n=4)
20µg/ml (n=4)
40µg/ml (n=4)
Treatment Concentration

c)

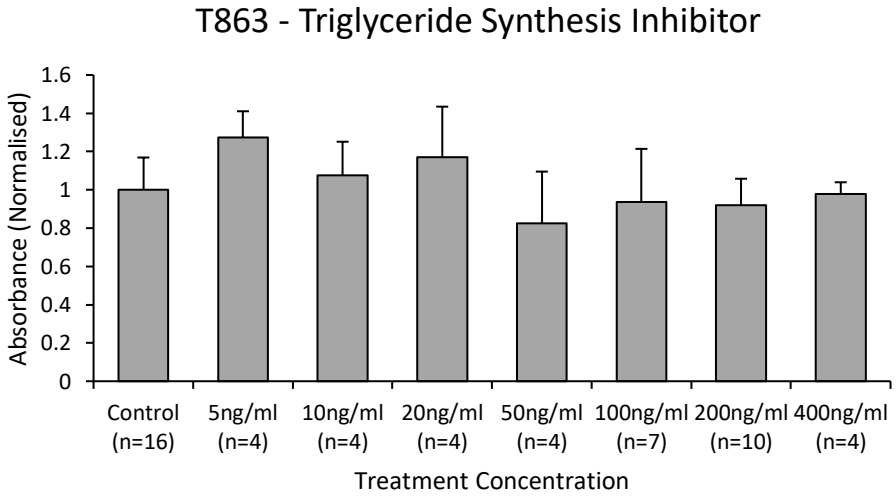
T863 - Triglyceride Synthesis Inhibitor
Absorbance (Normalised)
1.6
1.4
1.2
1
0.8
0.6
0.4
0.2
0
Control (n=16)
5ng/ml (n=4)
10ng/ml (n=4)
20ng/ml (n=4)
50ng/ml (n=4)
100ng/ml (n=7)
200ng/ml (n=10)
400ng/ml (n=4)
Treatment Concentration

d)

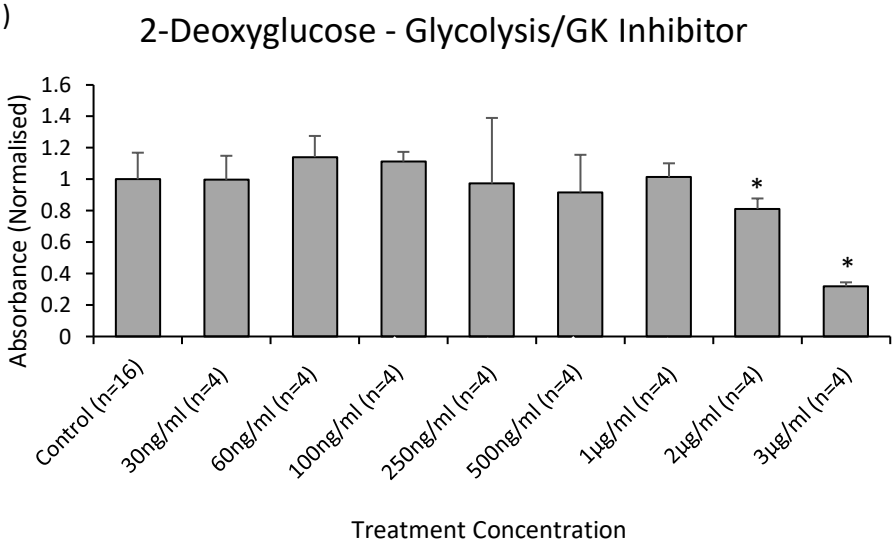

e)

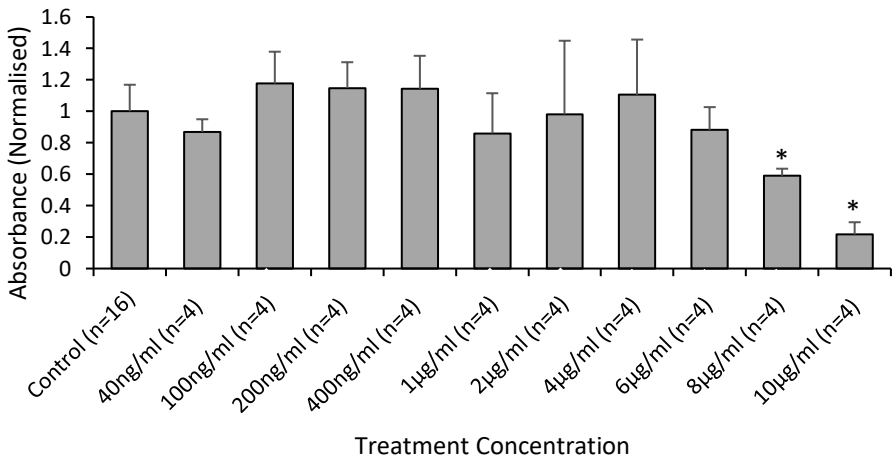

Figure S2.1: The effct of varying concentrations of TOFA, C75, T863, 2DG and 3BP on cell viability of 48 hours of treatment as assessed by the MTS assay. *The effect of varying concentrations of (a) TOFA, (b) C75, (c) T863, (d) 2-DG and (e) 3-BP on cell numbers of 48 hours of treatment as assessed by the MTS assay (section 5.2.4.1). Note that the number of repeats shown on the axes of the graphs are technical replicates and not independent repeats. Only one independent repeat was performed. Furthermore, the statistics calculations were based on these technical replicates. As a result, the data in these graphs were only used to determine approximate treatment ranges before validating these in a second trypan exclusion assay. The statistical significances of the differences calculated can only be considered to show a statistically significant change for the specific cells used under the exact conditions tested. * - p<0.05 compared with control. ±SD*

No significant change in MTS reading occurred for the range of T863 concentrations assessed (5ng/ml-400ng/ml) (figure S2.1c). Therefore, in the range measured, partial inhibition of DGAT1 by T863 did not cause a reduction in cell viability. On observation of the cells by eye, a clear reduction in lipid droplets was noted for treatments in the range 100-400ng/ml demonstrating that partial triglyceride

synthesis inhibition was occurring in this range (the effects of T863, along with the other treatments, on hepatic lipid levels is assessed in section 5.3.2).

3BP concentrations up to 6mg/ml caused no significant change in MTS reading (figure S2.1e). However, a significant decrease was measured when treating with 8µg/ml or higher. Treatment with 2µg/ml or higher 2DG significantly reduced the MTS reading, whilst lower concentrations did not significantly change the readings (figure S2.1d). Therefore, consistent with expectation for a cell culture line derived from hepatocellular carcinoma, inhibition of glycolysis above a certain threshold at either stage causes a reduction in the number of viable cells. However, below this, cells remained viable.

Treatment concentrations were selected below the concentrations at which reduced viability was measured in the MTS assay. For TOFA treatments concentrations of 2µg/ml and 4µg/ml were used. For C75, treatment concentrations of 1µg/ml and 2µg/ml were used. In both cases these test concentrations are well below the 20µg/ml concentration at which significant reductions in viability were measured by the MTS assay. For T863, treatment concentrations of 100ng/ml and 200ng/ml were tested. No change in viability occurred with T863 treatment in FA free medium (0-400ng/ml) but a reduction in the presence of lipid droplets was observed at 100ng/ml and 200ng/ml (quantitative assessment of the effects of T863 on steatosis is performed in section 5.3.2). For 2DG, treatment concentrations of 250ng/ml and 500ng/ml were used, corresponding to $^1/_8$ and $^1/_4$ of the 2µg/ml concentration at which a reduction in viability was measured. Similarly, for 3BP treatment concentrations of 1µg/ml and 2µg/ml were tested corresponding to $^1/_8$ and $^1/_4$ of the 8µg/ml concentration at which a reduction in viability was measured.

S2.2 Validation of treatment concentrations using a trypan blue exclusion assay

Due the lack of independent repeats of the MTS data, the impact of each treatment concentration on cell viability was next validated in a second trypan blue exclusion assay (figure S2.2). Consistent

with the MTS data, none of the proposed treatment concentrations caused a significant reduction in cell numbers at 48 hours. However, when the cells were treated with 2DG, nonsignificant decreases were seen in the number of viable cells for both 250ng/ml (1.81±0.15 (n=3) vs control: 2.02±0.07 (n=9); p=0.13) and 500ng/ml (1.85±0.19 (n=3); p=0.15) suggesting that at these concentrations, 2DG may cause a reduction in viable cells. However, this is small relative to the FFA induced cell death discussed in section 5.3.

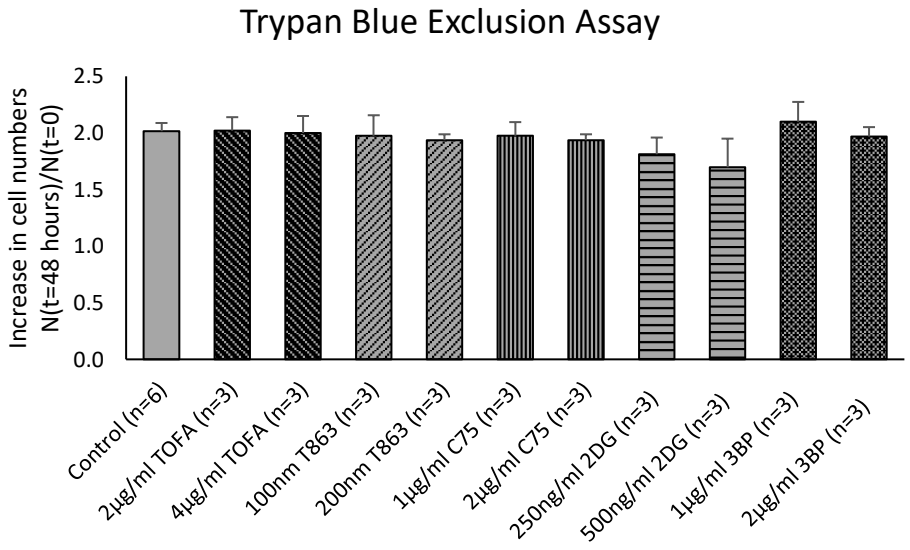

Figure S2.2: The effects of treatment concentrations for each inhibitor on viable HepG2 cell numbers. *The effects of the two treatment concentrations for each inhibitor (TOFA, T863, C75, 2DG and 3BP) on viable. HepG2 cell numbers after 48 hours of treatment as assessed by a trypan blue exclusion assay (section 5.2.4.4). The n numbers shown in the axes correspond to numbers of independent replicates. The mean ±SD is shown.*

References

1. UK, D., http://www.diabetes.org.uk/Documents/Reports/Diabetes_in_the_UK_2010.pdf. 2010.
2. UK, D., http://www.diabetes.org.uk/Guide-to-diabetes/What-is-diabetes/. 2013.
3. Mainous, A.G., 3rd, et al., *Prevalence of prediabetes in England from 2003 to 2011: population-based, cross-sectional study.* BMJ Open, 2014. **4**(6): p. e005002.
4. American Diabetes, A., *National Diabetes Statistics Report.* 2014.
5. OECD, *Health at a Glance: Europe 2014.* 2014.
6. NHS, *NHS Choices: Non-alcoholic fatty liver disease* http://www.nhs.uk/Conditions/fatty-liver-disease/Pages/Introduction.aspx, 2014.
7. McCullough, A.J., *The clinical features, diagnosis and natural history of nonalcoholic fatty liver disease.* Clin Liver Dis, 2004. **8**(3): p. 521-33, viii.
8. Byrne, C.D. and G. Targher, *NAFLD: a multisystem disease.* J Hepatol, 2015. **62**(1 Suppl): p. S47-64.

9. Ertle, J., et al., *Non-alcoholic fatty liver disease progresses to hepatocellular carcinoma in the absence of apparent cirrhosis.* Int J Cancer, 2011. **128**(10): p. 2436-43.
10. Starley, B.Q., C.J. Calcagno, and S.A. Harrison, *Nonalcoholic fatty liver disease and hepatocellular carcinoma: a weighty connection.* Hepatology, 2010. **51**(5): p. 1820-32.
11. Stickel, F. and C. Hellerbrand, *Non-alcoholic fatty liver disease as a risk factor for hepatocellular carcinoma: mechanisms and implications.* Gut, 2010. **59**(10): p. 1303-7.
12. Musso, G., et al., *Meta-analysis: natural history of non-alcoholic fatty liver disease (NAFLD) and diagnostic accuracy of non-invasive tests for liver disease severity.* Ann Med, 2011. **43**(8): p. 617-49.
13. Musso, G., et al., *Association of non-alcoholic fatty liver disease with chronic kidney disease: a systematic review and meta-analysis.* PLoS Med, 2014. **11**(7): p. e1001680.
14. Musso, G., et al., *Association of obstructive sleep apnoea with the presence and severity of non-alcoholic fatty liver disease. A systematic review and meta-analysis.* Obes Rev, 2013. **14**(5): p. 417-31.
15. Chalasani, N., et al., *Relationship of steatosis grade and zonal location to histological features of steatohepatitis in adult patients with non-alcoholic fatty liver disease.* J Hepatol, 2008. **48**(5): p. 829-34.
16. Brunt, E.M., *Pathology of fatty liver disease.* Mod Pathol, 2007. **20 Suppl 1**: p. S40-8.
17. Hijmans, B.S., et al., *Zonation of glucose and fatty acid metabolism in the liver: Mechanism and metabolic consequences.* Biochimie, 2014. **96**.
18. Bellentani, S., et al., *Prevalence of and risk factors for hepatic steatosis in Northern Italy.* Ann Intern Med, 2000. **132**(2): p. 112-7.
19. Kumar, V., et al., *Robbins and Cotran pathologic basis of disease*. 7th ed. 2005, Philadelphia: Elsevier Saunders. xv, 1525 p.
20. Arias, B., Fausto, Jakoby, Schachter, Shafritz, *The Liver Biology and Pathology*. Third Edition ed. 1994, New York: Raven Press.
21. Rappaport, A.M., *The microcirculatory acinar concept of normal and pathological hepatic structure.* Beitr Pathol, 1976. **157**(3): p. 215-43.
22. Kmiec, Z., *Cooperation of liver cells in health and disease.* Adv Anat Embryol Cell Biol, 2001. **161**: p. III-XIII, 1-151.
23. Bataller, R. and D.A. Brenner, *Liver fibrosis.* J Clin Invest, 2005. **115**(2): p. 209-18.
24. Jungermann, K. and T. Kietzmann, *Oxygen: modulator of metabolic zonation and disease of the liver.* Hepatology, 2000. **31**(2): p. 255-60.
25. Haussinger, D., *Regulation of hepatic ammonia metabolism: the intercellular glutamine cycle.* Adv Enzyme Regul, 1986. **25**: p. 159-80.
26. Donnelly, K.L., et al., *Sources of fatty acids stored in liver and secreted via lipoproteins in patients with nonalcoholic fatty liver disease.* J Clin Invest, 2005. **115**(5): p. 1343-51.
27. Falcon, A., et al., *FATP2 is a hepatic fatty acid transporter and peroxisomal very long-chain acyl-CoA synthetase.* American Journal of Physiology-Endocrinology and Metabolism, 2010. **299**(3): p. E384-E393.
28. Doege, H., et al., *Targeted deletion of FATP5 reveals multiple functions in liver metabolism: Alterations in hepatic lipid Homeostasis.* Gastroenterology, 2006. **130**(4): p. 1245-1258.
29. Mashek, D.G., *Hepatic fatty acid trafficking: multiple forks in the road.* Adv Nutr, 2013. **4**(6): p. 697-710.
30. Koonen, D.P.Y., et al., *Increased hepatic CD36 expression contributes to dyslipidemia associated with diet-induced obesity.* Diabetes, 2007. **56**(12): p. 2863-2871.
31. Greco, D., et al., *Gene expression in human NAFLD.* American Journal of Physiology-Gastrointestinal and Liver Physiology, 2008. **294**(5): p. G1281-G1287.
32. Mitsuyoshi, H., et al., *Analysis of hepatic genes involved in the metabolism of fatty acids and iron in nonalcoholic fatty liver disease.* Hepatology Research, 2009. **39**(4): p. 366-373.

33. Newberry, E.P., et al., *Decreased hepatic triglyceride accumulation and altered fatty acid uptake in mice with deletion of the liver fatty acid-binding protein gene.* Journal of Biological Chemistry, 2003. **278**(51): p. 51664-51672.
34. Kersten, S., *Mechanisms of nutritional and hormonal regulation of lipogenesis.* EMBO Rep, 2001. **2**(4): p. 282-6.
35. Beynen, A.C., W.J. Vaartjes, and M.J. Geelen, *Opposite effects of insulin and glucagon in acute hormonal control of hepatic lipogenesis.* Diabetes, 1979. **28**(9): p. 828-35.
36. Shimomura, I., Y. Bashmakov, and J.D. Horton, *Increased levels of nuclear SREBP-1c associated with fatty livers in two mouse models of diabetes mellitus.* J Biol Chem, 1999. **274**(42): p. 30028-32.
37. Browning, J.D. and J.D. Horton, *Molecular mediators of hepatic steatosis and liver injury.* J Clin Invest, 2004. **114**(2): p. 147-52.
38. Sanders, F.W. and J.L. Griffin, *De novo lipogenesis in the liver in health and disease: more than just a shunting yard for glucose.* Biol Rev Camb Philos Soc, 2016. **91**(2): p. 452-68.
39. Kohjima, M., et al., *SREBP-1c, regulated by the insulin and AMPK signaling pathways, plays a role in nonalcoholic fatty liver disease.* Int J Mol Med, 2008. **21**(4): p. 507-11.
40. Gunstone, F.D.H., J. L.; Dijkstra, A. J., *The Lipid Handbook with Cd-Rom. 3rd ed. Boca Raton: CRC Press ISBN 0849396883 | ISBN 978-0849396885.* 2007.
41. Kingsbury, K.J., et al., *The fatty acid composition of human depot fat.* Biochem J, 1961. **78**: p. 541-50.
42. Malcom, G.T., et al., *Fatty acid composition of adipose tissue in humans: differences between subcutaneous sites.* Am J Clin Nutr, 1989. **50**(2): p. 288-91.
43. Wendel, A.A., T.M. Lewin, and R.A. Coleman, *Glycerol-3-phosphate acyltransferases: rate limiting enzymes of triacylglycerol biosynthesis.* Biochim Biophys Acta, 2009. **1791**(6): p. 501-6.
44. Alves, T.C., et al., *Regulation of hepatic fat and glucose oxidation in rats with lipid-induced hepatic insulin resistance.* Hepatology, 2011. **53**(4): p. 1175-81.
45. Jungermann, K. and N. Katz, *Functional specialization of different hepatocyte populations.* Physiol Rev, 1989. **69**(3): p. 708-64.
46. Loud, A.V., *A quantitative stereological description of the ultrastructure of normal rat liver parenchymal cells.* J Cell Biol, 1968. **37**(1): p. 27-46.
47. Wimmer, M. and D. Pette, *Microphotometric studies on intraacinar enzyme distribution in rat liver.* Histochemistry, 1979. **64**(1): p. 23-33.
48. Novikoff, A.B., *Cell Heterogeneity within the Hepatic Lobule of the Rat (Staining Reactions).* Journal of Histochemistry & Cytochemistry, 1959. **7**(4): p. 240-244.
49. Chance, B., H. Sies, and A. Boveris, *Hydroperoxide metabolism in mammalian organs.* Physiol Rev, 1979. **59**(3): p. 527-605.
50. Jungermann, K. and T. Kietzmann, *Role of oxygen in the zonation of carbohydrate metabolism and gene expression in liver.* Kidney Int, 1997. **51**(2): p. 402-12.
51. Kudryavtseva, M.V., et al., *The metabolic zonation of glycogen synthesis in rat liver after fasting and refeeding.* Tissue Cell, 1992. **24**(1): p. 31-5.
52. Katz, N., et al., *Heterogeneous reciprocal localization of fructose-1,6-bisphosphatase and of glucokinase in microdissected periportal and perivenous rat liver tissue.* FEBS Lett, 1977. **83**(2): p. 272-6.
53. Lawrence, G.M., et al., *The compartmentation of glycolytic and gluconeogenic enzymes in rat kidney and liver and its significance to renal and hepatic metabolism.* Histochem J, 1986. **18**(1): p. 45-53.
54. Lawrence, G.M., I.P. Trayer, and D.G. Walker, *Histochemical and immunohistochemical localization of hexokinase isoenzymes in normal rat liver.* Histochem J, 1984. **16**(10): p. 1099-111.

55. Fischer, W., M. Ick, and N.R. Katz, *Reciprocal distribution of hexokinase and glucokinase in the periportal and perivenous zone of the rat liver acinus.* Hoppe Seylers Z Physiol Chem, 1982. **363**(4): p. 375-80.
56. Teutsch, H.F. and O.H. Lowry, *Sex specific regional differences in hepatic glucokinase activity.* Biochem Biophys Res Commun, 1982. **106**(2): p. 533-8.
57. Trus, M., et al., *Hexokinase and glucokinase distribution in the liver lobule.* J Histochem Cytochem, 1980. **28**(6): p. 579-81.
58. Eilers, F., H. Bartels, and K. Jungermann, *Zonal expression of the glucokinase gene in rat liver. Dynamics during the daily feeding rhythm and starvation-refeeding cycle demonstrated by in situ hybridization.* Histochemistry, 1993. **99**(2): p. 133-40.
59. Moorman, A.F., et al., *Pericentral expression pattern of glucokinase mRNA in the rat liver lobulus.* FEBS Lett, 1991. **287**(1-2): p. 47-52.
60. Kirchner, G., et al., *Zonation of glucokinase in rat liver changes during postnatal development.* FEBS Lett, 1993. **328**(1-2): p. 119-24.
61. Wals, P.A., M. Palacin, and J. Katz, *The zonation of liver and the distribution of fructose 2,6-bisphosphate in rat liver.* J Biol Chem, 1988. **263**(10): p. 4876-81.
62. Teutsch, H.F., *Quantitative determination of G6Pase activity in histochemically defined zones of the liver acinus.* Histochemistry, 1978. **58**(4): p. 281-8.
63. Katz, N., et al., *Heterogeneous distribution of glucose-6-phosphatase in microdissected periportal and perivenous rat liver tissue.* FEBS Lett, 1977. **76**(2): p. 226-30.
64. Royal-Free-Liver&Digestive-Health, *Unpublished Data.* 2013.
65. Frederiks, W.M., F. Marx, and C.J. Van Noorden, *Quantitative histochemical assessment of the heterogeneity of glycogen phosphorylase activity in liver parenchyma of fasted rats using the semipermeable membrane technique and the PAS reaction.* Histochem J, 1987. **19**(3): p. 150-6.
66. Giffin, B.F., et al., *Hepatic lobular patterns of phosphoenolpyruvate carboxykinase, glycogen synthase, and glycogen phosphorylase in fasted and fed rats.* J Histochem Cytochem, 1993. **41**(12): p. 1849-62.
67. Lamas, E., A. Kahn, and A. Guillouzo, *Detection of mRNAs present at low concentrations in rat liver by in situ hybridization: application to the study of metabolic regulation and azo dye hepatocarcinogenesis.* J Histochem Cytochem, 1987. **35**(5): p. 559-63.
68. Eilers, F., S. Modaressi, and K. Jungermann, *Predominant periportal expression of the fructose 1,6-bisphosphatase gene in rat liver: dynamics during the daily feeding rhythm and starvation-refeeding cycle.* Histochem Cell Biol, 1995. **103**(4): p. 293-300.
69. Nauck, M., et al., *Modulation of the glucagon-dependent induction of phosphoenolpyruvate carboxykinase and tyrosine aminotransferase by arterial and venous oxygen concentrations in hepatocyte cultures.* Eur J Biochem, 1981. **119**(3): p. 657-61.
70. Bartels, H., S. Freimann, and K. Jungermann, *Predominant periportal expression of the phosphoenolpyruvate carboxykinase gene in liver of fed and fasted mice, hamsters and rats studied by in situ hybridization.* Histochemistry, 1993. **99**(4): p. 303-9.
71. Bartels, H., H. Herbort, and K. Jungermann, *Predominant periportal expression of the phosphoenolpyruvate carboxykinase and tyrosine aminotransferase genes in rat liver. Dynamics during the daily feeding rhythm and starvation-refeeding cycle demonstrated by in situ hybridization.* Histochemistry, 1990. **94**(6): p. 637-44.
72. Bartels, H., H. Linnemann, and K. Jungermann, *Predominant localization of phosphoenolpyruvate carboxykinase mRNA in the periportal zone of rat liver parenchyma demonstrated by in situ hybridization.* FEBS Lett, 1989. **248**(1-2): p. 188-94.
73. Jones, C.G. and M.A. Titheradge, *Measurement of metabolic fluxes through pyruvate kinase, phosphoenolpyruvate carboxykinase, pyruvate dehydrogenase, and pyruvate carboxylate in hepatocytes of different acinar origin.* Arch Biochem Biophys, 1996. **326**(2): p. 202-6.

74. Chen, K.S. and J. Katz, *Zonation of glycogen and glucose syntheses, but not glycolysis, in rat liver.* Biochem J, 1988. **255**(1): p. 99-104.
75. Quistorff, B., *Gluconeogenesis in periportal and perivenous hepatocytes of rat liver, isolated by a new high-yield digitonin/collagenase perfusion technique.* Biochem J, 1985. **229**(1): p. 221-6.
76. Quistorff, B., J. Dich, and N. Grunnet, *Periportal and perivenous hepatocytes retain their zonal characteristics in primary culture.* Biochem Biophys Res Commun, 1986. **139**(3): p. 1055-61.
77. Wolfle, D. and K. Jungermann, *Long-term effects of physiological oxygen concentrations on glycolysis and gluconeogenesis in hepatocyte cultures.* Eur J Biochem, 1985. **151**(2): p. 299-303.
78. Lopez, C.H., et al., *Zonation of the action of ethanol on gluconeogenesis and ketogenesis studied in the bivascularly perfused rat liver.* Chem Biol Interact, 2009. **177**(2): p. 89-95.
79. Bartels, H., B. Vogt, and K. Jungermann, *Glycogen-Synthesis from Pyruvate in the Periportal and from Glucose in the Perivenous Zone in Perfused Livers from Fasted Rats.* Febs Letters, 1987. **221**(2): p. 277-283.
80. Nibourg, G.A., et al., *Liver progenitor cell line HepaRG differentiated in a bioartificial liver effectively supplies liver support to rats with acute liver failure.* PLoS One, 2012. **7**(6): p. e38778.
81. Katz, N.R., W. Fischer, and S. Giffhorn, *Distribution of enzymes of fatty acid and ketone body metabolism in periportal and perivenous rat-liver tissue.* Eur J Biochem, 1983. **135**(1): p. 103-7.
82. Morrison, G.R., et al., *Quantitative analysis of regenerating and degenerating areas within the lobule of the carbon tetrachloride-injured liver.* Arch Biochem Biophys, 1965. **111**(2): p. 448-60.
83. Guzman, M. and J. Castro, *Zonation of fatty acid metabolism in rat liver.* Biochem J, 1989. **264**(1): p. 107-13.
84. Bass, N.M., et al., *Acinar heterogeneity of fatty acid binding protein expression in the livers of male, female and clofibrate-treated rats.* Hepatology, 1989. **9**(1): p. 12-21.
85. Suzuki, T. and T. Ono, *Immunohistochemical studies on the distribution and frequency of fatty-acid-binding protein positive cells in human fetal, newborn and adult liver tissues.* J Pathol, 1987. **153**(4): p. 385-94.
86. Guzman, M. and J. Castro, *Zonal heterogeneity of the effects of chronic ethanol feeding on hepatic fatty acid metabolism.* Hepatology, 1990. **12**(5): p. 1098-105.
87. Guzman, M., C. Bijleveld, and M.J. Geelen, *Flexibility of zonation of fatty acid oxidation in rat liver.* Biochem J, 1995. **311 (Pt 3)**: p. 853-60.
88. Katz, N., J. Thiele, and S. Giffhorn-Katz, *Zonal distribution of fatty acid synthase in liver parenchyma of male and female rats.* Eur J Biochem, 1989. **180**(1): p. 185-9.
89. Katz, N.R., W. Fischer, and M. Ick, *Heterogeneous distribution of ATP citrate lyase in rat-liver parenchyma. Microradiochemical determination in microdissected periportal and perivenous liver tissue.* Eur J Biochem, 1983. **130**(2): p. 297-301.
90. Rieder, H., *NADP-dependent dehydrogenases in rat liver parenchyma. III. The description of a liponeogenic area on the basis of histochemically demonstrated enzyme activities and the neutral fat content during fasting and refeeding.* Histochemistry, 1981. **72**(4): p. 579-615.
91. Singer, II, et al., *Hydroxymethylglutaryl-coenzyme A reductase-containing hepatocytes are distributed periportally in normal and mevinolin-treated rat livers.* Proc Natl Acad Sci U S A, 1984. **81**(17): p. 5556-60.
92. Fitz, J.G., N.M. Bass, and R.A. Weisiger, *Hepatic transport of a fluorescent stearate derivative: electrochemical driving forces in intact rat liver.* Am J Physiol, 1991. **261**(1 Pt 1): p. G83-91.
93. Matsumura, T., et al., *O2 uptake in periportal and pericentral regions of liver lobule in perfused liver.* Am J Physiol, 1986. **250**(6 Pt 1): p. G800-5.

94. Kessler, M., J. Hoper, and B.A. Krumme, *Monitoring of tissue perfusion and cellular function.* Anesthesiology, 1976. **45**(2): p. 184-97.
95. Kietzmann, T., et al., *Regulation of the gluconeogenic phosphoenolpyruvate carboxykinase and glycolytic aldolase A gene expression by O2 in rat hepatocyte cultures. Involvement of hydrogen peroxide as mediator in the response to O2.* FEBS Lett, 1996. **388**(2-3): p. 228-32.
96. Lenart, J., et al., *Deficiency of manganese superoxide dismutase in hepatocytes disrupts zonated gene expression in mouse liver.* Arch Biochem Biophys, 2007. **462**(2): p. 238-44.
97. Miethke, H., et al., *Metabolic zonation in liver of diabetic rats. Zonal distribution of phosphoenolpyruvate carboxykinase, pyruvate kinase, glucose-6-phosphatase and succinate dehydrogenase.* Biol Chem Hoppe Seyler, 1985. **366**(5): p. 493-501.
98. Katz, N.R., M.A. Nauck, and P.T. Wilson, *Induction of glucokinase by insulin under the permissive action of dexamethasone in primary rat hepatocyte cultures.* Biochem Biophys Res Commun, 1979. **88**(1): p. 23-9.
99. Christ, B., et al., *Modulation of the glucagon-dependent induction of phosphoenolpyruvate carboxykinase by adenosine, but not ketone bodies or ammonia in rat hepatocyte cultures. Possible significance for the zonal heterogeneity of liver parenchyma.* Biol Chem Hoppe Seyler, 1987. **368**(12): p. 1579-87.
100. Christ, B., et al., *Regulation of the expression of the phosphoenolpyruvate carboxykinase gene in cultured rat hepatocytes by glucagon and insulin.* Eur J Biochem, 1988. **178**(2): p. 373-9.
101. Probst, I. and K. Jungermann, *The glucagon-insulin antagonism and glucagon-dexamethasone synergism in the induction of phosphoenolpyruvate carboxykinase in cultured rat hepatocytes.* Hoppe Seylers Z Physiol Chem, 1983. **364**(12): p. 1739-46.
102. England, P.H., http://fingertips.phe.org.uk/profile/liver-disease. 2016.
103. NHS, http://www.nhs.uk/Conditions/Liver-transplant/Pages/when-it-should-be-done.aspx. 2013.
104. NHS, http://www.organdonation.nhs.uk/about_transplants/waiting_time_to_transplant/index.asp. 2008-2011.
105. NHS, http://www.organdonation.nhs.uk/statistics/transplant_activity_report/current_activity_reports/ukt/liver_activity.pdf. 2012-2013.
106. Rinella, M.E., *Nonalcoholic fatty liver disease: a systematic review.* JAMA, 2015. **313**(22): p. 2263-73.
107. Maher, J.J., *Alcoholic steatosis and steatohepatitis.* Semin Gastrointest Dis, 2002. **13**(1): p. 31-9.
108. Ekstedt, M., et al., *Long-term follow-up of patients with NAFLD and elevated liver enzymes.* Hepatology, 2006. **44**(4): p. 865-73.
109. Cash, W.J., et al., *Current concepts in the assessment and treatment of hepatic encephalopathy.* QJM, 2010. **103**(1): p. 9-16.
110. Sakhuja, P., *Pathology of alcoholic liver disease, can it be differentiated from nonalcoholic steatohepatitis?* World J Gastroenterol, 2014. **20**(44): p. 16474-9.
111. Craig, D.G.N., Lee, A., Hayes, P. C. & Simpson, K. J., *Review article: the current management of acute liver failure.* Alimentary Pharmacology & Therapeutics,, 2010. **31** p. 345-358.
112. Laleman, W., et al., *Acute-on-chronic liver failure: current concepts on definition, pathogenesis, clinical manifestations and potential therapeutic interventions.* Expert Rev Gastroenterol Hepatol, 2011. **5**(4): p. 523-37; quiz 537.
113. Stadlbauer, V., G.A. Wright, and R. Jalan, *Role of artificial liver support in hepatic encephalopathy.* Metab Brain Dis, 2009. **24**(1): p. 15-26.

114. Organisation, W.H., *"Definition, Diagnosis and Classification of Diabetes Mellitus and its Complications".* 1999.
115. van Belle, T.L., K.T. Coppieters, and M.G. von Herrath, *Type 1 diabetes: etiology, immunology, and therapeutic strategies.* Physiol Rev, 2011. **91**(1): p. 79-118.
116. Prasad, R.B. and L. Groop, *Genetics of type 2 diabetes-pitfalls and possibilities.* Genes (Basel), 2015. **6**(1): p. 87-123.
117. Consensus, I., http://www.idf.org/webdata/docs/IDF_Meta_def_final.pdf.
118. Expert Panel on Detection, E. and A. Treatment of High Blood Cholesterol in, *Executive Summary of The Third Report of The National Cholesterol Education Program (NCEP) Expert Panel on Detection, Evaluation, And Treatment of High Blood Cholesterol In Adults (Adult Treatment Panel III).* JAMA, 2001. **285**(19): p. 2486-97.
119. Grundy, S.M., et al., *Definition of metabolic syndrome: report of the National Heart, Lung, and Blood Institute/American Heart Association conference on scientific issues related to definition.* Arterioscler Thromb Vasc Biol, 2004. **24**(2): p. e13-8.
120. Grundy, S.M., et al., *Diagnosis and management of the metabolic syndrome: an American Heart Association/National Heart, Lung, and Blood Institute Scientific Statement.* Circulation, 2005. **112**(17): p. 2735-52.
121. Ford, E.S., W.H. Giles, and W.H. Dietz, *Prevalence of the metabolic syndrome among US adults - Findings from the Third National Health and Nutrition Examination Survey.* Jama-Journal of the American Medical Association, 2002. **287**(3): p. 356-359.
122. Kahn, R., *Metabolic syndrome - what is the clinical usefulness?* Lancet, 2008. **371**(9628): p. 1892-1893.
123. Citrome, L., R.I.G. Holt, and T.G. Dinan, *The metabolic syndrome: Time for a critical appraisal: Joint statement from the American Diabetes Association and the European, Association for the Study of Diabetes - Response to Kahn et al.* Diabetes Care, 2006. **29**(1): p. 176-176.
124. Browning, J.D., et al., *Prevalence of hepatic steatosis in an urban population in the United States: impact of ethnicity.* Hepatology, 2004. **40**(6): p. 1387-95.
125. Blachier, M., et al., *The burden of liver disease in Europe: A review of available epidemiological data.* Journal of Hepatology, 2013. **58**(3): p. 593-608.
126. Bellentani, S., et al., *Epidemiology of Non-Alcoholic Fatty Liver Disease.* Digestive Diseases, 2010. **28**(1): p. 155-161.
127. Lavine, J.E. and J.B. Schwimmer, *Nonalcoholic fatty liver disease in the pediatric population.* Clin Liver Dis, 2004. **8**(3): p. 549-58, viii-ix.
128. Clark, J.M. and A.M. Diehl, *Nonalcoholic fatty liver disease: an underrecognized cause of cryptogenic cirrhosis.* JAMA, 2003. **289**(22): p. 3000-4.
129. Vos, B., et al., *Lean non-alcoholic fatty liver disease (Lean-NAFLD): a major cause of cryptogenic liver disease.* Acta Gastroenterol Belg, 2011. **74**(3): p. 389-94.
130. Charlton, M.R., et al., *Frequency and outcomes of liver transplantation for nonalcoholic steatohepatitis in the United States.* Gastroenterology, 2011. **141**(4): p. 1249-53.
131. Almeda-Valdes, P., D. Cuevas-Ramos, and C.A. Aguilar-Salinas, *Metabolic syndrome and non-alcoholic fatty liver disease.* Ann Hepatol, 2009. **8 Suppl 1**: p. S18-24.
132. Manchanayake, J., et al., *Postprandial hyperinsulinemia is universal in non-diabetic patients with nonalcoholic fatty liver disease.* Journal of Gastroenterology and Hepatology, 2011. **26**(3): p. 510-516.
133. Tolman, K.G., et al., *Spectrum of liver disease in type 2 diabetes and management of patients with diabetes and liver disease.* Diabetes Care, 2007. **30**(3): p. 734-43.
134. Kotronen, A. and H. Yki-Jarvinen, *Fatty liver - A novel component of the metabolic syndrome.* Arteriosclerosis Thrombosis and Vascular Biology, 2008. **28**(1): p. 27-38.
135. Kessoku, T., et al., *Insulin resistance correlated with the severity of liver histology in Japanese NAFLD patients: a multicenter retrospective study.* J Clin Gastroenterol, 2015. **49**(2): p. 169-70.

136. Kalra, S., et al., *Study of prevalence of nonalcoholic fatty liver disease (NAFLD) in type 2 diabetes patients in India (SPRINT).* J Assoc Physicians India, 2013. **61**(7): p. 448-53.
137. Prashanth, M., et al., *Prevalence of nonalcoholic fatty liver disease in patients with type 2 diabetes mellitus.* J Assoc Physicians India, 2009. **57**: p. 205-10.
138. Blachier, M., et al., *The burden of liver disease in Europe: a review of available epidemiological data.* J Hepatol, 2013. **58**(3): p. 593-608.
139. Reaven, G.M., et al., *Measurement of plasma glucose, free fatty acid, lactate, and insulin for 24 h in patients with NIDDM.* Diabetes, 1988. **37**(8): p. 1020-4.
140. Manco, M., et al., *Insulin resistance directly correlates with increased saturated fatty acids in skeletal muscle triglycerides.* Metabolism, 2000. **49**(2): p. 220-4.
141. Sindelka, G., et al., *Association of obesity, diabetes, serum lipids and blood pressure regulates insulin action.* Physiol Res, 2002. **51**(1): p. 85-91.
142. Jocken, J.W., et al., *Insulin-mediated suppression of lipolysis in adipose tissue and skeletal muscle of obese type 2 diabetic men and men with normal glucose tolerance.* Diabetologia, 2013. **56**(10): p. 2255-65.
143. Guilherme, A., et al., *Adipocyte dysfunctions linking obesity to insulin resistance and type 2 diabetes.* Nat Rev Mol Cell Biol, 2008. **9**(5): p. 367-77.
144. Zoppini, G., et al., *Mortality from chronic liver diseases in diabetes.* Am J Gastroenterol, 2014. **109**(7): p. 1020-5.
145. Marchesini, G. and A. Mazzotti, *NAFLD incidence and remission: Only a matter of weight gain and weight loss?* J Hepatol, 2015. **62**(1): p. 15-7.
146. Birkenfeld, A.L. and G.I. Shulman, *Nonalcoholic fatty liver disease, hepatic insulin resistance, and type 2 diabetes.* Hepatology, 2014. **59**(2): p. 713-23.
147. Kotronen, A., et al., *Liver fat is increased in type 2 diabetic patients and underestimated by serum alanine aminotransferase compared with equally obese nondiabetic subjects.* Diabetes Care, 2008. **31**(1): p. 165-9.
148. Church, T.S., et al., *Association of cardiorespiratory fitness, body mass index, and waist circumference to nonalcoholic fatty liver disease.* Gastroenterology, 2006. **130**(7): p. 2023-30.
149. Hsiao, T.J., J.C. Chen, and J.D. Wang, *Insulin resistance and ferritin as major determinants of nonalcoholic fatty liver disease in apparently healthy obese patients.* Int J Obes Relat Metab Disord, 2004. **28**(1): p. 167-72.
150. Kelley, D.E., et al., *Fatty liver in type 2 diabetes mellitus: relation to regional adiposity, fatty acids, and insulin resistance.* Am J Physiol Endocrinol Metab, 2003. **285**(4): p. E906-16.
151. Thamer, C., et al., *Intrahepatic lipids are predicted by visceral adipose tissue mass in healthy subjects.* Diabetes Care, 2004. **27**(11): p. 2726-9.
152. Kantartzis, K., et al., *The relationships of plasma adiponectin with a favorable lipid profile, decreased inflammation, and less ectopic fat accumulation depend on adiposity.* Clin Chem, 2006. **52**(10): p. 1934-42.
153. Wong, V.W., et al., *Incidence of non-alcoholic fatty liver disease in Hong Kong: A population study with paired proton-magnetic resonance spectroscopy.* J Hepatol, 2015. **62**(1): p. 182-9.
154. Suzuki, A., et al., *Effect of changes on body weight and lifestyle in nonalcoholic fatty liver disease.* J Hepatol, 2005. **43**(6): p. 1060-6.
155. Stefan, N., K. Kantartzis, and H.U. Haring, *Causes and metabolic consequences of Fatty liver.* Endocr Rev, 2008. **29**(7): p. 939-60.
156. Sadur, C.N., T.J. Yost, and R.H. Eckel, *Insulin responsiveness of adipose tissue lipoprotein lipase is delayed but preserved in obesity.* J Clin Endocrinol Metab, 1984. **59**(6): p. 1176-82.
157. Heilbronn, L., S.R. Smith, and E. Ravussin, *Failure of fat cell proliferation, mitochondrial function and fat oxidation results in ectopic fat storage, insulin resistance and type II diabetes mellitus.* Int J Obes Relat Metab Disord, 2004. **28 Suppl 4**: p. S12-21.

158. Roden, M., *Mechanisms of Disease: hepatic steatosis in type 2 diabetes--pathogenesis and clinical relevance.* Nat Clin Pract Endocrinol Metab, 2006. **2**(6): p. 335-48.
159. Montague, C.T. and S. O'Rahilly, *The perils of portliness: causes and consequences of visceral adiposity.* Diabetes, 2000. **49**(6): p. 883-8.
160. Lebovitz, H.E. and M.A. Banerji, *Point: visceral adiposity is causally related to insulin resistance.* Diabetes Care, 2005. **28**(9): p. 2322-5.
161. Harrison, S.A. and C.P. Day, *Benefits of lifestyle modification in NAFLD.* Gut, 2007. **56**(12): p. 1760-9.
162. Tilg, H. and A. Kaser, *Treatment strategies in nonalcoholic fatty liver disease.* Nat Clin Pract Gastroenterol Hepatol, 2005. **2**(3): p. 148-55.
163. Weisberg, S.P., et al., *Obesity is associated with macrophage accumulation in adipose tissue.* J Clin Invest, 2003. **112**(12): p. 1796-808.
164. Xu, H., et al., *Chronic inflammation in fat plays a crucial role in the development of obesity-related insulin resistance.* J Clin Invest, 2003. **112**(12): p. 1821-30.
165. Hotamisligil, G.S., *Inflammation and metabolic disorders.* Nature, 2006. **444**(7121): p. 860-7.
166. Trujillo, M.E. and P.E. Scherer, *Adipose tissue-derived factors: impact on health and disease.* Endocr Rev, 2006. **27**(7): p. 762-78.
167. Kadowaki, T. and T. Yamauchi, *Adiponectin and adiponectin receptors.* Endocr Rev, 2005. **26**(3): p. 439-51.
168. Lawlor, D.A., et al., *The associations of physical activity and adiposity with alanine aminotransferase and gamma-glutamyltransferase.* Am J Epidemiol, 2005. **161**(11): p. 1081-8.
169. Perseghin, G., et al., *Habitual physical activity is associated with intrahepatic fat content in humans.* Diabetes Care, 2007. **30**(3): p. 683-688.
170. O'Neill, H.M., *AMPK and Exercise: Glucose Uptake and Insulin Sensitivity.* Diabetes Metab J, 2013. **37**(1): p. 1-21.
171. Friedrichsen, M., et al., *Exercise-induced AMPK activity in skeletal muscle: role in glucose uptake and insulin sensitivity.* Mol Cell Endocrinol, 2013. **366**(2): p. 204-14.
172. Sui, X., et al., *Cardiorespiratory fitness and adiposity as mortality predictors in older adults.* JAMA, 2007. **298**(21): p. 2507-16.
173. Nguyen-Duy, T.B., et al., *Visceral fat and liver fat are independent predictors of metabolic risk factors in men.* Am J Physiol Endocrinol Metab, 2003. **284**(6): p. E1065-71.
174. Adams, L.A., et al., *A pilot trial of pentoxifylline in nonalcoholic steatohepatitis.* Am J Gastroenterol, 2004. **99**(12): p. 2365-8.
175. Kantartzis, K., et al., *High cardiorespiratory fitness is an independent predictor of the reduction in liver fat during a lifestyle intervention in non-alcoholic fatty liver disease.* Gut, 2009. **58**(9): p. 1281-8.
176. Stefan, N., K. Kantartzis, and H.U. Haring, *Cardiorespiratory fitness, adiposity, and mortality.* JAMA, 2008. **299**(9): p. 1013-4; author reply 1014.
177. Xu, C., et al., *Prevalence and risk factors for the development of nonalcoholic fatty liver disease in a nonobese Chinese population: the Zhejiang Zhenhai Study.* Am J Gastroenterol, 2013. **108**(8): p. 1299-304.
178. Younossi, Z.M., et al., *Nonalcoholic fatty liver disease in lean individuals in the United States.* Medicine (Baltimore), 2012. **91**(6): p. 319-27.
179. Kim, J.K., et al., *Mechanism of insulin resistance in A-ZIP/F-1 fatless mice.* J Biol Chem, 2000. **275**(12): p. 8456-60.
180. Gavrilova, O., et al., *Surgical implantation of adipose tissue reverses diabetes in lipoatrophic mice.* J Clin Invest, 2000. **105**(3): p. 271-8.
181. Greco, D., et al., *Gene expression in human NAFLD.* Am J Physiol Gastrointest Liver Physiol, 2008. **294**(5): p. G1281-7.

182. Fabbrini, E., et al., *Intrahepatic fat, not visceral fat, is linked with metabolic complications of obesity.* Proc Natl Acad Sci U S A, 2009. **106**(36): p. 15430-5.
183. Savage, D.B., et al., *Human metabolic syndrome resulting from dominant-negative mutations in the nuclear receptor peroxisome proliferator-activated receptor-gamma.* Diabetes, 2003. **52**(4): p. 910-7.
184. Matsusue, K., et al., *Liver-specific disruption of PPARgamma in leptin-deficient mice improves fatty liver but aggravates diabetic phenotypes.* J Clin Invest, 2003. **111**(5): p. 737-47.
185. Gavrilova, O., et al., *Liver peroxisome proliferator-activated receptor gamma contributes to hepatic steatosis, triglyceride clearance, and regulation of body fat mass.* J Biol Chem, 2003. **278**(36): p. 34268-76.
186. Akyuz, U., A. Yesil, and Y. Yilmaz, *Characterization of lean patients with nonalcoholic fatty liver disease: potential role of high hemoglobin levels.* Scand J Gastroenterol, 2015. **50**(3): p. 341-6.
187. Anstee, Q.M., D. Seth, and C.P. Day, *Genetic Factors That Affect Risk of Alcoholic and Nonalcoholic Fatty Liver Disease.* Gastroenterology, 2016. **150**(8): p. 1728-1744 e7.
188. Anstee, Q.M. and C.P. Day, *The Genetics of Nonalcoholic Fatty Liver Disease: Spotlight on PNPLA3 and TM6SF2.* Semin Liver Dis, 2015. **35**(3): p. 270-90.
189. Marzuillo, P., et al., *Understanding the pathophysiological mechanisms in the pediatric non-alcoholic fatty liver disease: The role of genetics.* World J Hepatol, 2015. **7**(11): p. 1439-43.
190. Liska, D., et al., *Interethnic differences in muscle, liver and abdominal fat partitioning in obese adolescents.* PLoS One, 2007. **2**(6): p. e569.
191. Johansson, L.E., et al., *Polymorphisms in the adiponutrin gene are associated with increased insulin secretion and obesity.* Eur J Endocrinol, 2008. **159**(5): p. 577-83.
192. Romeo, S., et al., *Genetic variation in PNPLA3 confers susceptibility to nonalcoholic fatty liver disease.* Nat Genet, 2008. **40**(12): p. 1461-5.
193. Kantartzis, K., et al., *Dissociation between fatty liver and insulin resistance in humans carrying a variant of the patatin-like phospholipase 3 gene.* Diabetes, 2009. **58**(11): p. 2616-23.
194. Ruhanen, H., et al., *PNPLA3 mediates hepatocyte triacylglycerol remodeling.* Journal of Lipid Research, 2014. **55**(4): p. 739-746.
195. Smagris, E., et al., *Inactivation of Tm6sf2, a Gene Defective in Fatty Liver Disease, Impairs Lipidation but Not Secretion of Very Low Density Lipoproteins.* J Biol Chem, 2016. **291**(20): p. 10659-76.
196. Mishra, S., et al., *Hyperinsulinemia predisposes to NAFLD.* Indian J Clin Biochem, 2008. **23**(2): p. 130-5.
197. Utzschneider, K.M. and S.E. Kahn, *Review: The role of insulin resistance in nonalcoholic fatty liver disease.* J Clin Endocrinol Metab, 2006. **91**(12): p. 4753-61.
198. Taskinen, M.R., *Diabetic dyslipidaemia: from basic research to clinical practice.* Diabetologia, 2003. **46**(6): p. 733-49.
199. Juurinen, L., et al., *Effects of insulin therapy on liver fat content and hepatic insulin sensitivity in patients with type 2 diabetes.* Am J Physiol Endocrinol Metab, 2007. **292**(3): p. E829-35.
200. Dentin, R., et al., *Liver-specific inhibition of ChREBP improves hepatic steatosis and insulin resistance in ob/ob mice.* Diabetes, 2006. **55**(8): p. 2159-70.
201. Bugianesi, E., et al., *Plasma adiponectin in nonalcoholic fatty liver is related to hepatic insulin resistance and hepatic fat content, not to liver disease severity.* Journal of Clinical Endocrinology & Metabolism, 2005. **90**(6): p. 3498-3504.
202. Lara-Castro, C., et al., *Adiponectin and the metabolic syndrome: mechanisms mediating risk for metabolic and cardiovascular disease.* Curr Opin Lipidol, 2007. **18**(3): p. 263-70.
203. Vasseur, F., D. Meyre, and P. Froguel, *Adiponectin, type 2 diabetes and the metabolic syndrome: lessons from human genetic studies.* Expert Rev Mol Med, 2006. **8**(27): p. 1-12.

204. Tomas, E., et al., *Enhanced muscle fat oxidation and glucose transport by ACRP30 globular domain: acetyl-CoA carboxylase inhibition and AMP-activated protein kinase activation.* Proc Natl Acad Sci U S A, 2002. **99**(25): p. 16309-13.
205. Yamauchi, T., et al., *Adiponectin stimulates glucose utilization and fatty-acid oxidation by activating AMP-activated protein kinase.* Nat Med, 2002. **8**(11): p. 1288-95.
206. Xu, A., et al., *The fat-derived hormone adiponectin alleviates alcoholic and nonalcoholic fatty liver diseases in mice.* J Clin Invest, 2003. **112**(1): p. 91-100.
207. Ukkola, O. and M. Santaniemi, *Adiponectin: a link between excess adiposity and associated comorbidities?* Journal of Molecular Medicine-Jmm, 2002. **80**(11): p. 696-702.
208. Polyzos, S.A., et al., *The role of adiponectin in the pathogenesis and treatment of non-alcoholic fatty liver disease.* Diabetes Obes Metab, 2010. **12**(5): p. 365-83.
209. Unger, R.H., *Minireview: weapons of lean body mass destruction: the role of ectopic lipids in the metabolic syndrome.* Endocrinology, 2003. **144**(12): p. 5159-65.
210. Petaja, E.M. and H. Yki-Jarvinen, *Definitions of Normal Liver Fat and the Association of Insulin Sensitivity with Acquired and Genetic NAFLD-A Systematic Review.* Int J Mol Sci, 2016. **17**(5).
211. Szczepaniak, L.S., et al., *Magnetic resonance spectroscopy to measure hepatic triglyceride content: prevalence of hepatic steatosis in the general population.* Am J Physiol Endocrinol Metab, 2005. **288**(2): p. E462-8.
212. Takahashi, Y. and T. Fukusato, *Histopathology of nonalcoholic fatty liver disease/nonalcoholic steatohepatitis.* World J Gastroenterol, 2014. **20**(42): p. 15539-48.
213. Chalasani, N., et al., *The diagnosis and management of non-alcoholic fatty liver disease: Practice guideline by the American Association for the Study of Liver Diseases, American College of Gastroenterology, and the American Gastroenterological Association.* Am J Gastroenterol, 2012. **107**(6): p. 811-26.
214. Yamada, T., et al., *Fatty liver predicts impaired fasting glucose and type 2 diabetes mellitus in Japanese undergoing a health checkup.* J Gastroenterol Hepatol, 2010. **25**(2): p. 352-6.
215. Sung, K.C., et al., *Combined influence of insulin resistance, overweight/obesity, and fatty liver as risk factors for type 2 diabetes.* Diabetes Care, 2012. **35**(4): p. 717-22.
216. Shibata, M., et al., *Nonalcoholic fatty liver disease is a risk factor for type 2 diabetes in middle-aged Japanese men.* Diabetes Care, 2007. **30**(11): p. 2940-4.
217. Okamoto, M., et al., *The association of fatty liver and diabetes risk.* J Epidemiol, 2003. **13**(1): p. 15-21.
218. Kim, C.H., et al., *Fatty liver is an independent risk factor for the development of Type 2 diabetes in Korean adults.* Diabet Med, 2008. **25**(4): p. 476-81.
219. Fan, J.G., et al., *Effects of nonalcoholic fatty liver disease on the development of metabolic disorders.* J Gastroenterol Hepatol, 2007. **22**(7): p. 1086-91.
220. Bae, J.C., et al., *Combined effect of nonalcoholic fatty liver disease and impaired fasting glucose on the development of type 2 diabetes: a 4-year retrospective longitudinal study.* Diabetes Care, 2011. **34**(3): p. 727-9.
221. Ryoo, J.H., et al., *The clinical availability of non alcoholic fatty liver disease as an early predictor of the metabolic syndrome in Korean men: 5-year's prospective cohort study.* Atherosclerosis, 2013. **227**(2): p. 398-403.
222. Kasturiratne, A., et al., *Influence of non-alcoholic fatty liver disease on the development of diabetes mellitus.* J Gastroenterol Hepatol, 2013. **28**(1): p. 142-7.
223. Chang, Y., et al., *Cohort study of non-alcoholic fatty liver disease, NAFLD fibrosis score, and the risk of incident diabetes in a Korean population.* Am J Gastroenterol, 2013. **108**(12): p. 1861-8.
224. Sung, K.C., S.H. Wild, and C.D. Byrne, *Resolution of fatty liver and risk of incident diabetes.* J Clin Endocrinol Metab, 2013. **98**(9): p. 3637-43.
225. Seki, S., et al., *In situ detection of lipid peroxidation and oxidative DNA damage in non-alcoholic fatty liver diseases.* J Hepatol, 2002. **37**(1): p. 56-62.

226. Racanelli, V. and B. Rehermann, *The liver as an immunological organ.* Hepatology, 2006. **43**(2 Suppl 1): p. S54-62.
227. Brehm, A., et al., *Increased lipid availability impairs insulin-stimulated ATP synthesis in human skeletal muscle.* Diabetes, 2006. **55**(1): p. 136-40.
228. Schmid, A.I., et al., *Liver ATP Synthesis Is Lower and Relates to Insulin Sensitivity in Patients With Type 2 Diabetes.* Diabetes Care, 2011. **34**(2): p. 448-453.
229. Roden, M., *Mechanisms of Disease: hepatic steatosis in type 2 diabetes - pathogenesis and clinical relevance.* Nature Clinical Practice Endocrinology & Metabolism, 2006. **2**(6): p. 335-348.
230. Wellen, K.E. and G.S. Hotamisligil, *Inflammation, stress, and diabetes.* Journal of Clinical Investigation, 2005. **115**(5): p. 1111-1119.
231. Wigg, A.J., et al., *The role of small intestinal bacterial overgrowth, intestinal permeability, endotoxaemia, and tumour necrosis factor alpha in the pathogenesis of non-alcoholic steatohepatitis.* Gut, 2001. **48**(2): p. 206-11.
232. Lichtman, S.N., et al., *Hepatic inflammation in rats with experimental small intestinal bacterial overgrowth.* Gastroenterology, 1990. **98**(2): p. 414-23.
233. Spinucci, G., et al., *Endogenous ethanol production in a patient with chronic intestinal pseudo-obstruction and small intestinal bacterial overgrowth.* Eur J Gastroenterol Hepatol, 2006. **18**(7): p. 799-802.
234. Solga, S.F. and A.M. Diehl, *Non-alcoholic fatty liver disease: lumen-liver interactions and possible role for probiotics.* J Hepatol, 2003. **38**(5): p. 681-7.
235. Lichtman, S.N., et al., *Hepatic injury associated with small bowel bacterial overgrowth in rats is prevented by metronidazole and tetracycline.* Gastroenterology, 1991. **100**(2): p. 513-9.
236. Li, Z., et al., *Probiotics and antibodies to TNF inhibit inflammatory activity and improve nonalcoholic fatty liver disease.* Hepatology, 2003. **37**(2): p. 343-50.
237. Drenick, E.J., J. Fisler, and D. Johnson, *Hepatic steatosis after intestinal bypass--prevention and reversal by metronidazole, irrespective of protein-calorie malnutrition.* Gastroenterology, 1982. **82**(3): p. 535-48.
238. Loguercio, C., et al., *Beneficial effects of a probiotic VSL#3 on parameters of liver dysfunction in chronic liver diseases.* J Clin Gastroenterol, 2005. **39**(6): p. 540-3.
239. Petersen, K.F., et al., *Reversal of nonalcoholic hepatic steatosis, hepatic insulin resistance, and hyperglycemia by moderate weight reduction in patients with type 2 diabetes.* Diabetes, 2005. **54**(3): p. 603-8.
240. Seppala-Lindroos, A., et al., *Fat accumulation in the liver is associated with defects in insulin suppression of glucose production and serum free fatty acids independent of obesity in normal men.* J Clin Endocrinol Metab, 2002. **87**(7): p. 3023-8.
241. Bajaj, M., et al., *Plasma resistin concentration, hepatic fat content, and hepatic and peripheral insulin resistance in pioglitazone-treated type II diabetic patients.* Int J Obes Relat Metab Disord, 2004. **28**(6): p. 783-9.
242. Ryysy, L., et al., *Hepatic fat content and insulin action on free fatty acids and glucose metabolism rather than insulin absorption are associated with insulin requirements during insulin therapy in type 2 diabetic patients.* Diabetes, 2000. **49**(5): p. 749-58.
243. Hwang, J.H., et al., *Increased intrahepatic triglyceride is associated with peripheral insulin resistance: in vivo MR imaging and spectroscopy studies.* Am J Physiol Endocrinol Metab, 2007. **293**(6): p. E1663-9.
244. Thamer, C., et al., *High visceral fat mass and high liver fat are associated with resistance to lifestyle intervention.* Obesity (Silver Spring), 2007. **15**(2): p. 531-8.
245. Byrne, C.D., *Dorothy Hodgkin Lecture 2012: non-alcoholic fatty liver disease, insulin resistance and ectopic fat: a new problem in diabetes management.* Diabet Med, 2012. **29**(9): p. 1098-107.

246. Byrne, C.D., *Ectopic fat, insulin resistance and non-alcoholic fatty liver disease.* Proc Nutr Soc, 2013. **72**(4): p. 412-9.
247. Sears, B. and M. Perry, *The role of fatty acids in insulin resistance.* Lipids Health Dis, 2015. **14**: p. 121.
248. Lipina, C. and H.S. Hundal, *Sphingolipids: agents provocateurs in the pathogenesis of insulin resistance.* Diabetologia, 2011. **54**(7): p. 1596-607.
249. Samuel, V.T., et al., *Inhibition of protein kinase Cepsilon prevents hepatic insulin resistance in nonalcoholic fatty liver disease.* J Clin Invest, 2007. **117**(3): p. 739-45.
250. Cantley, J.L., et al., *CGI-58 knockdown sequesters diacylglycerols in lipid droplets/ER-preventing diacylglycerol-mediated hepatic insulin resistance.* Proc Natl Acad Sci U S A, 2013. **110**(5): p. 1869-74.
251. Dresner, A., et al., *Effects of free fatty acids on glucose transport and IRS-1-associated phosphatidylinositol 3-kinase activity.* J Clin Invest, 1999. **103**(2): p. 253-9.
252. Samuel, V.T., et al., *Mechanism of hepatic insulin resistance in non-alcoholic fatty liver disease.* J Biol Chem, 2004. **279**(31): p. 32345-53.
253. Chavez, J.A. and S.A. Summers, *A ceramide-centric view of insulin resistance.* Cell Metab, 2012. **15**(5): p. 585-94.
254. Yamaguchi, K., et al., *Inhibiting triglyceride synthesis improves hepatic steatosis but exacerbates liver damage and fibrosis in obese mice with nonalcoholic steatohepatitis.* Hepatology, 2007. **45**(6): p. 1366-74.
255. Schenk, S., M. Saberi, and J.M. Olefsky, *Insulin sensitivity: modulation by nutrients and inflammation.* J Clin Invest, 2008. **118**(9): p. 2992-3002.
256. Leroux, A., et al., *Toxic lipids stored by Kupffer cells correlates with their pro-inflammatory phenotype at an early stage of steatohepatitis.* J Hepatol, 2012. **57**(1): p. 141-9.
257. Perry, R.J., et al., *The role of hepatic lipids in hepatic insulin resistance and type 2 diabetes.* Nature, 2014. **510**(7503): p. 84-91.
258. Hotamisligil, G.S., *Endoplasmic reticulum stress and the inflammatory basis of metabolic disease.* Cell, 2010. **140**(6): p. 900-17.
259. Tilg, H. and A.R. Moschen, *Insulin resistance, inflammation, and non-alcoholic fatty liver disease.* Trends Endocrinol Metab, 2008. **19**(10): p. 371-9.
260. Targher, G. and C.D. Byrne, *Clinical Review: Nonalcoholic fatty liver disease: a novel cardiometabolic risk factor for type 2 diabetes and its complications.* J Clin Endocrinol Metab, 2013. **98**(2): p. 483-95.
261. de Marco, R., et al., *Cause-specific mortality in type 2 diabetes. The Verona Diabetes Study.* Diabetes Care, 1999. **22**(5): p. 756-61.
262. Brunt, E.M., *Nonalcoholic steatohepatitis.* Semin Liver Dis, 2004. **24**(1): p. 3-20.
263. Targher, G., et al., *Nonalcoholic fatty liver disease and risk of future cardiovascular events among type 2 diabetic patients.* Diabetes, 2005. **54**(12): p. 3541-6.
264. Bhatia, L.S., et al., *Non-alcoholic fatty liver disease: a new and important cardiovascular risk factor?* Eur Heart J, 2012. **33**(10): p. 1190-200.
265. Ballestri, S., et al., *Risk of cardiovascular, cardiac and arrhythmic complications in patients with non-alcoholic fatty liver disease.* World J Gastroenterol, 2014. **20**(7): p. 1724-45.
266. Stepanova, M. and Z.M. Younossi, *Independent association between nonalcoholic fatty liver disease and cardiovascular disease in the US population.* Clin Gastroenterol Hepatol, 2012. **10**(6): p. 646-50.
267. Schindhelm, R.K., R.J. Heine, and M. Diamant, *Prevalence of nonalcoholic fatty liver disease and its association with cardiovascular disease among type 2 diabetic patients.* Diabetes Care, 2007. **30**(9): p. e94; author reply e95.
268. Addison, C.C., et al., *Relationship between medication use and cardiovascular disease health outcomes in the Jackson Heart Study.* Int J Environ Res Public Health, 2011. **8**(6): p. 2505-15.
269. Mirbagheri, S.A., et al., *Liver: an alarm for the heart?* Liver Int, 2007. **27**(7): p. 891-4.

270. Arslan, U., et al., *Association between nonalcoholic fatty liver disease and coronary artery disease.* Coron Artery Dis, 2007. **18**(6): p. 433-6.
271. Villanova, N., et al., *Endothelial dysfunction and cardiovascular risk profile in nonalcoholic fatty liver disease.* Hepatology, 2005. **42**(2): p. 473-80.
272. Targher, G., et al., *Relations between carotid artery wall thickness and liver histology in subjects with nonalcoholic fatty liver disease.* Diabetes Care, 2006. **29**(6): p. 1325-1330.
273. Brea, A., et al., *Nonalcoholic fatty liver disease is associated with carotid atherosclerosis: a case-control study.* Arterioscler Thromb Vasc Biol, 2005. **25**(5): p. 1045-50.
274. Targher, G., *Non-alcoholic fatty liver disease, the metabolic syndrome and the risk of cardiovascular disease: the plot thickens.* Diabet Med, 2007. **24**(1): p. 1-6.
275. Oni, E.T., et al., *A systematic review: burden and severity of subclinical cardiovascular disease among those with nonalcoholic fatty liver; should we care?* Atherosclerosis, 2013. **230**(2): p. 258-67.
276. Adams, L.A., et al., *The natural history of nonalcoholic fatty liver disease: a population-based cohort study.* Gastroenterology, 2005. **129**(1): p. 113-21.
277. Dam-Larsen, S., et al., *Long term prognosis of fatty liver: risk of chronic liver disease and death.* Gut, 2004. **53**(5): p. 750-5.
278. Soderberg, C., et al., *Decreased survival of subjects with elevated liver function tests during a 28-year follow-up.* Hepatology, 2010. **51**(2): p. 595-602.
279. Rafiq, N., et al., *Long-term follow-up of patients with nonalcoholic fatty liver.* Clin Gastroenterol Hepatol, 2009. **7**(2): p. 234-8.
280. Matteoni, C.A., et al., *Nonalcoholic fatty liver disease: a spectrum of clinical and pathological severity.* Gastroenterology, 1999. **116**(6): p. 1413-9.
281. Ekstedt, M., et al., *Fibrosis stage is the strongest predictor for disease-specific mortality in NAFLD after up to 33 years of follow-up.* Hepatology, 2015. **61**(5): p. 1547-54.
282. Perseghin, G., et al., *Increased mediastinal fat and impaired left ventricular energy metabolism in young men with newly found fatty liver.* Hepatology, 2008. **47**(1): p. 51-8.
283. Lautamaki, R., et al., *Liver steatosis coexists with myocardial insulin resistance and coronary dysfunction in patients with type 2 diabetes.* Am J Physiol Endocrinol Metab, 2006. **291**(2): p. E282-90.
284. Rijzewijk, L.J., et al., *Effects of hepatic triglyceride content on myocardial metabolism in type 2 diabetes.* J Am Coll Cardiol, 2010. **56**(3): p. 225-33.
285. Rijzewijk, L.J., et al., *Myocardial steatosis is an independent predictor of diastolic dysfunction in type 2 diabetes mellitus.* J Am Coll Cardiol, 2008. **52**(22): p. 1793-9.
286. Hallsworth, K., et al., *Cardiac structure and function are altered in adults with non-alcoholic fatty liver disease.* J Hepatol, 2013. **58**(4): p. 757-62.
287. Cassidy, S., et al., *Cardiac structure and function are altered in type 2 diabetes and non-alcoholic fatty liver disease and associate with glycemic control.* Cardiovasc Diabetol, 2015. **14**: p. 23.
288. Bonapace, S., et al., *Nonalcoholic fatty liver disease is associated with left ventricular diastolic dysfunction in patients with type 2 diabetes.* Diabetes Care, 2012. **35**(2): p. 389-95.
289. Bonapace, S., et al., *Nonalcoholic fatty liver disease is associated with aortic valve sclerosis in patients with type 2 diabetes mellitus.* PLoS One, 2014. **9**(2): p. e88371.
290. Kim, N.H., et al., *Non-alcoholic fatty liver disease, metabolic syndrome and subclinical cardiovascular changes in the general population.* Heart, 2014. **100**(12): p. 938-43.
291. Sinner, M.F., et al., *Relation of circulating liver transaminase concentrations to risk of new-onset atrial fibrillation.* Am J Cardiol, 2013. **111**(2): p. 219-24.
292. Alonso, A., et al., *Circulating levels of liver enzymes and incidence of atrial fibrillation: the Atherosclerosis Risk in Communities cohort.* Heart, 2014. **100**(19): p. 1511-6.

293. Targher, G., et al., *Non-alcoholic fatty liver disease is associated with an increased prevalence of atrial fibrillation in hospitalized patients with type 2 diabetes.* Clin Sci (Lond), 2013. **125**(6): p. 301-9.
294. Targher, G., et al., *Non-alcoholic fatty liver disease is associated with an increased incidence of atrial fibrillation in patients with type 2 diabetes.* PLoS One, 2013. **8**(2): p. e57183.
295. Targher, G., et al., *Association of nonalcoholic fatty liver disease with QTc interval in patients with type 2 diabetes.* Nutr Metab Cardiovasc Dis, 2014. **24**(6): p. 663-9.
296. Newton, J.L., et al., *Fatigue and autonomic dysfunction in non-alcoholic fatty liver disease.* Clin Auton Res, 2009. **19**(6): p. 319-26.
297. Otto, C.M. and B. Prendergast, *Aortic-valve stenosis--from patients at risk to severe valve obstruction.* N Engl J Med, 2014. **371**(8): p. 744-56.
298. Rossi, A., et al., *Aortic and mitral annular calcifications are predictive of all-cause and cardiovascular mortality in patients with type 2 diabetes.* Diabetes Care, 2012. **35**(8): p. 1781-6.
299. Markus, M.R., et al., *Hepatic steatosis is associated with aortic valve sclerosis in the general population: the Study of Health in Pomerania (SHIP).* Arterioscler Thromb Vasc Biol, 2013. **33**(7): p. 1690-5.
300. Targher, G., et al., *Non-alcoholic fatty liver disease is independently associated with an increased prevalence of chronic kidney disease and proliferative/laser-treated retinopathy in type 2 diabetic patients.* Diabetologia, 2008. **51**(3): p. 444-50.
301. Targher, G., et al., *Non-alcoholic fatty liver disease is independently associated with an increased prevalence of chronic kidney disease and retinopathy in type 1 diabetic patients.* Diabetologia, 2010. **53**(7): p. 1341-8.
302. Hwang, S.T., et al., *Impact of non-alcoholic fatty liver disease on microalbuminuria in patients with prediabetes and diabetes.* Intern Med J, 2010. **40**(6): p. 437-42.
303. Targher, G., et al., *Increased prevalence of chronic kidney disease in patients with Type 1 diabetes and non-alcoholic fatty liver.* Diabet Med, 2012. **29**(2): p. 220-6.
304. Yoshino, J., et al., *Resveratrol supplementation does not improve metabolic function in nonobese women with normal glucose tolerance.* Cell Metab, 2012. **16**(5): p. 658-64.
305. Ahn, A.L., et al., *Non-alcoholic Fatty Liver Disease and Chronic Kidney Disease in Koreans Aged 50 Years or Older.* Korean J Fam Med, 2013. **34**(3): p. 199-205.
306. Targher, G., et al., *Relationship between kidney function and liver histology in subjects with nonalcoholic steatohepatitis.* Clin J Am Soc Nephrol, 2010. **5**(12): p. 2166-71.
307. Yilmaz, Y., et al., *Microalbuminuria in nondiabetic patients with nonalcoholic fatty liver disease: association with liver fibrosis.* Metabolism, 2010. **59**(9): p. 1327-30.
308. Yasui, K., et al., *Nonalcoholic steatohepatitis and increased risk of chronic kidney disease.* Metabolism, 2011. **60**(5): p. 735-9.
309. Machado, M.V., et al., *Impaired renal function in morbid obese patients with nonalcoholic fatty liver disease.* Liver Int, 2012. **32**(2): p. 241-8.
310. Targher, G., et al., *Increased risk of CKD among type 2 diabetics with nonalcoholic fatty liver disease.* J Am Soc Nephrol, 2008. **19**(8): p. 1564-70.
311. Chang, Y., et al., *Nonalcoholic fatty liver disease predicts chronic kidney disease in nonhypertensive and nondiabetic Korean men.* Metabolism, 2008. **57**(4): p. 569-76.
312. Arase, Y., et al., *The development of chronic kidney disease in Japanese patients with non-alcoholic fatty liver disease.* Intern Med, 2011. **50**(10): p. 1081-7.
313. Targher, G., et al., *Nonalcoholic fatty liver disease is independently associated with an increased incidence of chronic kidney disease in patients with type 1 diabetes.* Diabetes Care, 2014. **37**(6): p. 1729-36.
314. Ratziu, V., Z. Goodman, and A. Sanyal, *Current efforts and trends in the treatment of NASH.* J Hepatol, 2015. **62**(1 Suppl): p. S65-75.

315. Dansinger, M.L., et al., *Meta-analysis: the effect of dietary counseling for weight loss.* Ann Intern Med, 2007. **147**(1): p. 41-50.
316. Bellentani, S., et al., *Behavior therapy for nonalcoholic fatty liver disease: The need for a multidisciplinary approach.* Hepatology, 2008. **47**(2): p. 746-54.
317. Ratziu, V., et al., *Lack of efficacy of an inhibitor of PDE4 in phase 1 and 2 trials of patients with nonalcoholic steatohepatitis.* Clin Gastroenterol Hepatol, 2014. **12**(10): p. 1724-30 e5.
318. Ratziu, V., et al., *A phase 2, randomized, double-blind, placebo-controlled study of GS-9450 in subjects with nonalcoholic steatohepatitis.* Hepatology, 2012. **55**(2): p. 419-28.
319. Chachay, V.S., et al., *Resveratrol does not benefit patients with nonalcoholic fatty liver disease.* Clin Gastroenterol Hepatol, 2014. **12**(12): p. 2092-103 e1-6.
320. Sanyal, A.J., et al., *No significant effects of ethyl-eicosapentanoic acid on histologic features of nonalcoholic steatohepatitis in a phase 2 trial.* Gastroenterology, 2014. **147**(2): p. 377-84 e1.
321. Keating, S.E., et al., *Exercise and non-alcoholic fatty liver disease: a systematic review and meta-analysis.* J Hepatol, 2012. **57**(1): p. 157-66.
322. Wen, C.P., et al., *Minimum amount of physical activity for reduced mortality and extended life expectancy: a prospective cohort study.* Lancet, 2011. **378**(9798): p. 1244-53.
323. Lee, I.M., et al., *Effect of physical inactivity on major non-communicable diseases worldwide: an analysis of burden of disease and life expectancy.* Lancet, 2012. **380**(9838): p. 219-29.
324. Kistler, K.D., et al., *Physical activity recommendations, exercise intensity, and histological severity of nonalcoholic fatty liver disease.* Am J Gastroenterol, 2011. **106**(3): p. 460-8; quiz 469.
325. Gordon, B.A., et al., *Resistance training improves metabolic health in type 2 diabetes: a systematic review.* Diabetes Res Clin Pract, 2009. **83**(2): p. 157-75.
326. Hallsworth, K., et al., *Resistance exercise reduces liver fat and its mediators in non-alcoholic fatty liver disease independent of weight loss.* Gut, 2011. **60**(9): p. 1278-83.
327. Helmerhorst, H.J., et al., *Objectively measured sedentary time may predict insulin resistance independent of moderate- and vigorous-intensity physical activity.* Diabetes, 2009. **58**(8): p. 1776-9.
328. Dunstan, D.W., et al., *Breaking up prolonged sitting reduces postprandial glucose and insulin responses.* Diabetes Care, 2012. **35**(5): p. 976-83.
329. Promrat, K., et al., *Randomized controlled trial testing the effects of weight loss on nonalcoholic steatohepatitis.* Hepatology, 2010. **51**(1): p. 121-9.
330. Lazo, M., et al., *Effect of a 12-month intensive lifestyle intervention on hepatic steatosis in adults with type 2 diabetes.* Diabetes Care, 2010. **33**(10): p. 2156-63.
331. Kral, J.G., et al., *Effects of surgical treatment of the metabolic syndrome on liver fibrosis and cirrhosis.* Surgery, 2004. **135**(1): p. 48-58.
332. Dixon, J.B., et al., *Nonalcoholic fatty liver disease: Improvement in liver histological analysis with weight loss.* Hepatology, 2004. **39**(6): p. 1647-54.
333. Lassailly, G., et al., *Bariatric Surgery Reduces Features of Nonalcoholic Steatohepatitis in Morbidly Obese Patients.* Gastroenterology, 2015. **149**(2): p. 379-88; quiz e15-6.
334. Moschen, A.R., et al., *Anti-inflammatory effects of excessive weight loss: potent suppression of adipose interleukin 6 and tumour necrosis factor alpha expression.* Gut, 2010. **59**(9): p. 1259-64.
335. Ryan, M.C., et al., *The Mediterranean diet improves hepatic steatosis and insulin sensitivity in individuals with non-alcoholic fatty liver disease.* J Hepatol, 2013. **59**(1): p. 138-43.
336. Petta, S., et al., *Industrial, not fruit fructose intake is associated with the severity of liver fibrosis in genotype 1 chronic hepatitis C patients.* J Hepatol, 2013. **59**(6): p. 1169-76.
337. Abdelmalek, M.F., et al., *Increased fructose consumption is associated with fibrosis severity in patients with nonalcoholic fatty liver disease.* Hepatology, 2010. **51**(6): p. 1961-71.

338. Ishimoto, T., et al., *High-fat and high-sucrose (western) diet induces steatohepatitis that is dependent on fructokinase.* Hepatology, 2013. **58**(5): p. 1632-43.
339. Stanhope, K.L., et al., *Consuming fructose-sweetened, not glucose-sweetened, beverages increases visceral adiposity and lipids and decreases insulin sensitivity in overweight/obese humans.* J Clin Invest, 2009. **119**(5): p. 1322-34.
340. Chiu, S., et al., *Effect of fructose on markers of non-alcoholic fatty liver disease (NAFLD): a systematic review and meta-analysis of controlled feeding trials.* Eur J Clin Nutr, 2014. **68**(4): p. 416-23.
341. Sievenpiper, J.L., et al., *Effect of fructose on body weight in controlled feeding trials: a systematic review and meta-analysis.* Ann Intern Med, 2012. **156**(4): p. 291-304.
342. Chiavaroli, L., et al., *Is industrial fructose just a marker of an unhealthy dietary pattern?* J Hepatol, 2014. **61**(1): p. 172-3.
343. Johnston, R.D., et al., *No difference between high-fructose and high-glucose diets on liver triacylglycerol or biochemistry in healthy overweight men.* Gastroenterology, 2013. **145**(5): p. 1016-1025 e2.
344. Adams, L.A., et al., *Nonalcoholic fatty liver disease increases risk of death among patients with diabetes: a community-based cohort study.* Am J Gastroenterol, 2010. **105**(7): p. 1567-73.
345. Zelber-Sagi, S., V. Ratziu, and R. Oren, *Nutrition and physical activity in NAFLD: an overview of the epidemiological evidence.* World J Gastroenterol, 2011. **17**(29): p. 3377-89.
346. Ouyang, X., et al., *Fructose consumption as a risk factor for non-alcoholic fatty liver disease.* J Hepatol, 2008. **48**(6): p. 993-9.
347. Zelber-Sagi, S., et al., *Long term nutritional intake and the risk for non-alcoholic fatty liver disease (NAFLD): a population based study.* J Hepatol, 2007. **47**(5): p. 711-7.
348. Ratziu, V., *Pharmacological agents for NASH.* Nat Rev Gastroenterol Hepatol, 2013. **10**(11): p. 676-85.
349. Sacks, F.M., et al., *Comparison of weight-loss diets with different compositions of fat, protein, and carbohydrates.* N Engl J Med, 2009. **360**(9): p. 859-73.
350. Sanyal, A.J., et al., *Pioglitazone, vitamin E, or placebo for nonalcoholic steatohepatitis.* N Engl J Med, 2010. **362**(18): p. 1675-85.
351. Kallwitz, E.R., A. McLachlan, and S.J. Cotler, *Role of peroxisome proliferators-activated receptors in the pathogenesis and treatment of nonalcoholic fatty liver disease.* World J Gastroenterol, 2008. **14**(1): p. 22-8.
352. Wu, Z., N.L. Bucher, and S.R. Farmer, *Induction of peroxisome proliferator-activated receptor gamma during the conversion of 3T3 fibroblasts into adipocytes is mediated by C/EBPbeta, C/EBPdelta, and glucocorticoids.* Mol Cell Biol, 1996. **16**(8): p. 4128-36.
353. Fajas, L., J.C. Fruchart, and J. Auwerx, *Transcriptional control of adipogenesis.* Curr Opin Cell Biol, 1998. **10**(2): p. 165-73.
354. Kim, J.B. and B.M. Spiegelman, *ADD1/SREBP1 promotes adipocyte differentiation and gene expression linked to fatty acid metabolism.* Genes Dev, 1996. **10**(9): p. 1096-107.
355. Yu, J.G., et al., *The effect of thiazolidinediones on plasma adiponectin levels in normal, obese, and type 2 diabetic subjects.* Diabetes, 2002. **51**(10): p. 2968-74.
356. Soden, J.S., et al., *Subcutaneous vitamin E ameliorates liver injury in an in vivo model of steatocholestasis.* Hepatology, 2007. **46**(2): p. 485-95.
357. Sokol, R.J., et al., *Vitamin E reduces oxidant injury to mitochondria and the hepatotoxicity of taurochenodeoxycholic acid in the rat.* Gastroenterology, 1998. **114**(1): p. 164-74.
358. Azzi, A., et al., *Vitamin E mediates cell signaling and regulation of gene expression.* Ann N Y Acad Sci, 2004. **1031**: p. 86-95.
359. Belfort, R., et al., *A placebo-controlled trial of pioglitazone in subjects with nonalcoholic steatohepatitis.* N Engl J Med, 2006. **355**(22): p. 2297-307.

360. Aithal, G.P., et al., *Randomized, placebo-controlled trial of pioglitazone in nondiabetic subjects with nonalcoholic steatohepatitis.* Gastroenterology, 2008. **135**(4): p. 1176-84.
361. Levin, D., et al., *Pioglitazone and bladder cancer risk: a multipopulation pooled, cumulative exposure analysis.* Diabetologia, 2015. **58**(3): p. 493-504.
362. Lavine, J.E., et al., *Effect of vitamin E or metformin for treatment of nonalcoholic fatty liver disease in children and adolescents: the TONIC randomized controlled trial.* JAMA, 2011. **305**(16): p. 1659-68.
363. Ferrara, A., et al., *Cohort study of pioglitazone and cancer incidence in patients with diabetes.* Diabetes Care, 2011. **34**(4): p. 923-9.
364. Lewis, J.D., et al., *Risk of bladder cancer among diabetic patients treated with pioglitazone: interim report of a longitudinal cohort study.* Diabetes Care, 2011. **34**(4): p. 916-22.
365. Lutchman, G., et al., *The effects of discontinuing pioglitazone in patients with nonalcoholic steatohepatitis.* Hepatology, 2007. **46**(2): p. 424-9.
366. Nobili, V., et al., *Lifestyle intervention and antioxidant therapy in children with nonalcoholic fatty liver disease: a randomized, controlled trial.* Hepatology, 2008. **48**(1): p. 119-28.
367. Bjelakovic, G., et al., *Mortality in randomized trials of antioxidant supplements for primary and secondary prevention: systematic review and meta-analysis.* JAMA, 2007. **297**(8): p. 842-57.
368. Schurks, M., et al., *Effects of vitamin E on stroke subtypes: meta-analysis of randomised controlled trials.* BMJ, 2010. **341**: p. c5702.
369. Klein, E.A., et al., *Vitamin E and the risk of prostate cancer: the Selenium and Vitamin E Cancer Prevention Trial (SELECT).* JAMA, 2011. **306**(14): p. 1549-56.
370. Pearson, P., et al., *The pro-oxidant activity of high-dose vitamin E supplements in vivo.* BioDrugs, 2006. **20**(5): p. 271-3.
371. Zhou, G., et al., *Role of AMP-activated protein kinase in mechanism of metformin action.* J Clin Invest, 2001. **108**(8): p. 1167-74.
372. Ekstedt, M., et al., *Statins in non-alcoholic fatty liver disease and chronically elevated liver enzymes: a histopathological follow-up study.* J Hepatol, 2007. **47**(1): p. 135-41.
373. Neuschwander-Tetri, B.A., et al., *Farnesoid X nuclear receptor ligand obeticholic acid for non-cirrhotic, non-alcoholic steatohepatitis (FLINT): a multicentre, randomised, placebo-controlled trial.* Lancet, 2015. **385**(9972): p. 956-65.
374. Chae, M.K., et al., *Pentoxifylline attenuates methionine- and choline-deficient-diet-induced steatohepatitis by suppressing TNF-alpha expression and endoplasmic reticulum stress.* Exp Diabetes Res, 2012. **2012**: p. 762565.
375. Zein, C.O., et al., *Pentoxifylline improves nonalcoholic steatohepatitis: a randomized placebo-controlled trial.* Hepatology, 2011. **54**(5): p. 1610-9.
376. Hardy, T., Q.M. Anstee, and C.P. Day, *Nonalcoholic fatty liver disease: new treatments.* Curr Opin Gastroenterol, 2015. **31**(3): p. 175-83.
377. Abdelmalek, M.F. and A.M. Diehl, *Nonalcoholic fatty liver disease as a complication of insulin resistance.* Medical Clinics of North America, 2007. **91**(6): p. 1125-+.
378. Popper, H. and C.S. Lieber, *Histogenesis of alcoholic fibrosis and cirrhosis in the baboon.* Am J Pathol, 1980. **98**(3): p. 695-716.
379. Tsukamoto, H. and X.P. Xi, *Incomplete compensation of enhanced hepatic oxygen consumption in rats with alcoholic centrilobular liver necrosis.* Hepatology, 1989. **9**(2): p. 302-6.
380. Hijmans, B.S., et al., *Zonation of glucose and fatty acid metabolism in the liver: mechanism and metabolic consequences.* Biochimie, 2014. **96**: p. 121-9.
381. Brown, M.S. and J.L. Goldstein, *Selective versus total insulin resistance: a pathogenic paradox.* Cell Metab, 2008. **7**(2): p. 95-6.

382. MacDonald, G.A., et al., *Lipid peroxidation in hepatic steatosis in humans is associated with hepatic fibrosis and occurs predominately in acinar zone 3.* J Gastroenterol Hepatol, 2001. **16**(6): p. 599-606.
383. Kim, J., G.M. Saidel, and M.E. Cabrera, *Multi-scale computational model of fuel homeostasis during exercise: effect of hormonal control.* Ann Biomed Eng, 2007. **35**(1): p. 69-90.
384. Xu, K., et al., *A whole-body model for glycogen regulation reveals a critical role for substrate cycling in maintaining blood glucose homeostasis.* PLoS Comput Biol, 2011. **7**(12): p. e1002272.
385. Liu, W., C. Hsin, and F. Tang, *A molecular mathematical model of glucose mobilization and uptake.* Math Biosci, 2009. **221**(2): p. 121-9.
386. Balakrishnan, N.P., G.P. Rangaiah, and L. Samavedham, *Review and Analysis of Blood Glucose (BG) Models for Type 1 Diabetic Patients.* Industrial & Engineering Chemistry Research, 2011. **50**(21): p. 12041-12066.
387. Somvanshi, P.P., A.; Bhartiyab, S.; Venkatesh, K., *Influence of plasma macronutrient levels on hepatic metabolism: role of regulatory networks in homeostasis and disease states.* RSC Advances, 2016. **6**: p. 14344-14371.
388. Konig, M., S. Bulik, and H.G. Holzhutter, *Quantifying the Contribution of the Liver to Glucose Homeostasis: A Detailed Kinetic Model of Human Hepatic Glucose Metabolism.* Plos Computational Biology, 2012. **8**(6).
389. Hetherington, J., et al., *A composite computational model of liver glucose homeostasis. I. Building the composite model.* J R Soc Interface, 2012. **9**(69): p. 689-700.
390. Sumner, T., et al., *A composite computational model of liver glucose homeostasis. II. Exploring system behaviour.* J R Soc Interface, 2012. **9**(69): p. 701-6.
391. Chalhoub, E., R.W. Hanson, and J.M. Belovich, *A computer model of gluconeogenesis and lipid metabolism in the perfused liver.* Am J Physiol Endocrinol Metab, 2007. **293**(6): p. E1676-86.
392. Calvetti, D., A. Kuceyeski, and E. Somersalo, *Sampling-based analysis of a spatially distributed model for liver metabolism at steady state.* Multiscale Modeling & Simulation, 2008. **7**(1): p. 407-431.
393. Bogle, I.D.L.J., R.; Shephard, E.; Seymour, R.; Finkelstein, A.; Sumner, T.; Warner A., *Systems Biology of the Liver.* Reviews in Cell Biology and Molecular Medicine, 2012.
394. Fisher, C.P., et al., *Systems biology approaches for studying the pathogenesis of non-alcoholic fatty liver disease.* World J Gastroenterol, 2014. **20**(41): p. 15070-8.
395. Ohno, H., et al., *Construction of a biological tissue model based on a single-cell model: a computer simulation of metabolic heterogeneity in the liver lobule.* Artif Life, 2008. **14**(1): p. 3-28.
396. Anissimov, Y.G. and M.S. Roberts, *A compartmental model of hepatic disposition kinetics: 1. Model development and application to linear kinetics.* J Pharmacokinet Pharmacodyn, 2002. **29**(2): p. 131-56.
397. Sheikh-Bahaei, S., J.J. Maher, and C. Anthony Hunt, *Computational experiments reveal plausible mechanisms for changing patterns of hepatic zonation of xenobiotic clearance and hepatotoxicity.* J Theor Biol, 2010. **265**(4): p. 718-33.
398. Pang, K.S., M. Weiss, and P. Macheras, *Advanced pharmacokinetic models based on organ clearance, circulatory, and fractal concepts.* AAPS J, 2007. **9**(2): p. E268-83.
399. Konig, M., H.G. Holzhutter, and N. Berndt, *Metabolic gradients as key regulators in zonation of tumor energy metabolism: a tissue-scale model-based study.* Biotechnol J, 2013. **8**(9): p. 1058-69.
400. Davidson, A.J., M.J. Ellis, and J.B. Chaudhuri, *A theoretical approach to zonation in a bioartificial liver.* Biotechnol Bioeng, 2012. **109**(1): p. 234-43.

401. Ashworth, W.B., N.A. Davies, and I.D. Bogle, *A Computational Model of Hepatic Energy Metabolism: Understanding Zonated Damage and Steatosis in NAFLD.* PLoS Comput Biol, 2016. **12**(9): p. e1005105.
402. Ashworth, W., et al., *Liver function as an engineering system.* AICHEj, 2016. **62**(9): p. 3285–3297.
403. Eipel, C., K. Abshagen, and B. Vollmar, *Regulation of hepatic blood flow: the hepatic arterial buffer response revisited.* World J Gastroenterol, 2010. **16**(48): p. 6046-57.
404. Davy, K.P. and D.R. Seals, *Total blood volume in healthy young and older men.* J Appl Physiol (1985), 1994. **76**(5): p. 2059-62.
405. Critchley, L.A. and J.A. Critchley, *A meta-analysis of studies using bias and precision statistics to compare cardiac output measurement techniques.* J Clin Monit Comput, 1999. **15**(2): p. 85-91.
406. Teutsch, H.F., *A new sample isolation procedure for microchemical analysis of functional liver cell heterogeneity.* J Histochem Cytochem, 1986. **34**(2): p. 263-7.
407. Johnson, J.H., et al., *The high Km glucose transporter of islets of Langerhans is functionally similar to the low affinity transporter of liver and has an identical primary sequence.* J Biol Chem, 1990. **265**(12): p. 6548-51.
408. Jung, C.Y. and A.L. Rampal, *Cytochalasin B binding sites and glucose transport carrier in human erythrocyte ghosts.* J Biol Chem, 1977. **252**(15): p. 5456-63.
409. Buschiazzo, H., J.H. Exton, and C.R. Park, *Effects of glucose on glycogen synthetase, phosphorylase, and glycogen deposition in the perfused rat liver.* Proc Natl Acad Sci U S A, 1970. **65**(2): p. 383-7.
410. Schomburg, D. *BRENDA: The Comprehensive Enzyme Information System*. 2016.
411. Reshef, L., et al., *Glyceroneogenesis and the triglyceride/fatty acid cycle.* J Biol Chem, 2003. **278**(33): p. 30413-6.
412. Dolinsky, V.W., et al., *Regulation of the enzymes of hepatic microsomal triacylglycerol lipolysis and re-esterification by the glucocorticoid dexamethasone.* Biochem J, 2004. **378**(Pt 3): p. 967-74.
413. Zheng, Q., et al., *Glucose regulation of glucose transporters in cultured adult and fetal hepatocytes.* Metabolism, 1995. **44**(12): p. 1553-8.
414. Agius, L., *Glucokinase and molecular aspects of liver glycogen metabolism.* Biochemical Journal, 2008. **414**: p. 1-18.
415. Gloyn, A.L., et al., *Insights into the structure and regulation of glucokinase from a novel mutation (V62M), which causes maturity-onset diabetes of the young.* Journal of Biological Chemistry, 2005. **280**(14): p. 14105-14113.
416. Brocklehurst, K.J., R.A. Davies, and L. Agius, *Differences in regulatory properties between human and rat glucokinase regulatory protein.* Biochemical Journal, 2004. **378**: p. 693-697.
417. Ahn, K.J., et al., *Enzymatic properties of the N- and C-terminal halves of human hexokinase II.* Bmb Reports, 2009. **42**(6): p. 350-355.
418. Goward, C.R., et al., *The purification and characterization of glucokinase from the thermophile Bacillus stearothermophilus.* Biochem J, 1986. **237**(2): p. 415-20.
419. Heredia, V.V., et al., *Glucose-induced conformational changes in glucokinase mediate allosteric regulation: transient kinetic analysis.* Biochemistry, 2006. **45**(24): p. 7553-62.
420. van Schaftingen, E., et al., *The regulatory protein of liver glucokinase.* Adv Enzyme Regul, 1992. **32**: p. 133-48.
421. van Schaftingen, E. and I. Gerin, *The glucose-6-phosphatase system.* Biochem J, 2002. **362**(Pt 3): p. 513-32.
422. Henry-Vitrac, C., et al., *Contribution of chlorogenic acids to the inhibition of human hepatic glucose-6-phosphatase activity in vitro by Svetol, a standardized decaffeinated green coffee extract.* J Agric Food Chem, 2010. **58**(7): p. 4141-4.

423. Turnquist, R.L., T.A. Gillett, and R.G. Hansen, *Uridine diphosphate glucose pyrophosphorylase. Crystallization and properties of the enzyme from rabbit liver and species comparisons.* J Biol Chem, 1974. **249**(23): p. 7695-700.
424. Turnquist, R.L.H., R.G.; , *Uridine diphosphoryl glucose pyrophosphorylase*, in *The Enzymes, 3rd. Ed (Boyer, P.D., ed.)* 1973. p. 8.
425. Daly, M.E., et al., *Acute effects on insulin sensitivity and diurnal metabolic profiles of a high-sucrose compared with a high-starch diet.* Am J Clin Nutr, 1998. **67**(6): p. 1186-96.
426. Albe, K.R., M.H. Butler, and B.E. Wright, *Cellular Concentrations of Enzymes and Their Substrates.* Journal of Theoretical Biology, 1990. **143**(2): p. 163-195.
427. Rawat, A.K., *Effects of ethanol infusion on the redox state and metabolite levels in rat liver in vivo.* Eur J Biochem, 1968. **6**(4): p. 585-92.
428. Taylor, R., et al., *Direct assessment of liver glycogen storage by 13C nuclear magnetic resonance spectroscopy and regulation of glucose homeostasis after a mixed meal in normal subjects.* J Clin Invest, 1996. **97**(1): p. 126-32.
429. Veech, R.L., D. Veloso, and M.A. Mehlman, *Thiamin deficiency: liver metabolite levels and redox and phosphorylation states in thiamin-deficient rats.* J Nutr, 1973. **103**(2): p. 267-72.
430. Faupel, R.P., et al., *The problem of tissue sampling from experimental animals with respect to freezing technique, anoxia, stress and narcosis. A new method for sampling rat liver tissue and the physiological values of glycolytic intermediates and related compounds.* Arch Biochem Biophys, 1972. **148**(2): p. 509-22.
431. Mandarino, L.J., et al., *Effects of insulin infusion on human skeletal muscle pyruvate dehydrogenase, phosphofructokinase, and glycogen synthase. Evidence for their role in oxidative and nonoxidative glucose metabolism.* J Clin Invest, 1987. **80**(3): p. 655-63.
432. Baskaran, S., et al., *Structural basis for glucose-6-phosphate activation of glycogen synthase.* Proc Natl Acad Sci U S A, 2010. **107**(41): p. 17563-8.
433. Assaf, S.A. and A.A. Yunis, *Physicochemical and Catalytic Properties of Crystallized Human Muscle Glycogen-Phosphorylase.* Annals of the New York Academy of Sciences, 1973. **210**(Feb9): p. 139-152.
434. Prando, R., et al., *Blood Lactate Behavior after Glucose-Load in Diabetes-Mellitus.* Acta Diabetologica Latina, 1988. **25**(3): p. 247-256.
435. Berndt, J., et al., *Fatty acid synthase gene expression in human adipose tissue: association with obesity and type 2 diabetes.* Diabetologia, 2007. **50**(7): p. 1472-80.
436. Bruser, A., J. Kirchberger, and T. Schoneberg, *Altered allosteric regulation of muscle 6-phosphofructokinase causes Tarui disease.* Biochemical and Biophysical Research Communications, 2012. **427**(1): p. 133-137.
437. Bruser, A., et al., *Functional linkage of adenine nucleotide binding sites in mammalian muscle 6-phosphofructokinase.* J Biol Chem, 2012. **287**(21): p. 17546-53.
438. Mediavilla, D., I. Meton, and I.V. Baanante, *Purification and kinetic properties of 6-phosphofructo-1-kinase from gilthead sea bream muscle.* Biochim Biophys Acta, 2007. **1770**(4): p. 706-15.
439. Dombrauckas, J.D., B.D. Santarsiero, and A.D. Mesecar, *Structural basis for tumor pyruvate kinase M2 allosteric regulation and catalysis.* Biochemistry, 2005. **44**(27): p. 9417-29.
440. Weber, G., M.A. Lea, and N.B. Stamm, *Inhibition of pyruvate kinase and glucokinase by acetyl CoA and inhibition of glucokinase by phosphoenolpyruvate.* Life Sciences, 1967. **6**(22): p. 2441–2452.
441. Dharmarajan, L., et al., *Tyr235 of human cytosolic phosphoenolpyruvate carboxykinase influences catalysis through an anion-quadrupole interaction with phosphoenolpyruvate carboxylate.* FEBS J, 2008. **275**(23): p. 5810-9.
442. Kiselevsky, Y.V., S.A. Ostrovtsova, and S.A. Strumilo, *Kinetic characterization of the pyruvate and oxoglutarate dehydrogenase complexes from human heart.* Acta Biochim Pol, 1990. **37**(1): p. 135-9.

443. Edgerton, D.S., et al., *Effects of insulin on the metabolic control of hepatic gluconeogenesis in vivo.* Diabetes, 2009. **58**(12): p. 2766-75.
444. Ainscow, E.K. and M.D. Brand, *Top-down control analysis of ATP turnover, glycolysis and oxidative phosphorylation in rat hepatocytes.* Eur J Biochem, 1999. **263**(3): p. 671-85.
445. Eaton, S., *Control of mitochondrial beta-oxidation flux.* Prog Lipid Res, 2002. **41**(3): p. 197-239.
446. Schulz, H., *Regulation of fatty acid oxidation in heart.* J Nutr, 1994. **124**(2): p. 165-71.
447. Kim, J.H., T.M. Lewin, and R.A. Coleman, *Expression and characterization of recombinant rat Acyl-CoA synthetases 1, 4, and 5. Selective inhibition by triacsin C and thiazolidinediones.* J Biol Chem, 2001. **276**(27): p. 24667-73.
448. Van Horn, C.G., et al., *Characterization of recombinant long-chain rat acyl-CoA synthetase isoforms 3 and 6: identification of a novel variant of isoform 6.* Biochemistry, 2005. **44**(5): p. 1635-42.
449. Marcel, Y.L. and G. Suzue, *Kinetic studies on the specificity of long chain acyl coenzyme A synthetase from rat liver microsomes.* J Biol Chem, 1972. **247**(14): p. 4433-6.
450. Stinnett, L., T.M. Lewin, and R.A. Coleman, *Mutagenesis of rat acyl-CoA synthetase 4 indicates amino acids that contribute to fatty acid binding.* Biochim Biophys Acta, 2007. **1771**(1): p. 119-25.
451. Zierz, S. and A.G. Engel, *Different sites of inhibition of carnitine palmitoyltransferase by malonyl-CoA, and by acetyl-CoA and CoA, in human skeletal muscle.* Biochem J, 1987. **245**(1): p. 205-9.
452. Daly, M.E., et al., *Acute fuel selection in response to high-sucrose and high-starch meals in healthy men.* Am J Clin Nutr, 2000. **71**(6): p. 1516-24.
453. Seal, C.J., et al., *Postprandial carbohydrate metabolism in healthy subjects and those with type 2 diabetes fed starches with slow and rapid hydrolysis rates determined in vitro.* Br J Nutr, 2003. **90**(5): p. 853-64.
454. Mukherjee, A., et al., *Studies on human heart citrate synthase.* Adv Myocardiol, 1980. **1**: p. 329-37.
455. Bald, D., et al., *ATP synthesis by F0F1-ATP synthase independent of noncatalytic nucleotide binding sites and insensitive to azide inhibition.* J Biol Chem, 1998. **273**(2): p. 865-70.
456. Soga, N., et al., *Efficient ATP synthesis by thermophilic Bacillus FoF1-ATP synthase.* FEBS J, 2011. **278**(15): p. 2647-54.
457. Richard, P., B. Pitard, and J.L. Rigaud, *ATP synthesis by the F0F1-ATPase from the thermophilic Bacillus PS3 co-reconstituted with bacteriorhodopsin into liposomes. Evidence for stimulation of ATP synthesis by ATP bound to a noncatalytic binding site.* J Biol Chem, 1995. **270**(37): p. 21571-8.
458. Lam, S.C. and M.A. Packham, *Isolation and kinetic studies of nucleoside diphosphokinase from human platelets and effects of cAMP phosphodiesterase inhibitors.* Biochem Pharmacol, 1986. **35**(24): p. 4449-55.
459. Kimura, N. and N. Shimada, *Membrane-associated nucleoside diphosphate kinase from rat liver. Purification, characterization, and comparison with cytosolic enzyme.* J Biol Chem, 1988. **263**(10): p. 4647-53.
460. Fukuchi, T., et al., *Recombinant rat nucleoside diphosphate kinase isoforms (alpha and beta): purification, properties and application to immunological detection of native isoforms in rat tissues.* Biochim Biophys Acta, 1994. **1205**(1): p. 113-22.
461. Tsuboi, K.K. and C.H. Chervenka, *Adenylate kinase of human erythrocyte. Isolation and properties of the predominant inherited form.* J Biol Chem, 1975. **250**(1): p. 132-40.
462. Abu-Elheiga, L., et al., *The subcellular localization of acetyl-CoA carboxylase 2.* Proc Natl Acad Sci U S A, 2000. **97**(4): p. 1444-9.
463. Cheng, D., et al., *Expression, purification, and characterization of human and rat acetyl coenzyme A carboxylase (ACC) isozymes.* Protein Expr Purif, 2007. **51**(1): p. 11-21.

464. Carlisle-Moore, L., et al., *Substrate recognition by the human fatty-acid synthase.* J Biol Chem, 2005. **280**(52): p. 42612-8.
465. Jayakumar, A., et al., *Human fatty acid synthase: properties and molecular cloning.* Proc Natl Acad Sci U S A, 1995. **92**(19): p. 8695-9.
466. Monti, L.D., et al., *Myocardial insulin resistance associated with chronic hypertriglyceridemia and increased FFA levels in Type 2 diabetic patients.* Am J Physiol Heart Circ Physiol, 2004. **287**(3): p. H1225-31.
467. Saggerson, E.D. and A.L. Greenbaum, *The regulation of triglyceride synthesis and fatty acid synthesis in rat epididymal adipose tissue.* Biochem J, 1970. **119**(2): p. 193-219.
468. Zammit, V.A. and C.G. Corstorphine, *Inhibition of acetyl-CoA carboxylase activity in isolated rat adipocytes incubated with glucagon. Interactions with the effects of insulin, adrenaline and adenosine deaminase.* Biochem J, 1982. **208**(3): p. 783-8.
469. Halestrap, A.P. and R.M. Denton, *Hormonal regulation of adipose-tissue acetyl-Coenzyme A carboxylase by changes in the polymeric state of the enzyme. The role of long-chain fatty acyl-Coenzyme A thioesters and citrate.* Biochem J, 1974. **142**(2): p. 365-77.
470. Vancura, A. and D. Haldar, *Purification and characterization of glycerophosphate acyltransferase from rat liver mitochondria.* J Biol Chem, 1994. **269**(44): p. 27209-15.
471. Farese, R.V., et al., *Insulin-induced activation of glycerol-3-phosphate acyltransferase by a chiro-inositol-containing insulin mediator is defective in adipocytes of insulin-resistant, type II diabetic, Goto-Kakizaki rats.* Proc Natl Acad Sci U S A, 1994. **91**(23): p. 11040-4.
472. Duncan, R.E., et al., *Regulation of lipolysis in adipocytes.* Annu Rev Nutr, 2007. **27**: p. 79-101.
473. Kaplan, A. and M.H. Teng, *Interaction of beef liver lipase with mixed micelles of tripalmitin and Triton X-100.* J Lipid Res, 1971. **12**(3): p. 324-30.
474. Chakraborty, K. and R.P. Raj, *An extra-cellular alkaline metallolipase from Bacillus licheniformis MTCC 6824: Purification and biochemical characterization.* Food Chemistry, 2008. **109**(4): p. 727-736.
475. Westergaard, N., P. Madsen, and K. Lundgren, *Characterization of glycerol uptake and glycerol kinase activity in rat hepatocytes cultured under different hormonal conditions.* Biochim Biophys Acta, 1998. **1402**(3): p. 261-8.
476. Rajaraman, G., et al., *Membrane binding proteins are the major determinants for the hepatocellular transmembrane flux of long-chain fatty acids bound to albumin.* Pharmaceutical Research, 2005. **22**(11): p. 1793-1804.
477. Stump, D.D., et al., *Characteristics of Oleate Binding to Liver Plasma-Membranes and Its Uptake by Isolated Hepatocytes.* Journal of Hepatology, 1992. **16**(3): p. 304-315.
478. Buque, X., et al., *High insulin levels are required for FAT/CD36 plasma membrane translocation and enhanced fatty acid uptake in obese Zucker rat hepatocytes.* Am J Physiol Endocrinol Metab, 2012. **303**(4): p. E504-14.
479. Stahl, A., et al., *Insulin causes fatty acid transport protein translocation and enhanced fatty acid uptake in adipocytes.* Dev Cell, 2002. **2**(4): p. 477-88.
480. Ge, F., et al., *Insulin- and leptin-regulated fatty acid uptake plays a key causal role in hepatic steatosis in mice with intact leptin signaling but not in ob/ob or db/db mice.* Am J Physiol Gastrointest Liver Physiol, 2010. **299**(4): p. G855-66.
481. Durrington, P.N., et al., *Effects of Insulin and Glucose on Very Low-Density Lipoprotein Triglyceride Secretion by Cultured Rat Hepatocytes.* Journal of Clinical Investigation, 1982. **70**(1): p. 63-73.
482. Nelson, R.H., et al., *Triglyceride uptake and lipoprotein lipase-generated fatty acid spillover in the splanchnic bed of dogs.* Diabetes, 2007. **56**(7): p. 1850-5.
483. Quarfordt, S.H., et al., *Differing uptake of emulsion triglyceride by the fed and fasted rat liver.* J Clin Invest, 1982. **69**(5): p. 1092-8.

484. Bergman, E.N., et al., *Quantitative studies of the metabolism of chylomicron triglycerides and cholesterol by liver and extrahepatic tissues of sheep and dogs.* J Clin Invest, 1971. **50**(9): p. 1831-9.
485. McDonald, G.B., et al., *Portal venous transport of long-chain fatty acids absorbed from rat intestine.* Am J Physiol, 1980. **239**(3): p. G141-50.
486. Jackson, R.C., H.P. Morris, and G. Weber, *Partial purification, properties and regulation of inosine 5'phosphate dehydrogenase in normal and malignant rat tissues.* Biochem J, 1977. **166**(1): p. 1-10.
487. Guzman, M. and J. Castro, *Zonal Heterogeneity of the Effects of Chronic Ethanol Feeding on Hepatic Fatty-Acid Metabolism.* Hepatology, 1990. **12**(5): p. 1098-1105.
488. Frederiks, W.M., F. Marx, and C.J. van Noorden, *Homogeneous distribution of phosphofructokinase in the rat liver acinus: a quantitative histochemical study.* Hepatology, 1991. **14**(4 Pt 1): p. 634-9.
489. Bass, N.M., *Fatty acid-binding protein expression in the liver: its regulation and relationship to the zonation of fatty acid metabolism.* Mol Cell Biochem, 1990. **98**(1-2): p. 167-76.
490. Krones, A., T. Kietzmann, and K. Jungermann, *Perivenous localization of insulin receptor protein in rat liver, and regulation of its expression by glucose and oxygen in hepatocyte cultures.* Biochem J, 2000. **348 Pt 2**: p. 433-8.
491. Krones, A., T. Kietzmann, and K. Jungermann, *Periportal localization of glucagon receptor mRNA in rat liver and regulation of its expression by glucose and oxygen in hepatocyte cultures.* FEBS Lett, 1998. **421**(2): p. 136-40.
492. Lewis, G.F., et al., *Disordered fat storage and mobilization in the pathogenesis of insulin resistance and type 2 diabetes.* Endocr Rev, 2002. **23**(2): p. 201-29.
493. Benhamed, F., et al., *The lipogenic transcription factor ChREBP dissociates hepatic steatosis from insulin resistance in mice and humans.* Journal of Clinical Investigation, 2012. **122**(6): p. 2176-2194.
494. Uyeda, K. and J.J. Repa, *Carbohydrate response element binding protein, ChREBP, a transcription factor coupling hepatic glucose utilization and lipid synthesis.* Cell Metabolism, 2006. **4**(2): p. 107-110.
495. Michael, M.D., et al., *Loss of insulin signaling in hepatocytes leads to severe insulin resistance and progressive hepatic dysfunction.* Mol Cell, 2000. **6**(1): p. 87-97.
496. Fisher, S.J. and C.R. Kahn, *Insulin signaling is required for insulin's direct and indirect action on hepatic glucose production.* Journal of Clinical Investigation, 2003. **111**(4): p. 463-468.
497. Haeusler, R.A. and D. Accili, *The double life of Irs.* Cell Metab, 2008. **8**(1): p. 7-9.
498. Dong, X.C., et al., *Inactivation of hepatic Foxo1 by insulin signaling is required for adaptive nutrient homeostasis and endocrine growth regulation.* Cell Metabolism, 2008. **8**(1): p. 65-76.
499. Kubota, N., et al., *Dynamic functional relay between insulin receptor substrate 1 and 2 in hepatic insulin signaling during fasting and feeding.* Cell Metabolism, 2008. **8**(1): p. 49-64.
500. Haeusler, R.A. and D. Accili, *The double life of Irs.* Cell Metabolism, 2008. **8**(1): p. 7-9.
501. Gusdon, A.M., K.X. Song, and S. Qu, *Nonalcoholic Fatty Liver Disease: Pathogenesis and Therapeutics from a Mitochondria-Centric Perspective.* Oxidative Medicine and Cellular Longevity, 2014.
502. Hammad, E.S., J.S. Striffler, and R.R. Cardell, Jr., *Morphological and biochemical observations on hepatic glycogen metabolism in mice on a controlled feeding schedule. II. Streptozotocin-diabetic mice.* Dig Dis Sci, 1982. **27**(8): p. 692-700.
503. Diraison, F., P. Moulin, and M. Beylot, *Contribution of hepatic de novo lipogenesis and reesterification of plasma non esterified fatty acids to plasma triglyceride synthesis during non-alcoholic fatty liver disease.* Diabetes Metab, 2003. **29**(5): p. 478-85.
504. Lambert, J.E., et al., *Increased De Novo Lipogenesis Is a Distinct Characteristic of Individuals With Nonalcoholic Fatty Liver Disease.* Gastroenterology, 2014. **146**(3): p. 726-735.

505. Henly, D.C., J.W. Phillips, and M.N. Berry, *Suppression of glycolysis is associated with an increase in glucose cycling in hepatocytes from diabetic rats.* Journal of Biological Chemistry, 1996. **271**(19): p. 11268-11271.
506. Bugianesi, E., et al., *Insulin resistance in non-diabetic patients with non-alcoholic fatty liver disease: sites and mechanisms.* Diabetologia, 2005. **48**(4): p. 634-42.
507. Lazarin Mde, O., et al., *Liver mitochondrial function and redox status in an experimental model of non-alcoholic fatty liver disease induced by monosodium L-glutamate in rats.* Exp Mol Pathol, 2011. **91**(3): p. 687-94.
508. Iozzo, P., et al., *Fatty Acid Metabolism in the Liver, Measured by Positron Emission Tomography, Is Increased in Obese Individuals.* Gastroenterology, 2010. **139**(3): p. 846-U203.
509. Hodson, L., et al., *Greater dietary fat oxidation in obese compared with lean men: an adaptive mechanism to prevent liver fat accumulation?* Am J Physiol Endocrinol Metab, 2010. **299**(4): p. E584-92.
510. Carmiel-Haggai, M., A.I. Cederbaum, and N. Nieto, *A high-fat diet leads to the progression of non-alcoholic fatty liver disease in obese rats.* Faseb Journal, 2004. **18**(14): p. 136-+.
511. Jiang, Y., M.Y. Zhao, and W. An, *Increased hepatic apoptosis in high-fat diet-induced NASH in rats may be associated with downregulation of hepatic stimulator substance.* Journal of Molecular Medicine-Jmm, 2011. **89**(12): p. 1207-1217.
512. Serviddio, G., et al., *Alterations of hepatic ATP homeostasis and respiratory chain during development of non-alcoholic steatohepatitis in a rodent model.* European Journal of Clinical Investigation, 2008. **38**(4): p. 245-252.
513. Cortez-Pinto, H., et al., *Alterations in liver ATP homeostasis in human nonalcoholic steatohepatitis - A pilot study.* Jama-Journal of the American Medical Association, 1999. **282**(17): p. 1659-1664.
514. Serviddio, G., et al., *Uncoupling protein-2 (UCP2) induces mitochondrial proton leak and increases susceptibility of non-alcoholic steatohepatitis (NASH) liver to ischaemia-reperfusion injury.* Gut, 2008. **57**(7): p. 957-965.
515. Garciaruiz, C., et al., *Role of Oxidative Stress Generated from the Mitochondrial Electron-Transport Chain and Mitochondrial Glutathione Status in Loss of Mitochondrial-Function and Activation of Transcription Factor Nuclear Factor-Kappa-B - Studies with Isolated-Mitochondria and Rat Hepatocytes.* Molecular Pharmacology, 1995. **48**(5): p. 825-834.
516. Hensley, K., et al., *Dietary choline restriction causes complex I dysfunction and increased H2O2 generation in liver mitochondria.* Carcinogenesis, 2000. **21**(5): p. 983-989.
517. Shimomura, I., Y. Bashmakov, and J.D. Horton, *Increased levels of nuclear SREBP-1c associated with fatty livers in two mouse models of diabetes mellitus.* Journal of Biological Chemistry, 1999. **274**(42): p. 30028-30032.
518. Burns, S.P., et al., *Zonation of gluconeogenesis, ketogenesis and intracellular pH in livers from normal and diabetic ketoacidotic rats: evidence for intralobular redistribution of metabolic events in ketoacidosis.* Biochem J, 1999. **343 Pt 1**: p. 273-80.
519. Stefan, N., et al., *Genetic variations in PPARD and PPARGC1A determine mitochondrial function and change in aerobic physical fitness and insulin sensitivity during lifestyle intervention.* J Clin Endocrinol Metab, 2007. **92**(5): p. 1827-33.
520. Wang, Y.X., et al., *Peroxisome-proliferator-activated receptor delta activates fat metabolism to prevent obesity.* Cell, 2003. **113**(2): p. 159-70.
521. Wei, Y., et al., *Nonalcoholic fatty liver disease and mitochondrial dysfunction.* World J Gastroenterol, 2008. **14**(2): p. 193-9.
522. Goodpaster, B.H., A. Katsiaras, and D.E. Kelley, *Enhanced fat oxidation through physical activity is associated with improvements in insulin sensitivity in obesity.* Diabetes, 2003. **52**(9): p. 2191-7.
523. Corbett, J.W. and J.H. Harwood, Jr., *Inhibitors of mammalian acetyl-CoA carboxylase.* Recent Pat Cardiovasc Drug Discov, 2007. **2**(3): p. 162-80.

524. Abu-Elheiga, L., et al., *Continuous fatty acid oxidation and reduced fat storage in mice lacking acetyl-CoA carboxylase 2.* Science, 2001. **291**(5513): p. 2613-2616.
525. Abu-Elheiga, L., et al., *Acetyl-CoA carboxylase 2 mutant mice are protected against obesity and diabetes induced by high-fat/high-carbohydrate diets.* Proceedings of the National Academy of Sciences of the United States of America, 2003. **100**(18): p. 10207-10212.
526. Savage, D.B., et al., *Reversal of diet-induced hepatic steatosis and hepatic insulin resistance by antisense oligonucleotide inhibitors of acetyl-CoA carboxylases 1 and 2.* Journal of Clinical Investigation, 2006. **116**(3): p. 817-824.
527. Ritchie, S.A. and J.M. Connell, *The link between abdominal obesity, metabolic syndrome and cardiovascular disease.* Nutr Metab Cardiovasc Dis, 2007. **17**(4): p. 319-26.
528. Fox, C.S., et al., *Abdominal visceral and subcutaneous adipose tissue compartments: association with metabolic risk factors in the Framingham Heart Study.* Circulation, 2007. **116**(1): p. 39-48.
529. Doege, H., et al., *Silencing of hepatic fatty acid transporter protein 5 in vivo reverses diet-induced non-alcoholic fatty liver disease and improves hyperglycemia.* J Biol Chem, 2008. **283**(32): p. 22186-92.
530. Salpeter, S.R., et al., *Risk of fatal and nonfatal lactic acidosis with metformin use in type 2 diabetes mellitus: systematic review and meta-analysis.* Arch Intern Med, 2003. **163**(21): p. 2594-602.
531. Choi, C.S., et al., *Liver-specific pyruvate dehydrogenase complex deficiency upregulates lipogenesis in adipose tissue and improves peripheral insulin sensitivity.* Lipids, 2010. **45**(11): p. 987-95.
532. Neschen, S., et al., *Prevention of hepatic steatosis and hepatic insulin resistance in mitochondrial acyl-CoA:glycerol-sn-3-phosphate acyltransferase 1 knockout mice.* Cell Metab, 2005. **2**(1): p. 55-65.
533. Wendel, A.A., et al., *Glycerol-3-phosphate acyltransferase 1 deficiency in ob/ob mice diminishes hepatic steatosis but does not protect against insulin resistance or obesity.* Diabetes, 2010. **59**(6): p. 1321-9.
534. Brown, G.K., et al., *Pyruvate dehydrogenase deficiency.* J Med Genet, 1994. **31**(11): p. 875-9.
535. Sidhu, S., et al., *Tissue-specific pyruvate dehydrogenase complex deficiency causes cardiac hypertrophy and sudden death of weaned male mice.* Am J Physiol Heart Circ Physiol, 2008. **295**(3): p. H946-H952.
536. Chirala, S.S., et al., *Fatty acid synthesis is essential in embryonic development: Fatty acid synthase null mutants and most of the heterozygotes die in utero.* Proceedings of the National Academy of Sciences of the United States of America, 2003. **100**(11): p. 6358-6363.
537. Chakravarthy, M.V., et al., *"New" hepatic fat activates PPARalpha to maintain glucose, lipid, and cholesterol homeostasis.* Cell Metab, 2005. **1**(5): p. 309-22.
538. Harada, N., et al., *Hepatic de novo lipogenesis is present in liver-specific ACC1-deficient mice.* Molecular and Cellular Biology, 2007. **27**(5): p. 1881-1888.
539. Wu, M., et al., *Antidiabetic and antisteatotic effects of the selective fatty acid synthase (FAS) inhibitor platensimycin in mouse models of diabetes.* Proceedings of the National Academy of Sciences of the United States of America, 2011. **108**(13): p. 5378-5383.
540. Lodhi, I.J., et al., *Inhibiting adipose tissue lipogenesis reprograms thermogenesis and PPARgamma activation to decrease diet-induced obesity.* Cell Metab, 2012. **16**(2): p. 189-201.
541. Kim, K.H., *Regulation of mammalian acetyl-coenzyme A carboxylase.* Annu Rev Nutr, 1997. **17**: p. 77-99.
542. Abu-Elheiga, L., et al., *Mutant mice lacking acetyl-CoA carboxylase 1 are embryonically lethal.* Proc Natl Acad Sci U S A, 2005. **102**(34): p. 12011-6.

543. Mao, J., et al., *Liver-specific deletion of acetyl-CoA carboxylase 1 reduces hepatic triglyceride accumulation without affecting glucose homeostasis.* Proceedings of the National Academy of Sciences of the United States of America, 2006. **103**(22): p. 8552-8557.
544. Arbeeny, C.M., et al., *Inhibition of fatty acid synthesis decreases very low density lipoprotein secretion in the hamster.* J Lipid Res, 1992. **33**(6): p. 843-51.
545. Alkhouri, N., C. Carter-Kent, and A.E. Feldstein, *Apoptosis in nonalcoholic fatty liver disease: diagnostic and therapeutic implications.* Expert Rev Gastroenterol Hepatol, 2011. **5**(2): p. 201-12.
546. Wang, K., *Molecular mechanisms of hepatic apoptosis.* Cell Death Dis, 2014. **5**: p. e996.
547. Begriche, K., et al., *Mitochondrial dysfunction in NASH: causes, consequences and possible means to prevent it.* Mitochondrion, 2006. **6**(1): p. 1-28.
548. Begriche, K., et al., *Mitochondrial adaptations and dysfunctions in nonalcoholic fatty liver disease.* Hepatology, 2013. **58**(4): p. 1497-507.
549. Gariani, K., J. Philippe, and F.R. Jornayvaz, *Non-alcoholic fatty liver disease and insulin resistance: from bench to bedside.* Diabetes Metab, 2013. **39**(1): p. 16-26.
550. Bugianesi, E., et al., *Insulin resistance in nonalcoholic fatty liver disease.* Curr Pharm Des, 2010. **16**(17): p. 1941-51.
551. Barbara B. Knowles, D.P.A., *Human hepatoma derived cell line, process for preparation thereof, and uses therefor 4,393,133*. 1983: United States.
552. Schardt, C., et al., *Characterization of insulin-like growth factor II receptors in human small cell lung cancer cell lines.* Exp Cell Res, 1993. **204**(1): p. 22-9.
553. Ranade, A.R., et al., *High Content Imaging and Analysis Enable Quantitative In Situ Assessment of CYP3A4 Using Cryopreserved Differentiated HepaRG Cells.* J Toxicol, 2014. **2014**: p. 291054.
554. Gibbons, G.F., et al., *Lipid balance in HepG2 cells: active synthesis and impaired mobilization.* J Lipid Res, 1994. **35**(10): p. 1801-8.
555. Hugo-Wissemann, D., et al., *Differences in glycolytic capacity and hypoxia tolerance between hepatoma cells and hepatocytes.* Hepatology, 1991. **13**(2): p. 297-303.
556. Vander Heiden, M.G., L.C. Cantley, and C.B. Thompson, *Understanding the Warburg effect: the metabolic requirements of cell proliferation.* Science, 2009. **324**(5930): p. 1029-33.
557. Garcia-Ruiz, I., et al., *In vitro treatment of HepG2 cells with saturated fatty acids reproduces mitochondrial dysfunction found in nonalcoholic steatohepatitis.* Dis Model Mech, 2015. **8**(2): p. 183-91.
558. Gao, Z., et al., *Butyrate improves insulin sensitivity and increases energy expenditure in mice.* Diabetes, 2009. **58**(7): p. 1509-17.
559. Puddu, A., et al., *Evidence for the gut microbiota short-chain fatty acids as key pathophysiological molecules improving diabetes.* Mediators Inflamm, 2014. **2014**: p. 162021.
560. Chempro. http://www.chempro.in/fattyacid.htm. 2016.
561. Wein, S., et al., *Medium-chain fatty acids ameliorate insulin resistance caused by high-fat diets in rats.* Diabetes Metab Res Rev, 2009. **25**(2): p. 185-94.
562. Mensink, R.P., et al., *Effects of dietary fatty acids and carbohydrates on the ratio of serum total to HDL cholesterol and on serum lipids and apolipoproteins: a meta-analysis of 60 controlled trials.* Am J Clin Nutr, 2003. **77**(5): p. 1146-55.
563. Fischer, C.L., et al., *Antibacterial activity of sphingoid bases and fatty acids against Gram-positive and Gram-negative bacteria.* Antimicrob Agents Chemother, 2012. **56**(3): p. 1157-61.
564. Shilling, M., et al., *Antimicrobial effects of virgin coconut oil and its medium-chain fatty acids on Clostridium difficile.* J Med Food, 2013. **16**(12): p. 1079-85.
565. Harding, R., et al., *Meeting the communication and information needs of chronic heart failure patients.* J Pain Symptom Manage, 2008. **36**(2): p. 149-56.

566. Organisation, W.H., *Diet, nutrition and the prevention of chronic diseases.*

. Report of the joint WHO/FAO expert consultation. WHO Technical Report Series, No. 916, 2003.
567. Reynoso, R., L.M. Salgado, and V. Calderon, *High levels of palmitic acid lead to insulin resistance due to changes in the level of phosphorylation of the insulin receptor and insulin receptor substrate-1.* Mol Cell Biochem, 2003. **246**(1-2): p. 155-62.
568. Grossi, M.M., G., *Fast and Accurate Determination of Olive Oil Acidity by Electrochemical Impedance Spectroscopy.* IEEE Sensors Journal, 2014. **14**(9): p. 2947 - 2954.
569. Temme, E.H., R.P. Mensink, and G. Hornstra, *Comparison of the effects of diets enriched in lauric, palmitic, or oleic acids on serum lipids and lipoproteins in healthy women and men.* Am J Clin Nutr, 1996. **63**(6): p. 897-903.
570. Teres, S., et al., *Oleic acid content is responsible for the reduction in blood pressure induced by olive oil.* Proc Natl Acad Sci U S A, 2008. **105**(37): p. 13811-6.
571. Farvid, M.S., et al., *Dietary linoleic acid and risk of coronary heart disease: a systematic review and meta-analysis of prospective cohort studies.* Circulation, 2014. **130**(18): p. 1568-78.
572. Moloney, F., et al., *Conjugated linoleic acid supplementation, insulin sensitivity, and lipoprotein metabolism in patients with type 2 diabetes mellitus.* Am J Clin Nutr, 2004. **80**(4): p. 887-95.
573. Shadman, Z., et al., *Effect of conjugated linoleic acid and vitamin E on glycemic control, body composition, and inflammatory markers in overweight type2 diabetics.* J Diabetes Metab Disord, 2013. **12**(1): p. 42.
574. Riserus, U., et al., *Treatment with dietary trans10cis12 conjugated linoleic acid causes isomer-specific insulin resistance in obese men with the metabolic syndrome.* Diabetes Care, 2002. **25**(9): p. 1516-21.
575. McCune, S.A. and R.A. Harris, *Mechanism responsible for 5-(tetradecyloxy)-2-furoic acid inhibition of hepatic lipogenesis.* J Biol Chem, 1979. **254**(20): p. 10095-101.
576. Halvorson, D.L. and S.A. McCune, *Inhibition of fatty acid synthesis in isolated adipocytes by 5-(tetradecyloxy)-2-furoic acid.* Lipids, 1984. **19**(11): p. 851-6.
577. Huang, H., et al., *Inhibitors of Fatty Acid Synthesis Induce PPAR alpha -Regulated Fatty Acid beta -Oxidative Genes: Synergistic Roles of L-FABP and Glucose.* PPAR Res, 2013. **2013**: p. 865604.
578. Wu, M., et al., *Antidiabetic and antisteatotic effects of the selective fatty acid synthase (FAS) inhibitor platensimycin in mouse models of diabetes.* Proc Natl Acad Sci U S A, 2011. **108**(13): p. 5378-83.
579. Kempen, H.J., et al., *Secretion of apolipoproteins A-I and B by HepG2 cells: regulation by substrates and metabolic inhibitors.* J Lipid Res, 1995. **36**(8): p. 1796-806.
580. Triscari, J. and A.C. Sullivan, *Anti-obesity activity of a novel lipid synthesis inhibitor.* Int J Obes, 1984. **8 Suppl 1**: p. 227-39.
581. Fukuda, N. and J.A. Ontko, *Interactions between fatty acid synthesis, oxidation, and esterification in the production of triglyceride-rich lipoproteins by the liver.* J Lipid Res, 1984. **25**(8): p. 831-42.
582. Harwood, H.J., Jr., et al., *Isozyme-nonselective N-substituted bipiperidylcarboxamide acetyl-CoA carboxylase inhibitors reduce tissue malonyl-CoA concentrations, inhibit fatty acid synthesis, and increase fatty acid oxidation in cultured cells and in experimental animals.* J Biol Chem, 2003. **278**(39): p. 37099-111.
583. Kuhajda, F.P., et al., *Synthesis and antitumor activity of an inhibitor of fatty acid synthase.* Proc Natl Acad Sci U S A, 2000. **97**(7): p. 3450-4.
584. Loftus, T.M., et al., *Reduced food intake and body weight in mice treated with fatty acid synthase inhibitors.* Science, 2000. **288**(5475): p. 2379-81.

585. Cao, J., et al., *Targeting Acyl-CoA:diacylglycerol acyltransferase 1 (DGAT1) with small molecule inhibitors for the treatment of metabolic diseases.* J Biol Chem, 2011. **286**(48): p. 41838-51.
586. Ganapathy-Kanniappan, S., et al., *Glyceraldehyde-3-phosphate dehydrogenase (GAPDH) is pyruvylated during 3-bromopyruvate mediated cancer cell death.* Anticancer Res, 2009. **29**(12): p. 4909-18.
587. Ehrke, E., C. Arend, and R. Dringen, *3-bromopyruvate inhibits glycolysis, depletes cellular glutathione, and compromises the viability of cultured primary rat astrocytes.* J Neurosci Res, 2015. **93**(7): p. 1138-46.
588. Vandercammen, A. and E. Van Schaftingen, *Competitive inhibition of liver glucokinase by its regulatory protein.* Eur J Biochem, 1991. **200**(2): p. 545-51.
589. Chen, W. and M. Gueron, *The inhibition of bovine heart hexokinase by 2-deoxy-D-glucose-6-phosphate: characterization by 31P NMR and metabolic implications.* Biochimie, 1992. **74**(9-10): p. 867-73.
590. Turner, N., et al., *Excess lipid availability increases mitochondrial fatty acid oxidative capacity in muscle: evidence against a role for reduced fatty acid oxidation in lipid-induced insulin resistance in rodents.* Diabetes, 2007. **56**(8): p. 2085-92.
591. Nassir, F. and J.A. Ibdah, *Role of mitochondria in nonalcoholic fatty liver disease.* Int J Mol Sci, 2014. **15**(5): p. 8713-42.
592. Chow, L., A. From, and E. Seaquist, *Skeletal muscle insulin resistance: the interplay of local lipid excess and mitochondrial dysfunction.* Metabolism, 2010. **59**(1): p. 70-85.
593. Mansouri, A., et al., *An alcoholic binge causes massive degradation of hepatic mitochondrial DNA in mice.* Gastroenterology, 1999. **117**(1): p. 181-90.
594. Pessayre, D., A. Mansouri, and B. Fromenty, *Nonalcoholic steatosis and steatohepatitis. V. Mitochondrial dysfunction in steatohepatitis.* Am J Physiol Gastrointest Liver Physiol, 2002. **282**(2): p. G193-9.
595. Spanidis, Y., et al., *Assessment of the redox status in patients with metabolic syndrome and type 2 diabetes reveals great variations.* Exp Ther Med, 2016. **11**(3): p. 895-903.
596. Rael, L.T., et al., *Plasma oxidation-reduction potential and protein oxidation in traumatic brain injury.* J Neurotrauma, 2009. **26**(8): p. 1203-11.
597. Spanidis, Y., et al., *Assessment of Oxidative Stress in Septic and Obese Patients Using Markers of Oxidation-reduction Potential.* In Vivo, 2015. **29**(5): p. 595-600.
598. Bar-Or, D., et al., *Oxidative stress in severe acute illness.* Redox Biol, 2015. **4**: p. 340-5.
599. Bar-Or, R., et al., *Raman spectral signatures of human liver perfusates correlate with oxidation reduction potential.* Mol Med Rep, 2009. **2**(2): p. 175-80.
600. Holm, S., *A simple sequentially rejective multiple test procedure.* Scandinavian Journal of Statistics, 1979. **6**(2): p. 65-70.
601. Renner, K., et al., *Changes of mitochondrial respiration, mitochondrial content and cell size after induction of apoptosis in leukemia cells.* Biochim Biophys Acta, 2003. **1642**(1-2): p. 115-23.
602. Wang, C., et al., *Acetyl-CoA carboxylase-a as a novel target for cancer therapy.* Front Biosci (Schol Ed), 2010. **2**: p. 515-26.
603. Dilip, A., et al., *Mitochondria-targeted antioxidant and glycolysis inhibition: synergistic therapy in hepatocellular carcinoma.* Anticancer Drugs, 2013. **24**(9): p. 881-8.
604. Pedersen, P.L., *3-Bromopyruvate (3BP) a fast acting, promising, powerful, specific, and effective "small molecule" anti-cancer agent taken from labside to bedside: introduction to a special issue.* J Bioenerg Biomembr, 2012. **44**(1): p. 1-6.
605. Flavin, R., et al., *Fatty acid synthase as a potential therapeutic target in cancer.* Future Oncol, 2010. **6**(4): p. 551-62.
606. Lee, J.Y., H.K. Cho, and Y.H. Kwon, *Palmitate induces insulin resistance without significant intracellular triglyceride accumulation in HepG2 cells.* Metabolism, 2010. **59**(7): p. 927-34.

607. Ishii, M., et al., *Palmitate induces insulin resistance in human HepG2 hepatocytes by enhancing ubiquitination and proteasomal degradation of key insulin signaling molecules.* Arch Biochem Biophys, 2015. **566**: p. 26-35.
608. Tang, Z., et al., *TRAM1 protect HepG2 cells from palmitate induced insulin resistance through ER stress-JNK pathway.* Biochem Biophys Res Commun, 2015. **457**(4): p. 578-84.
609. Soardo, G., et al., *Oxidative Stress Is Activated by Free Fatty Acids in Cultured Human Hepatocytes.* Metabolic Syndrome and Related Disorders, 2011. **9**(5): p. 397-401.
610. Ralser, M., et al., *A catabolic block does not sufficiently explain how 2-deoxy-D-glucose inhibits cell growth.* Proc Natl Acad Sci U S A, 2008. **105**(46): p. 17807-11.
611. Li, S., et al., *TOFA suppresses ovarian cancer cell growth in vitro and in vivo.* Mol Med Rep, 2013. **8**(2): p. 373-8.
612. Benoist, F. and T. Grand-Perret, *ApoB-100 secretion by HepG2 cells is regulated by the rate of triglyceride biosynthesis but not by intracellular lipid pools.* Arterioscler Thromb Vasc Biol, 1996. **16**(10): p. 1229-35.
613. Sigma. http://www.sigmaaldrich.com/catalog/product/sigma/t6575. 2016.
614. Wang, C., et al., *Acetyl-CoA carboxylase-alpha inhibitor TOFA induces human cancer cell apoptosis.* Biochem Biophys Res Commun, 2009. **385**(3): p. 302-6.
615. Impheng, H., et al., *[6]-Gingerol inhibits de novo fatty acid synthesis and carnitine palmitoyltransferase-1 activity which triggers apoptosis in HepG2.* Am J Cancer Res, 2015. **5**(4): p. 1319-36.
616. Williamson DH, B.J., Concentrations of metabolites in animal tissues. In: Methods of enzymatic analysis (Bergmeyer HV ed.) pp. 2266-2302. New York: Academic Press.
617. Zhou, W., et al., *Fatty acid synthase inhibition triggers apoptosis during S phase in human cancer cells.* Cancer Res, 2003. **63**(21): p. 7330-7.
618. Landree, L.E., et al., *C75, a fatty acid synthase inhibitor, modulates AMP-activated protein kinase to alter neuronal energy metabolism.* J Biol Chem, 2004. **279**(5): p. 3817-27.
619. Gao, Y., et al., *Growth arrest induced by C75, A fatty acid synthase inhibitor, was partially modulated by p38 MAPK but not by p53 in human hepatocellular carcinoma.* Cancer Biol Ther, 2006. **5**(8): p. 978-85.
620. Scott, S.A., et al., *Chemical modulation of glycerolipid signaling and metabolic pathways.* Biochim Biophys Acta, 2014. **1841**(8): p. 1060-84.
621. Muhlenberg, T., et al., *Inhibition of KIT-glycosylation by 2-deoxyglucose abrogates KIT-signaling and combination with ABT-263 synergistically induces apoptosis in gastrointestinal stromal tumor.* PLoS One, 2015. **10**(3): p. e0120531.
622. Zhao, S., et al., *[3-bromopyruvate enhances cisplatin sensitivity of hepatocellular carcinoma cells in vitro].* Nan Fang Yi Ke Da Xue Xue Bao, 2014. **34**(1): p. 25-30.
623. Ganapathy-Kanniappan, S., R. Kunjithapatham, and J.F. Geschwind, *Anticancer efficacy of the metabolic blocker 3-bromopyruvate: specific molecular targeting.* Anticancer Res, 2013. **33**(1): p. 13-20.